An investigation of heme-protein covalent links and active site cross-links in heme peroxidases

Thesis submitted for the degree of Doctor of Philosophy at the
University of Leicester

by

Zoi Pipirou, Ptychion Chemistry

Department of Chemistry
Faculty of Science
University of Leicester

November 2007

UMI Number: U495426

UMI

Dissertation Publishing

ProQuest

To Paris, Despoina and Savvas

Statement

Unless otherwise acknowledged, the experimental work described in this thesis has been carried out by the author in the Department of Chemistry and Henry Wellcome laboratories for Structural Biology, at the University of Leicester between October 2004 and November 2007. The work has not been submitted, and is not presently being submitted for any other degree at this or any other university.

Signed: Date:

Department of Chemistry

University of Leicester

University Road

Leicester

LE1 7RH

UK

An investigation of heme-protein covalent links and active site cross-links in heme peroxidases

Zoi Pipirou

Abstract

Proteins and enzymes that contain a heme group form a diverse family that are involved in a truly overwhelming range of biological processes. Many heme proteins contain iron protoporphyrin IX, however, it is now becoming clear that a large number of other proteins, e.g. the mammalian peroxidases, use modified versions of iron protoporphyrin IX in which the heme is covalently linked to the protein. This thesis presents an investigation of covalent heme attachment in APX and plant proteins.

In Chapter 2, it was shown that reaction of APX with H_2O_2 leads to the formation of a covalent link from the heme to Trp41 residue under non-catalytic conditions. Formation of this covalent link was proposed to proceed through a Compound I species bearing a porphyrin π-cation radical. Formation of a protein radical at Trp41 is also implicated, in a reaction mechanism that is analogous to that proposed for formation of a covalent Trp-Tyr-Met link in the closely related catalase-peroxidase (KatG) enzymes. It was also shown that the same covalent link is formed into the S207E variant of APX.

In Chapter 3, it was shown that a covalent link between the heme and Trp51 cannot be supported by wild type CcP, but can be engineered into the W191F variant of CcP where formation of a Compound I species bearing a porphyrin π-cation radical is sustainable. A comparison of the similarities and differences between the mechanisms used by the members of the Class I family of plant peroxidases is made in both Chapters 2 and 3.

In Chapter 4, the reaction of the S160Y variant of APX with H_2O_2 was examined and it was shown that Tyr160 forms a covalent link to the heme in an autocatalytic reaction that also leads to formation of a second covalent link to Trp41, as above. The formation of these links was found to have a profound effect on the redox properties of the heme iron. The implications of these data are discussed in terms of both current understanding of heme group reactivity and the conditions needed for any heme protein to duplicate the active site architecture observed in the mammalian peroxidases.

Although several questions still remain unanswered, the work in this thesis has given valuable insight into the formation of covalent links in heme proteins, using plant proteins as model systems and has demonstrated how plant proteins can provide alternative routes for studying covalent heme attachment.

Acknowledgements

Contents

Chapter 1   Introduction

Chapter 2 Autocatalytic formation of a covalent link between Trp41 and the heme in APX

Chapter 3 Investigation of heme-protein covalent link formation in C*c*P and the W191F variant

Chapter 4 The reactivity of heme in biological systems: Autocatalytic formation of both tyrosine-heme and tryptophan-heme covalent links in a single protein architecture

Chapter 5   Summary

Chapter 6   Experimental

Abbreviations

Amino Acids are abbreviated according to the three-letter codes recommended by the I. U. P. A.C. Joint Commission on Biochemical Nomenclature (1985).

Enzymes

APX	ascorbate peroxidase
rpAPX	recombinant cytosolic pea ascorbate peroxidase
rsAPX	recombinant cytosolic soybean ascorbate peroxidase
CcP	cytochrome c peroxidase
KatG	catalase-peroxidase
HRP	horseradish peroxidase
MnP	manganese peroxidase
Hb	hemoglobin
HAO	hydroxylamine oxidoreductase
MPO	myeloperoxidase
LPO	lactoperoxidase
TPO	thyroid peroxidase
EPO	eosinophil peroxidase
DNase	deoxyribonuclease
RNase	ribonuclease

Amino acids

Ala	A	alanine
Asn	N	asparagine
Asp	D	aspartic acid
Arg	R	arginine
Cys	C	cysteine
Glu	E	glutamic acid
Gln	Q	glutamine
Gly	G	glycine
His	H	histidine

Met	M	methionine
Pro	P	proline
Ser	S	serine
Thr	T	threonine
Tyr	Y	tyrosine
Lys	K	lysine
Leu	L	leucine
Ile	I	isoleucine
Phe	F	phenylalanine
Trp	W	tryptophan`
Val	V	valine

Chemicals

Amp	ampicillin
Kan	kanamycin
dNTPs	deoxynucleotide triphosphates
EDTA	ethylenediaminetetraacetic acid
HEPES	N-2-hydroxyethylpiperazine-N'-2-ethanesulphonic acid
IPTG	isopropyl-β-D thiogalactopyanoside
NTA	nitrilotriacetic acid
PEG 4000	poly-ethylene glycol of average molecular weight 4000
SDS	sodium dodecyl sulphate
DTT	dithiothreitol
LB	Luria-Bertani broth
NADH	nicotinamide adenine dinucleotide (reduced form)
PMSF	phenylmethanesulphonylfluoride
TFA	trifluoroacetic acid
kpi	potassium phosphate

Techniques

EPR	electron paramagnetic resonance
ENDOR	electron nuclear double resonance

FTIR	fourier transform infrared spectroscopy
HPLC	high performance liquid chromatography
MALDI-TOF	m atrix-assisted laser desorption/ionization - time of flight
FPLC	fast protein liquid chromatography
NMR	nuclear magnetic resonance
PAGE	polyacrylamide gel electophoresis
PCR	polymerase chain reaction
R_z	Reinheitzahl
UV	ultra violet
Vis	visible `

Units/Symbols

A	absorption
c	concentration
ε	absorption coefficient
Å	Ångström (1 Å = 10^{-10} m)
°C	degrees Celsius
°	degrees
g	grams
μ	ionic strength
kDa	kiloDaltons
kb	kilobases
l	litres
m	metres
min	minutes
M	molar
rpm	revolutions per minute
s	seconds
V	volts
λ	wavelength
w/v	weight per volume
n	whole number

OD	optical density
Hz	Hhertz
W	Watt
amu	atomic mass units

Miscellaneous

DNA	deoxyribonucleic acid
cDNA	complementary deoxyribonucleic acid
FAD	flavin adenine dinucleotide
E. coli	*Escherichia coli*
mt	*mycobacterium tuberculosis*
FFQ	fast flow Q Sepharose
I. U. P. A.C.	International Union of Pure and Applied Chemistry
PDB	Protein Data Bank
PNACL	Protein and Nucleic Acid Chemistry Laboratory

Chapter 1

Introduction

1.1　Heme

Iron protoporphyrin IX, also known as heme, is an iron-containing macrocycle that is an integral component of many proteins in bacteria, plants and animals. It is the component of hemoglobin (Figure 1.1a) that gives blood its red color. Heme consists of a protoporphyrin ring and a central iron (Fe) atom. A protoporphyrin ring is made up of four pyrrole rings linked by methene bridges. Four methyl, two vinyl, and two propionate side chains are attached. (Figure 1.1b) The iron can either be in the ferrous (Fe^{II}) or the ferric (Fe^{III}) oxidation state.
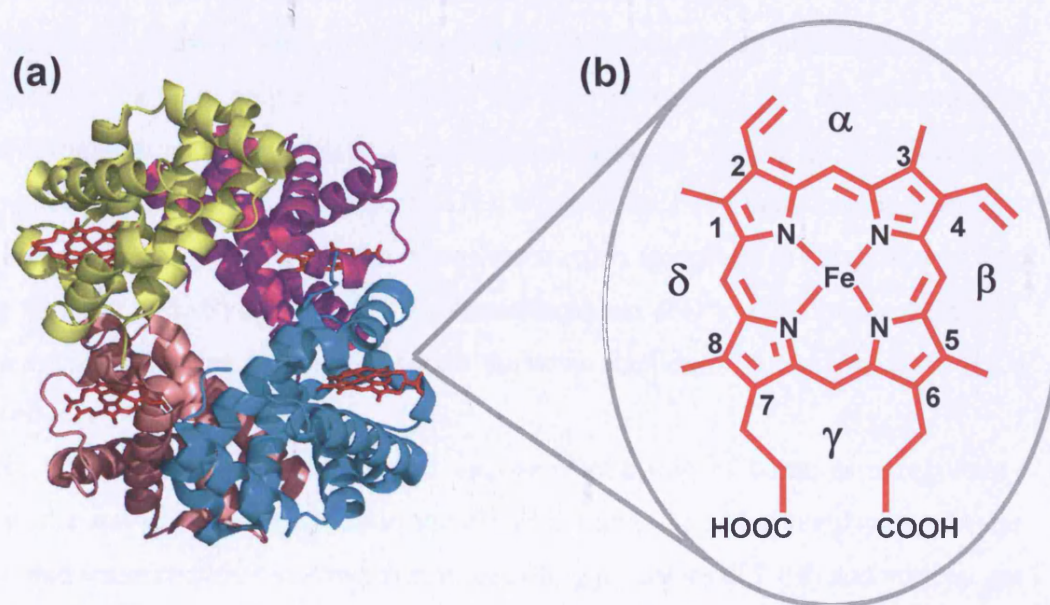
Figure 1.1: (a) Crystal structure of hemoglobin (PDB accession code 1GZX). (b) The structure of heme. The methene bridges are designated α, β, γ and δ.

Strictly speaking, ferriprotoporphyrin IX (Fe^{III}) is known as hemin whereas ferroprotoporphyrin IX (Fe^{II}) is known as heme. However, since the heme iron used in proteins can have many oxidation states, any form of iron-containing protoporphyrin IX is usually denoted heme and the oxidation state is given. The net charge of the heme with four-coordinate Fe^{III} is +1 (*1*). It is well known that heme is involved in various biological reactions as a prosthetic group of the proteins, so-called hemoproteins.

1.2 Heme proteins

Heme proteins display a wide range of biological functions and the area has been reviewed fairly extensively (*2-8*). Although many of these proteins possess the same prosthetic group, that of an iron protoporphyrin IX (Figure 1.2), the functions they perform can vary enormously. Heme proteins participate in a wide array of biological processes and can be grouped into three categories (*9*):

(i)   Electron transfer (*e.g. b-* and *c*-type cytochromes),

(ii)   Oxygen transport and storage (*e.g.* hemoglobin and myoglobin), and

(iii)   Redox enzymes (*e.g.* peroxidases and P450s).

Cytochromes, mostly found in the respiratory pathways, act as one-electron carrier proteins by shuttling between Fe^{II} and Fe^{III} at their active site (*3-5, 10*). Hemoglobin and myoglobin are able to maintain a balanced supply of oxygen by functioning as oxygen transport and binding proteins (*11*), whereas the P450 heme enzymes can act as mono-oxygenases by using dioxygen (*via* oxygen insertion) to catalyse aromatic and aliphatic hydroxylations (*12, 13*). Peroxidases are able to reduce peroxides and, as a consequence, are utilised to prevent the accumulation of potentially toxic H_2O_2 in cells (*14*).

More recent work however, has also uncovered the role of heme as a regulatory molecule and as a gas sensor, so to the above list must be added regulatory proteins that bind heme resulting in downstream signalling processes (*15, 16*) and various gas sensing proteins like guanylate cyclase, FixL, CooA, *etc (17-19)*.

Both the redox and coordination chemistry of the porphyrin iron – which is itself controlled by a number of variables imposed upon the molecule by the surrounding protein structure - can influence the function of the metalloprotein. This flexibility in function, more than likely, arises from a combination of differences in both the polypeptide and heme constituents of the various heme proteins.

A representation of heme in heme proteins is shown in Figure 1.2. The general coordination geometry of the iron in heme proteins is five or six. The two axial ligands are referred to as proximal and distal and can vary between proteins. In many cases the proximal ligand is a histidine, while the distal ligand can vary from low to strong field ligands and result in high- or low-spin heme, respectively.
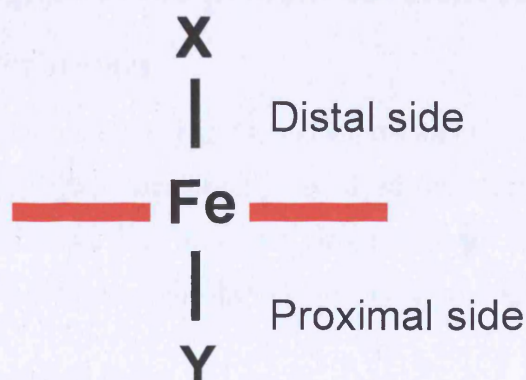
Figure 1.2: A representation of heme. The red lines represent the heme plane and X and Y represent the 5th and 6th ligand respectively.

1.3 Heme modification and heme-protein covalent links

Heme is a widely distributed cofactor found in proteins with diverse functions such as electron transfer, the binding of gases and many types of catalysis, as mentioned previously. Although the heme is non-covalently bound to many of these proteins, heme is found to attach covalently to others with different modes of attachment. Covalent attachment of the heme to the protein can either happen as an autocatalytic process (*e.g.* mammalian peroxidases) or through a process that requires the catalytic participation of additional proteins (*e.g.* cytochrome *c*). Autocatalytic modification of the heme group can be further divided into two general classes:

(i)   Processes that have evolved as part of the normal function of the proteins in question.

(ii)   Processes that are abnormal ("pathological") and result in non-physiological modification and/or degradation of the heme.

1.4   Physiological heme-protein covalent links

1.4.1 c-type cytochromes

Archaea, bacteria, fungi, plant thylakoids, and almost all higher organisms use c-type cytochromes (20-22). They are usually involved in electron transfer (e.g. in respiratory chains) (22-24), but they can also be found at the catalytic site of enzymes (25, 26), and in higher cells they are involved in apoptosis (27).

1.4.1.1 Nature of covalent links

In c-type cytochromes, heme is bound covalently by two thioether bonds to a conserved CXXCH motif of the apoprotein in a post-translational process referred to as cytochrome c maturation (28-30). The biogenesis process to produce c-type cytochromes involves the formation of two thioether bonds between the α-carbons of the heme vinyl groups and the thiol sulfurs from two cysteine residues of a CXXCH motif in the protein (Figure 1.3). The stereochemistry of the attachment is universally conserved and generally the process of attachment requires the involvement of other proteins (20, 31).

Rare exceptions to the CXXCH motif are either attachment to a CXXXCH, CXXXXCH, or CXXCK motif or attachment via a single thioether bond to an A/FXXCH motif, the latter presently known only in a group of eukaryotes, the Euglenozoa (28, 29). The H (or K) is always one of the axial ligands to the heme iron. The second axial ligand can either be a methionine (e.g. mitochondrial cytochrome c, Figure 1.3a,b) or a histidine (e.g. bacterial multiheme c-type cytochromes); these ligands are supplied by residues distant in the sequence from the CXXCH motif (29).

It has also been found that the heme chaperone CcmE, which is an essential intermediate in the process of cytochrome c biogenesis, also binds heme covalently before transferring heme to apocytochromes (32, 33). A single covalent bond is involved and occurs between a heme vinyl group and a histidine residue of CcmE (Figure 1.4) (31).
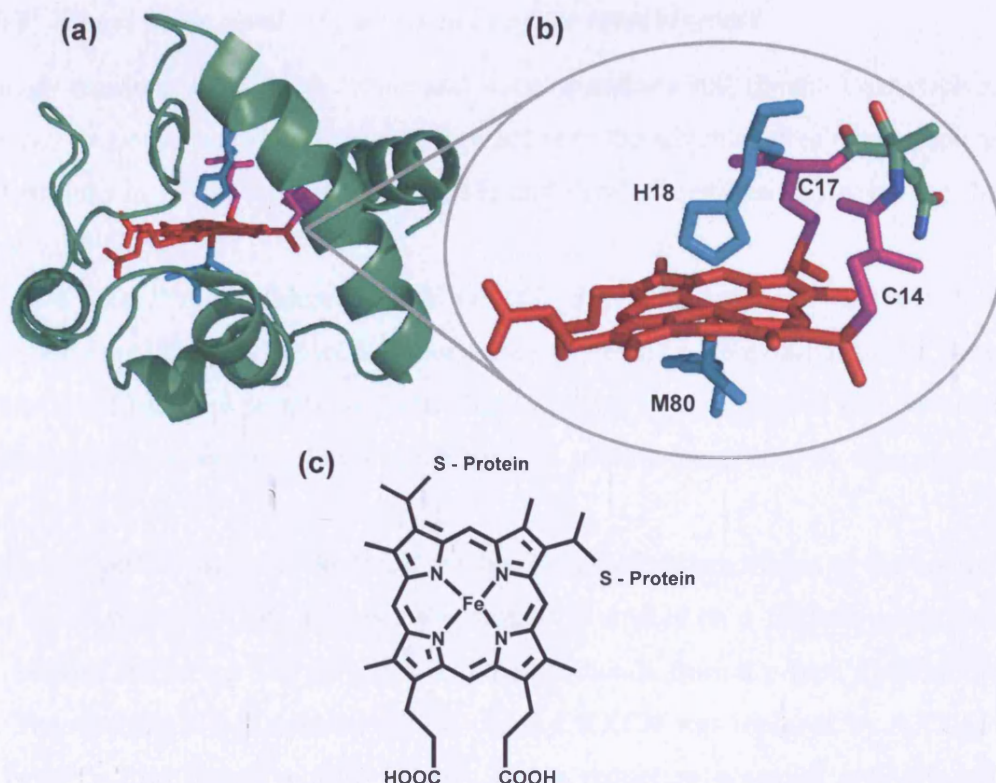
Figure 1.3: (a) Crystal structure of horse heart (mitochondrial) cytochrome *c* (PDB accession code 1HRC) (*34*), (b) Active site structure representing the single thioether bonds between the heme vinyl groups and the cysteine side chains (Cys14 and Cys17) in magenta. The remaining aminoacids of the CXXCH motif are shown in green, the heme is shown in red and the axial proximal (Met80) and distal (His18) ligands in cyan, (c) Structure of the heme in *c*-type cytochromes.
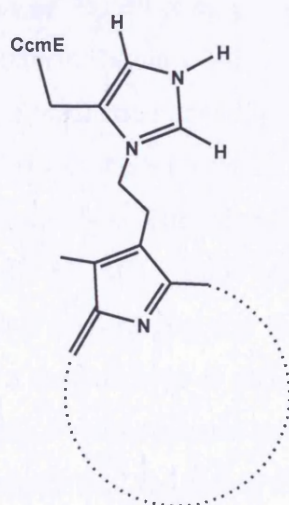
Figure 1.4: The structure of the covalent bond between an essential histidine sidechain of CcmE and heme as determined by NMR (35) (showing only one pyrrole ring for simplicity) (36).

6

1.4.1.2 Why is heme covalently attached in c-type cytochromes?

Although there has been great debate and many questions still remain unanswered, numerous proposals have been brought forward as to the advantages of heme-protein covalent links in c-type cytochromes. Barker and Ferguson extensively reviewed the area in 1999 (20).

The issue was first considered by Wood (37, 38) who proposed that covalent attachment could act as a device to prevent loss of heme to the external media from proteins in the bacterial periplasm. Later studies though have suggested that covalent attachment of heme is not solely a mechanism to prevent heme loss by dissociation (20).

Another suggestion was that the two thioether bonds might contribute to the control of the redox potential. This proposal was tested by studies on a folded protein that was obtained following loss of both the thioether bonds from a c-type cytochrome (39). The resulting b-type cytochrome, in which CXXCH was replaced by AXXAH (the heme is thus non-covalently bound), had a reduction potential only 70 mV different from the wild type protein, a difference that could surely be compensated, if needed, by adjustment of the micro-environment of the heme group. However, conversion of a c-type into a b-type cytochrome resulted in decreased thermal and chemical stability of both the oxidised and reduced form (39). This last observation has been further supported by studies which showed that heme is required for the stable fold of these proteins and might also provide a nucleation site for direction of folding (20, 21, 40-42). Even more, Rosell et al. proposed that loss of just one of the two thioether bonds to the porphyrin ring in C14S variant of yeast iso-1-cytochrome results in destabilization of the overall structure (43).

Recent studies have also emphasized the importance of the thioether links in tuning the redox potential of cytochrome c (44). Thus it was proposed that the mobility and conformational dynamics of the CXXCH motif can play a role in tuning heme potential by influencing the His-Fe interaction and therefore, covalent heme binding in cytochrome c may allow for a greater range of potentials to be accessed (44).

Other advantages of covalent link formation could be the economy of minimizing the the amino acid residue to heme ratio and the ability to position hemes spatially close and aid well-defined packing in multiheme proteins (20), such as c_3-type cytochromes (45). Finally, studies of variants of cytochrome b_{562} with cysteine in the

heme binding site have also shown the value of the covalent linkage for retaining otherwise unstable ligand environments involving methionine ligation (*46*).

1.4.2   Hydroxylamine oxidoreductase (HAO) and cytochrome P460

Heme P460 is a novel protein-bound *c*-type heme cofactor that has to date been characterized in only two proteins: the enzyme hydroxylamine oxidoreductase (HAO) (Figure 1.5a) (*47*) and the periplasmic cytochrome P460 (Figure 1.5b) (*48, 49*). Heme P460 is named for its characteristic ferrous Soret peak maximum at 460 nm (*47*).

HAO of *Nitrosomonas europaea* catalyses the oxidation of hydroxylamine to nitrite, the second step in ammonia oxidation, a process that accounts for the majority of ammonia oxidation in the biosphere (*50*). The physiological function of cytochrome P460 has not been established, but it has a weak hydroxylamine oxidation/cytochrome *c* reduction activity (*48, 51-53*).
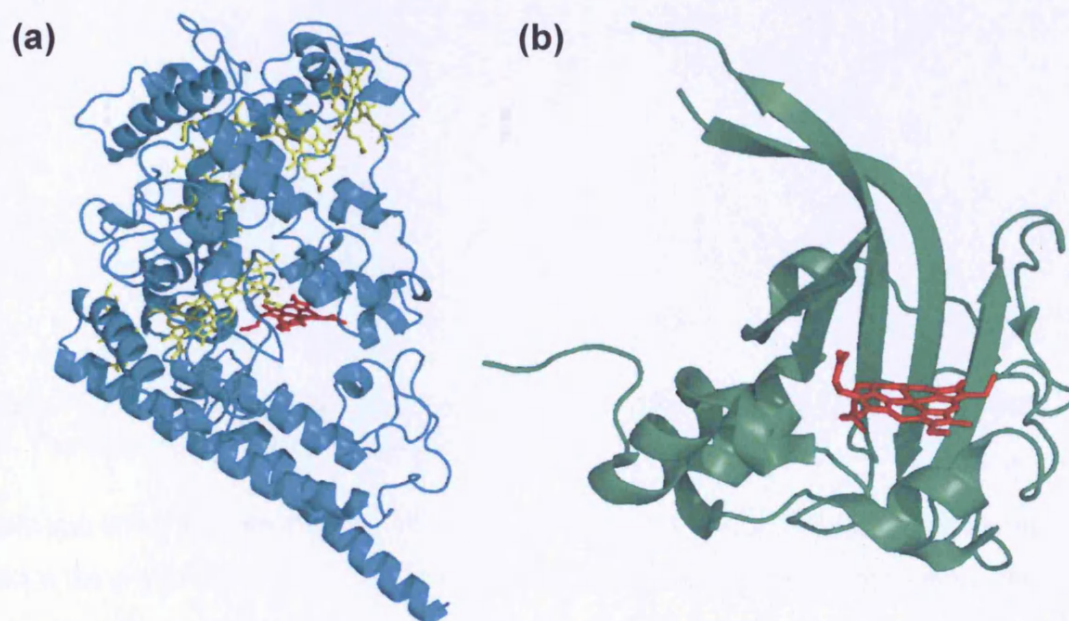
Figure 1.5: (a) Crystal structure of HAO monomer (PDB accession code 1FGJ) (*25*). Each HAO monomer contains 7 *c*-type hemes, shown in yellow, and one heme P460, shown in red, which forms the catalytic site. (b) Crystal structure of cytochrome P460 monomer (PDB accession code 2JE2) (*49*). Heme P460 is shown in red.

Both HAO and cytochrome P460 bear two thioether covalent links between the 2 vinyl groups of the heme and two cysteine residues of a CXXCH motif, as observed in cytochromes c. The X-ray crystal structure of HAO (Figure 1.5a) (*25*) confirmed earlier studies showing that there is an additional protein-derived tyrosine cross-link via a heme *meso*-carbon, in addition to the two thioether bonds typical of c-type cytochromes (Figure 1.6a) (*25, 51*). Similar biochemical studies carried out on cytochrome P460 and confirmed by X-ray crystallography, indicated that its heme P460 also possessed a third proteinaceous cross-link, but in this case to a conserved lysine residue (Figure 1.6b) (*49, 54, 55*). The formation of the cross-link to heme P460 in cytochrome P460 has been proposed to be an autocatalytic event (*54, 55*). As in the heme P460 of HAO, the third cross-link is to a *meso* carbon of the porphyrin ring. However, in the case of cytochrome P460 the cross-link is to the 13'-*meso* carbon, opposite the 5'-*meso* carbon linked to tyrosine in HAO (*49*).
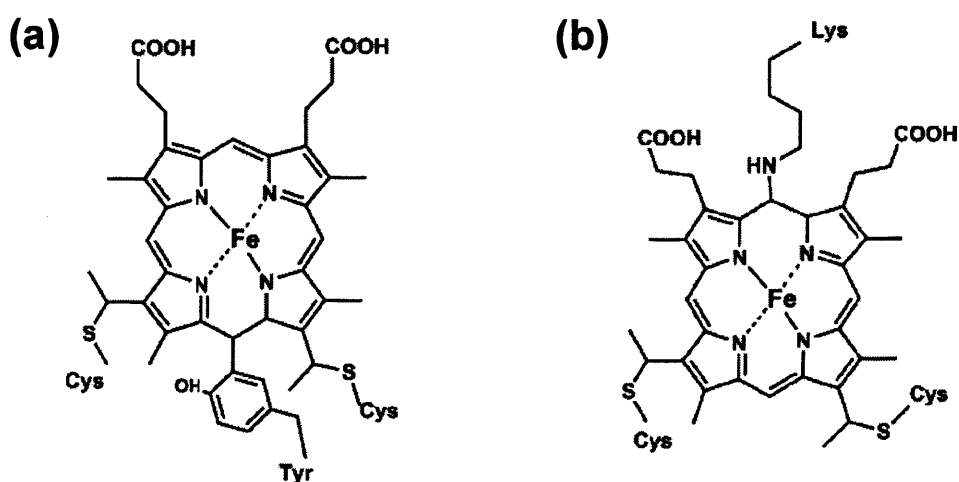
Figure 1.6: Schematic of the heme P460 structure in HAO (a) and cytochrome P460 (b). The figure is reproduced from reference (*49*).

Although HAO and cytochrome P460 both contain heme P460, the only similarity in fold is the c-type heme binding helix containing the CXXCH motif. Furthermore, the location of the extra cross-link to the opposite sides of the porphyrin ring indicates that the unusual spectral properties of heme P460 do not require the cross-link to be with a specific *meso*-carbon of the heme. This observation demonstrates that the formation of heme P460 can occur in multiple protein scaffolds, although it has so far only been identified in these two proteins (*49*).

1.4.3 Mammalian peroxidases

Mammalian peroxidases catalyse reactions of crucial importance to a wide range of biological processes, including thyroid hormone biosynthesis (thyroid peroxidase (TPO)) (*56*), control of inflammatory response (eosinophil peroxidase (EPO)) (*57*) and antimicrobial and antifungal action (myeloperoxidase (MPO), lactoperoxidase (LPO)) (*1, 58, 59*).

The most striking feature of the mammalian peroxidases is the existence of two to three covalent bonds between the prosthetic group and the protein in the functional, mature enzymes (*58*). The heme is covalently attached to the protein through ester bonds to heme methyl groups, in the case of LPO (*60*), EPO (*61*) and TPO (*62*) and through an additional sulfonium link to a heme vinyl group in the case of MPO (*63-65*).

1.4.3.1 Nature of covalent links

The patterns of these bonds, postulated early on (*66, 67*), have been clearly demonstrated for MPO by crystallography (*68*), for LPO by NMR and mass spectrometry (*69, 70*), and for EPO/LPO by mass spectrometry and peptide sequencing (*65*). The presence of ester links in all three enzymes has furthermore been corroborated by difference FTIR (*71*). Compelling evidence, based on sequence similarity and biochemical analysis, suggests the presence of similar heme-protein crosslinks in TPO (*62*).

The bonds between the heme and the protein are of two types:

    (i)   two ester bonds, observed in all four members, one linking a hydroxyl group on the 1-methyl substituent to a glutamic acid carboxylic group and the other a hydroxyl group on the 5-methyl substituent to the carboxyl group of an aspartyl residue,

    (ii) a vinyl-sulfonium bond, only present in MPO, linking the β-carbon of the 2-vinyl substituent and the sulfur of Met243 (*72*) (Figure 1.7).

The prosthetic group in these enzymes is therefore derived from Fe^{III} protoporphyrin IX by the formal replacement of one of the hydrogen atoms on the 1- and 5-methyls by an ester oxygen and one of the vinyl β-hydrogens by a methionine sulfur (Figure 1.8) (*58*).
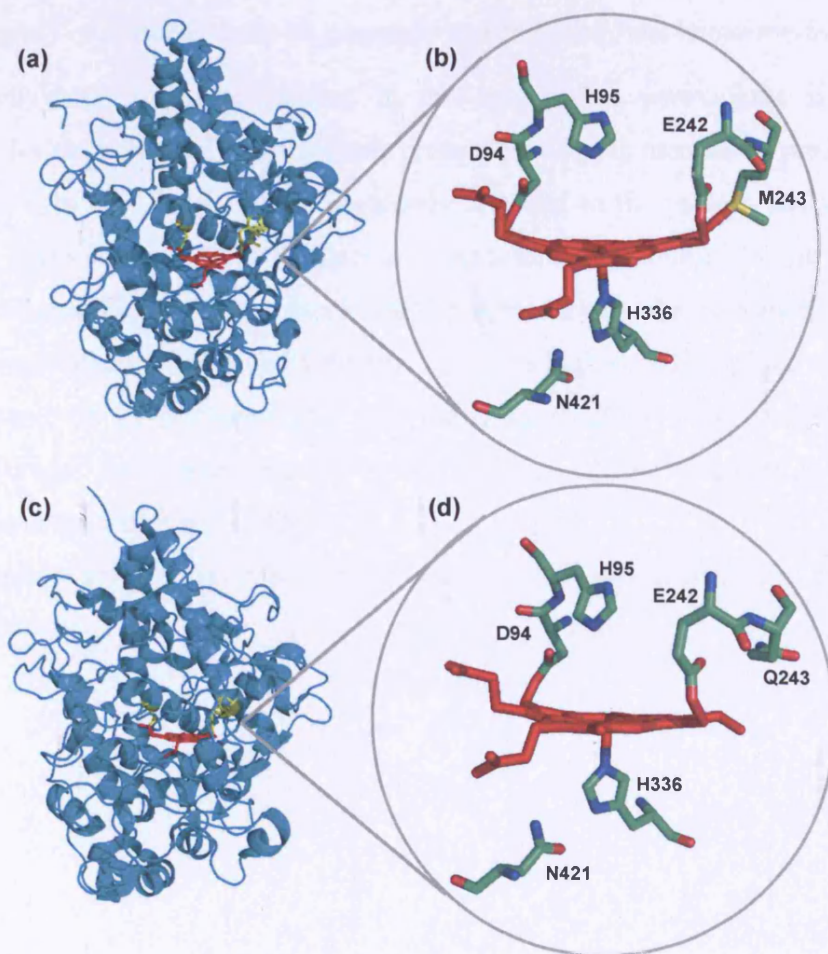
Figure 1.7: Overall (a,c) and active site (b,d) structures of human myeloperoxidase and bovine lactoperoxidase, respectively (PDB accession codes 1CXP and 2GJ1, respectively) (*73*). Residues that are covalently bound to the heme are indicated in yellow in (a) and (c).
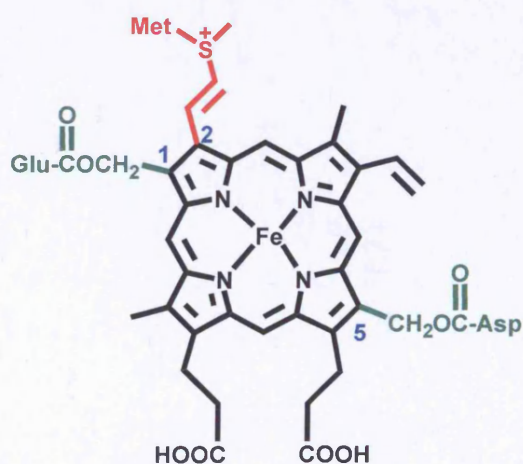
Figure 1.8: Covalent binding pattern of heme in mammalian peroxidases. The ester linkages between the 1- and 5-methyl carbons and Glu242 and Asp94, respectively, are conserved in all members of the mammalian peroxidases. The sulfonium ion linkage between the sulfur atom of Met243 and the β-carbon of the 2-vinyl group is present only in MPO.

1.4.3.2 Impact of covalent links on enzyme properties and functional implications

The unusual mode of heme binding in the mammalian peroxidases is partly responsible for their peculiar spectroscopic properties (73). As mentioned previously, the heme in both MPO and LPO is covalently attached to the protein through two ester links, but in the case of MPO there is an additional sulfonium ion link (Figure 1.8). As a consequence, the heme ring in MPO assumes a bow-shaped structure and a pronounced out-of-plane location of the iron ion in its high spin Fe^{III} state, while the two ester bonds in LPO cause a less distorted heme (Figure 1.7b,d, respectively). These differences have been proposed to be the cause of the variations in optical properties between MPO and LPO.

The electronic absorption spectra of MPO and LPO are shown in Figure 1.9a and 1.9b, respectively.
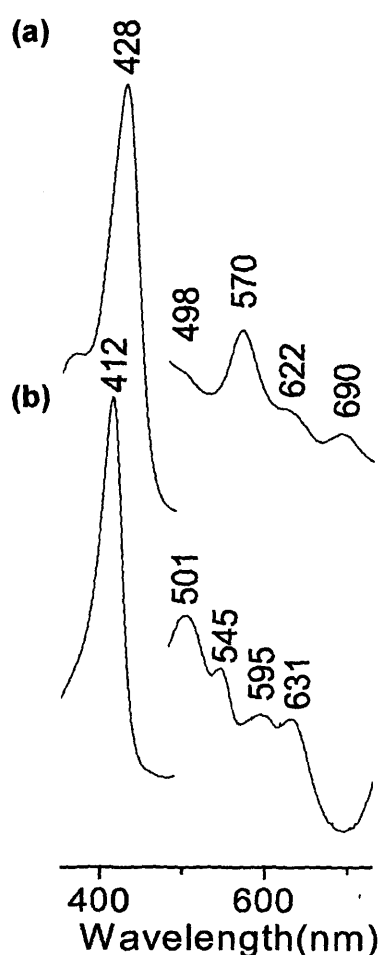
Figure 1.9: Electronic absorption spectra of the Fe^{III} forms of MPO (a) and LPO (b) in phosphate buffer, pH 7.0. The intensity in the visible region is four-fold expanded The figure is reproduced from reference (73).

The Soret band of LPO is fairly sharp with a maximum at 412 nm, and the visible spectrum exhibits maxima at 501, 545, 595, and 631 nm (74). Both EPO and TPO exhibit similar spectral features to LPO (1, 75). The electronic absorption maxima of the ferric form of MPO are red-shifted compared to LPO. The Soret band is at 428 nm and the spectrum shows additional bands at 498, 570, 622, and 690 nm (76, 77). However, upon mutation of Met243 the UV-visible spectrum becomes similar to LPO, confirming that the sulfonium ion linkage, is responsible for the MPO-typical spectral properties (63, 78, 79). In addition to the sulfonium ion linkage, its neighbouring residue Glu242 contributes to the distortion from the planar conformation and the lowered symmetry (63). Raman studies have also showed that the three covalent linkages significantly lower the heme group symmetry and thus the RR spectra of MPO are extremely rich (79-81).

The unique sulfonium link in MPO is also thought to be directly linked to the higher oxidizing potential of this enzyme as compared to the other three. LPO has a Fe^{3+}/Fe^{2+} reduction potential of -190 mV, which is in the same range as seen for plant type heme peroxidases (range from -180 to -300 mV). For EPO and TPO no reduction potentials have been reported, but because the active site structures are very similar (82), it is reasonable to assume that they are close to that of LPO. However, MPO has a Fe^{3+}/Fe^{2+} reduction potential in the range of +5 to +21 mV (83-85), which is similar to the globins (myoglobin and hemoglobin) that have to be stable in the ferrous form to function as reversible oxygen carriers. The main contribution to the high Fe^{3+}/Fe^{2+} reduction potential in MPO has been proposed to stem from the positive charge of the sulfur atom in the sulfonium ion linkage (65). The presence of such an electron withdrawing group strongly influences the basicity of the four pyrrole nitrogens and thus decreases the electron density at the heme iron. Furthermore, the more pronounced heme distortion in MPO and, as a consequence, the out-of-plane iron position is likely to also contribute to the globin like reduction potential of MPO, that makes it unique in its ability to oxidize chloride ion (Cl^-) at pH 7 (58, 73).

The covalent heme to protein links in the mammalian peroxidases have also been proposed to reinforce the rigidity of the active site and thus protect the heme from modification during the oxidation of their physiological substrates, i.e. halides and thiocyanate (86-88). It has therefore been suggested that anchoring the heme to the protein will dampen the natural dynamic breathing motions and could facilitate

protection of the vinyl groups (*88*). Studies on horseradish peroxidase (HRP), that has a non-covalently bound heme, showed that autocatalytic modification of the heme in HRP occurs during halide (*86*) and thiocyanate (*87*) oxidation. Even more, a single engineered heme-protein link in HRP seemed to protect the heme from such modification (*89*) and thus further supported the above argument.

Recent studies also revealed that mutations of Arg499 and Gly501 in MPO compromised the oxidizing potential of the enzyme and resulted in myeloperoxidase deficiency (*90*). The Soret band for each mutant was shifted from the normal 430 to ~412 nm, confirming that heme was incorporated but suggesting that the number of covalent bonds or other structural aspects of the heme pocket were disrupted by the mutations and further emphasized the vitality of these heme-protein covalent links for correct function of mammalian peroxidases (*90*).

1.4.4 CYP4A family of P450s

Similar type of covalent heme attachment, as seen for mammalian peroxidases, was initially identified in the CYP4A (*91*) family of cytochrome P450 enzymes and later on in more subfamilies of the same enzymes, such as CYP4B and CYP4F (*92, 93*). The covalent link in these cases has been assigned as a single ester bond to the 5-methyl group of the heme (*94, 95*).

The CYP4 family of P450 enzymes catalyze the ω- and $(\omega - 1)$-hydroxylation of fatty acids. In mammals, the CYP4 enzymes exhibit a preference for ω-hydroxylation. It has been proposed that covalent binding of the heme to the protein, by anchoring the heme to the protein, may allow a finer discrimination against exposure of the $(\omega - 1)$-methylene group to the ferryl species and thus enhance the ω-regiospecificity of the enzyme (*58, 91, 92*).

1.4.5 *Synechocystis* hemoglobin

The recombinant products of the cyanobacterial hemoglobins from *Synechocystis* sp. PCC 6803 and *Synechocystis* sp. PCC 7002 have been found capable of spontaneously forming a covalent bond, linking one of the heme vinyl groups to His117 located in the C-terminal helix (Figure 1.10). S6803 rHb is expressed as a noncovalent complex, named rHb-R but during NMR experiments it was observed to convert spontaneously to an alternative form, rHb-A (*96*). Optical and mass spectroscopy, as well as NMR techniques, were used to identify the position of

covalent linkage (*97, 98*). It was also found that covalent linking of His117 to the heme is facilitated under aerobic conditions by the presence of dithionite (*97*), although the exact mechanism of formation of this link has not yet been defined.

The presence of the heme adduct in preparations of the soluble holoprotein from *E. coli* extracts suggests that the reaction takes place *in vivo* and results in a physiologically relevant species (*99*). S6803 Hb and *Synechocystis* sp. PCC 7002 Hb are unique in having a histidine at or near position 117. Thus, it was suggested that the cross-link may play a functional role particular to these cyanobacteria, for example to increase the stability of the holoprotein, as proposed for cytochrome *c* (*20, 39*), or to prevent heme loss (*98*). It was indeed found that the cross-link stabilized the protein with respect to thermal and acid denaturation (*100*).
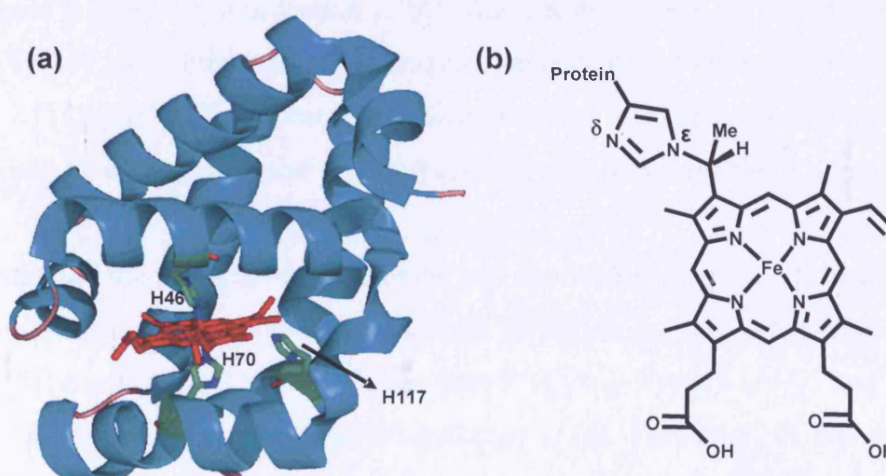
Figure 1.10: (a) Solution structure of S6803 rHb-R (PDB accession code 1RTX) (*101*). The heme, His46, His 70 and His 117 are indicated. (b) Structure of the covalent cross-link observed in rHb-A. The reactive histidine is His 117.

1.5   Non-physiological heme modification

There are also examples of modification of heme groups by radicals or other reactive species generated during the catalytic turnover of heme proteins (*58*). These kind of non-physiological heme modifications have mainly been reported for heme proteins such as the peroxidases and cytochrome P450 enzymes that catalyse the relatively nonspecific oxidation of xenobiotics (*102-104*).

There are various cases in which autocatalytic reactions cause non-physiological modifications of heme, as has been observed in cytochromes P450 (*58*) and P450$_{cam}$ (*105*). Similar ester links as those seen in LPO have recently been engineered into

HRP by introducing aspartate and glutamic acid residues at positions suitably orientated towards the heme methyl groups (*106*). Another example of a covalent tetrapyrrole adduct is the heme-myoglobin complex that is formed during the reductive debromination of $BrCCl_3$, in which a histidine residue becomes covalently attached to a heme vinyl group (*107*).

1.6 Modifications around the heme active site

In addition to heme-protein covalent links, as discussed above, there is also a growing list of metalloenzymes that have aromatic amino acids covalently modified in their active sites. Perhaps the most well-known example is the existence of a Met-Tyr-Trp cross-link in the active site of catalase-peroxidase (KatG) (*108, 109*), which is discussed in more detail in section 1.10.1. Another example is the Cu_B-coordinated His240-Tyr244 cross-link at the O_2-activating heme center of cytochrome *c* oxidase (Figure 1.11a) (*110-112*); the cross-link was proposed to have prevented damaging ˙OH release at electron transfer to dioxygen and thus have enabled O_2 respiration (*112*).

Other examples of such cross-links include: *Mycobacterium tuberculosis* hemoglobin O (Tyr_{23}-Tyr_{36}) (Figure 1.11b) (*113*), catalase HPII (His_{392}–Tyr_{415}) (*114*), galactose oxidase (Tyr_{272}–Cys_{228}) (*115, 116*), catalase-1 (Cys_{356}–Tyr_{379}) (*117*), and amine oxidase (2,4,5-trihydroxyphenylalanine quinone) (*118*). Formation of the covalent bonds in these systems is believed to occur through metal-mediated autocatalytic processes, with the resulting modified amino acids possessing altered redox and pK_a properties that affect enzyme chemistry.
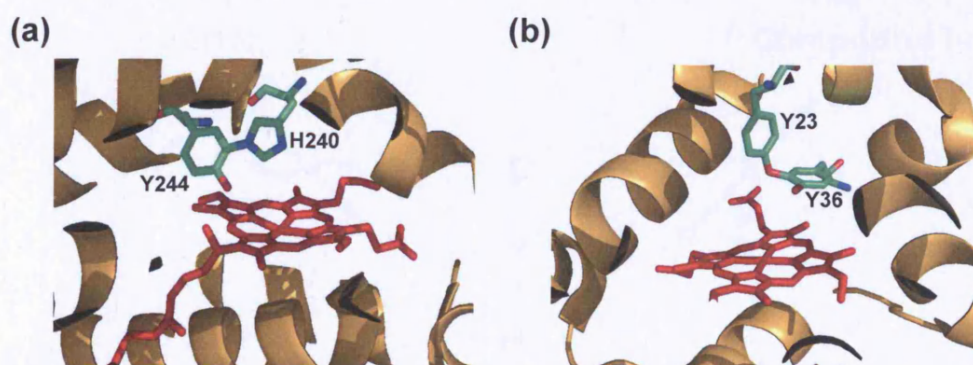
Figure 1.11: (a) Active site structure of cytochrome *c* oxidase (PDB accession code 1V55), showing the presence of a Cu_B-coordinated His240-Tyr244 cross-link (*112, 119*). (b) Active site structure of *Mycobacterium tuberculosis* hemoglobin O (PDB accession code 1NGK), showing the presence of Tyr23-Tyr36 covalent link (*113*).

1.7   Heme peroxidases

Peroxidases are used for a variety of purposes in biology. For example, lignin degradation (lignin and manganese peroxidases) (*120, 121*), hydrogen peroxide removal in eye disease (*122*) or in plants (ascorbate peroxidase) (*123, 124*), bacterial killing (myeloperoxidase (*125*) and lactoperoxidase (*126*)) and hormone synthesis (thyroid peroxidase) (*127*).

Heme-containing peroxidases catalyse the H_2O_2-dependent oxidation of a wide range of organic and inorganic substrates (*1, 57, 128, 129*). The overall equation for the reaction catalysed by a peroxidase is given by Equation 1.1:

$$H_2O_2 + 2S_{red} \quad \rightarrow \quad 2S_{ox} + 2H_2O \qquad \qquad ...(1.1)$$
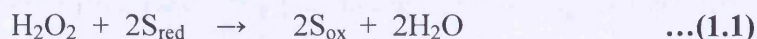
where S_{red} is the reducing substrate and S_{ox} the oxidised product. Consequently, the function of a peroxidase is wholly dependent upon its substrate recognition properties.

The catalytic cycle is common to all types of heme peroxidase and proceeds through two detectable oxyferryl ($Fe^{IV}=O$) intermediates, known as Compound I and Compound II (Figure 1.12).
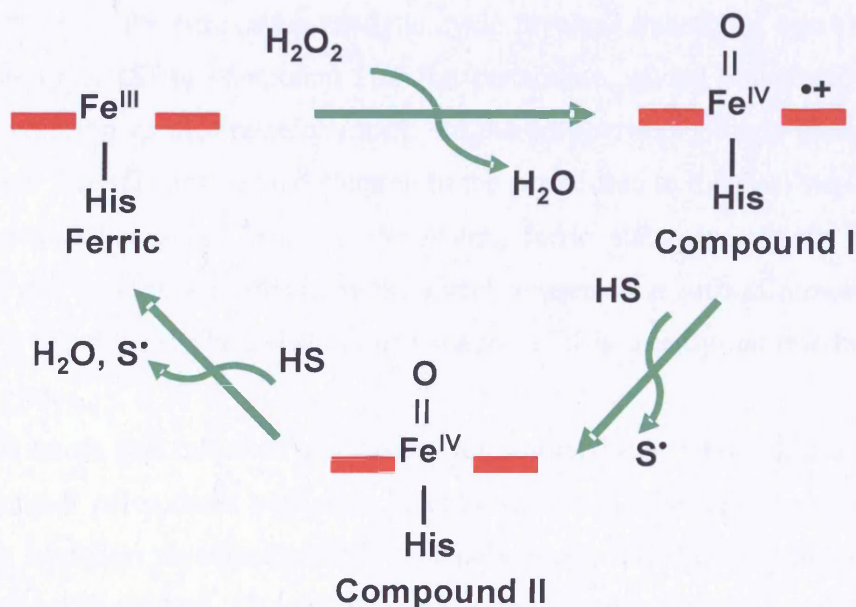
Figure 1.12: The catalytic cycle of peroxidases. HS represents reduced substrate and $S^{\bullet}$ represents oxidised substrate.

The first step of peroxidase catalysis consists of reaction of the ferric enzyme with H_2O_2 to form a doubly oxidised oxyferryl species, named Compound I. The iron is in the ferryl state, and the second oxidising equivalent is stored as either a porphyrin π-cation radical or as a protein based radical.

When the X-ray crystal structure of cytochrome c peroxidase was solved (130), Poulos and Kraut proposed a detailed mechanism for the formation of compound I (131) (Figure 1.13). This involves the binding of neutral hydrogen peroxide to the ferric heme iron, with the concomitant donation of a proton to the distal histidine (His52 in Figure1.13) from the α-oxygen atom. The positively charged guanidinum side chain of the distal arginine (Arg48 in Figure 1.13) is proposed to interact directly with the anionic peroxide ligand, thus promoting the build-up of negative charge on the β-oxygen atom. Reorientation of the arginine, coupled with proton transfer from the distal histidine to the terminal oxygen of the peroxide (β-oxygen), results in the general acid-catalysed heterolytic cleavage of the oxygen-oxygen bond, and the formation of a ferryl $Fe^{IV}=O$ species (compound I) and a molecule of water. Compound I is formed by heterolytic cleavage of the peroxide bond and requires two electrons from the protein, one of which comes from the iron atom, the second oxidising equivalent is stored in the form of either a porphyrin π-cation radical or a protein-based radical (132).

The second step in the peroxidase catalytic cycle involves transfer of one electron from the substrate (S) to compound I of the peroxidase, giving compound II, in which the oxyferryl species remains intact, but the porphyrin or protein radical has been reduced. Transfer of a second electron to the peroxidase in the final step of the cycle reduces compound II back to the resting ferric state, and results in the protonation and subsequent release of the ferryl oxygen as a second molecule of water (130), Figure1.13. The reduction of Compound II is usually the rate-limiting step in the cycle.

Based on structure and function, peroxidases are grouped into three superfamilies: catalases, animal peroxidases and plant peroxidases (133). The animal peroxidase superfamily includes myeloperoxidase, lactoperoxidase, thyroid peroxidase and eonisophil peroxidase (134). They contain similar helices to the plant peroxidases in the region binding the heme (135), but the crystal structures of myeloperoxidase

(*136*) and prostaglandin H synthase (*135*), as well as sequence correlations (*137*), indicate that animal and plant peroxidases are separate superfamilies.
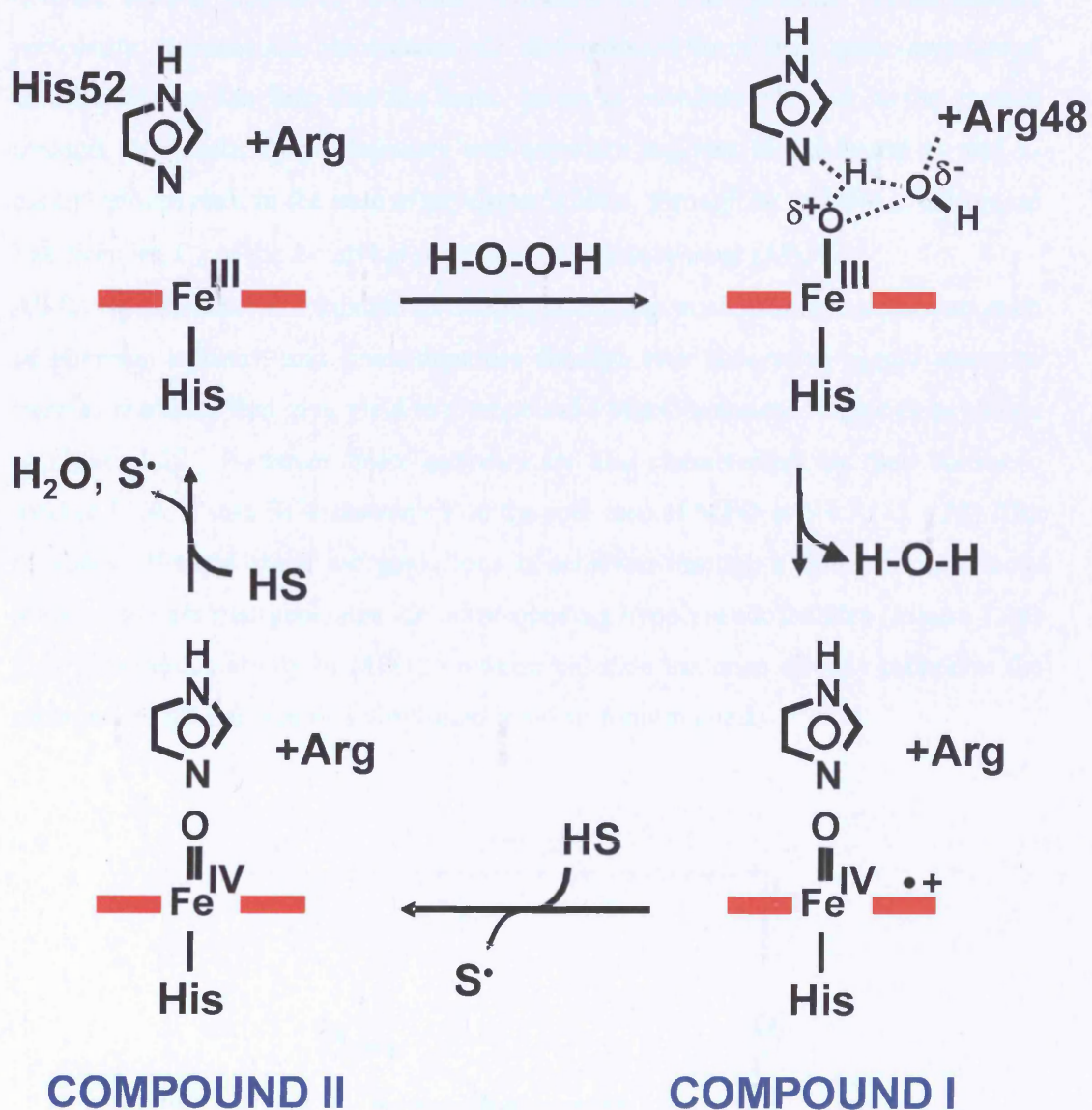
Figure 1.13: Schematic representation of the catalytic mechanism cytochrome *c* peroxidase. HS represents reduced substrate and S• represents oxidised substrate.

1.8   Mammalian peroxidases

The mammalian peroxidases myeloperoxidase (MPO), lactoperoxidase (LPO), eosinophil peroxidases (EPO), and thyroid peroxidase (TPO) participate in host defense against infection, hormone synthesis and pathogenesis. As mentioned previously, mammalian peroxidases are distinguished from their plant and fungal counterparts by the fact that the heme group is covalently bound to the protein through ester links from glutamate and aspartate residues to the heme 1- and 5-methyl groups and, in the case of myeloperoxidase, through an additional sulfonium link from the C_β of the 2-vinyl group to a methionine residue (*58*).

All four peroxidases are capable of directly oxidizing small aromatic substrates such as phenols, anilines, and phenothiazines through two successive single electron-transfer reactions that give yield to Compound I and Compound II species as shown in Figure 1.12. However, these enzymes are also characterized by their ability to oxidize I^-, SCN^- and Br^- and even Cl^- in the sole case of MPO at pH 7 (*75, 138*). The oxidation of these small inorganic ions is achieved through a direct two-electron-transfer process that generates the corresponding hypo(pseudo)halides (Figure 1.14) (*58*). The unique ability of MPO to oxidize chloride has been directly related to the presence in that enzyme of a vinyl-methionyl sulfonium bond.
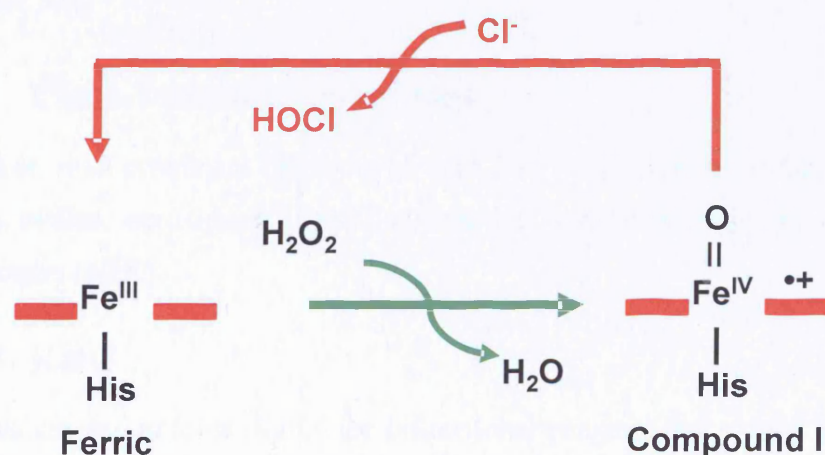
Figure 1.14: The catalytic cycle of chloride oxidation by MPO.

1.9 Plant peroxidases

The majority of known peroxidases belong to the so-called "plant peroxidase superfamily", which is characterized by a protein fold consisting of a central heme group sandwiched between a distal and proximal domain. Based on protein sequence homologies, Welinder proposed a classification of the plant peroxidase superfamily that subdivided the enzymes into three peroxidase families (*133*).

(i) Class I constitutes intracellular peroxidases of prokaryotic origin. These include yeast cytochrome *c* peroxidase (C*c*P), chloroplast and cytosolic ascorbate peroxidases (APX) (*139*). Class I peroxidases have no carbohydrate, no cysteine bridges, no calcium ions, and no signal peptide secretion.

(ii) Class II consists of secretory fungal peroxidases. Examples are the lignin (LnP) and manganese (MnP) peroxidases. The proximal tryptophan residue, conserved in the Class I peroxidases, is replaced by phenylalanine or leucine in Class II.

(iii) Class III is comprised of the classical secretory plant peroxidases. The most extensively studied example is horseradish peroxidase (HRP).

Both class II and class III peroxidases contain two conserved calcium ions, one in each of the proximal and distal domains and both classes also contain four disulphide bridges (*140*).

1.10 Class I plant peroxidases

The three most prominent members of the Class I superfamily of plant peroxidases are the catalase-peroxidases (KatG), cytochrome *c* peroxidases (C*c*P) and ascorbate peroxidases (APX).

1.10.1 KatG

The catalase-peroxidases (KatG) are bifunctional enzymes that exhibit both catalatic and peroxidatic activity (*140*). There has been considerable interest in the KatG due to its role in activating the pro-drug isoniazid (INH) (*141*), the frontline antibiotic used to treat tuberculosis.

1.10.1.1 Catalysis

KatG are anomalies: they have a high sequence homology with prokaryotic peroxidases, including fungal cytochrome *c* peroxidase and plant ascorbate peroxidase (*142*), and as such possess substantial peroxidase activity, yet also exhibit catalatic activity (Figure 1.15) equivalent to that of the monofunctional catalases despite having low sequence homology with the latter (*143*).
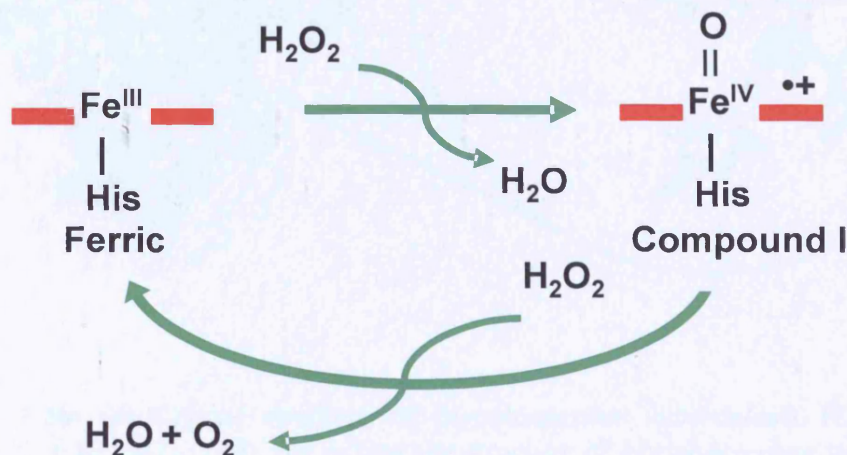
Figure 1.15: The catalytic cycle of catalases.

1.10.1.2 The X-Ray crystal structure of KatG: Role of the Met-Tyr-Trp cross-link

Interest in the catalase-peroxidases has also been spurred by the publication of three crystal structures of KatG from different sources: *Haloarcula marismortui (144)*, *Burkholderia pseudomonas (145)*, and *Mycobacterium tuberculosis* (Figure 1.16a) (*146*). A common feature in each crystal structure is the presence of two covalent bonds between three amino acid side chains, Trp107, Tyr229, and Met255 (*Mycobacterium tuberculosis* numbering) located on the distal side of the heme active site (Figure 1.16b). The consistent observation of a Met-Tyr-Trp "cross-link" suggests that it is a characteristic common to all KatG, and, as it is not found in the monofunctional peroxidases, implies that this structural element may impart catalatic activity to the KatG (*146*). Indeed, several mutagenesis studies have confirmed that the cross-link is required for catalatic, but not for peroxidatic, activity (*108, 147-149*).
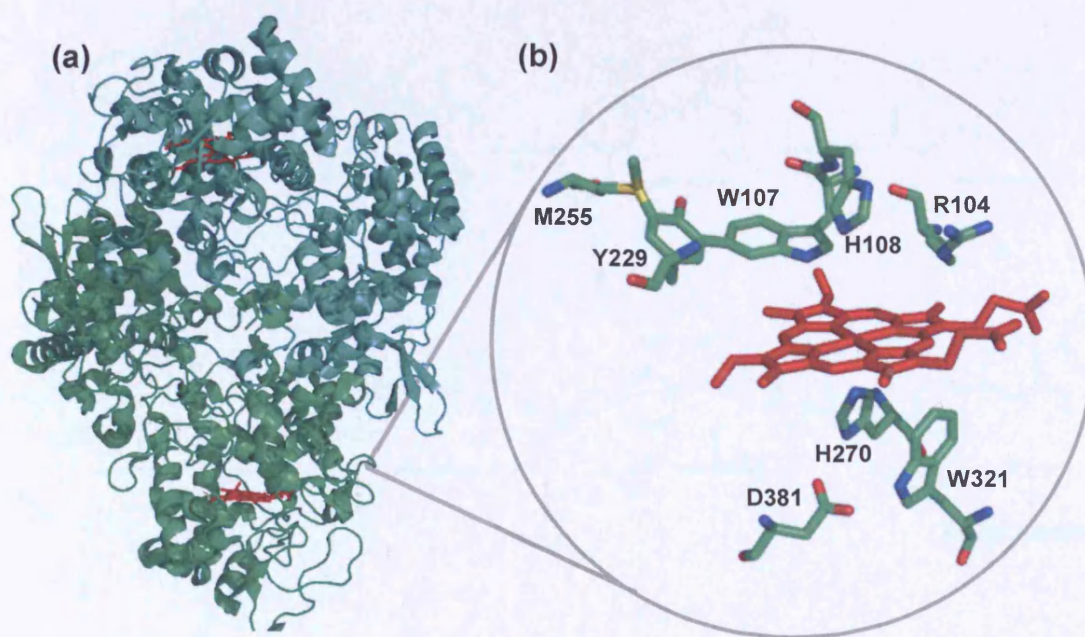
Figure 1.16: (a) Crystal structure of *Mycobacterium tuberculosis* KatG (PDB accession code 1SJ2) (*146*). (b) Active site structure of *Mycobacterium tuberculosis* KatG, showing the covalent cross-link between Met255, Tyr229 and Trp107.

Formation of a Met-Tyr-Trp cross link in KatG has been proposed to form through an autocatalytic process (*109*) on reaction with H_2O_2 and proceed through a Compound I intermediate as seen for heme-protein covalent links (see section 1.11). More specifically, the mechanism was proposed to proceed as follows: Formation of compound I (Scheme1.1, step a) leads to oxidation of both Tyr229 and Trp107. Both of these redox active residues are within the threshold for long-range electron transfer (*5, 150*) and are capable of being oxidized by compound I with concomitant formation of Trp107˙ and Tyr229˙. Both protein radicals are formed simultaneously from a single turnover event, and coupling of the two radicals (step c) results in formation of the Tyr-Trp bond (step d). Formation of a second compound I intermediate (step e) results in further oxidation of the Tyr-Trp cross-link (step f), nucleophilic attack of the sulfur atom of Met255 on Tyr-Trp (step h) occurs (step i), yielding the Met-Tyr-Trp cross-link (*109, 151*).
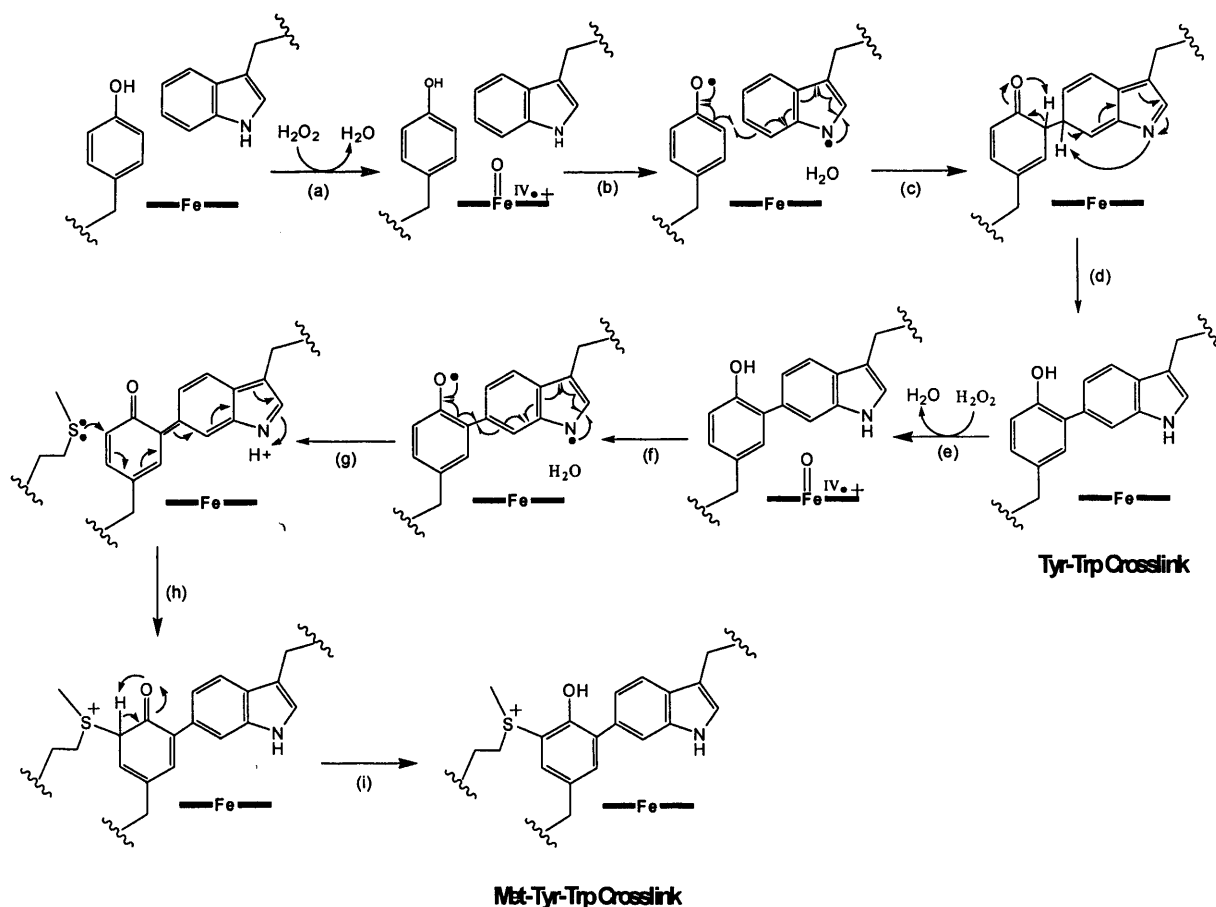
Scheme 1.1: Proposed mechanism for the formation of the Met-Tyr-Trp cross-link in *Mycobacterium tuberculosis* KatG (*109*).

1.10.2 Cytochrome *c* Peroxidase

Cytochrome *c* peroxidases (CcP) is found in the mitochondria of baker's yeast, *Saccharomyces cervisiae*, protecting the organism from the deleterious effects of hydrogen peroxide (*152*).

1.10.2.1 Catalysis

CcP catalyses the reduction of hydrogen peroxide to water using the reducing equivalents from two molecules of ferrocytochrome *c*, as shown in Equation 1.2, where c^{2+} and c^{3+} represent ferro- and ferricytochrome *c*, respectively (*153*).

$$CcP + H_2O_2 + 2\ c^{2+} + 2H^+ \rightarrow CcP + 2H_2O + 2c^{3+} \qquad \text{...(1.2)}$$
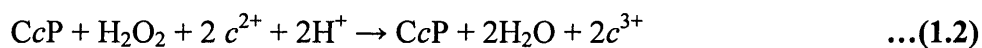
1.10.2.2 The X-Ray crystal structures of CcP

CcP was discovered in 1940 (*154*) and in 1978 it became the first heme peroxidase to have its crystallographic structure solved (Figure 1.17) (*130, 131, 155*). Based upon the initial crystal structure of CcP, Poulos and Kraut (*156*) proposed a mechanism for the formation of Compound I, as shown previously in Figure 1.13.
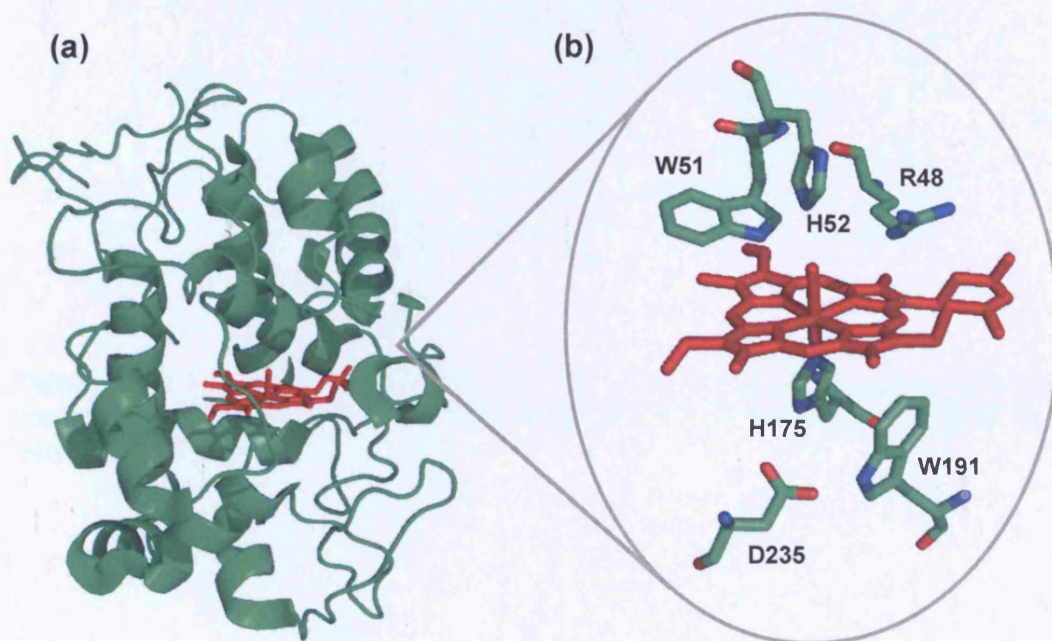
Figure 1.17: (a) Crystal structure of CcP (PDB accession code 2PCB) (*130*). (b) Active site structure of CcP.

1.10.2.3 CcP Compound I

In CcP, the EPR spectrum for Compound I (Figure 1.18b) indicated that the radical was not on the porphyrin (*157*). Site-directed mutagenesis (*158*) and ENDOR studies (*159, 160*) eventually led to the identification of proximal Trp191 (Figure 1.17b) as the site of the radical. In most heme peroxidases, Compound I consists of an oxyferryl iron species bearing a porphyrin π-cation radical but CcP is unique in using a stable protein-based radical to store the second oxidising equivalent of Compound I. The X-ray structure of the noncovalent complex between CcP and its physiological substrate (Figure 1.19), cytochrome *c*, revealed that the latter is bound at the surface of CcP to maximize electron transfer to the Trp191 radical following reduction of H_2O_2 (*161*). The Compound I spectrum of CcP looks like the Compound II spectrum of other peroxidases with a shift in the Soret peak to 420 nm and no decrease in intensity of the Soret peak (Figure 1.18a).
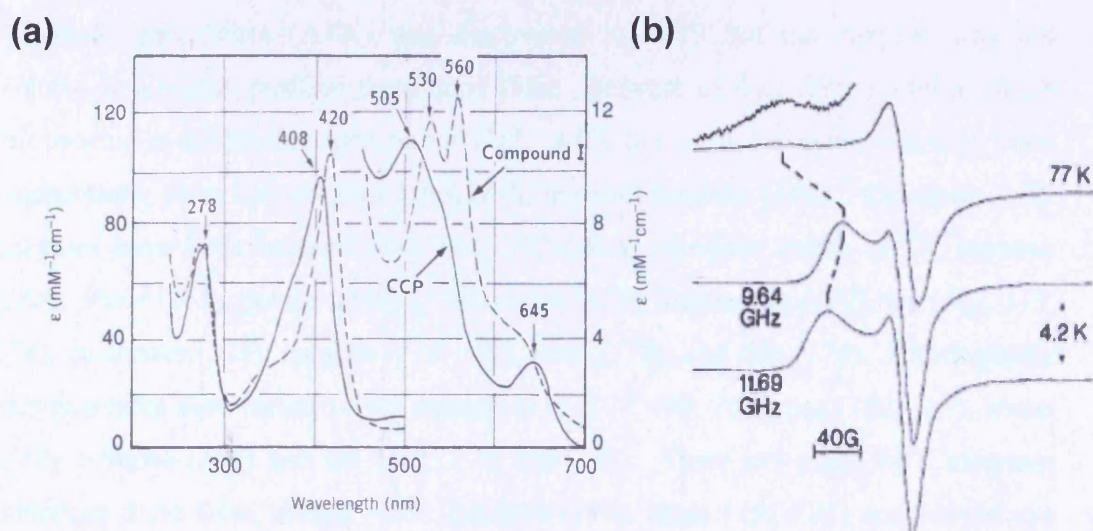
Figure 1.18: (a) UV-visible spectra of C*c*P: native (solid line) and Compound I (dashed line). (b) EPR spectra of C*c*P Compound I. The figure is reproduced from reference (*157*).

Figure 1.19: Crystal structure of the noncovalent complex between C*c*P (shown in green) and cytochrome *c* (shown in cyan) (PDB accession code 2PCB) (*161*). The distal His52, proximal His175 and proximal Trp191 are shown in yellow.

1.10.3 Ascorbate Peroxidase

Ascorbate peroxidase (APX) was discovered in 1979 but the enzyme was not isolated in a highly purified form until 1989. Because of this, there is not as much information available for APX as for CcP. APX is a class I enzyme found in plant chloroplasts, plant cytosol and nitrogen-fixing root nodules (*162*). Cytosolic APX enzymes have been isolated from pea (*163-166*), Japanese radish (*167*), soybean (*168*), wheat (*169*), potato tubers (*170*), maize (*171*), komatsuna (*172*), tea (*162, 173, 174*), cucumber (*175*), spinach (*176, 177*), bean (*178*), and rice (*179*). Chloroplastic enzymes have been isolated from spinach (*176, 177, 180, 181*), pea (*182, 183*), wheat (*184*), tobacco (*185*) and tea (*162, 173, 186-188*). There are other APX enzymes including those from insects (*189*), bacteria (*190*), algae (*191-193*) and bovine eye (*194*).

APXs from tea leaves (*162, 186*), soybean root nodules (*168*), *E. gracilis* (*191*) and peas (*163, 195, 196*) have been purified and characterized. A few APX enzymes have been expressed in recombinant form, including pea APX (rpAPX) (*195, 196*) and soybean APX (rsAPX) (*197*), enabling preparation of wild-type and variant proteins in high enough yields for analytical characterization (*57*).

1.10.3.1 Catalysis

Within all living organisms, hydrogen peroxide is generated as a potentially toxic by-product of molecular oxygen metabolism (*198*). Ascorbate peroxidases belong to the Class I plant peroxidases (*133*) and are heme-containing enzymes that catalyse the reduction of hydrogen peroxide to water in plants and algae, using ascorbate (*i.e.* vitamin C) as a substrate (*199*) (Equation 1.3). Although ascorbate is the preferred physiological substrate, APXs can also catalyse the oxidation of non-physiological substrates, such as sulfides and phenolic compounds (*199, 200*).

$$2 \text{ ascorbate} + H_2O_2 + 2H^+ \rightarrow 2 \text{ monodehydroascorbate} + 2 H_2O \quad ...(1.3)$$
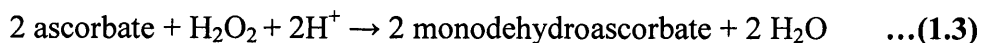
According to Equation 1.3, the immediate product of the oxidative reaction is monodehydroascorbate. However, this product is a fairly reactive and unstable radical and two monodehydroascorbate free radicals disproportionate back to ascorbate and dehydroascorbate (*201*) (Figure 1.20).

ascorbate

mono-dehydroascorbate
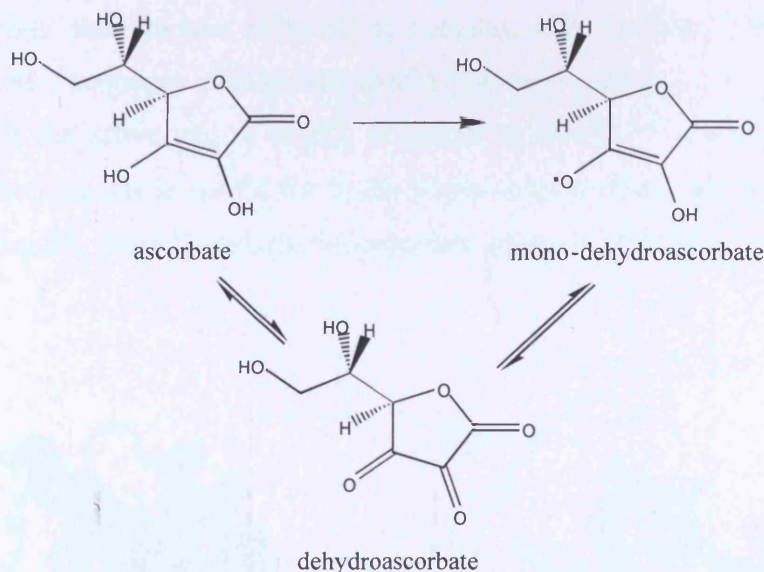
dehydroascorbate

Figure 1.20: Conversion of ascorbate into monodehydroascorbate and dehydroascorbate.

1.10.3.2 The X-Ray crystal structures of rpAPX and rsAPX

The X-ray crystal structure of rpAPX was solved in 1995 by Patterson and Poulos (*139*) (Figure 1.21a) and revealed a non-covalently bound dimer. A cation near Trp179 was identified in rpAPX and was assigned as a potassium ion (Figure 1.21b) (*139*). The interpretation of the original X-ray crystal structure data was based on the CcP structure as APX has high (37%) sequence identity with CcP.
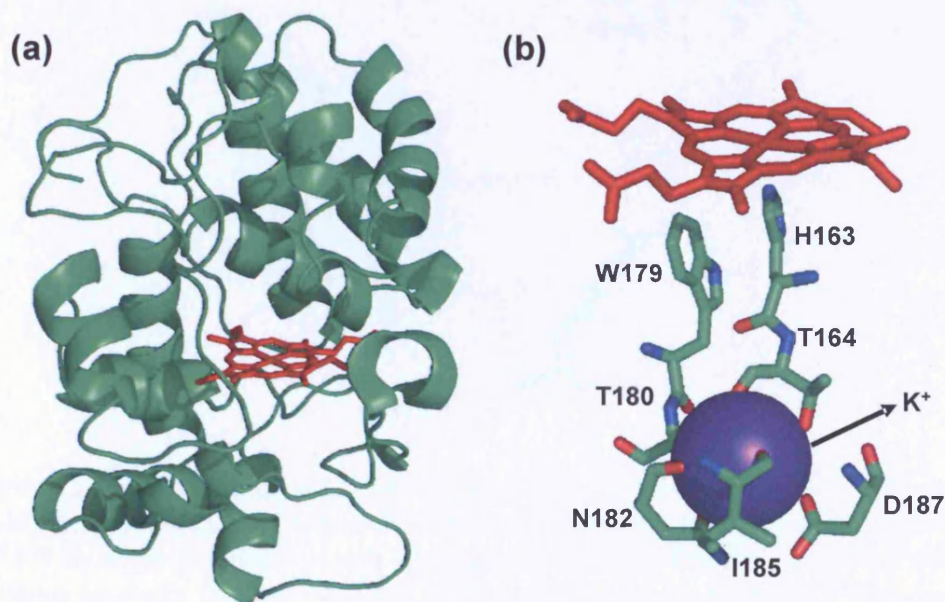
Figure 1.21: (a) The overall structure of rpAPX monomer (PDB accession code 1APX) (*139*). (b) Active site structure of rpAPX showing the potassium (K$^+$) binding site in purple.

More recently, the structure of rsAPX in complex with ascorbate (Figure 1.22a,b), which has 91% sequence identity with rpAPX, has been reported to 1.75Å (*202*). The structure of the active site of rsAPX is similar to rpAPX. It was shown that the ascorbate binding site in rsAPX lies in the γ-heme edge and that ascorbate hydrogen-bonds to Lys30, Arp172 and the 6-propionate group of the heme (Figure 1.22c) (*202*).
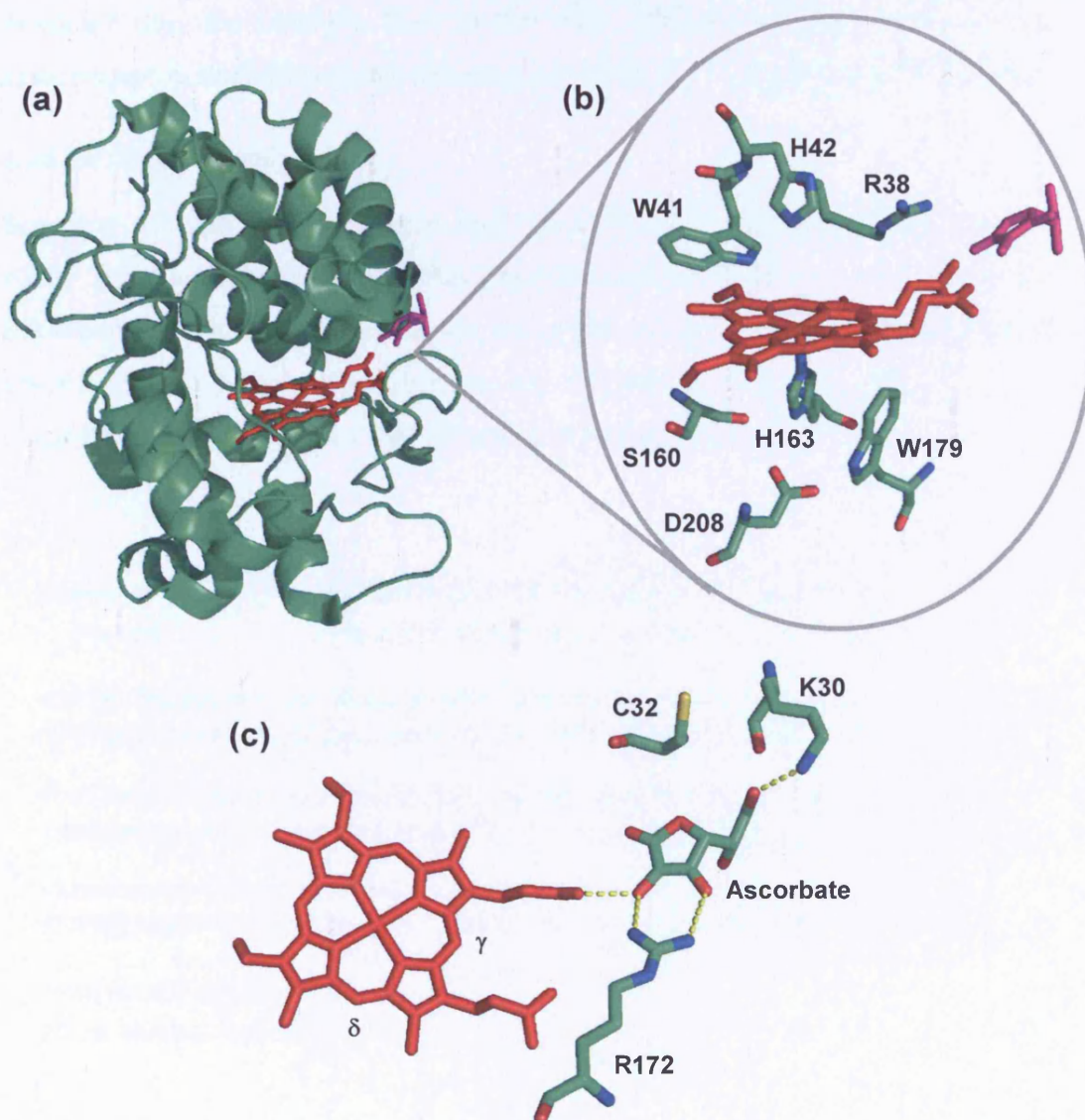
Figure 1.22: (a) Crystal structure of the rsAPX-ascorbate complex (PDB accession code 1OAF) (*202*). Ascorbate is shown in magenta. (b) The active structure of rsAPX showing the heme in red, ascorbate in magenta and the rest of the active site residues in green. (c) The structure of the rsAPX-ascorbate complex showing the γ-*meso* and δ-*meso* positions of the heme and binding of ascorbate. Hydrogen bonds are indicated as yellow, dotted lines.

1.10.3.3 Active Site Residues

The active sites of rpAPX (*139*) and rsAPX (*202*) are essentially identical and are both very similar to CcP. The active site structure of rsAPX is shown in Figure 1.22b. The heme is bound to the protein through a coordinate bond from the iron to His163. The key active site residues (Arg38, Trp41, His42) observed in the distal pocket of CcP (Arg48, Trp51, His52) (Figure 1.17b) are also seen in APX. On the proximal side, the catalytic His-Asp-Trp triad (His163-Asp208-Trp179) is also apparent and is analogous to that observed in CcP (His175, Asp235, Trp191) (*199*).

1.10.3.4 APX Sequences

Sequence analysis of sequences coding for APX (*203*), results in seven types of APX. There are five cytosolic APXs (three of these are membrane bound) and two chloroplastic APXs. Key residues are conserved throughout the seven, and they all contain residues for a potassium binding site. Alignment of the amino acid sequences of rpAPX and rsAPX, shows a 90 % backbone homology (Figure 1.23).

```
                 1                   20
Soybean APX      MGKSYPTVSADYQKAVEKAKKKLRGFIAEKRCAPLMLRLAWHSA
   Pea APX       -GKSYPTVSPDYQKAIEKAKRKLRGFIAEKKCAPLILRLAWHSA

                                 81
                 GTFDKGTKTGGPFATIKHPAELAHSANNGLDIAVRLLEPLKAEFPILSYADFYQLAGVVAVE
                 GTFDSKTKTGGPFATIKHQAELAHGANNGLDIAVRLLEPIKEQFPIVSYADFYQLAGVVAVE

                                141
                 VTGGPEVPFHPGREDKPEPPPEGRLPDATKGSDHLRDVFGKAMGLTDQDIVALSGGHTIGAA
                 ITGGPEVPFHPGREDKPEPPPEGRLPDATKGSDHLRDVFGKAMGLSDQDIVALSGGHTIGAA

                                206
                 HKERSGFEGPWTSNPLIFDNSYFTELLSGEKEGLLQLPSDKALLSDPVFRPLVDKYAADEDA
                 HKERSGFEGPWTSNPLIFDNSYFTELLTGEKDGLLQLPSDKALLTDSVFRPLVEKYAADEDV

                 FFADYAEAHQKLSELGFADA
                 FFADYAEAHLKLSELGFAEA
```

Figure 1.23: Sequence alignment of rpAPX and rsAPX with the differences underlined. The two sequences are 90% identical. The active site residues are highlighted in red. Residues involved in ascorbate binding are highlighted in green and residues involved in potassium binding are highlighted in blue.

1.10.3.5 Compounds I and II

The crystal structure shows APX has a tryptophan residue on the proximal side of the heme (Trp179, Figure 1.22b). The corresponding residue in CcP (Trp191, Figure 1.17b) is the site of the Compound I radical. Amazingly, as determined by EPR and optical spectroscopy, Compound I of APX contains a conventional porphyrin π-cation radical (204, 205). More specifically, the UV-visible spectrum of Compound I of APX shows a decrease in the absorbance of the Soret peak, which is characteristic of a porphyrin π-cation radical (Figure 1.24a) (205); EPR spectroscopy also yielded a species with g-values (g = 3.52, g = 1.998) consistent with the existence of a porphyrin π-cation radical (Figure 1.24b) (204).

It was suggested that this is because APX has a metal ion binding site near the proximal tryptophan (Figure 1.21b) (204). Thus, the presence of a nearby positive ion would make it more difficult for electron transfer to occur from the tryptophan to the porphyrin, and from that standpoint the higher the charge on the metal ion, the better (1). In support of this proposal, it has also been shown that engineering the corresponding potassium-site into CcP, which originally lacks an equivalent metal ion site, resulted in destabilization of protein radical formation at Trp191 (206-209).

However, these differences between and APX and CcP can not be solely explained on electrostatic grounds. Thus, comparison of the substrate-bound crystal structures of CcP and APX (Figures 1.19 and 1.22, respectively), provides more convincing rationalization of the different properties of the two enzymes. Hence, as mentioned previously, the ascorbate-bound crystal structure of rsAPX (210) revealed that there is direct coupling of the substrate to the heme group, through the heme 6-propionate (Figure 1.22c), and reduction of Compound I therefore occurs through a porphyrin π-cation intermediate, completely by-passing the need for involvement of Trp179. This is in contrast to the substrate binding orientation in the CcP-cytochrome c complex (161) (Figure 1.19), in which cytochrome c binds to CcP in an orientation that involves Trp191 as part of an electron transfer pathway to the heme. For CcP therefore, Trp191 would be expected to be essential for enzyme activity, which is indeed observed (211).
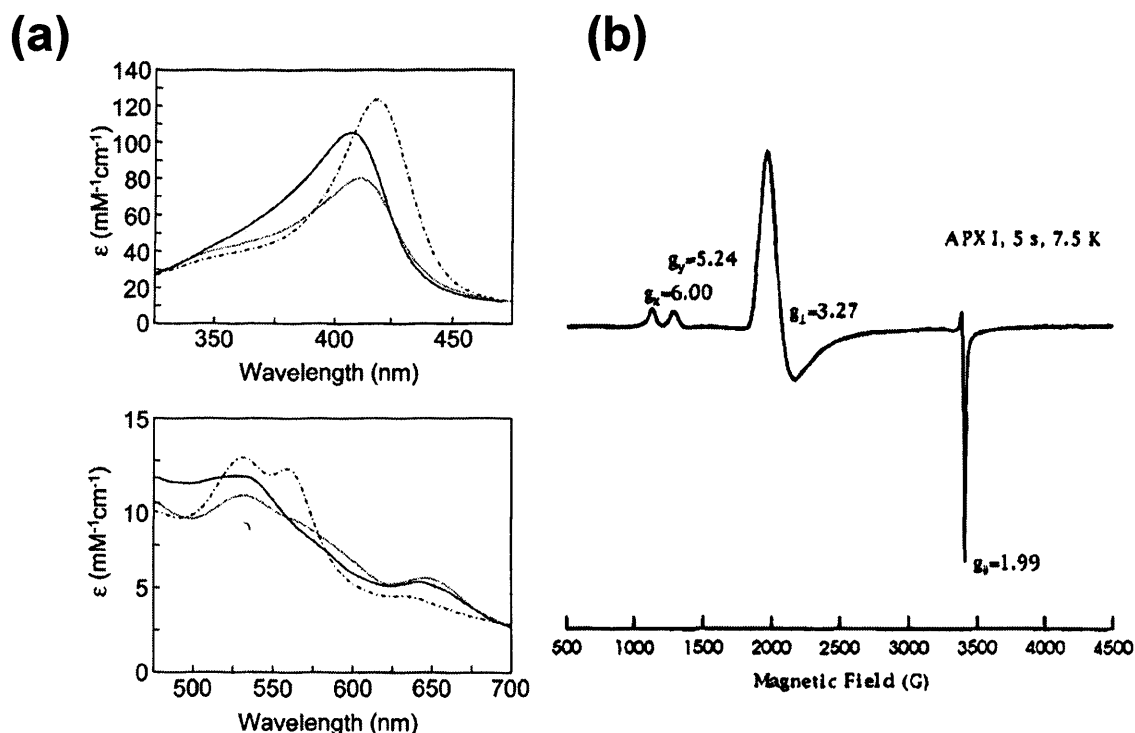
Figure 1.24: (a) UV-visible spectra of native (solid line), Compound I (dotted line) and Compound II (dashed and dotted line) rsAPX; the figure is reproduced from reference (*212*). (b) EPR spectrum of rpAPX Compound I; the figure is reproduced from reference (*213*).

1.11 Proposed mechanisms for covalent bond formation

1.11.1 Heme-protein covalent links in mammalian peroxidases

Incubation of recombinant LPO with low amounts of H_2O_2 increases both the extent of covalent heme binding and the catalytic activity (*70*). These results provided the first evidence that the heme to protein bonds could be formed through an autocatalytic process and were further supported by studies in EPO and TPO (*61, 214*).

The demonstration that formation of the ester bonds in LPO can be achieved simply by reaction of the heme-LPO complex with H_2O_2 (*70*) suggests that formation of a compound I-like intermediate is followed by a process that removes a hydrogen from each of the two methyl groups involved in cross-link formation. Removal of a hydrogen atom would generate a carbon radical that would be converted to a carbocation by transfer of one electron to the Fe^{IV} of the ferryl species. In this mechanism, the ester bond is then formed by trapping of the carbocation by the protein carboxylic acid group (*58*) (Scheme 1.2).
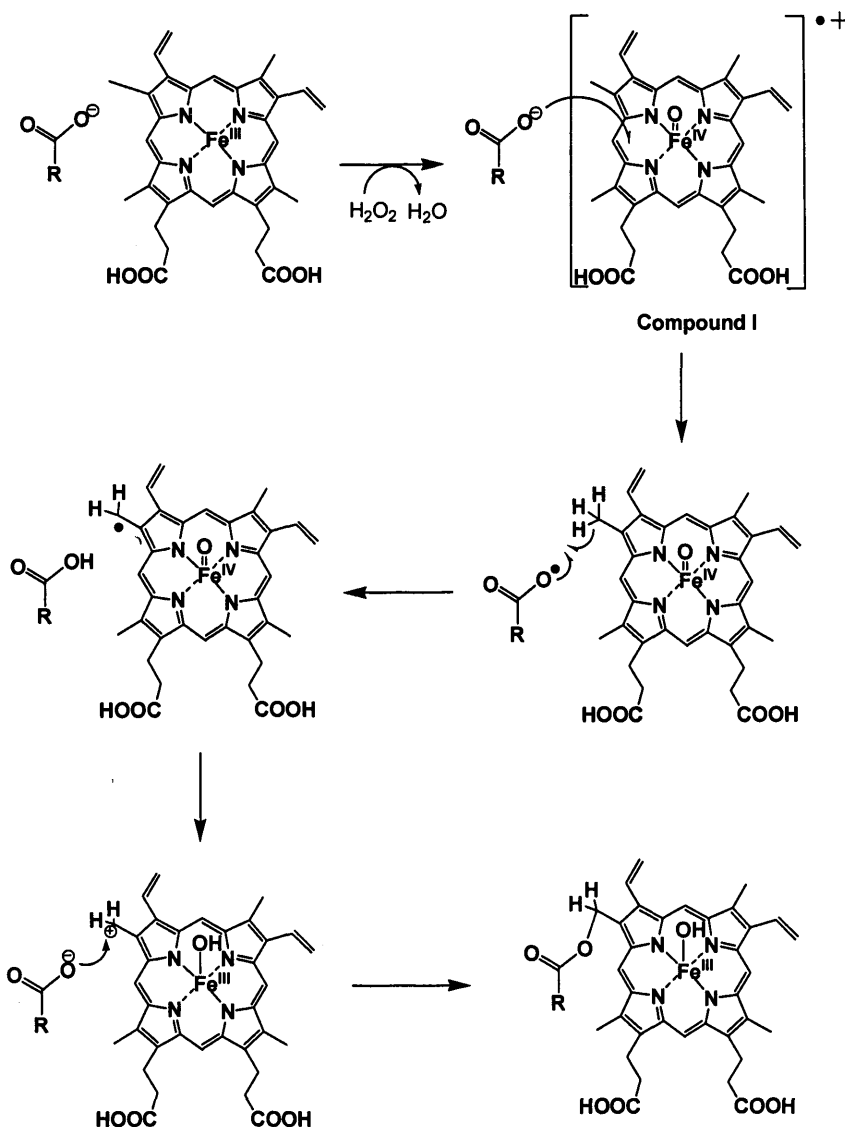
Scheme 1.2: Proposed mechanism for the H_2O_2 dependent autocatalytic formation of the ester bonds in mammalian peroxidases (58).

A key question with regard to this mechanism is the identity of the species that abstracts the hydrogen atom from the methyl group. As it is sterically impossible for the ferryl species of compound I to directly remove the hydrogen atom, this mechanism requires that Compound I first oxidize a protein side chain to a radical species that, in turn, removes the hydrogen from the methyl group (*58*). It was proposed that the carboxylic acid groups themselves could be oxidized to radical species that abstract the hydrogen from the methyl groups and then, in a subsequent step, also trap the carbocation intermediates (*58*).

Despite the demonstration that the ester links in the mammalian peroxidases can be formed through an autocatalytic process (*70*), little is known about the details of covalent bond formation or about the mechanism that forms the vinyl-sulfonium

cross-link in MPO. A mechanism for formation of the vinyl-sulfonium bond in MPO has been proposed by Colas and Ortiz de Montellano (*58*), that is based on the autocatalytic mechanism invoked for formation of the ester links. Thus, oxidation of the methionine sulfur by compound I would generate a thioether radical cation that attacks the β-carbon of the 2-vinyl substituent. Electron transfer to the ferryl iron followed by deprotonation would produce the desired vinyl sulfonium link (Scheme 1.3). The β-regiochemistry of the bond between the sulfur and the vinyl group is consistent with such an electrophilic attack of the sulfur on the vinyl group (*58*).

Compound I
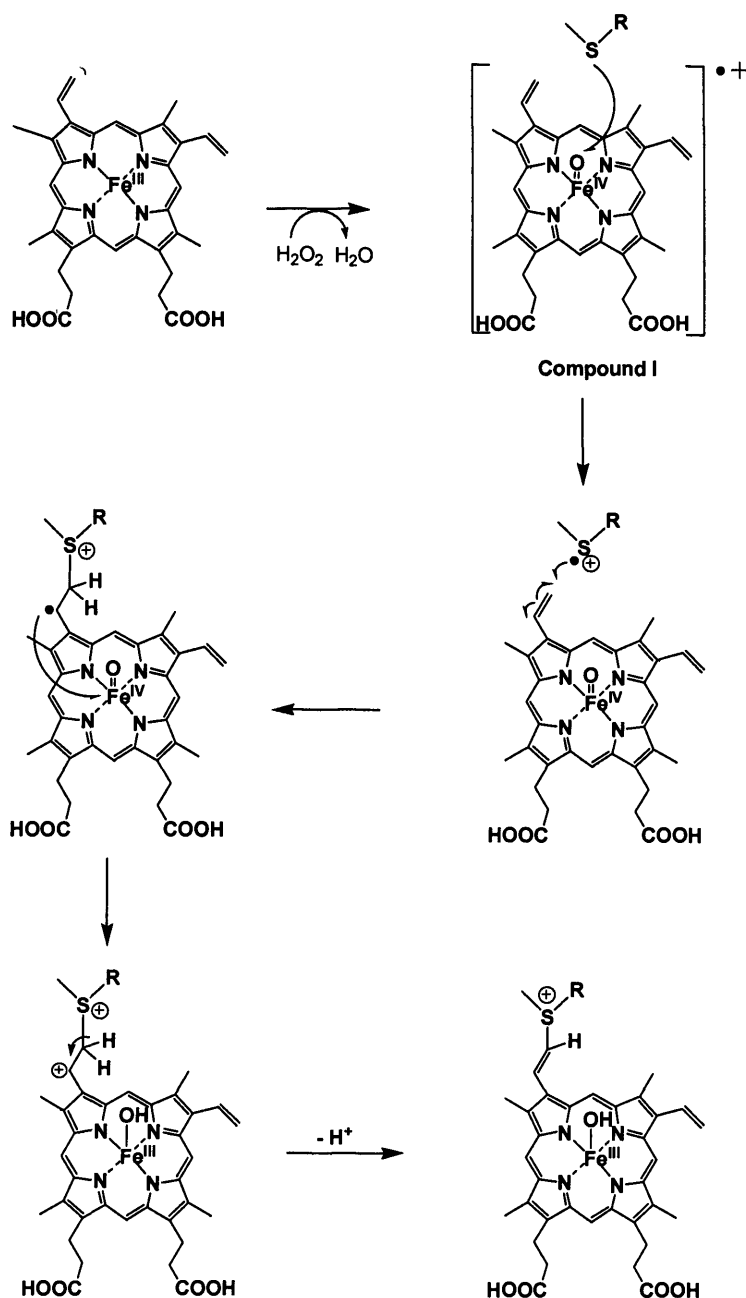
Scheme 1.3: Suggested mechanism for autocatalytic formation of the methionyl-vinyl sulfonium link in MPO (*58*).

1.11.2 Formation of an ester link in CYP4 family of P450s

As discussed previously, the CYP4 family of P450s can accommodate formation of a single ester bond from a glutamate residue to the 5-methyl group of the heme, similar to what is seen in the mammalian peroxidases (*92, 93, 215*). Recent studies by Baer *et al.* have provided the first experimental support for the mechanism of ester bond formation in a wild type CYP4 enzyme (*216*). Their studies with ^{18}O labeled glutamate residues of CYP4B1 demonstrated that 100% of the oxygen from Glu310 carboxylate is transferred to the P450 monoester linkage. These data support a mechanism in which the iron-oxo P450 oxidant removes an electron from the glutamic acid carboxylate, followed by abstraction of hydrogen from the C-5 position of the heme group. Intramolecular electron transfer within the heme forms the methyl carbocation, which is then quenched by Glu310 to generate the ester bond (Scheme 1.4) (*216*). This mechanism is similar to what has been previously proposed for formation of ester links in LPO (*58*) and further supports the idea that the carboxylic acid group that forms the ester link is the radical species that abstracts the hydrogen from the methyl groups.
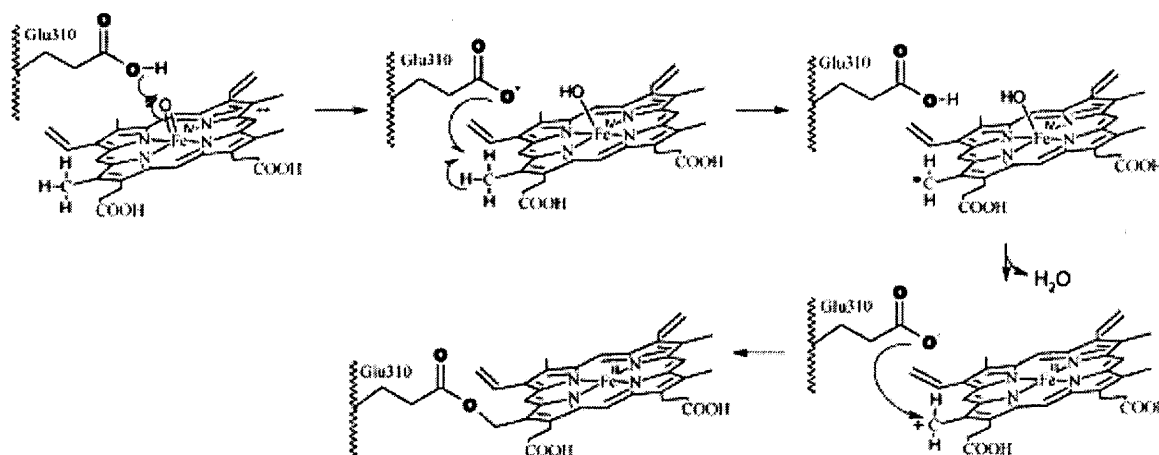
Scheme 1.4: Proposed mechanism for covalent heme attachment involving hydrogen abstraction by the iron-oxo species in CYP4B1 P450. The labeled oxygens (boldface) were traced throughout the reactions. This mechanism results in 100% incorporation of glutamate ^{18}O into the ester linkage. The scheme is reproduced from reference (*216*).

1.12 Experiments on plant-type peroxidases

As mentioned previously, the mammalian peroxidases bear covalent links between the protein and the heme prosthetic group. So far, there is very limited information on the mechanism of covalent linkage formation in the mammalian peroxidases. This is an important question not only because it promotes our more general understanding of the chemical, biological, and biomedical properties of the mammalian enzymes, but also because it is relevant to our understanding of covalent heme formation in other proteins.

Mechanistic studies in the mammalian peroxidases raise a number of difficulties, the more important of which lies in the fact that the covalent links are fully formed after expression of mammalian peroxidases, which makes their mechanism of formation impossible to study in the mature form of the enzymes.

To address this deficiency, several groups have used indirect methods, such as protein engineering techniques in plant peroxidases (that bear a non-covalently bound heme group), in an attempt to duplicate the heme-protein covalent links seen in the mammalian enzymes and study their mechanism of formation. Thus, there have been several attempts to mimic formation of either an ester or sulfonium link in plant proteins.

- Studies on LPO suggested that the ester links form through a H_2O_2 dependent, autocatalytic process (see Section 1.11.1) (*58, 70*). Attempts to duplicate heme-protein ester links in horseradish peroxidase (HRP) further supported this argument (*217*). More specifically, aspartate and/or glutamate residues were introduced into the distal cavity of HRP by site-directed mutagenesis. The HRP mutants (F41E and S73E) were isolated with no covalently bound heme, but the heme was completely covalently bound upon incubation with H_2O_2. Thus, it was suggested that covalent binding via ester bonds occurs fully autocatalytically after formation of compound I mediated by H_2O_2 (*217*), as had been previously proposed for the ester links in LPO (*70*).

- The formation of ester linkages was further investigated by studies on the $P450_{cam}$ G248E variant (*105*). A glutamate residue was engineered into $P450_{cam}$ close to the heme 5-methyl group. Incubation of the G248E variant with camphor, putidaredoxin, putidaredoxin reductase, and NADH results in

partial covalent binding of the heme to the protein. These results establish that a properly positioned carboxyl group is the sole requirement for autocatalytic formation of a heme-protein link in P450 enzymes (*105*).

- In contrast to formation of the ester linkages in mammalian peroxidases, until recently there was no information at all on the mechanism of formation of the sulfonium ion linkage (*58*). To duplicate the sulfonium link in MPO, a methionine residue close to the 2-vinyl group of the heme (Figure 1.25) was engineered in S160M variant of rpAPX and it was shown that a covalent sulfonium ion linkage could be formed autocatalytically upon incubation with H_2O_2 (*218*). A mechanism based on the autocatalytic formation of the ester bond was proposed, namely oxidation of the methionine sulfur by compound I thereby generating a thioether radical cation that attacks the vinyl carbon. Finally, electron transfer to the ferryl iron followed by deprotonation produces the sulfonium ion link (Scheme 1.5) (*58, 218*). In this proposed mechanism, the Compound I intermediate was detected directly and provided the first direct evidence of the presence of such a species during formation of a sulfonium ion link (*218*). Another observation was the proposed nucleophilic attack of H_2O at the final step of the proposed mechanism to give a heme structure consistent with the addition of a hydroxyl group. For MPO, addition of a hydroxyl group clearly does not occur, and an alternative pathway, involving loss of H^+ from the same cation intermediate and retention of the double bond, has been suggested (*58*).
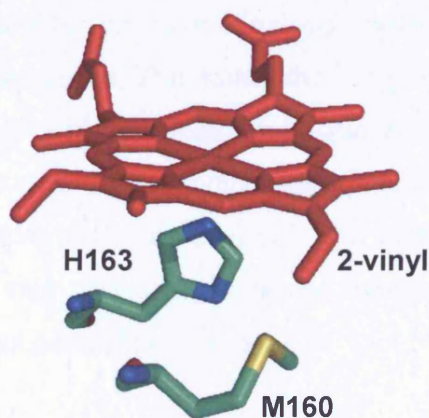
Figure 1.25: Model structure of the active site of S160M variant of rpAPX, showing His163, Met160 and the 2-vinyl group of the heme.
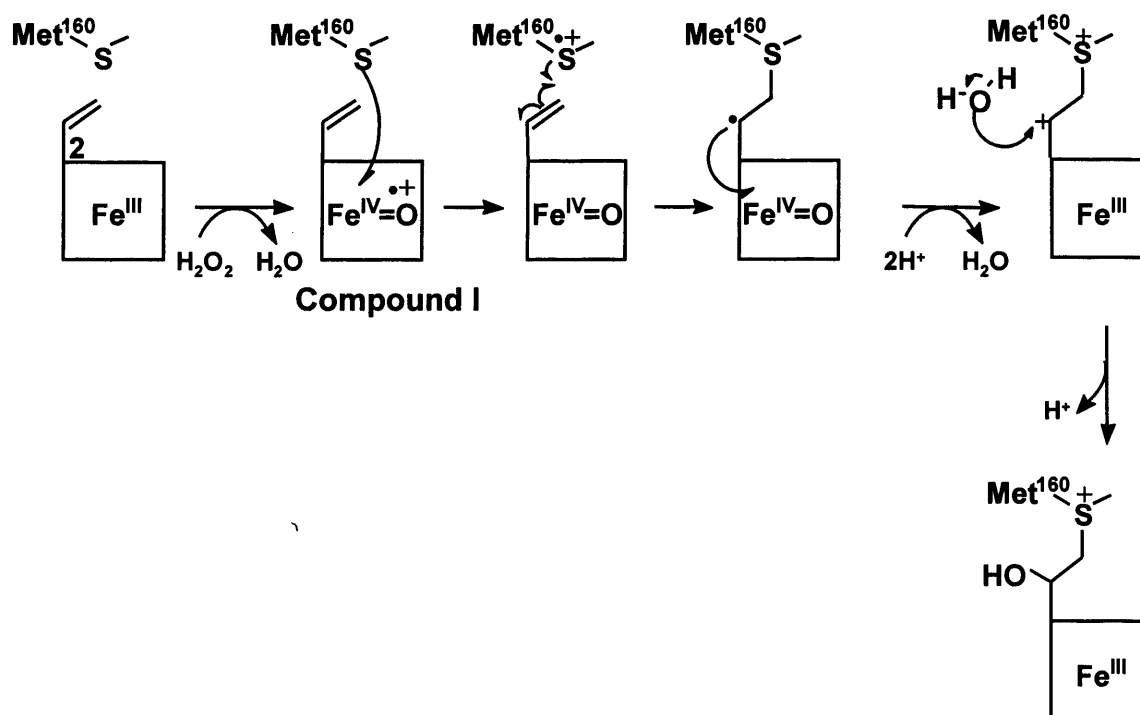
Scheme 1.5: Suggested mechanism for autocatalytic formation of a covalent link between Met160 and the 2-vinyl group of the heme in rpPAX (*218*).

These results provided the first direct evidence that covalent linkage formation between the methionine residue and the heme vinyl group occurs as an H_2O_2-dependent process (*218*). This is important because it showed that the strategic positioning of a suitable methionine residue close to the heme and contained within a catalytically competent structural architecture is sufficient for methionine-heme crosslinking to occur.

Overall, the study of plant-type peroxidase mutants has revealed that there are no specific requirements other than the presence of an appropriately located residue for heme-protein covalent link formation. This raises the intriguing possibility that, in principle, any heme peroxidase with appropriately positioned residues can duplicate the active site architecture observed in the mammalian peroxidases. If this is the case, it would provide an alternative route for exploring the effects of these covalent linkages on heme function that avoids the inherent experimental complications associated with the mammalian peroxidase enzyme.

1.13 Thesis aims

In the context of the above discussion, an investigation into the formation of heme-protein covalent links in plant peroxidases is presented in this thesis. The objectives of this research were:

- To use APX as a platform to investigate heme-protein covalent link formation in plant peroxidases.

- To establish the conditions needed to duplicate the same chemistry in other heme architectures.

- To investigate the mechanism of formation of these links.

- To look into the functional role of heme-protein covalent links and investigate their effect on the properties of the enzyme.

- To investigate the reactivity of rsAPX in comparison to other members of the Class I plant peroxidases in which covalent protein links are observed.

1.14 References

(1)   Dunford, H. B. (1999) *Heme Peroxidases*, John Wiley & Sons, New York.

(2)   Review edited by Raven, E. L., and Ortiz de montellano, P. R. (2007) The chemistry and biochemistry of heme proteins. *Nat. Prod. Rep. 24*, 489-644.

(3)   Ator, M. A., and Ortiz de Montellano, P. R. (1987) Protein control of prosthetic heme reactivity. Reaction of substrates with the heme edge of horseradish peroxidase. *J. Biol. Chem. 262*, 1542-1551.

(4)   Dawson, J. H. (1988) Probing structure-function relations in heme-containing oxygenases and peroxidases. *Science 240*, 433-439.

(5)   Gray, H. B., and Winkler, J. R. (1996) Electron transfer in proteins. *Annu. Rev. Biochem. 65*, 537-561.

(6)   Ortiz de Montellano, P. R. (1987) Control of the catalytic activity of prosthetic heme by the structure of hemoproteins. *Acc. Chem. Res. 20*, 289-294.

(7)   Springer, B. A., Sligar, S. G., Olson, J. S., and Phillips, G. N. (1994) Mechanisms of ligand recognition in myoglobin. *Chem. Rev. 94*, 699-714.

(8)   English, A. M., and Tsaprailis, G. (1995) Catalytic structure-function relationships in heme peroxidases. *Adv. Inorg. Chem. 43*, 79-125.

(9)   Reedy, C. J., and Gibney, B. R. (2003) Heme protein assemblies. *Chem. Rev. 104*, 617-649.

(10) Fenton, D. E. (1995) *Biocoordination Chemistry*, Oxford University Press.

(11) Antonini, M., and Brunori, E. (1971) *Hemoglobin and Myoglobin and their reactions with ligands*, North Holland Publishers, Amsterdam.

(12) Sono, M., Roach, M. P., Coulter, E. D., and Dawson, J. H. (1996) Heme-Containing Oxygenases. *Chem. Rev. 96*, 2841-2888.

(13) Wong, L. L. (1998) Cytochrome P450 monooxygenases. *Curr. Opin. Chem. Biol. 2*, 263-268.

(14) Bosshard, H. R., Anni, H., and Yonetoni, T. (1991) *Peroxidases in Chemistry and Biology*, Vol. 2, CRS Press Boca Raton.

(15) Chen, J.-J. (2000) *Translational control of gene expression*, Cold Spring Harbor Laboratory Press, Cold Spring Harbor, New York.

(16) Zhang, L., and Hach, A. (1999) Molecular mechanism of heme signaling in yeast: the transcriptional activator Hap1 serves as the key mediator. *Cell Mol. Life Sci. 56*, 415-426.

(17) Rodgers, K. R. (1999) Heme-based sensors in biological systems. *Curr. Opin. Chem. Biol. 3*, 158-167.

(18) Poulos, T. L. (2007) The Janus nature of heme. *Nat. Prod. Rep. 24*, 504-510.

(19) Gilles-Gonzalez, M. A., and Gonzalez, G. (2005) Heme-based sensors: defining characteristics, recent developments, and regulatory hypotheses. *J. Inorg. Biochem. 99*, 1-22.

(20) Barker, P. D., and Ferguson, S. J. (1999) Still a puzzle: why is haem covalently attached in *c*-type cytochromes? *Structure 7*, R281-290.

(21) Page, M. D., Sambongi, Y., and Ferguson, S. J. (1998) Contrasting routes of *c*-type cytochrome assembly in mitochondria, chloroplasts and bacteria. *Trends Biochem. Sci. 23*, 103-108.

(22) Moore, G. R., and Pettigrew, G. W. (1990) *Cytochromes c: evolutionary, structural and physicochemical aspects*, Springer-Verlag, New York.

(23) Moore, G. R., and Pettigrew, G. W. (1987) *Cytochromes c: Biological aspects*, Springer, New York.

(24) Scott, R. A., and Mauk, A. G. (1995) *Cytochrome c: A multidisciplinary approach*, University Science Books, Mill Valley, CA.

(25) Igarashi, N., Moriyama, H., Fujiwara, T., Fukumori, Y., and Tanaka, N. (1997) The 2.8 A structure of a hydroxylamine oxidoreductase from a denitrifying chemoautotrophic bacterium, *Nitrosomonas europaea. Nat. Struct. Biol. 4*, 276-284.

(26) Einsle, O., Messerschmidt, A., Stach, P., Bourenkov, G. P., Bartunik, H. D., Huber, R., and Kroneck, P. M. (1999) Structure of cytochrome *c* nitrite reductase. *Nature 400*, 476-480.

(27) Martinou, J. C., Desagher, S., and Antonsson, B. (2000) Cytochrome *c* release from mitochondria: all or nothing. *Nat. Cell Biol. 2*, E41-43.

(28) Allen, J. W., Daltrop, O., Stevens, J. M., and Ferguson, S. J. (2003) *C*-type cytochromes: diverse structures and biogenesis systems pose evolutionary problems. *Philos. Trans. R. Soc. Lond. B Biol. Sci. 358*, 255-266.

(29)   Stevens, J. M., Daltrop, O., Allen, J. W., and Ferguson, S. J. (2004) *C*-type cytochrome formation: chemical and biological enigmas. *Acc. Chem. Res. 37*, 999-1007.

(30)   Daltrop, O., and Ferguson, S. J. (2003) Cytochrome *c* maturation. The in vitro reactions of horse heart apocytochrome *c* and Paracoccus dentrificans apocytochrome c550 with heme. *J. Biol. Chem. 278*, 4404-4409.

(31)   Stevens, J. M., Uchida, T., Daltrop, O., and Ferguson, S. J. (2005) Covalent cofactor attachment to proteins: cytochrome *c* biogenesis. *Biochem. Soc. Trans. 33*, 792-795.

(32)   Daltrop, O., Allen, J. W., Willis, A. C., and Ferguson, S. J. (2002) In vitro formation of a *c*-type cytochrome. *Proc. Natl. Acad. Sci. U S A 99*, 7872-7876.

(33)   Schulz, H., Hennecke, H., and Thony-Meyer, L. (1998) Prototype of a heme chaperone essential for cytochrome *c* maturation. *Science 281*, 1197-1200.

(34)   Bushnell, G. W., Louie, G. V., and Brayer, G. D. (1990) High-resolution three-dimensional structure of horse heart cytochrome *c*. *J. Mol. Biol. 214*, 585-595.

(35)   Lee, D., Pervushin, K., Dischof, D., Braun, M., and Thony-Meyer, L. (2005) Unusual heme-histidine bond in the active site of a chaperone. *J. Am. Chem. Soc. 127*, 3716-3717.

(36)   Allen, J. W., Barker, P. D., Daltrop, O., Stevens, J. M., Tomlinson, E. J., Sinha, N., Sambongi, Y., and Ferguson, S. J. (2005) Why isn't 'standard' heme good enough for *c*-type and d1-type cytochromes? *Dalton Trans.*, 3410-3418.

(37)   Wood, P. M. (1983) Why do *c*-type cytochromes exist? *FEBS Lett. 164*, 223-226.

(38)   Wood, P. M. (1991) Why do *c*-type cytochromes exist? Reprise. *Biochim. Biophys. Acta 1058*, 5-7.

(39)   Tomlinson, E. J., and Ferguson, S. J. (2000) Conversion of a *c* type cytochrome to a *b* type that spontaneously forms in vitro from apo protein and heme: implications for *c* type cytochrome biogenesis and folding. *Proc. Natl. Acad. Sci. U S A 97*, 5156-5160.

(40)   Stellwagen, E., Rysavy, R., and Babul, G. (1972) The conformation of horse heart apocytochrome *c*. *J. Biol. Chem. 247*, 8074-8077.

(41)   Cohen, J. S., Fisher, W. R., and Schechter, A. N. (1974) Spectroscopic studies on the conformation of cytochrome *c* and apocytochrome *c*. *J. Biol. Chem. 249*, 1113-1118.

(42)   Dumont, M. E., Corin, A. F., and Campbell, G. A. (1994) Noncovalent binding of heme induces a compact apocytochrome *c* structure. *Biochemistry 33*, 7368-7378.

(43)   Rosell, F. I., and Mauk, A. G. (2002) Spectroscopic properties of a mitochondrial cytochrome *c* with a single thioether bond to the heme prosthetic group. *Biochemistry 41*, 7811-7818.

(44)   Michel, L, V., Ye, T., Bowman, S. E., Levin, B. D., Hahn, M. A., Russell, B. S., Elliott, S. J., and Bren, K. L. (2007) Heme attachment motif mobility tunes cytochrome *c* redox potential. *Biochemistry 46*, 11753-11760.

(45)   Norager, S., Legrand, P., Pieulle, L., Hatchikian, C., and Roth, M. (1999) Crystal structure of the oxidised and reduced acidic cytochrome *c3* from Desulfovibrio africanus. *J. Mol. Biol. 290*, 881-902.

(46)   Barker, P. D., Nerou, E. P., Cheesman, M. R., Thomson, A. J., de Oliveira, P., and Hill, H. A. (1996) Bis-methionine ligation to heme iron in mutants of cytochrome b562. 1. Spectroscopic and electrochemical characterization of the electronic properties. *Biochemistry 35*, 13618-13626.

(47)   Hooper, A. B., Maxwell, P. C., and Terry, K. R. (1978) Hydroxylamine oxidoreductase from *Nitrosomonas*: absorption spectra and content of heme and metal. *Biochemistry 17*, 2984-2989.

(48)   Erickson, R. H., and Hooper, A. B. (1972) Preliminary characterization of a variant co-binding heme protein from *Nitrosomonas*. *Biochim. Biophys. Acta 275*, 231-244.

(49)   Pearson, A. R., Elmore, B. O., Yang, C., Ferrara, J. D., Hooper, A. B., and Wilmot, C. M. (2007) The crystal structure of cytochrome P460 of *Nitrosomonas europaea* reveals a novel cytochrome fold and heme-protein cross-link. *Biochemistry 46*, 8340-8349.

(50)   Kowalchuk, G. A., and Stephen, J. R. (2001) Ammonia-oxidizing bacteria: a model for molecular microbial ecology. *Annu. Rev. Microbiol. 55*, 485-529.

(51)   Arciero, D. M., Hooper, A. B., Cai, M., and Timkovich, R. (1993) Evidence for the structure of the active site of heme P460 in hydroxylamine oxidoreductase of *Nitrosomonas europaea*. *Biochemistry 32*, 9370-9378.

(52) Numata, M., Saito, T., Yamazaki, T., Fukumori, Y., and Yamanaka, T. (1990) Cytochrome P460 of *Nitrosomonas europaea*: further purification and further characterization. *J. Biochem. (Tokyo) 108*, 1016-1021.

(53) Bergmann, D. J., and Hooper, A. B. (1994) The primary structure of cytochrome P460 of *Nitrosomonas europaea* - Presence of a *c*-heme binding motif. *FEBs Lett. 353*, 324-326.

(54) Elmore, B. O., Pearson, A. R., Wilmot, C. M., and Hooper, A. B. (2006) Expression, purification, crystallization and preliminary X-ray diffraction of a novel *Nitrosomonas europaea* cytochrome, cytochrome P460. *Acta Crystallogr., Sect. F: Struct. Biol. Cryst. Commun. 62*, 395-398.

(55) Bergmann, D. J., and Hooper, A. B. (2003) Cytochrome P460 of *Nitrosomonas europaea*- Formation of the heme-lysine cross-link in a heterologous host and mutagenic conversion to a non-cross-linked cytochrome *c'*. *Eur. J. Biochem. 270*, 1935-1941.

(56) McLachlan, S. M., and Rapoport, B. (1992) The molecular biology of thyroid peroxidase: cloning, expression and role as autoantigen in autoimmune thyroid disease. *Endocr. Rev. 13*, 192-206.

(57) Dalton, D. A. (1991) *Peroxidases in Chemistry and Biology*, Vol. 2, CRC Press Boca Raton.

(58) Colas, C., and Ortiz de Montellano, P. R. (2003) Autocatalytic radical reactions in physiological prosthetic heme modification. *Chem. Rev. 103*, 2305-2332.

(59) Watanabe, S., Varsalona, F., Yoo, Y. C., Guillaume, J. P., Bollen, A., Shimazaki, K., and Moguilevsky, N. (1998) Recombinant bovine lactoperoxidase as a tool to study the heme environment in mammalian peroxidases. *FEBS Lett. 441*, 476-479.

(60) Colas, C., Kuo, J. M., and Ortiz de Montellano, P. R. (2002) Asp225 and Glu375 in autocatalytic attachment of the prosthetic heme group of lactoperoxidase. *J. Biol. Chem. 277*, 7191-7200.

(61) Oxvig, C., Thomsen, A. R., Overgaard, M. T., Sorensen, E. S., Hojrup, P., Bjerrum, M. J., Gleich, G. J., and Sottrup-Jensen, L. (1999) Biochemical evidence for heme linkage through esters with Asp93 and Glu241 in human eosinophil peroxidase. The ester with Asp93 is only partially formed in vivo. *J. Biol. Chem. 274*, 16953-16958.

(62)   Fayadat, L., Niccoli-Sire, P., Lanet, J., and Franc, J. L. (1999) Role of heme
        in intracellular trafficking of thyroperoxidase and involvement of H_2O_2
        generated at the apical surface of thyroid cells in autocatalytic covalent heme
        binding. *J. Biol. Chem. 274*, 10533-10538.

(63)   Kooter, I. M., Moguilevsky, N., Bollen, A., van der Veen, L. A., Otto, C.,
        Dekker, H. L., and Wever, R. (1999) The sulfonium ion linkage in
        myeloperoxidase. Direct spectroscopic detection by isotopic labeling and
        effect of mutation. *J. Biol. Chem. 274*, 26794-26802.

(64)   Kooter, I. M., Pierik, A. J., Merkx, M., Averill, B. A., Moguilevsky, N.,
        Bollen, A., and Wever, R. (1997) Difference fourier transform infrared
        evidence for ester bonds linking the heme group in myeloperoxidase,
        lactoperoxidase, and eosinophil Peroxidase *J. Am. Chem. Soc. 119*, 11542-
        11543.

(65)   Fiedler, T. J., Davey, C. A., and Fenna, R. E. (2000) X-ray crystal structure
        and characterization of halide-binding sites of human myeloperoxidase at 1.8
        Å resolution. *J. Biol. Chem. 275*, 11964-11971.

(66)   Taylor, K. L., Strobel, F., Yue, K. T., Ram, P., Pohl, J., Woods, A. S., and
        Kinkade, J. M., Jr. (1995) Isolation and identification of a protoheme IX
        derivative released during autolytic cleavage of human myeloperoxidase.
        Arch. Biochem. Biophys. 316, 635-642.

(67)   Andersson, L. A., Bylkas, S. A., and Wilson, A. E. (1996) Spectral analysis
        of lactoperoxidase. Evidence for a common heme in mammalian peroxidases.
        J. Biol. Chem. 271, 3406-12.

(68)   Fenna, R., Zeng, J., and Davey, C. (1995) Structure of the green heme in
        myeloperoxidase. *Arch. Biochem. Biophys. 316*, 653-656.

(69)   Ortiz de Montellano, P. R., and Wilks, P. R. (2000) *Adv. Inorg. Chem. 51*,
        359.

(70)   DePillis, G. D., Ozaki, S., Kuo, J. M., Maltby, D. A., and Ortiz de
        Montellano, P. R. (1997) Autocatalytic processing of heme by
        lactoperoxidase produces the native protein-bound prosthetic group. *J. Biol.
        Chem. 272*, 8857-8860.

(71)   Kooter, I. M., Pierik, A. J., Merkx, M., Averill, B. A., Moguilevsky, N., Bollen, A., and Wever, R. (1997) Difference fourier transform infrared evidence for ester bonds linking the heme group in myeloperoxidase, lactoperoxidase and eosinophil peroxiadse. *J. Am. Chem. Soc. 119*, 11542-11543.

(72)   Rae, T. D., and Goff, H. M. (1998) The heme prosthetic group of lactoperoxidase. Structural characteristics of heme l and heme l-peptides. *J. Biol. Chem. 273*, 27968-27977.

(73)   Zederbauer, M., Furtmuller, P. G., Brogioni, S., Jakopitsch, C., Smulevich, G., and ,Obinger, C. (2007) Heme to protein linkages in mammalian peroxidases: impact on spectroscopic, redox and catalytic properties. *Nat. Prod. Rep. 24*, 571-584.

(74)   Sievers, G. (1980) Structure of milk lactoperoxidase. A study using circular dichroism and difference absorption spectroscopy. *Biochim. Biophys. Acta. 624*, 249-259.

(75)   Furtmuller, P. G., Obinger, C., Hsuanyu, Y., and Dunford, H. B. (2000) Mechanism of reaction of myeloperoxidase with hydrogen peroxide and chloride ion. *Eur. J. Biochem. 267*, 5858-5864.

(76)   Andrews, P. C., and Krinsky, N. I. (1981) The reductive cleavage of myeloperoxidase in half, producing enzymically active hemi-myeloperoxidase. *J. Biol. Chem. 256*, 4211-4218.

(77)   Wever, R., and Plat, H. (1981) Spectral properties of myeloperoxidase and its ligand complexes. *Biochim. Biophys. Acta 661*, 235-239.

(78)   Kooter, I. M., Moguilevsky, N., Bollen, A., Sijtsema, N. M., Otto, C., and Wever, R. (1997) Site-directed mutagenesis of Met243, a residue of myeloperoxidase involved in binding of the prosthetic group. *J. Biol. Inorg. Chem. 2*, 191-197.

(79)   Kooter, I. M., Koehler, B. P., Moguilevsky, N., Bollen, A., Wever, R., and Johnson, M. K. (1999) The Met243 sulfonium ion linkage is responsible for the anomalous magnetic circular dichroism and optical spectral properties of myeloperoxidase. *J. Biol. Inorg. Chem. 4*, 684-691.

(80) Brogioni, S., Feis, A., Marzocchi, M. P., Zederbauer, M., Furtmuller, P. G., Obinger, C., and Smulevich, G. (2006) Resonance Raman assignment of myeloperoxidase and the selected mutants Asp94Val and Met243Thr. Effect of the heme distortion. *J. Raman Spectrosc. 37*, 263-276.

(81) Kooter, I. M., Moguilevsky, N., Bollen, A., Sijtsema, N. M., Otto, C., Dekker, H. L., and Wever, R. (1999) Characterization of the Asp94 and Glu242 mutants in myeloperoxidase, the residues linking the heme group via ester bonds. *Eur. J. Biochem. 264*, 211-217.

(82) Furtmuller, P. G., Zederbauer, M., Jantschko, W., Helm, J., Bogner, M., Jakopitsch, C., and Obinger, C. (2006) Active site structure and catalytic mechanisms of human peroxidases. *Arch. Biochem. Biophy.s 445*, 199-213.

(83) Harrison, J. E., and Schultz, J. (1978) Myeloperoxidase: confirmation and nature of heme-binding inequivalence. Resolution of a carbonyl-substituted heme. *Biochim. Biophys. Acta 536*, 341-349.

(84) Ikeda-Saito, M., and Prince, R. C. (1985) The effect of chloride on the redox and EPR properties of myeloperoxidase. *J. Biol. Chem. 260*, 8301-8305.

(85) Battistuzzi, G., Bellei, M., Zederbauer, M., Furtmuller, P. G., Sola, M., and Obinger, C. (2006) Redox thermodynamics of the Fe(III)/Fe(II) couple of human myeloperoxidase in its high-spin and low-spin forms. *Biochemistry 45*, 12750-12755.

(86) Huang, L., Colas, C., and Ortiz de Montellano, P. R. (2004) Oxidation of carboxylic acids by horseradish peroxidase results in prosthetic heme modification and inactivation. *J. Am. Chem. Soc. 126*, 12865-12873.

(87) Wojciechowski, G., Huang, L., and Ortiz de Montellano, P. R. (2005) Autocatalytic modification of the prosthetic heme of horseradish but not lactoperoxidase by thiocyanate oxidation products. A role for heme-protein covalent cross-linking. *J. Am. Chem. So.c 127*, 15871-15879.

(88) Huang, L., and Ortiz de Montellano, P. R. (2006) Heme-protein covalent bonds in peroxidases and resistance to heme modification during halide oxidation. *Arch. Biochem. Biophys. 446*, 77-83.

(89) Huang, L., Wojciechowski, G., and Ortiz de Montellano, P. R. (2006) Role of heme-protein covalent bonds in mammalian peroxidases. Protection of the heme by a single engineered heme-protein link in horseradish peroxidase. *J. Biol. Chem. 281*, 18983-18988.

(90) Goedken, M., McCormick, S., Leidal, K. G., Suzuki, K., Kameoka, Y., Astern, J. M., Huang, M., Cherkasov, A., and Nauseef, W. M. (2007) Impact of two novel mutations on the structure and function of human myeloperoxidase. *J. Biol. Chem. 282*, 27994-28003.

(91) LeBrun, L. A., Hoch, U., and Ortiz de Montellano, P. R. (2002) Autocatalytic mechanism and consequences of covalent heme attachment in the cytochrome P4504A family. *J. Biol. Chem. 277*, 12755-12761.

(92) LeBrun, L. A., Xu, F., Kroetz, D. L., and Ortiz de Montellano, P. R. (2002) Covalent attachment of the heme prosthetic group in the CYP4F cytochrome P450 family. *Biochemistry 41*, 5931-5937.

(93) Henne, K. R., Kunze, K. L., Zheng, Y. M., Christmas, P., Soberman, R. J., and Rettie, A. E. (2001) Covalent linkage of prosthetic heme to CYP4 family P450 enzymes. *Biochemistry 40*, 12925-12931.

(94) Hoch, U., and Ortiz De Montellano, P. R. (2001) Covalently linked heme in cytochrome p4504a fatty acid hydroxylases. *J. Biol. Chem. 276*, 11339-11346.

(95) Henne, K. R., Kunze, K. L., Zheng, Y.-M., Christmas, P., Soberman, R. J., and Rettie, A. E. (2001) Covalent linkage of prosthetic heme to CYP4 family of P450 enzymes. *Biochemistry 40*, 12925-12931.

(96) Lecomte, J. T., Scott, N. L., Vu, B. C., and Falzone, C. J. (2001) Binding of ferric heme by the recombinant globin from the cyanobacterium Synechocystis sp. PCC 6803. *Biochemistry 40*, 6541-6552.

(97) Scott, N. L., Falzone, C. J., Vuletich, D. A., Zhao, J., Bryant, D. A., and Lecomte, J. T. (2002) Truncated hemoglobin from the cyanobacterium *Synechococcus sp.* PCC 7002: evidence for hexacoordination and covalent adduct formation in the ferric recombinant protein. *Biochemistry 41*, 6902-6910.

(98) Vu, B. C., Jones, A. D., and Lecomte, J. T. (2002) Novel histidine-heme covalent linkage in a hemoglobin. *J. Am. Chem. So.c 124*, 8544-8545.

(99) Scott, N. L., and Lecomte, J. T. (2000) Cloning, expression, purification, and preliminary characterization of a putative hemoglobin from the cyanobacterium *Synechocystis sp.* PCC 6803. *Protein Sci 9*, 587-597.

(100) Vu, B. C., Vuletich, D. A., Kuriakose, S. A., Falzone, C. J., and Lecomte, J. T. (2004) Characterization of the heme-histidine cross-link in cyanobacterial hemoglobins from *Synechocystis sp.* PCC 6803 and *Synechococcus sp.* PCC 7002. *J. Biol. Inorg. Chem.* *9*, 183-194.

(101) Hoy, J. A., Kundu, S., Trent III, J. T., Ramaswamy, S., and Hargrove, M. S. (2004) The crystal structure of *Synechocystis* hemoglobin with a covalent heme linkage. *J. Biol. Chem.* *279*, 16535-16542.

(102) Ortiz de Montellano, P. R. (1990) Arylhydrazines as probes of hemoprotein structure and function. *Pharmacol. Ther.* *48*, 95.

(103) Ortiz de Montellano, P. R. (1995) *Cytochrome P450: Structure, Mechanism, and Biochemistry*, Plenum Press: New York, London.

(104) Ortiz de Montellano, P. R. (1990) Free radical modification of prosthetic heme groups. *Pharmacol. Ther.* *48*, 95-120.

(105) Limburg, J., LeBrun, L. A., and Ortiz de Montellano, P. R. (2005) The P450cam G248E mutant covalently binds its prosthetic heme group. *Biochemistry 44*, 4091-4099.

(106) Colas, C., and De Montellano, P. R. (2004) Horseradish peroxidase mutants that autocatalytically modify their prosthetic heme group: insights into mammalian peroxidase heme-protein covalent bonds. *J. Biol. Chem.* *279*, 24131-24140.

(107) Osawa, Y., Highet, R. J., Bax, A., and Pohl, L. R. (1991) Characterization by NMR of the heme-myoglobin adduct formed during the reductive metabolism of BrCCl3. Covalent bonding of the proximal histidine to the ring I vinyl group. *J. Biol. Chem.* *266*, 3208-3214.

(108) Jakopitsch, C., Kolarich, D., Petutschnig, G., Furtmuller, P. G., and Obinger, C. (2003) Distal side tryptophan, tyrosine and methionine in catalase-peroxidases are covalently linked in solution. *FEBS Lett.* *552*, 135-140.

(109) Ghiladi, R. A., Knudsen, G. M., Medzihradszky, K. F., and Ortiz de Montellano, P. R. (2005) The Met-Tyr-Trp cross link in *Mycobacterium tuberculosis* catalase peroxidase. *J. Biol. Chem.* *280*, 22651-22663.

(110) Ostermeier, C., Harrenga, A., Ermler, U., and Michel, H. (1997) Structure at 2.7 Å resolution of the *Paracoccus denitrificans* two-subunit cytochrome *c* oxidase complexed with an antibody FV fragment. *Proc. Natl. Acad. Sci. U S A 94*, 10547-10553.

(111) Yoshikawa, S., Shinzawa-Itoh, K., Nakashima, R., Yaono, R., Yamashita, E., Inoue, N., Yao, M., Fei, M. J., Libeu, C. P., Mizushima, T., Yamaguchi, H., Tomizaki, T., and Tsukihara, T. (1998) Redox-coupled crystal structural changes in bovine heart cytochrome c oxidase. *Science 280*, 1723-1729.

(112) Buse, G., Soulimane, T., Dewor, M., Meyer, H. E., and Bluggel, M. (1999) Evidence for a copper-coordinated histidine-tyrosine cross-link in the active site of cytochrome c oxidase. *Protein Sci. 8*, 985-990.

(113) Milani, M., Savard, P. Y., Ouellet, H., Ascenzi, P., Guertin, M., and Bolognesi, M. (2003) A TyrCD1/TrpG8 hydrogen bond network and a TyrB10TyrCD1 covalent link shape the heme distal site of *Mycobacterium tuberculosis* hemoglobin O. *Proc. Natl. Acad. Sci. U S A 100*, 5766-5771.

(114) Bravo, J., Fita, I., Ferrer, J. C., Ens, W., Switala, J., and Loewen, P. C. (1997) Identification of a novel bond between a histidine and the essential tyrosine in catalase HPII of *Esherichia coli. Prot. Sci. 6*, 1016-1023.

(115) Ito, N., Phillips, S. E., Stevens, C., Ogel, Z. B., McPherson, M. J., Keen, J. N., Yadav, K. D., and Knowles, P. F. (1991) Novel thioether bond revealed by a 1.7 Å crystal structure of galactose oxidase. *Nature 350*, 87-90.

(116) Ito, N., Phillips, S. E., Yadav, K. D., and Knowles, P. F. (1994) Crystal structure of a free radical enzyme, galactose oxidase. *J. Mol. Biol. 238*, 794-814.

(117) Diaz, A., Horjales, E., Rudino-Pinera, E., Arreola, R., and Hansberg, W. (2004) Unusual Cys-Tyr covalent bond in a large catalase. *J. Mol. Biol. 342*, 971-985.

(118) Parsons, M. R., Convery, M. A., Wilmot, C. M., Yadav, K. D., Blakeley, V., Corner, A. S., Phillips, S. E., McPherson, M. J., and Knowles, P. F. (1995) Crystal structure of a quinoenzyme: copper amine oxidase of *Escherichia coli* at 2 Å resolution. *Structure 3*, 1171-1184.

(119) Tsukihara, T., Aoyama, H., Yamashita, E., Tomizaki, T., Yamaguchi, H., Shinzawa-Itoh, K., Nakashima, R., Yaono, R., and Yoshikawa, S. (1996) The whole structure of the 13-subunit oxidized cytochrome c oxidase at 2.8 Å. *Science 272*, 1136-1144.

(120) Kirk, T. K., and Farrell, R. L. (1987) Enzymatic "combustion": the microbial degradation of lignin. *Annu. Rev. Microbiol. 41*, 465-505.

(121) Wariishi, H., Marquez, L., Dunford, H. B., and Gold, M. H. (1990) Lignin peroxidase compounds II and III. Spectral and kinetic characterization of reactions with peroxides. *J. Biol. Chem. 265*, 11137-11142.

(122) Wada, N., Kinoshita, S., Matsuo, M., Amako, K., Miyake, C., and Asada, K. (1998) Purification and molecular properties of ascorbate peroxidase from bovine eye. *Biochem. Biophys. Res. Commun. 242*, 256-261.

(123) Groden, D., and Beck, E. (1979) H_2O_2 destruction by ascorbate-dependent systems from chloroplasts. *Biochim. Biophys. Acta 546*, 426-435.

(124) Kelly, G. J., and Latzko, E. (1979) Soluble ascorbate peroxidase: detection in plants and use in vitamim C estimation. *Naturwissenschaften 66*, 617-619.

(125) Sips, H. J., and Hamers, M. N. (1981) Mechanism of the bactericidal action of myeloperoxidase: increased permeability of the *Escherichia coli* cell envelope. *Infect. Immun. 31*, 11-16.

(126) Hogg, D. M., and Jago, G. R. (1970) The antibacterial action of lactoperoxidase. The nature of the bacterial inhibitor. *Biochem. J. 117*, 779-790.

(127) Hosoya, T., and Morrison, M. (1967) A study of the hemoproteins of thyroid microsomes with emphasis on the thyroid peroxidase. *Biochemistry 6*, 1021-1026.

(128) English, A. M., and Tsaprailis. (1995) *Adv. Inorg. Chem. 43*, 79.

(129) English, A. M. (1994) *Encyclopaedia of inorganic chemistry: Iron haem proteins, peroxidases and catalysis*, Vol. 4, Wiley.

(130) Poulos, T. L., Freer, S. T., Alden, R. A., Edwards, S. L., Skogland, U., Takio, K., Eriksson, B., Xuong, N., Yonetani, T., and Kraut, J. (1980) The crystal structure of cytochrome *c* peroxidase. *J. Biol. Chem. 255*, 575-580.

(131) Finzel, B. C., Poulos, T. L., and Kraut, J. (1984) Crystal structure of cytochrome *c* peroxidase refined at 1.7 Å resolution. *J. Biol. Chem. 259*, 13027-13036.

(132) Hiner, A. N., Raven, E. L., Thorneley, R. N., Garcia-Canovas, F., and Rodriguez-Lopez, J. N. (2002) Mechanisms of compound I formation in heme peroxidases. *J. Inorg. Biochem. 91*, 27-34.

(133) Welinder, K. G. (1992) *Current Opinions in Structural Biology 2*, 388-393.

(134) Kimura, S., and Ikeda-Saito, M. (1988) Human myeloperoxidase and thyroid peroxidase, two enzymes with separate and distinct physiological functions, are evolutionarily related members of the same gene family. *Proteins 3*, 113-120.

(135) Picot, D., Loll, P. J., and Garavito, R. M. (1994) The X-ray crystal structure of the membrane protein prostaglandin H2 synthase-1. *Nature 367*, 243-249.

(136) Zeng, J., and Fenna, R. E. (1992) X-ray crystal structure of canine myeloperoxidase at 3 Å resolution. *J. Mol. Biol. 226*, 185-207.

(137) Poulos, T. L., and Fenna, R. E. (1994) *Metal Ions in Biological systems*, Vol. 30, New York.

(138) Furtmuller, P. G., Jantschko, W., Regelsberger, G., Jakopitsch, C., Arnhold, J., and Obinger, C. (2002) Reaction of lactoperoxidase compound I with halides and thiocyanate. *Biochemistry 41*, 11895-11900.

(139) Patterson, W. R., and Poulos, T. L. (1995) Crystal structure of recombinant pea cytosolic ascorbate peroxidase. *Biochemistry 34*, 4331-4341.

(140) Welinder, K. G. (1992) Superfamily of plant, fungal and bacterial peroxidases. *Current Opinion in Chemical Biology 2*, 388-393.

(141) Riley, L. W. (1996) *Tuberculosis*, Little, Brown and Company, Boston.

(142) Welinder, K. G. (1991) Bacterial catalase-peroxidases are gene duplicated members of the plant peroxidase superfamily. *Biochim. Biophys. Acta 1080*, 215-220.

(143) Zamocky, M., Regelsberger, G., Jakopitsch, C., and Obinger, C. (2001) The molecular peculiarities of catalase-peroxidases. *FEBS Lett. 492*, 177-182.

(144) Yamada, Y., Fujiwara, T., Sato, T., Igarashi, N., and Tanaka, N. (2002) The 2.0 angstrom crystal structure of catalase-peroxidase from *Haloarcula marismortui*. *Nature. Struct. Biol. 9*, 691-695.

(145) Carpena, X., Loprasert, S., Mongkolsuk, S., Switala, J., Loewen, P. C., and Fita, I. (2003) Catalase-peroxidase KatG of Burkholderia pseudomallei at 1.7 Å. *J. Mol. Biol. 327*, 475-489.

(146) Bertrand, T., Eady, N. A. J., Jones, J. N., Bodiguel, J., Jesmin, Nagy, J. M., Raven, E. L., Jamart-Gregoire, B., and Brown, K. H. (2004) Crystal Structure of *Mycobacterium tuberculosis* Catalase-Peroxidase. *J. Biol. Chem. 279*, 38991-38999.

(147) Santoni, E., Jakopitsch, C., Obinger, C., and Smulevich, G. (2004) Manipulating the covalent link between distal side tryptophan, tyrosine, and methionine in catalase-peroxidases: an electronic absorption and resonance Raman study. *Biopolymers 74*, 46-50.

(148) Jakopitsch, C., Ivancich, A., Schmuckenschlager, F., Wanasinghe, A., Poltl, G., Furtmuller, P. G., Ruker, F., and Obinger, C. (2004) Influence of the unusual covalent adduct on the kinetics and formation of radical intermediates in *Synechocytic* catalase peroxidase. *J. Biol. Chem. 279*, 46082-46095.

(149) Jakopitsch, C., Auer, M., Ivancich, A., Ruker, F., Furtmuller, P. G., and Obinger, C. (2003) Total conversion of bifunctional catalase-peroxidase (KatG) to monofunctional peroxidase by exchange of a conserved distal side tyrosine. *J. Biol. Chem. 278*, 20185-20191.

(150) Gray, H. B., and Winkler, J. R. (2003) Electron tunneling through proteins. *Q. Rev. Biophys. 36*, 341-372.

(151) Ghiladi, R. A., Medzihradszky, K. F., and Ortiz de Montellano, P. R. (2005) Role of the Met-Tyr-Trp cross link in *Mycobacterium tuberculosis* catalase peroxidase (KatG) as revealed by KatG(M255I). *Biochemistry 44*, 15093-15105.

(152) Bosshard, H. R., Anni, H., and Yonetani, T. (1991) Yeast cytochrome *c* peroxidase, in *Peroxidases in Chemistry and Biology* (Everse, J., Everse, K. E., and Grisham, M. B., Eds.) pp 51-84, CRC Press, Boca Raton.

(153) Erman, J. E. (1998) Cytochrome *c* peroxidase: a model heme protein. *J. Biochem. Mol. Biol. 31*, 307-327.

(154) Altschul, A. M., Abrams, R., and Hogness, T. R. (1940) Cytochrome *c* peroxidase. *J. Biol. Chem. 136*, 777-794.

(155) Poulos, T. L., Freer, S. T., Alden, R. A., Xuong, N., Edwards, S. L., Hamlin, R. C., and Kraut, J. (1978) Crystallographic determination of the heme orientation and location of the cyanide binding site in yeast cytochrome *c* peroxidase. *J. Biol. Chem. 253*, 3730-3735.

(156) Poulos, T. L., and Kraut, J. (1980) The stereochemistry of peroxidase catalysis. *J. Biol. Chem. 255*, 8199-8205.

(157) Hoffman, B. M., Roberts, J. E., Kang, C. H., and Margoliash, E. (1981) Electron paramagnetic and electron nuclear double resonance of the hydrogen peroxide compound of cytochrome c peroxidase. *J. Biol. Chem. 256*, 6556-6564.

(158) Erman, J. E., Vitello, L. B., Mauro, J. M., and Kraut, J. (1989) Detection of an oxyferryl porphyrin pi-cation-radical intermediate in the reaction between hydrogen peroxide and a mutant yeast cytochrome c peroxidase. Evidence for tryptophan-191 involvement in the radical site of compound I *Biochemistry 28*, 7992-7995.

(159) Huyett, J. E., Doan, P. E., Gurbiel, R., Houseman, A. L. P., Sivaraja, M., Goodin, D. B., and Hoffman, B. M. (1995) Compound ES of cytochrome c peroxidase contains a Trp pi-cation radical: characterization by continuous wave and pulsed Q-band external nuclear double resonance spectroscopy *J. Am. Chem. Soc. 117*, 9033-9041.

(160) Houseman, A. L. P., Doan, P. E., Goodin, D. B., and Hoffman, B. M. (1993) Comprehensive explanation of the anomalous EPR spectra of wild-type and mutant cytochrome c peroxidase compound ES *Biochemistry 32*, 4430-4443.

(161) Pelletier, H., and Kraut, J. (1992) Crystal structure of a complex between electron transfer partners, cytochrome c peroxidase and cytochrome c. *Science 258*, 1748-1755.

(162) Chen, G. X., and Asada, K. (1989) *Plant and Cell Phys.30*, 987-998.

(163) Mittler, R., and Zilinskas, B. A. (1991) *Plant Phys. 97*, 962-968.

(164) Kelly, G. J., and Latzko, E. (1979) *Naturwissenschaften 66*, 617-618.

(165) Groden, D., and Beck, E. (1979) *Biochim. Biophys. Acta 546*, 426-435.

(166) Gerbling, K.-P., kelly, G. J., Fischer, K.-H., and Latzko, E. (1984) *J. Plant Phys. 115*, 59-67.

(167) Ohya, T., Morimura, Y., Saji, T., Mihara, T., and Ikawa, T. (1997) *Plant Science 125*, 137-145.

(168) Dalton, D. A., Hanus, F. J., Russell, S. A., and Evans, H. J. (1987) *Plant Physiology 83*, 789-794.

(169) De Gara, L., de Pinto, M. C., and Arrigoni, O. (1997) *Physiologia Plantarum 100*, 894-900.

(170) Elia, M. R., Borracino, G., and Dipierro, S. (1992) *Plant Science 85*, 17-21.

(171) Koshiba, T. (1993) *Plant and Cell Phys. 34*, 713-721.

(172) Ishikawa, T., Takeda, T., and Shigeaka, S. (1996) *Plant Science 120*, 11-18.

(173) Amako, K., Chen, G.-X., and Asada, K. (1994) *Plant and Cell Phys. 35*, 497-504.

(174) Kvaratskhelia, M., Winkel, C., and Thorneley, R. N. F. (1997) *Plant Phys.y 114*, 1237-1245.

(175) Battistuzzi, G., D'Onofrio, M., Loschi, L., and Sola, M. (2001) *Arch. Biochem. Biophys.388*, 100-112.

(176) Tanaka, K., Takeuchi, E., Kubo, A., Sakaki, T., Haraguchi, K., and Kawamura, Y. (1991) *Arch. Biochem. Biophys. 286*, 371-375.

(177) Yoshimura, K., Ishikawa, T., Nakumura, Y., Tamoi, M., Takeda, T., Tada, T., Nishimura, K., and Shigeaka, S. (1998) *Arch. Biochem. Biophys. 353*, 55-63.

(178) Preger, V., Pesaresi, A., Pupillo, P., and Trost, P. (2001) *Protoplasma 217*, 137-145.

(179) Ushimara, T., Maki, Y., Sano, S., Koshiba, K., Asada, K., and Tsuji, H. (1997) *Plant and Cell Phys. 38*, 541-549.

(180) Miyake, C., Cao, W.-H., and Asada, K. (1993) *Plant and Cell Phys. 34*, 881-995.

(181) Nakano, Y., and Asada, K. (1987) *Plant and Cell Phys. 28*, 131-140.

(182) Gillham, D. J., and Dodge, A. D. (1986) *Planta 167*, 246-251.

(183) Jablonski, P. P., and Anderson, J. W. (1982) *Plant Phys. 69*, 1407-1413.

(184) Meneguzzo, S., Sgherri, C. L. M., Navari-Izzo, F., and Izzo, R. (1998) *Physiologia Plantarum 104*, 735-740.

(185) Wada, K., Tada, T., Nakamura, Y., Yabuta, Y., Yoshimura, K., Takeda, T., Shigoeka, S., and Nishimura, K. (2002) crystallization and preliminary x-ray diffraction analysis of chloroplastic ascorbate peroxidase of tobacco plants. *Acta Crystallographica D58*, 559-561.

(186) Chen, G. X., Sano, S., and Asada, K. (1992) *Plant and Cell Phys. 33*, 109-116.

(187) Kvaratskhelia, M., Winkel, C., Naldrett, M. T., and Thorneley, R. N. F. (1999) A novel high activity cationic ascorbate peroxidase from tea -A class III peroxidase with unusual substrate specificity. *J. Plant Phys. 154*, 273-282.

(188) Heering, H. A., Jansen, M. A. K., Thorneley, R. N. F., and Smulevich, G. (2001) Cationic ascorbate peroxidase isozyme II from tea: structural insights in to the heme pocket of a unique hybrid enzyme. *Biochemistry 40*, 10360-10370.

(189) Mathews, M. C., Summers, C. B., and Felton, G. W. (1997) *Arch. Ins. Biochem. Phys. 34*, 57-68.

(190) Tel-Or, E., Huflejt, M. E., and Packer, L. (1986) *Arch. Biochem. Biophys. 246*, 396-402.

(191) Shigeoka, S., Nakano, Y., and Kitaoka, S. (1980) *Arch. Biochem. Biophys. 201*, 121-127.

(192) Takeda, T., Yoshimura, K., Ishikawa, T., and Shigeaka, S. (1998) *Biochimie 80*, 295-301.

(193) Takeda, T., Yoshimura, K., Yoshii, M., Kanahoshi, H., Miyasaka, H., and Shigeoka, S. (2000) *Arch. Biochem. Biophys. 376*, 82-90.

(194) Wada, N., Kinoshita, S., Matsuo, M., Amako, K., Miyake, C., and Asada, K. (1998) *Biochem. Biophys. Res. Comm. 242*, 256-261.

(195) Mittler, R., and Zilinskas, B. A. (1992) Molecular cloning and characterization of a gene encoding pea cytosolic ascorbate peroxidase *J. Biol. Chem. 267*, 21802-21807.

(196) Mittler, R., and Zilinskas, B. A. (1991) Molecular cloning and nucleotide sequence analysis of a cDNA encoding pea cytosolic ascorbate peroxidase *FEBS Lett. 289*, 257-259.

(197) Dalton, D. A., del Castillo, L. D., Kahn, M. L., Joyner, S. L., and Chatfield, J. M. (1996) Heterologous expression and charaterization of soybean cytosolic ascorbate peroxidase. *Arch. Biochem. Biophys. 328*, 1-8.

(198) Foyer, C. H., and Mullineaux, P. M. (1998) The presence of dehydroascorbate and dehydroascorbate reductase in plant tissues. *FEBS Lett. 425*, 528-529.

(199) Raven, E. L. (2003) Understanding functional diversity and substrate specificity in haem peroxidases: what can we learn from ascorbate peroxidase? *Nat. Prod. Rep. 20*, 367-381.

(200) Celik, A., Cullis, P. M., Sutcliffe, M. J., Sangar, R., and Raven, E. L. (2001) Engineering the active site of ascorbate peroxidase. *Eur. J. Biochem. 268*, 78-85.

(201) Kelley, P. M., Jalukar, V., and Njus, D. (1990) Rate of electron transfer between cytochrome b561 and extravesicular ascorbic acid. *J. Biol. Chem.* *265*, 19409-19413.

(202) Sharp, K. H., Mewies, M., Moody, P. C., and Raven, E. L. (2003) Crystal structure of the ascorbate peroxidase-ascorbate complex. *Nat. Struct. Biol. 10*, 303-307.

(203) Jespersen, H. M., Kjaersgard, I. V. H., Ostergaard, L., and Welinder, K. G. (1997) From sequence analysis of three novel ascorbate peroxidases from *Arabidopsis thaliana* to structure, function and evolution of seven types of ascorbate peroxidase. *Biochem. J. 326*, 305-310.

(204) Patterson, W. R., Poulos, T. L., and Goodin, D. B. (1995) Identification of a porphyrin pi cation radical in ascorbate peroxidase compound I. *Biochemistry 34*, 4342-4345.

(205) Marquez, L. A., Quitoriano, M., Zilinskas, B. A., and Dunford, H. B. (1996) Kinetic and spectral properties of pea cytosolic ascorbate peroxidase. *FEBS Lett. 389*, 153-156.

(206) Bonagura, C. A., Sundaramoorthy, M., Bhaskar, B., and L, P. T. (1999) The effects of an engineered cation site on the structure, activity and EPR properties of cytochrome *c* peroxidase. *Biochemistry 38*, 5538-5545.

(207) Bonagura, C. A., Sundaramoorthy, M., Pappa, H. S., Patterson, W. R., and Poulos, T. L. (1996) An engineered cation site in cytochrome *c* peroxidase alters the reactivity of the redox active tryptophan. *Biochemistry 35*, 6107-6115.

(208) Bhaskar, B., Bonagura, C. A., Li, H., and Poulos, T. L. (2002) Cation-induced stabilisation of the engineered cation-binding loop in cytochrome *c* peroxidase (CcP). *Biochemistry 41*, 2684-2693.

(209) Bonagura, C. A., Bhaskar, B., Sundaramoorthy, M., and Poulos, T. L. (1999) Conversion of an engineered potassium-binding site into a calcium-selective site in cytochrome *c* peroxidase. *J. Biol. Chem. 274*, 37827-27833.

(210) Sharp, K. H., Mewies, M., Moody, P. C. E., and Raven, E. L. (2003) The crystal structure of the ascorbate peroxidase/ascorbate complex. *Nat. Struct. Biol. 10*, 303-307.

(211) Mauro, J. M., Fishel, L. A., Hazzard, J. T., Meyer, T. E., Tollin, G., Cusanovich, M. A., and Kraut, J. (1988) Tryptophan-191-phenylalanine, a proximal-side mutation in yeast cytochrome c peroxidase that strongly affects the kinetics of ferrocytochrome c oxidation. *Biochemistry 27*, 6243-6256.

(212) Lad, L., Mewies, M., and Raven, E. L. (2002) Substrate binding and catalytic mechanism in APX: evidence for two ascorbate binding sites. *Biochemistry 41*, 13774-13781.

(213) Patterson, W. R., Poulos, T. L., and Goodin, D. B. (1995) Identification of a porphyrin π–cation radical in ascorbate peroxidase compound I. *Biochemistry 34*, 4342-4345.

(214) Fayadat, L., Niccoli-Sire, P., Lanet, J., and Franc, J.-L. (1999) Role of heme in intramolecular trafficking of thyroperoxidase and involvement of H_2O_2 generated at the apical surface of thyroid cells in autocatalytic covalent heme binding. *J. Biol. Chem. 274*, 10533-10538.

(215) Zheng, Y.-M., Baer, B. R., Kneller, B., Henne, K. R., Kunze, K. L., and Rettie, A. E. (2003) Covalent heme binding to CYP4B1 via Glu310 and a carbocation porphyrin intermediate. *Biochemistry 42*, 4601-4606.

(216) Baer, B. R., Kunze, K. L., and Rettie, A. E. (2007) Mechanism of Formation of the Ester Linkage between Heme and Glu310 of CYP4B1: (18)O Protein Labeling Studies. *Biochemistry 46*, 11598-115605.

(217) Colas, C., and Ortiz de Montellano, P. R. (2004) Horseradish peroxidase mutants that autocatalytically modify their heme prosthetic group. *J. Biol. Chem. 279*, 24131-24140.

(218) Metcalfe, C. L., Ott, M., Patel, N., Singh, K., Mistry, S. C., Goff, H. M., and Raven, E. L. (2004) Autocatalytic formation of green heme: evidence for H_2O_2-dependent formation of a covalent methionine-heme linkage in ascorbate peroxidase. *J. Am. Chem. Soc. 126*, 16242-8.

Chapter 2

Autocatalytic formation of a covalent link between Trp41 and the heme in APX

2.1   Introduction

In contrast to other heme proteins, heme peroxidases can react with hydrogen peroxide to form a stable oxidized intermediate, known as Compound I. Peroxidase catalytic turnover (Equations 2.1 – 2.3) proceeds through two detectable intermediates (*1*), known as Compound I and Compound II:

$$\text{Peroxidase (Fe}^{III},\text{P)} + \text{H}_2\text{O}_2 \rightarrow \text{Peroxidase (Fe}^{IV}=\text{O,P}^{\bullet+}) + \text{H}_2\text{O} \qquad ...(2.1)$$

$$\text{Peroxidase (Fe}^{IV}=\text{O, P}^{\bullet+}) + \text{S}_{red} \rightarrow \text{Peroxidase (Fe}^{IV}=\text{O,P)} + \text{S}_{ox} \qquad ...(2.2)$$

$$\text{Peroxidase (Fe}^{IV}=\text{O,P)} + \text{S}_{red} + 2\text{H}^+ \rightarrow \text{Peroxidase (Fe}^{III},\text{P)} + \text{S}_{ox} + \text{H}_2\text{O} \qquad ...(2.3)$$
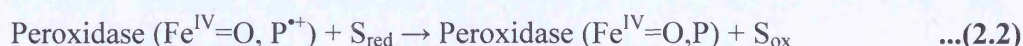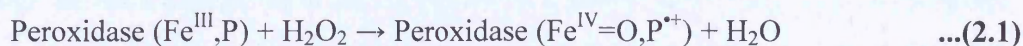
where S_{red} & S_{ox} are the reduced and oxidised forms of the substrate, S; Fe^{III},P corresponds to the peroxidase resting-state; $\text{Fe}^{IV}=\text{O,P}^{\bullet+}$ and $\text{Fe}^{IV}=\text{O,P}$ are the intermediates Compound I and Compound II, respectively. Both Compound I and Compound II are oxyferryl species, $\text{Fe}^{IV}=\text{O,P}$. Compound I stores the second oxidising equivalent either as a porphyrin π-cation radical, $\text{P}^{\bullet+}$ or as a protein radical (*1*).

As mentioned in Chapter 1, the three most prominent members of the class I superfamily of heme peroxidases (*2*) are cytochrome *c* peroxidase (C*c*P), ascorbate peroxidase (APX) and the bifunctional catalase-peroxidase (KatG) enzymes. These class I enzymes are distinguished from other peroxidases in the superfamily by the presence of a distal tryptophan residue, in place of the more usual phenylalanine residue, and a second active site tryptophan adjacent to the proximal histidine ligand, Figure 2.1.
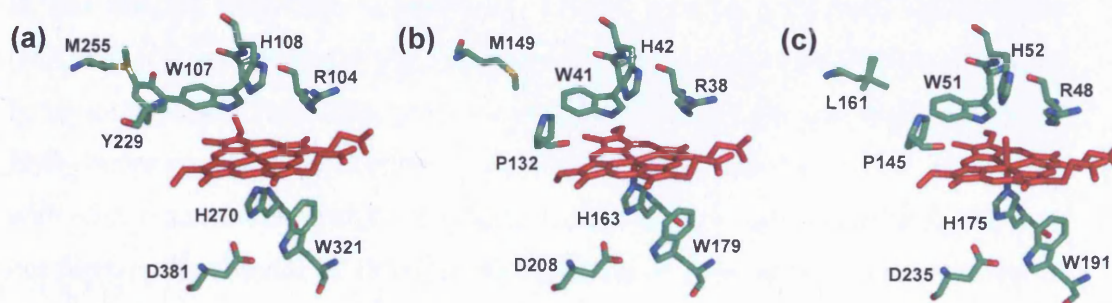
Figure 2.1: Comparison of the active site structures of (a) *mt*KatG (PDB accession code 1SJ2), (b) rsAPX (1OAG) and (c) C*c*P (2CYP), showing the covalent links between residues W107, Y229 and M255 in mtKatG and the residues occupying the equivalent positions in rsAPX and C*c*P.

The catalase-peroxidases contain a unique structural feature, however, that distinguishes them from all other heme peroxidases: in all catalase-peroxidase enzymes for which crystal structures have appeared (3-5), a covalently-bound Trp-Tyr-Met cross link has been observed (involving Trp107, Tyr229 and Met255 in the *M. tuberculosis* KatG enzyme, Figure 2.1a). The formation of the Trp-Tyr-Met link is therefore believed to be a feature of all KatGs and is proposed (6, 7) to be formed through an autocatalytic mechanism involving reaction with H_2O_2. The tryptophan and tyrosine residues are essential for complete formation of the link, but replacement of the methionine is tolerated if both tryptophan and tyrosine are present (6-8). The functional role of this covalent link is not clearly established, but the fact that it is not observed in the monofunctional peroxidases (APX and CcP), Figures 2.1b and 2.1c, suggests that it might be connected with catalatic activity in KatG. Mutagenesis data support this suggestion (8-12).

A key feature in the proposed mechanism (6, 7) of formation of the Trp-Tyr-Met link, is the formation of a protein radical at the distal tryptophan residue. At present, it is not clear whether other, related heme proteins are able to support oxidation of the distal tryptophan residue. The only example of protein radical formation in the class I peroxidases is in cytochrome *c* peroxidase, which uses a protein radical as a part of its reaction mechanism (13). More than forty years ago, CcP was suggested to form a stable protein radical in Compound I (traditionally known as Compound ES) (14) and two decades later proximal Trp191 was unambiguously identified as the site of the radical species (15). Most other peroxidases, including APX and the KatG enzymes, are known to form porphyrin π-cation radicals during their catalytic cycle (2, 16, 17).

In this chapter, electronic spectroscopy, HPLC analyses and mass spectrometry (MALDI-TOF and MS/MS) have been used to show that a covalent link from the heme to the distal Trp41 can occur on exposure of ascorbate peroxidase (APX) to H_2O_2 under non-catalytic conditions. Parallel analyses with the W41A variant and with APX reconstituted with deuteroheme clearly indicate that the covalent link does not form in the absence of either Trp41 or the heme vinyl groups. The presence of substrate also precludes formation of the link. Formation of a protein radical at Trp41 is implicated, in a reaction mechanism that is analogous to that proposed (7) for formation of a covalent Trp-Tyr-Met link in the closely related catalase-peroxidase

(KatG) enzymes. Data for the S207E variant indicate that formation of a covalent link between Trp41 and the heme can occur not only in the wild type enzyme.

Collectively, the data suggest that radical formation at the distal tryptophan position is not an exclusive feature of the KatG enzymes and may be used more widely across other members of the class I heme peroxidase family. Overall, this gives further insight into the factors affecting radical formation and stability across plant peroxidases.

2.2   Results

2.2.1   Expression and purification

2.2.1.1   Expression system

Samples of rsAPX were prepared from *E. coli* SG1300 cells (containing the pREP4 vector) incorporating a pQE30-derived expression vector and purified as described previously (*18*), using the incorporated His-tag (six histidine residues on the C-terminal end of the protein). Samples (~30 mg/ml) of rsAPX were stored in deionised water in 100 μl aliquots at -80 °C. Concentrations of enzyme were determined using the molar absorption coefficient for rsAPX (ε_{407} = 107 mM^{-1}cm^{-1} (*19*)).

2.2.1.2   Affinity / Gel-filtration chromatography

Protein samples were purified by means of affinity chromatography, using a Ni^{2+}-nitrilotriacetic acid (NTA) agarose column (Qiagen). The final elution from the Ni^{2+}-nitrilotriacetic acid agarose column (Qiagen) was using pH (4.2) rather than using imidazole. The protein was then further purified by Fast Protein Liquid Chromatography, FPLC (Figure 2.2).
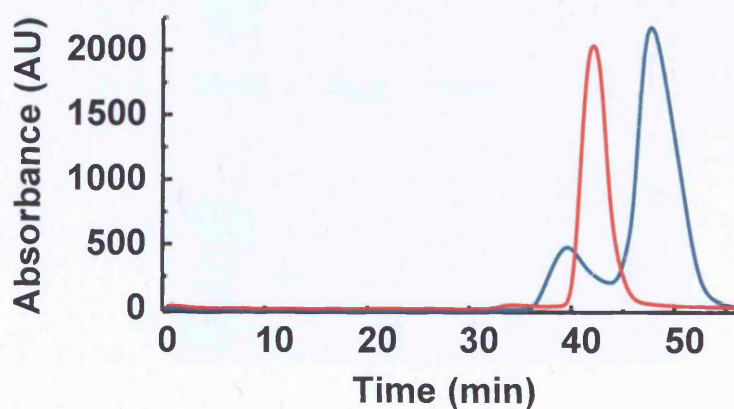
Figure 2.2: Absorbance trace of rsAPX at 280 nm before (blue line) and after (red line) FPLC purification. Conditions: Superdex 75 HR 10/30 gel filtration column, 150 mM potassium phosphate, pH 7.0, 150 μl injection of purified rsAPX, run time 60 minutes.

2.2.1.3 Reinheitzahl values

The purity of rsAPX was primarily assessed by calculating the R_z values. The ratio of the absorbance of the Soret peak and that of the protein peak at 280 nm is the Reinheitzahl (R_z) number and relates to the purity of the peroxidase. The higher the R_z number the higher the purity. The absorbance at 280 nm is due to aromatic residues with a contribution from the heme and the Soret peak is due to the heme. rsAPX with an R_z value greater than two is considered pure (*20*).

2.2.1.4 SDS-PAGE analysis

Protein purity was also monitored using SDS-PAGE gel electrophoresis. The SDS-PAGE gel showed only one band after the purification procedure was carried out. A typical SDS-PAGE gel for rsAPX is shown in Figure 2.3 and was characteristic for all batches of protein expressed.
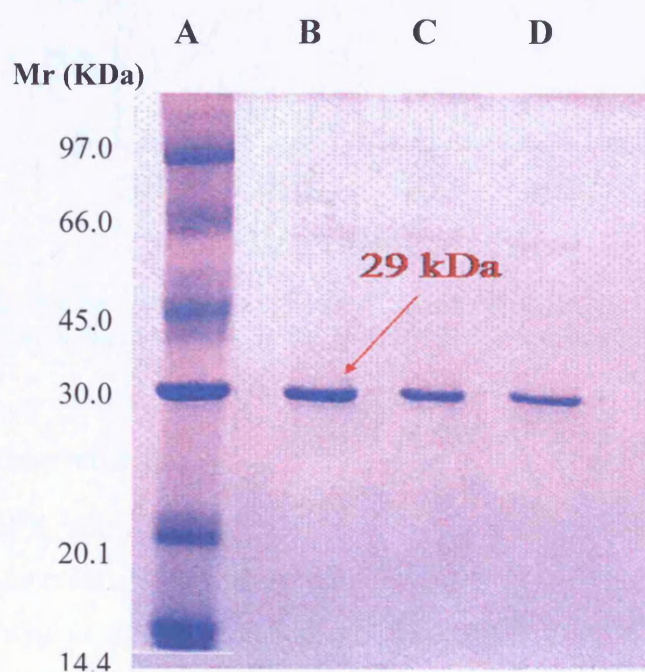
Figure 2.3: A 15% SDS-PAGE gel of rsAPX. From the left: marker standards (lane A), rsAPX from a typical expression and purification procedure (lanes B-D).

2.2.2   Electronic absorption spectra

The Soret band absorption coefficient value for recombinant forms of wild-type soybean cytosolic APX has been reported as 107 mM^{-1} cm^{-1} (*18*).

Analysis of UV-visible spectra for rsAPX (100 mM potassium phosphate, pH 7.0, 25 °C) reveals wavelength maxima at 407, 525 and ~636 nm (Figure 2.4), which is consistent with the values reported previously (*19*).
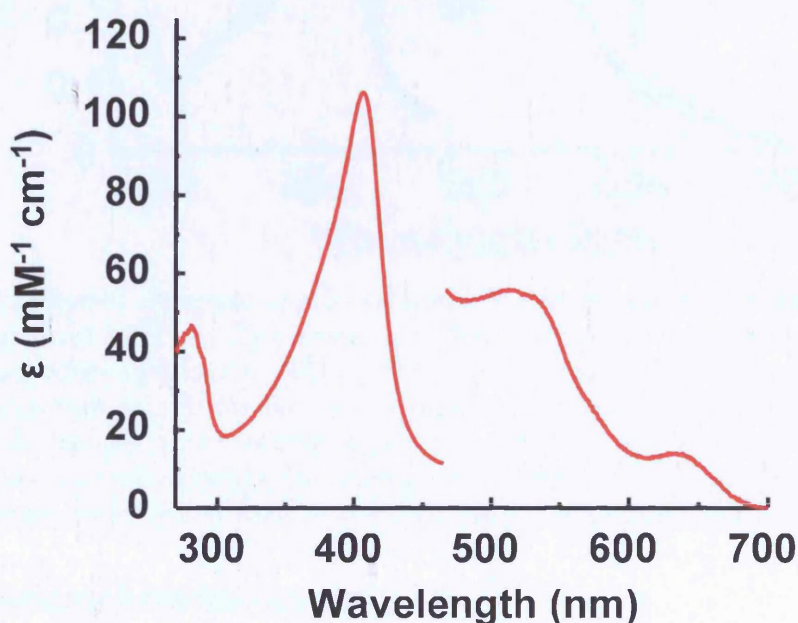
Figure 2.4: UV-visible absorption spectra of ferric rsAPX. The visible region has been multiplied by a factor of 5. Conditions: 100 mM potassium phosphate buffer, pH 7.0, 25 °C.

2.2.3   Reaction with H$_2$O$_2$

Reaction of rsAPX with 6 equivalents of H$_2$O$_2$ resulted in the initial formation of a Compound I intermediate, as observed previously (*21*). This is followed by immediate conversion of this Compound I to a more stable Compound II-type species, Figure 2.5. This latter species then decays over a period of ~8 hours to a final product that has a spectrum that is similar but not identical to that of rsAPX, Figure 2.5. The activity of rsAPX against ascorbic acid was monitored before and after reaction with H$_2$O$_2$ under the conditions described above. Values for k_{cat} after reaction with H$_2$O$_2$ were essentially unchanged (k_{cat} = 275 ± 67 s^{-1}) from those of the wild type enzyme (k_{cat} = 272 ± 32 s^{-1} (*21*)).
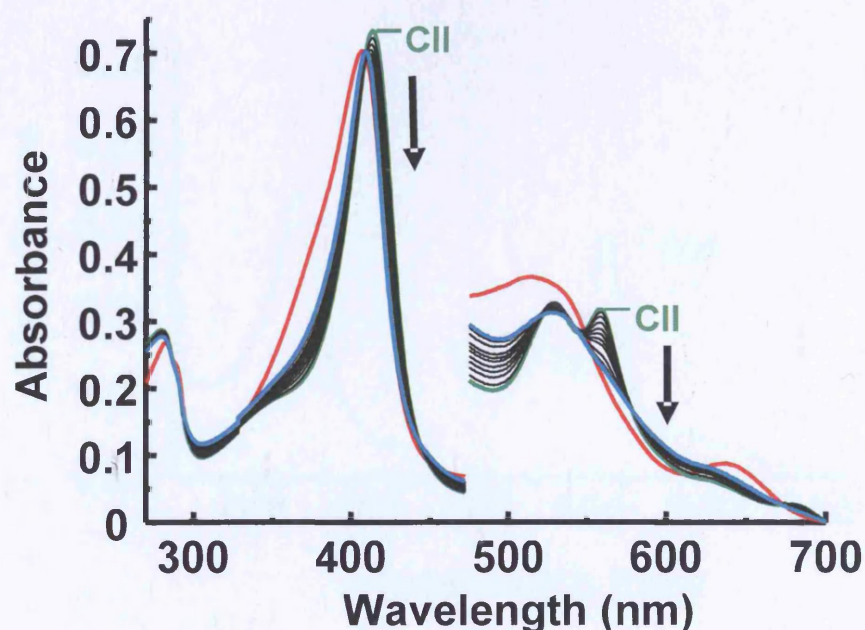
Figure 2.5: Selected electronic spectra collected during the reaction of ferric rsAPX with 6 equivalents of H_2O_2. Conversion of rsAPX (red line) to the initial Compound II-type intermediate (green line, indicated as CII on the Figure) is observed, followed by conversion back to a ferric-like species (blue line). Intermediate spectra between CII and ferric-like are shown as black lines. The total reaction time was 8 hours. The visible region has been multiplied by a factor of 5. Sample conditions: [Enzyme] = 5 μM, [Hydrogen peroxide] = 30 μM, 100 mM potassium phosphate, pH 7.0, 25 °C.

2.2.4   Pyridine hemochromagen assay

A pyridine hemochromagen assay was carried out on rsAPX both before and after reaction with H_2O_2. For rsAPX before treatment with H_2O_2, the spectrum of the reduced pyridine hemochromagen complex obtained in this way showed a maximum at 556 nm, Figure 2.6. In this experiment, complete extraction of the heme from the protein is observed and the spectrum of the hemochromagen complex is consistent with a non-covalently bound heme structure, in which neither heme vinyl group is modified (22). When the same experiment was carried out with rsAPX after treatment with H_2O_2, the peak was shifted to 553 nm, Figure 2.6. These spectroscopic changes are diagnostic of covalent attachment to one of the two vinyl groups on the heme (23).
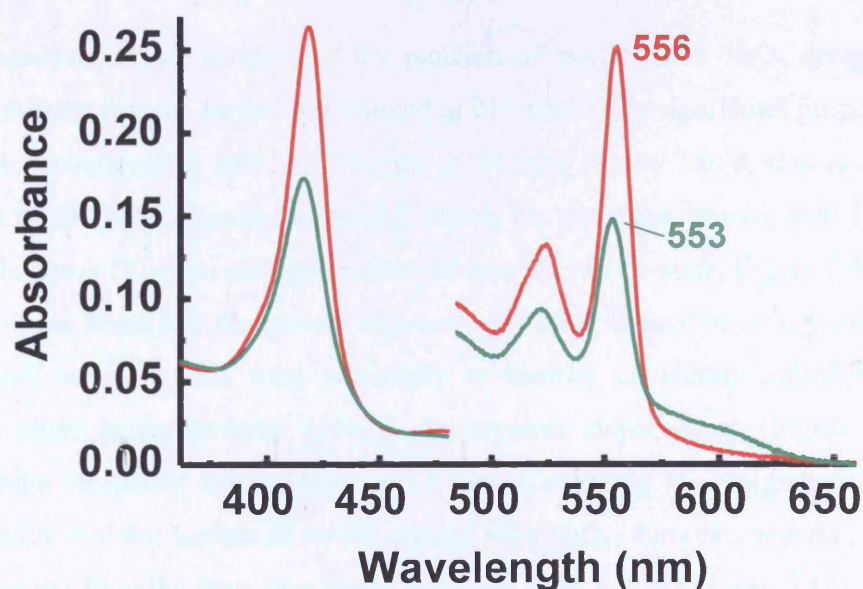
Figure 2.6: Spectra of the reduced pyridine hemochromagen complexes of rsAPX before (red line) and after (green line) reaction with H_2O_2.

2.2.5 Acidified butanone extraction

An acid butanone extraction after reaction of rsAPX with H_2O_2 did not remove all the heme from the protein, Figure 2.7b; which is a clear indication of covalent attachment of some proportion of the heme to the protein; in contrast, control experiments with rsAPX before reaction with H_2O_2 showed complete extraction of heme into the organic layer, Figure 2.7a. These effects were examined in more detail below.
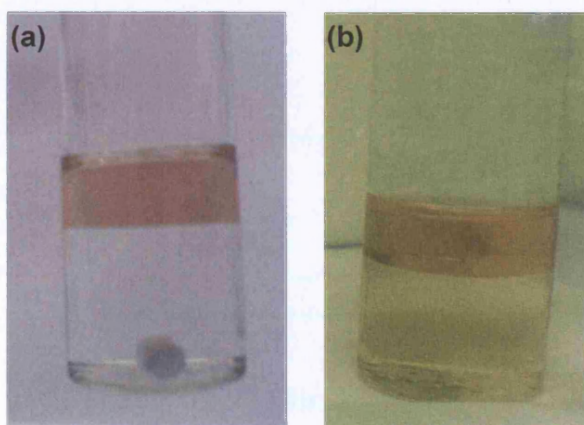
Figure 2.7: Acidified butanone extraction on rsAPX before (a) and after (b) reaction with H_2O_2.

2.2.6   HPLC analysis

HPLC analysis of the product of the reaction of rsAPX with H_2O_2 (prepared as above) showed that the protein (monitored at 215 nm) and a significant proportion of the heme (monitored at 398 nm) co-elute at 24 min, Figure 2.8c,d; this is in direct contrast to the HPLC profile of rsAPX which has not been treated with H_2O_2, in which the heme (11 min) and the protein (24 min) do not co-elute, Figure 2.8a,b. Co-elution of the heme and the protein fragments is a clear indication of covalent heme attachment and has been used previously to identify covalently linked heme in various other heme proteins (24-29). In separate experiments (Figure 2.9), a commercial sample of hemin eluted at 11 min, confirming the assignment for free heme above. For the sample of rsAPX treated with H_2O_2, there is a second peak that elutes earlier (4 min) than free heme (labelled with a * in Figure 2.8c). This is indicative of a hydroxylated heme product (25), and a similar assignment is proposed here. MALDI-TOF analysis of this heme fragment confirmed this assignment: a mass of 650 Da was observed (Figure 2.10), which is consistent with a doubly hydroxylated heme species. Non-specific hydroxylation of heme groups has been reported in other peroxidase systems (27, 30).
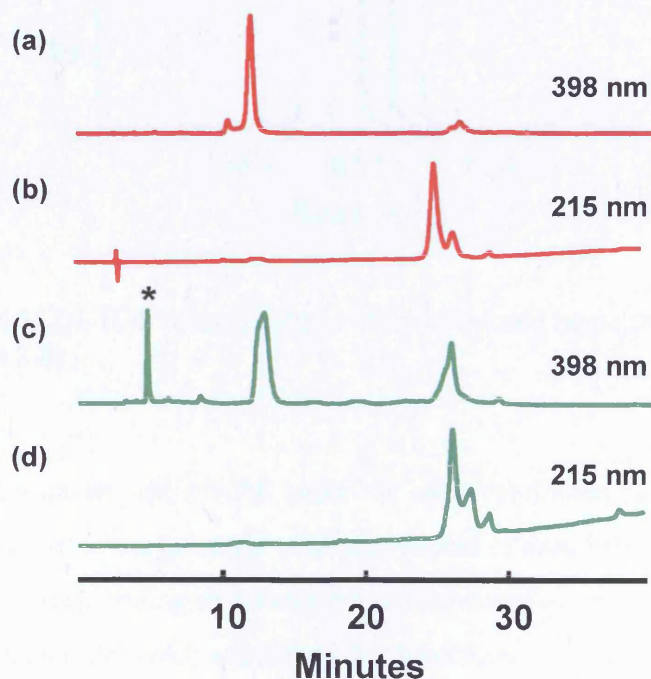
Figure 2.8: HPLC analyses of rsAPX before and after reaction with H_2O_2 monitored at 398 nm and 215 nm. (a,b) rsAPX before reaction with H_2O_2, (c,d) rsAPX after reaction with H_2O_2.
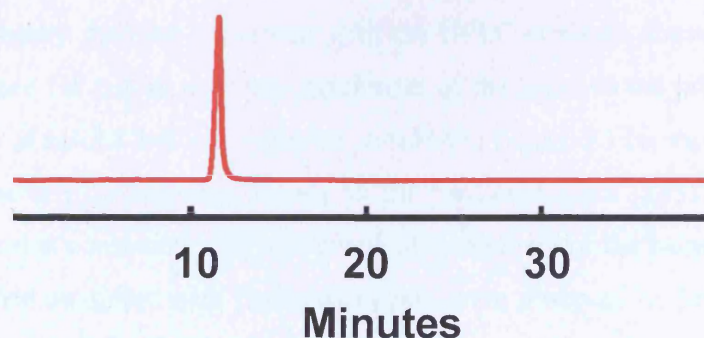
Figure 2.9: HPLC analyses of a commercial sample of free heme.
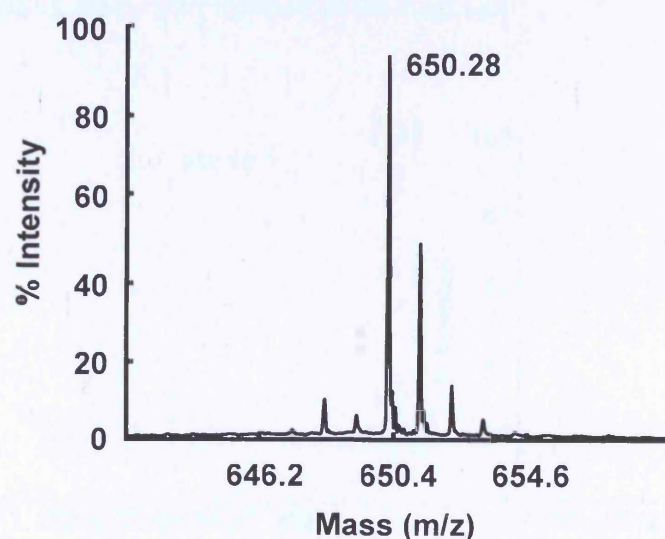
Figure 2.10: MALDI-TOF mass spectrum of hydroxylated heme fragment, eluting at 4 min in Figure 2.8c.

In separate experiments with rsAPX under the same conditions as those used above for Figure 2.8c,d but in the presence of a large excess of ascorbate, it was shown that no HPLC peak corresponding to protein-bound heme was observed at ~24 min. This indicates that under turnover conditions no formation of covalently-bound heme occurs.

2.2.7 MALDI-TOF analysis before and after reaction with H_2O_2

Mass spectrometry data are consistent with the HPLC analyses above and provided further evidence for partial covalent attachment of the heme to the protein. MALDI-TOF analysis of rsAPX before treatment with H_2O_2, Figure 2.11a, showed a mass of 28312.0 Da which corresponds closely to the predicted mass (28318.9 Da) of the apo-protein and is consistent with non-covalent attachment of the heme to the protein in rsAPX. After treatment with H_2O_2, two peaks were observed in the MALDI-TOF spectrum, Figure 2.11b. The first is at 28320.6 Da, which is consistent with the mass of the apo-protein (as above). The second peak is at 28954.3 Da, which corresponds to an increase in mass of 634 Da over the apo-protein, and is consistent with covalent attachment of the heme (616 Da) to the protein. The additional mass of 18 amu is assigned as arising from hydroxylation of the fragment.
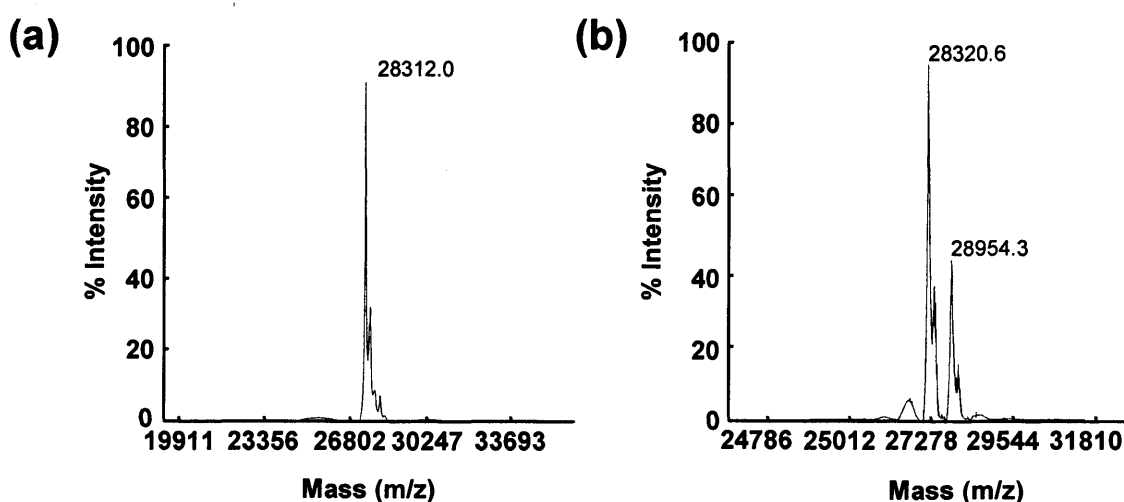
Figure 2.11: MALDI-TOF mass spectrum of rsAPX before (a) and after (b) reaction with 6 equivalents of H_2O_2.

2.2.8 Crystal screens on rsAPX and soaks of crystals with H_2O_2

To gain some insight into the exact position of covalent link formation between the heme and the protein backbone of rsAPX, crystals of the protein were soaked in H_2O_2 and the crystallographic data were analysed. Examination of the electron density for rsAPX, soaked with H_2O_2, around Trp41 indicates that there is positive F_o - F_c density close to the γ-carbon of Trp41 (Figure 2.12). Although the extra density could not account for the presence of a hydroxyl group or give proof of covalent

attachment to the heme, it gave indication of some possible modification at this position [a].
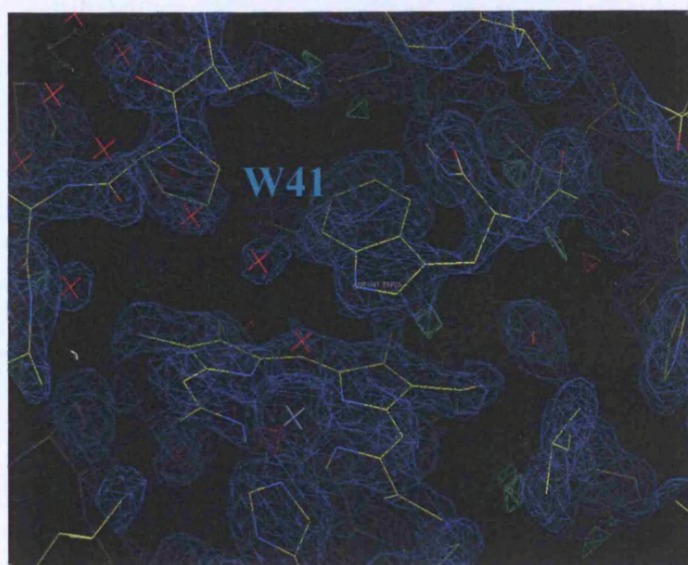
Figure 2.12: Active site of rsAPX crystals soaked in H_2O_2, showing the electron density around atoms and the observed difference density. $2F_o - F_c$ electron density is shown in blue and positive $F_o - F_c$ electron density is shown in green.

2.2.9   Tryptic digest and MALDI-TOF mass spectrometry

To establish the nature of the heme-protein covalent link, tryptic digestion of the product of the reaction of rsAPX with H_2O_2 was carried out and HPLC was used to isolate heme-containing peptide fragments (*i.e.* showing both heme and protein absorbancies) from the resulting peptide mixture, Figure 2.13.

There were three peaks with significant absorbance at 398 nm. The MALDI-TOF mass spectrum of the product eluting at 35.1 min gave a mass of 616 Da, indicating that this HPLC peak corresponds to free heme species. MALDI-TOF mass spectrometry of the peptide fragments eluting at 26.4 and 27.5 min both gave spectra with identical masses of 1863.9 Da, indicating that both HPLC peaks are assigned to a single peptide (Figure 2.14).

The mass of 1863.9 Da observed for this fragment, Figure 2.14, is 16 Da higher than the calculated mass of 1848 Da expected for the $L^{39}AW^{41}HSAGTFDK^{49}$ peptide fragment containing heme covalently bound to Trp41.

---

[a] Data analyses was carried out by Dr Peter Moody at the X-ray laboratories of the Department of Biochemistry.
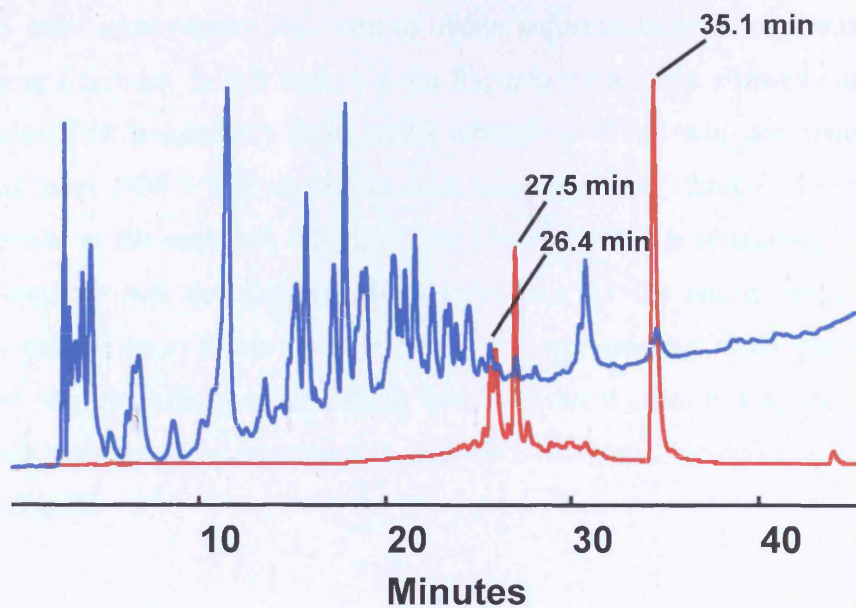
Figure 2.13: HPLC analyses of a tryptic digest of rsAPX after reaction with H_2O_2, monitored at 215 nm (blue line) and 398 nm (red line). Elution times of heme-containing peptides (26.4 and 27.5 min) as well as free heme (35.1 min) are indicated.
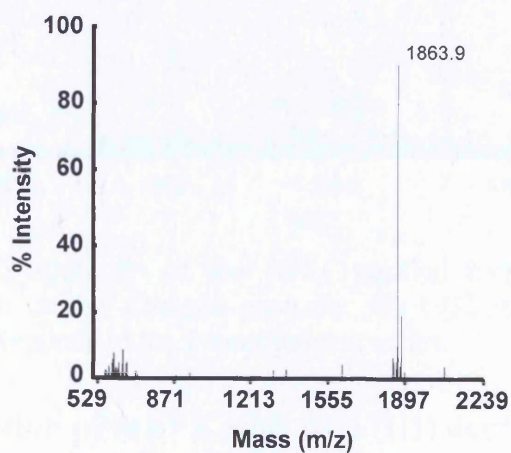
Figure 2.14: MALDI-TOF mass spectrum of the HPLC-purified heme-containing peptide fragment obtained after reaction of rsAPX with H_2O_2.

2.2.10 MS/MS analysis of heme-containing peptide fragment

MS/MS mass spectrometry was used to obtain sequence information for this heme-containing fragment. In this case, a y-ion fragmentation series allowed amino acids to be identified sequentially from His42 through to Thr46 with the remaining C-terminal mass (409.1 Da) consistent with residues Phe47 through Lys49, which corresponds to the sequence HSAGTFDK, Figure 2.15. The remaining N-terminal mass, together with the absence of fragment ions for the amino acids (LAW[41]) indicate that the heme forms a covalent cross link with this part of the peptide. Since Leu and Ala are unlikely to be able to form a covalent cross link to the heme, the data are interpreted as being consistent with the formation of a covalent link from the heme toTrp41.
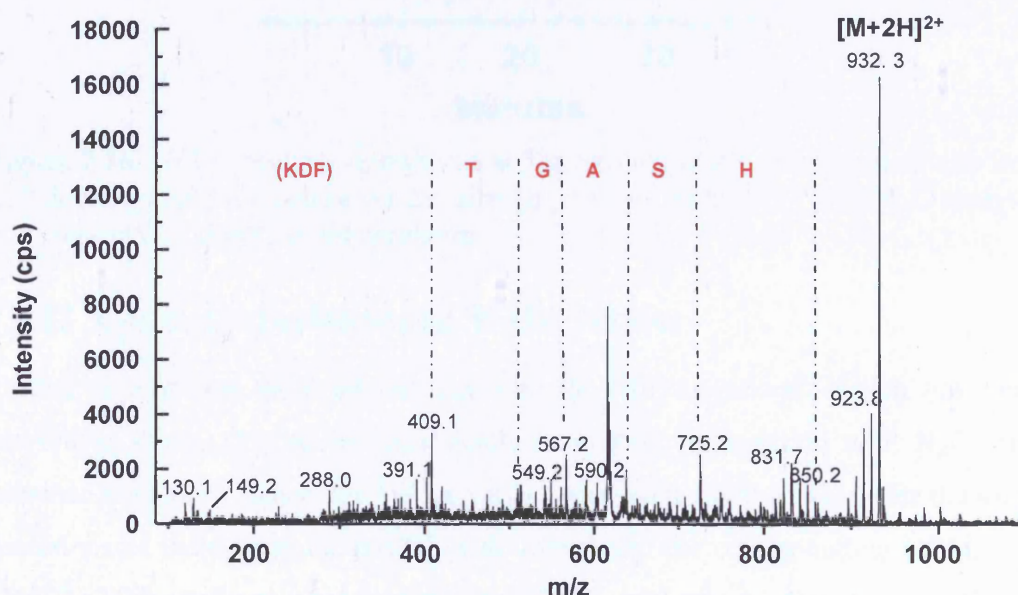
Figure 2.15: MS/MS spectrum of the HPLC-purified heme-containing peptide fragment showing the doubly charged precursor ion (932.56 Da). The annotated peptide sequence corresponds to the y-ion fragment series.

2.2.11 Reconstitution of rsAPX with iron (III) deuteroporphyrin IX chloride and reaction with H_2O_2

To provide further information on the nature of the covalent attachment, a sample of apo-rsAPX was reconstituted with iron(III) deuteroporphyrin, in which hydrogen atoms replace the 2- and 4-vinyl groups, and subsequently reacted with H_2O_2 as above. No peak corresponding to covalently bound heme was observed by HPLC,

because heme was released from the protein and eluted at 5 min both before (Figure 2.16a) and after (Figure 2.16b) reaction with H_2O_2. A commercial sample of deuteroheme was also shown to elute at 5 min (Figure 2.16c). This indicates that a vinyl group is necessary for formation of a covalent link with the protein.
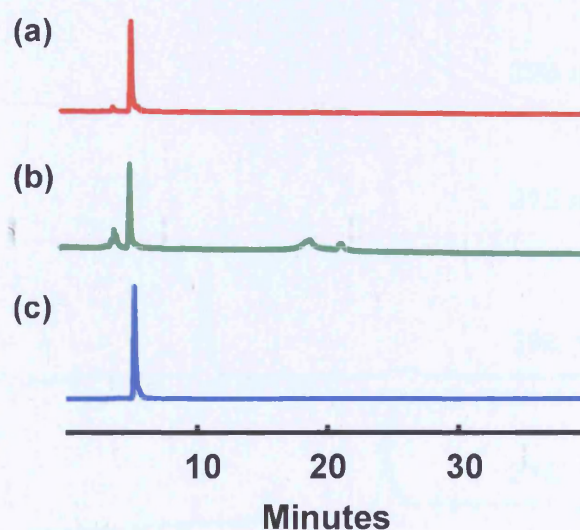
Figure 2.16: HPLC analysis (monitored at 398 nm) of rsAPX reconstituted with iron (III) deuteroporphyrin, before (a) and after (b) reaction with H_2O_2; (c) HPLC analysis of a commercial sample of deuteroheme.

2.2.12 Control experiments on W41A variant

Further experiments were carried out with the W41A variant[b], which has been previously shown (31) to be catalytically competent for reaction with H_2O_2 and substrate oxidation. Hence, the W41A variant was reacted with H_2O_2 under the same conditions as those used for rsAPX (*vide supra*) and the corresponding HPLC and MALDI-TOF analyses were carried out. HPLC analysis prior to treatment with H_2O_2, Figure 2.17a,b, showed that the heme and the protein elute separately as for rsAPX under the same conditions. However, on treatment with H_2O_2 no change in the HPLC elution profile was observed, indicating that no covalent attachment of the heme to the protein had occurred in this case, Figure 2.17c,d. In addition, and in contrast to rsAPX, there is no evidence for formation of a hydroxylated heme species in the HPLC analyses.

MALDI-TOF analyses, Figure 2.18; confirmed these observations since essentially identical molecular masses are observed for W41A before (28207.1 Da) and after

---

[b] W41A variant was kindly provided by Miss Sandip Badyal.

(28202.5 Da) treatment with H_2O_2 [c]. Both of these values are in good agreement with the calculated mass for the apo-W41A variant (28203.7 Da).

These observations further support the initial hypothesis that Trp41 is essential for covalent link formation on treatment of rsAPX with H_2O_2.
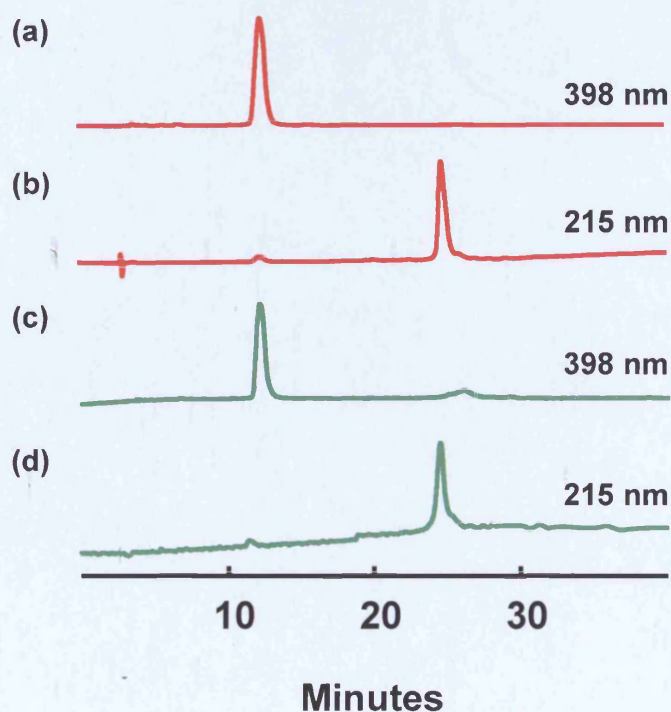
Figure 2.17: HPLC analyses of W41A before (a,b) and after (c,d) reaction with H_2O_2 monitored at 398 nm and 215 nm.
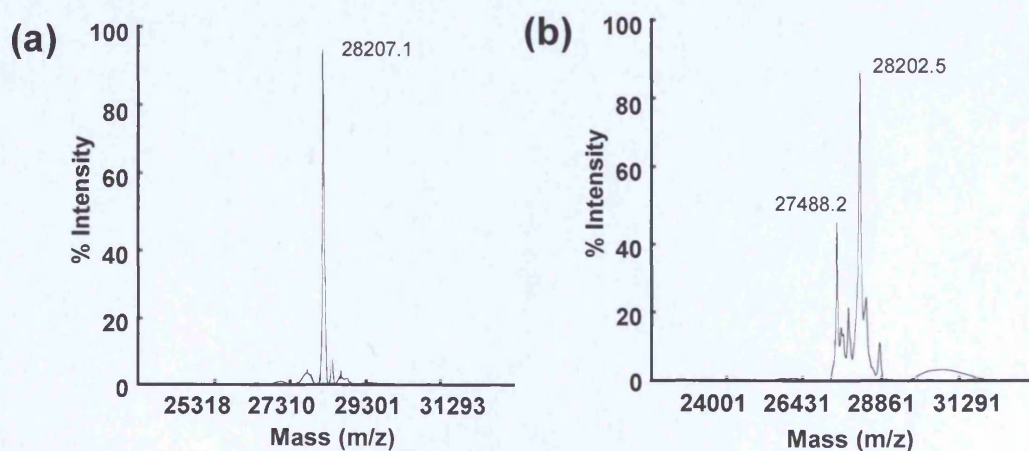
Figure 2.18: MALDI-TOF mass spectrum of W41A before (a) and after (b) reaction with 6 equivalents of H_2O_2.

---

[c] A minor peak at 27488.2 Da is also observed, which may arise from non-specific cleavage of the protein

2.2.13 Electron Paramagnetic Resonance spectroscopy

EPR spectroscopy was carried out by Dr. Dimitri Svistunenko at the University of Essex and was used to further characterize the heme environment in rsAPX. Low temperature EPR of rsAPX (Figure 2.19a) reveals high- and low-spin species as reported before (19). The EPR spectrum of rsAPX, has a high-spin signal, significantly departed from tetragonality (g = 5.96, 5.23 and 1.98), and a low-spin heme signal with $g = 2.68, 2.21$, and 1.78 (19).

EPR spectroscopy was also used to obtain further evidence for the possible formation of a protein radical on reaction of rsAPX with H_2O_2. The EPR spectrum of rsAPX after treatment with one equivalent of H_2O_2 is shown in Figure 2.19b. In agreement with previous reports (17), reaction of rsAPX with H_2O_2 yields a species with apparent g-values (g_{max} = 3.52, g_{min} = 1.998) consistent with the existence of a porphyrin π-cation radical (Figure 2.20a). Simulation of this EPR signal (Figure 2.20b) allows more accurate determination of the principal g-factors: 3.48, 3.28 and 1.9991. Maximum concentration of Compound I (in the 80 μM / 80 μM heme/peroxide system) was observed at 9 s after mixing and was 27 μM. Small amounts of protein free radicals are also detected.
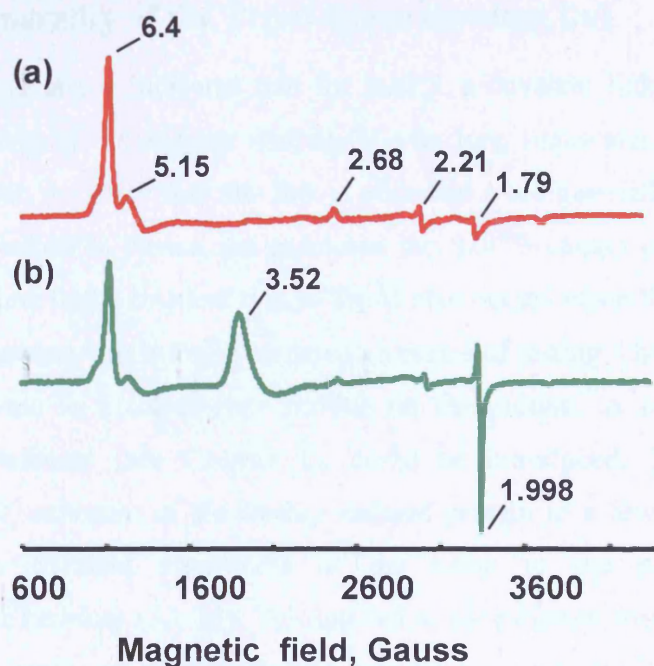
Figure 2.19: The EPR spectra of rsAPX (80 μM enzyme, 50 mM potassium phosphate, pH 7.0) before (a) and after (b) addition of 80 μM H_2O_2 (final concentrations, pH 7.0). The spectra were measured at 10 K, other instrumental conditions were: modulation frequency $\nu_m = 100$ kHz, modulation amplitude $A_m = 5$ G, sweep rate $\nu = 22.6$ G/s, time constant $\tau = 82$ ms, microwave frequency $\nu = 9.4667$ GHz, microwave power P = 3.188 mW.
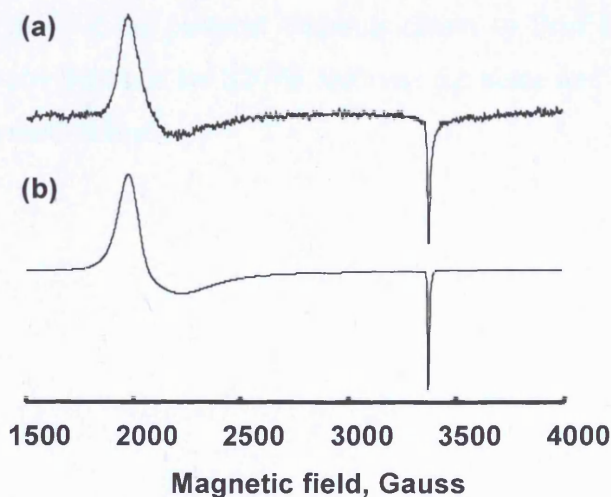
Figure 2.20: (a) Compound I pure EPR signal obtained as a difference spectrum: the spectrum of the 1:1 rsAPX + H_2O_2 sample frozen 4 s after addition of H_2O_2, was measured at 0.20 mW (30 dB), has been multiplied by 1.672 and subtracted from the spectrum of the same sample measure at 3.18 mW (18 dB). (b) Spectrum (a) simulated for $g_x = 3.48$, $g_y = 3.28$, $g_z = 1.9991$, $\Delta H_x = 80$ G, $\Delta H_y = 270$ G and $\Delta H_z = 7$.

2.3   The generality of the Trp41-heme covalent link

The data presented above indicated that for rsAPX a covalent link to Trp41 was formed on treatment of the enzyme with H_2O_2 over long timescales. In the second half of this chapter, we show that this link is observed more generally in other site-directed variants of APX. Hence, we examined the S207E variant of APX and we present data to show that a covalent link to Trp41 also occurs when S207E is treated with H_2O_2. This variant was initially prepared as means of testing whether a covalent link from the heme to a carboxylate residue on the protein, as observed in the mammalian peroxidases (see Chapter 1), could be introduced. In the case of recombinant LPO, exposure of the freshly isolated protein to a few equivalents of H_2O_2 results in covalent attachment of the heme to the protein through glutamate/asparate residues (*32*, *33*). This has led to the proposal that covalent bond formation is the result of an autocatalytic process (*33*, *34*). Similar studies had already shown that the vinyl-Met link in the mammalian peroxidases could, indeed, be duplicated under a similar autocatalytic mechanism in the S160M variant (*35*) and serine 207 was considered to be close enough to the 1-methyl group of the heme (Figure 2.21). However, the S207E variant did not show a methyl-ester linkage, even though separate work in the laboratory of Professor Paul Ortiz de Montellano showed that this was possible in HRP (*36*) (although the vinyl-methionine link could not be replicated in HRP, POM personal communication to Prof Emma Raven). Instead, we observe a covalent link for S207E, between the heme and Trp41, as seen for rsAPX and as described below.
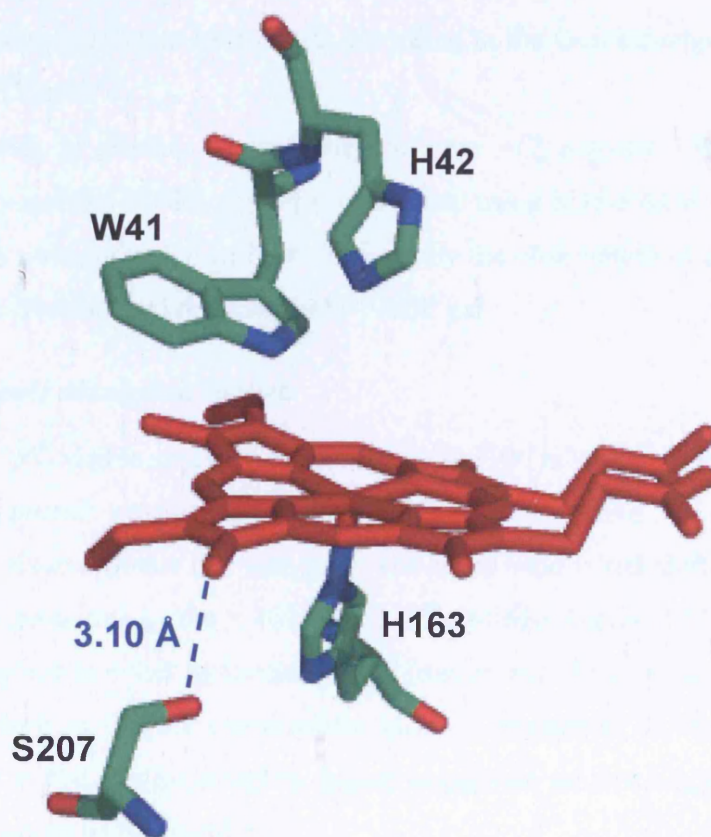
Figure 2.21: Active site structure of rsAPX showing the distance between Ser207, and the 1-methyl group of the heme.

2.3.1 Expression, purification and characterization of S207E variant

Site-directed mutagenesis was performed, according to the Quickchange^{TM} protocol, as described in Chapter 6.

The typical yields of purified variant enzyme were ~13 mg/litre LB-media. The purity of freshly isolated S207E variant was checked using SDS-PAGE analysis, and the preparations were judged to be homogeneous by the observation of a single band on a Coomassie Blue-stained reducing SDS-PAGE gel.

2.3.1.1 Electronic absorption spectra

Analysis of the UV-visible spectra for S207E variant (100 mM potassium phosphate, pH 7.0, 25 °C), reveals wavelength maxima at 350^{sh}, 412, 530 and 560 nm, which is consistent with six-coordinate low spin iron. The Soret band is red-shifted compared to the wild-type protein (λ_{max}/nm = 407, 506, 540^{sh} and 636, Figure 2.22). This could possibly be assigned to either hydroxide-bound iron or one of the amino acids in the active site binding in the six coordination place. Comparison of the UV-visible spectrum (λ_{max}) to that of a bis-histidine ligated myoglobin mutant suggested that the heme in S207E could be bis-histidine.
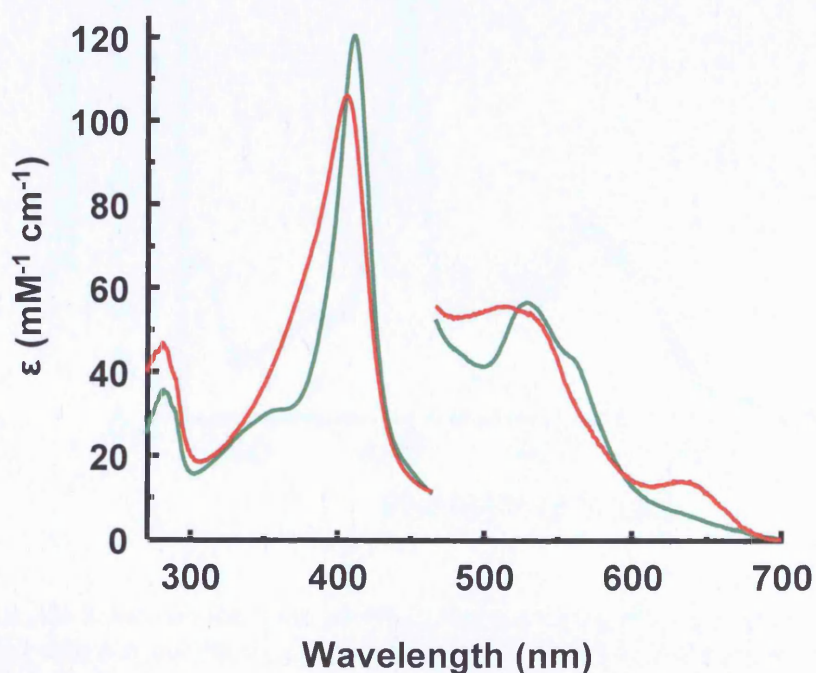
Figure 2.22: UV-visible absorption spectra of ferric rsAPX (red line) and ferric S207E (green line). The visible region has been multiplied by a factor of 5. Conditions: 100 mM potassium phosphate buffer, pH 7.0, 25 °C.

The absorption coefficient of S207E was calculated using an average of three heme contents measured using the pyridine hemochromagen assay (*22*). An average absorption coefficient value of $\varepsilon_{412} = 120 \pm 1$ mM^{-1} cm^{-1} was obtained. This value is higher than that reported for wild type rsAPX (107 mM^{-1}cm^{-1} (*19*)) and is also characteristic of low-spin iron formation.

2.3.2 Reaction with H₂O₂ and covalent link formation

2.3.2.1 Reaction with H₂O₂ followed by UV-visible spectroscopy

To test whether S207E undergoes heme-protein cross-linking under oxidative conditions, the enzyme was treated with H_2O_2, varying the amount of equivalents and the time of incubation Reaction of S207E with H_2O_2 yielded a product with a UV-visible spectrum (λ_{max}/nm = 410, 530, 560) that is distinct from that of S207E. Reaction of S207E with H_2O_2 did not show any evidence for formation of either Compound I or Compound II using conventional electronic spectroscopy. Instead, the reaction resulted in a final product with wavelength maxima at 410, 530 and 560 nm (Figure 2.23).
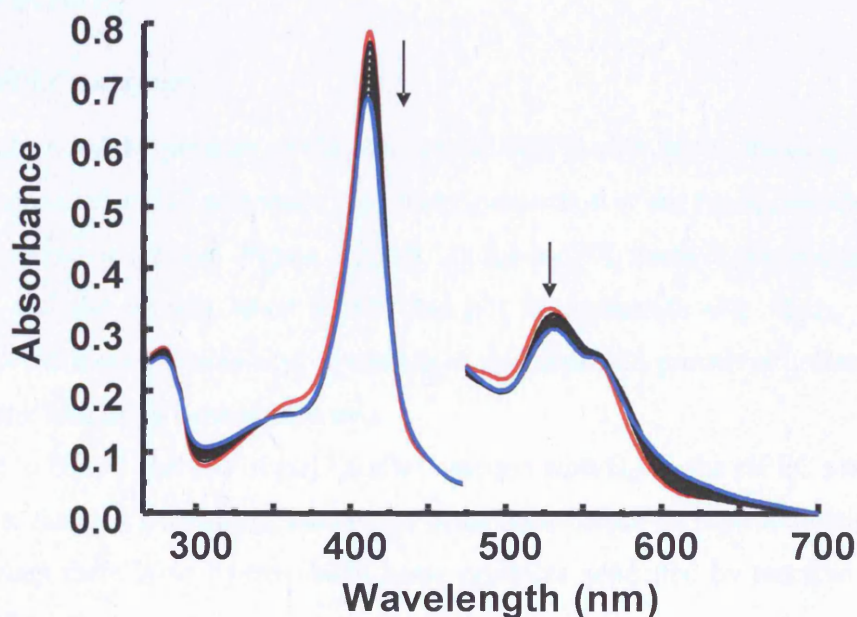
Figure 2.23: Selected electronic spectra collected during the reaction of ferric S207E (red line) with 6 equivalents of H_2O_2. Intermediate spectra between ferric S207E and final product (blue line) are shown as black lines. The visible region has been multiplied by a factor of 5. Sample conditions: [Enzyme] = 6 μM, [Hydrogen peroxide] = 36 μM, 100 mM potassium phosphate, pH 7.0, 25 °C.

2.3.2.2 Acidified butanone extraction

An acid butanone extraction after reaction of S207E with H_2O_2, as in the case of rsAPX, did not remove the heme from the protein (Figure 2.24b), which is a clear indication of covalent attachment of the heme to the protein; in contrast, control experiments with S207E before reaction with H_2O_2 showed complete extraction of heme into the organic layer (Figure 2.24a).
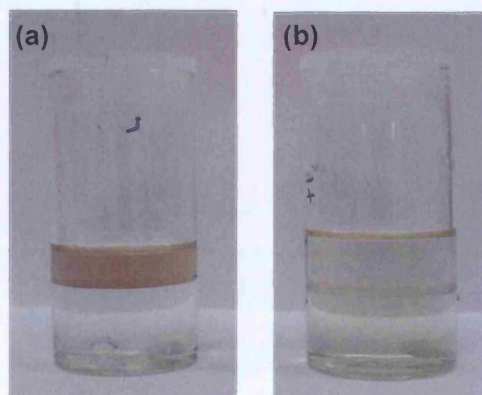
Figure 2.24: Acidified butanone extraction on S207E before (a) and after (b) reaction with H_2O_2.

2.3.2.3 HPLC analyses

HPLC analysis of the product of the reaction of S207E with H_2O_2 showed that the protein (monitored at 215 nm) and a significant proportion of the heme (monitored at 398 nm) co-elute at 28 min, Figure 2.25c,d. As for rsAPX, there is no co-elution of the heme and the protein when S207E has not been treated with H_2O_2, Figure 2.25a,b. As mentioned previously, co-elution of the heme and protein is indicative of covalent link formation between the two.

In contrast to HPLC analysis of rsAPX after reaction with H_2O_2, the HPLC profile of S207E after reaction with H_2O_2, showed no heme peak before 11 min, indicating that in this variant there is no hydroxylated heme products generated by reaction of the protein with H_2O_2.
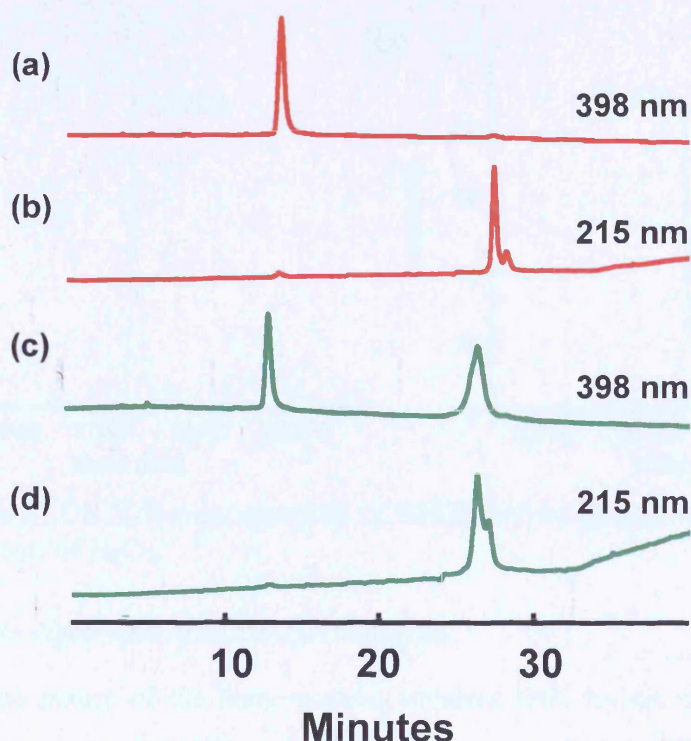
Figure 2.25: HPLC analyses of S207E before and after reaction with H_2O_2 monitored at 398 nm and 215 nm. (a,b) rsAPX before reaction with H_2O_2, (c,d) rsAPX after reaction with H_2O_2.

2.3.2.4 MALDI-TOF analysis before and after reaction with H_2O_2

Mass spectrometry data are consistent with the HPLC analyses above and provided further evidence for partial covalent attachment of the heme to the protein in S207E. MALDI-TOF analysis of S207E before treatment with H_2O_2, Figure 2.26a, showed a mass of 28367.95 Da which corresponds closely to the predicted mass (28360.91 Da) of the apo-protein and is consistent with non-covalent attachment of the heme to the protein in rsAPX. After treatment with H_2O_2, two peaks were observed in the MALDI-TOF spectrum, Figure 2.26b. The first is at 28372.50 Da, which is within the theoretical error (~0.05%) of the mass of the apo-protein (as above). The second peak is at 28998.88 Da, which corresponds to an increase in mass of 627 Da over the apo-protein, and is consistent with covalent attachment of the heme (616 Da) to the protein. This additional mass of 627 Da lies between the theoretical mass of 616 Da for addition of heme and 632 Da for addition of heme with an extra hydroxyl group. Thus, the lack of mass accuracy due to the large mass of the protein did not allow the covalently linked heme to be assigned as hydroxylated or not at this stage.
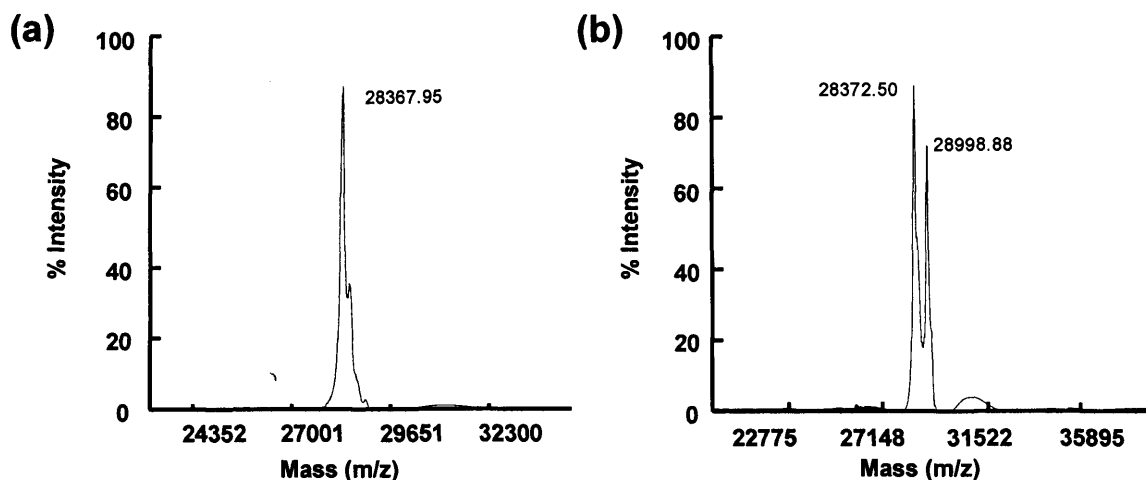
Figure 2.26: MALDI-TOF mass spectrum of S207E before (a) and after (b) reaction with 6 equivalents of H_2O_2.

2.3.2.5 Tryptic digest and MALDI-TOF analysis

To establish the nature of the heme-protein covalent link, tryptic digestion of the product of the reaction of S207E with H_2O_2 was carried out and HPLC was used to isolate heme-containing peptide fragments (*i.e.* showing both heme and protein absorbancies) from the resulting peptide mixture.

There were three peaks with significant absorbance at 398 nm. The MALDI-TOF mass spectrum of the product eluting at 36.4 min gave a mass of 616 Da, indicating that this HPLC peak corresponds to free heme species. MALDI-TOF mass spectrometry of the peptide fragments eluting at 29.1 and 30.3 min both gave spectra with identical masses of 1864.06 Da (Figure 2.28), indicating that both HPLC peaks are assigned to a single peptide (Figure 2.27) [d].

The mass of 1864.06 Da observed for this fragment, Figure 2.28, is 16 Da higher than the calculated mass of 1848 Da expected for the $L^{39}AW^{41}HSAGTFDK^{49}$ peptide fragment containing heme covalently bound to Trp41. This mass is almost identical to the mass of 1864.06 Da, observed for the heme-containing fragment isolated after the reaction of rsAPX with H_2O_2. As there was no other heme-containing fragment isolated by HPLC, this indicated that reaction of S207E variant with H_2O_2 might be leading to formation of a covalent link between the heme and Trp41, as for rsAPX. Better mass accuracy of this mass spectrum, also allowed the

---

[d] An additional heme peak at 28.6 min could not be separated from the peak at 29.1 min and so both peaks were analysed together.

heme containing fragment to be assigned as arising from a hydroxylated heme product as observed for rsAPX.
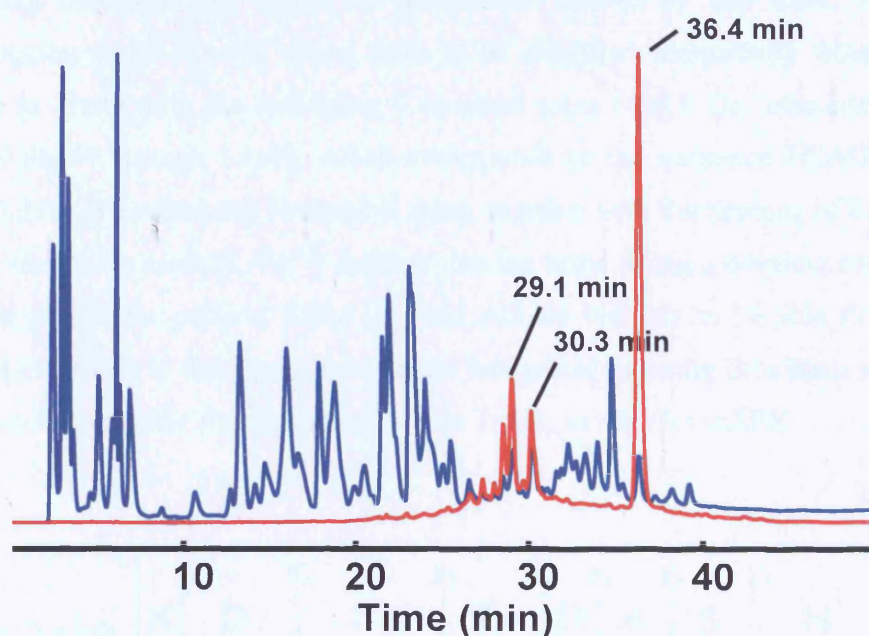
Figure 2.27: HPLC analyses of a tryptic digest of S207E after reaction with H_2O_2, monitored at 215 nm (blue line) and 398 nm (red line). Elution times of heme-containing peptides (29.1 and 30.3 min) as well as free heme (36.4 min) are indicated.
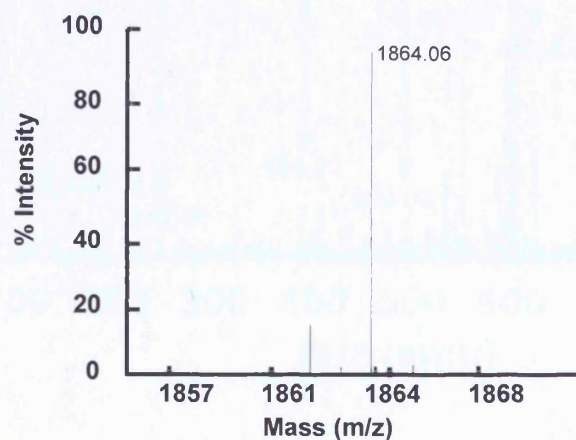
Figure 2.28: MALDI-TOF mass spectrum of the HPLC-purified heme-containing peptide fragment obtained after reaction of S207E with H_2O_2.

2.3.2.6 MS/MS analysis of heme-containing peptide fragment

MS/MS mass spectrometry was used to obtain sequence information for this heme-containing fragment and verify its assignment above. In this case, a y-ion fragmentation series allowed amino acids to be identified sequentially from His42 through to Thr46 with the remaining C-terminal mass (409.1 Da) consistent with residues Phe47 through Lys49, which corresponds to the sequence HSAGTFDK, Figure 2.27a. The remaining N-terminal mass, together with the absence of fragment ions for the amino acids (LAW^{41}) indicate that the heme forms a covalent cross link with this part of the peptide. Since Leu and Ala are unlikely to be able to form a covalent cross link to the heme, the data are interpreted as being consistent with the formation of a covalent link from the heme to Trp41, as seen for rsAPX.
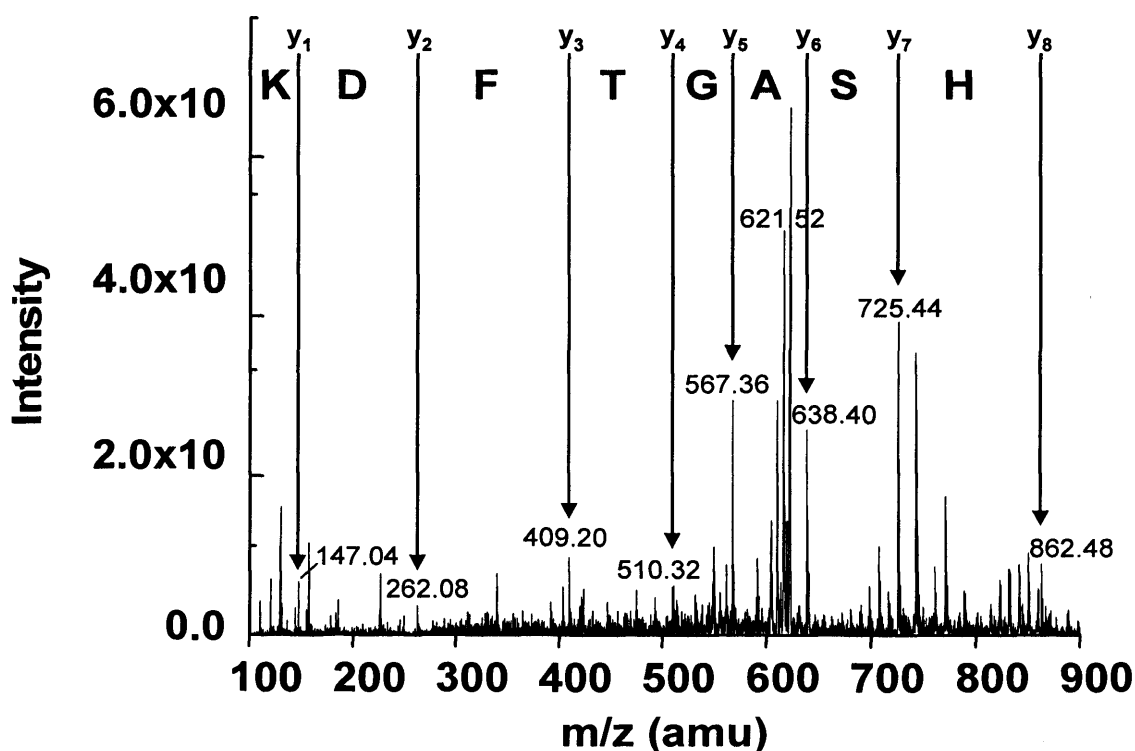
Figure 2.29: MS/MS spectrum of the HPLC-purified heme-containing peptide fragment showing the triply charged precursor ion (621.52 Da). The annotated peptide sequence corresponds to the y-ion fragment series.

2.3.2.7 Crystal screens

Crystal screens were set up for S207E under the same conditions used for crystallization of wild type rsAPX (*37*). All screens were performed at 19 °C, with a protein concentration of ~10 mg/ml in water. Sitting drop plates were used for all screens with 2 μl drops of protein solution and 2 μl of well solution over 1ml wells. All pH values given are of 1.0 M buffer solutions before addition to the wells. The pH values were measured on stock solutions, as this is how the commercial screens are prepared. The conditions for the screens were: 0.1 M Hepes pH 8.0 to pH 9.5, lithium sulphate 1.5 M to 2.25 M. A second set of screens was set up by repeating the exact conditions (0.1 M Hepes 2.25 M, pH 8.3) for crystallisation of the wild type protein in all 24 wells. Commercial crystal screens MDL I and II (Appendix D) were also set up for S207E. None of the above conditions gave yield to crystals for S207E variant.

2.4   Discussion

In the mammalian heme peroxidases, it is known that different types of covalent link from protein amino acids to the heme group are used (*38*). Although covalently-bound heme groups are not observed in other peroxidases, there is an increasing amount of evidence to show that these links can be engineered into an existing peroxidase framework if the correct residue is inserted at the correct site and if the peroxidase in question is competent for reaction with H_2O_2 (see for example (*24, 27*)). This represents a substantial change in the way we think about these modified peroxidases: collectively, what it tells us is that there no intrinsic reason why any peroxidase, or any heme protein for that matter, cannot form a particular covalent link under the right conditions. *In extremis,* this might even mean that some proteins may need to be poised in an environment that specifically 'switches off' these covalent links. Collectively, and in view of the very similar active site structures of the class I peroxidase enzymes, these ideas indicated that the same principle may apply to the covalent Trp-Tyr-Met link in KatG (at least in the class I enzymes). More specifically, that the mechanisms that lead to formation of the Trp-Tyr-Met link in KatG might also be accessible under certain conditions in other class I peroxidases.

The proposed mechanism (*6, 7*) of formation of the Trp-Tyr-Met link involves initial reaction with H_2O_2 to form a Compound I intermediate (containing a ferryl heme and a porphyrin π-cation radical). This is followed by oxidation of both Trp229 and Tyr107 (numbering according to Figure 2.30a) by Compound I to form protein radicals at both residues. Thus, the formation of both Trp and Tyr radicals is proposed to follow a normal oxidative peroxidase mechanism (*6, 7*). Radical cross-linking reactions then occur to form the Trp-Tyr link. A second cycle of reaction with H_2O_2 is then proposed for formation of the Tyr-Met link (Scheme 2.1).
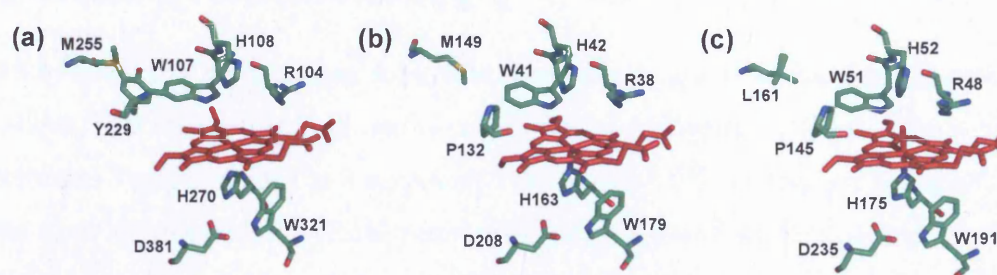
Figure 2.30: Comparison of active site structures of (a) mtKatG, (b) rsAPX and (c) C*c*P.
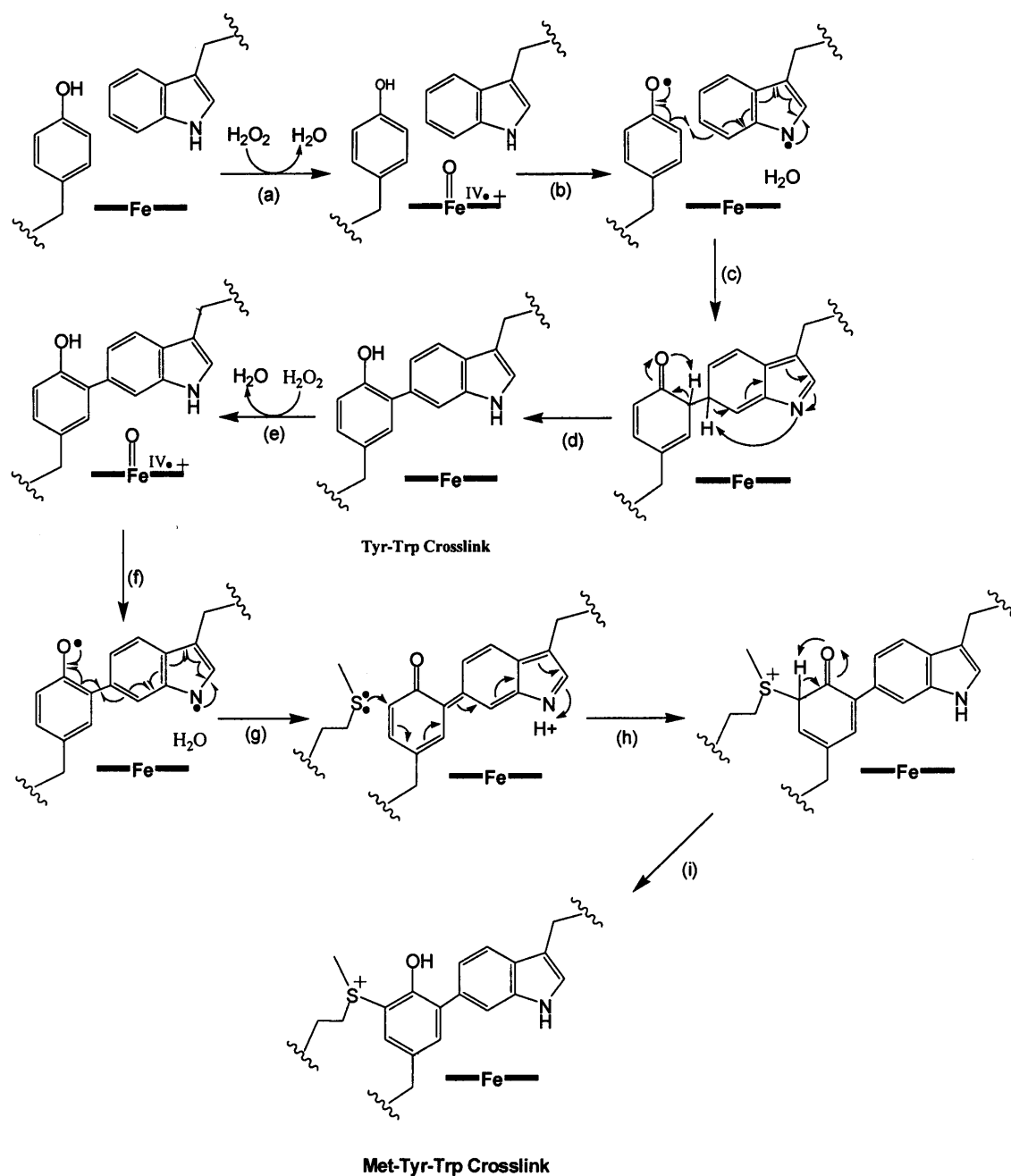
Scheme 2.1: Proposed mechanism for the formation of the Met-Tyr-Trp cross-link in *Mycobacterium Tuberculosis* KatG (*6*).

A key feature is the proposed formation of a protein radical at the distal tryptophan residue, in a mechanism that can be considered as analogous to the oxidation of the proximal Trp191 residue in Compound I of CcP (*39-42*). At present, however, it is not clear whether other, related heme proteins are able to support oxidation of the distal tryptophan residue. Although both CcP and APX contain a distal tryptophan residue in an essentially identical structural environment to that observed in KatG,

Figure 2.30, the Trp-Tyr-Met link is not observed in either of these enzymes because the active site Tyr residue is missing in APX [e], Figure 2.30b; and because both Tyr and Met are missing in C*c*P, Figure 2.30c.
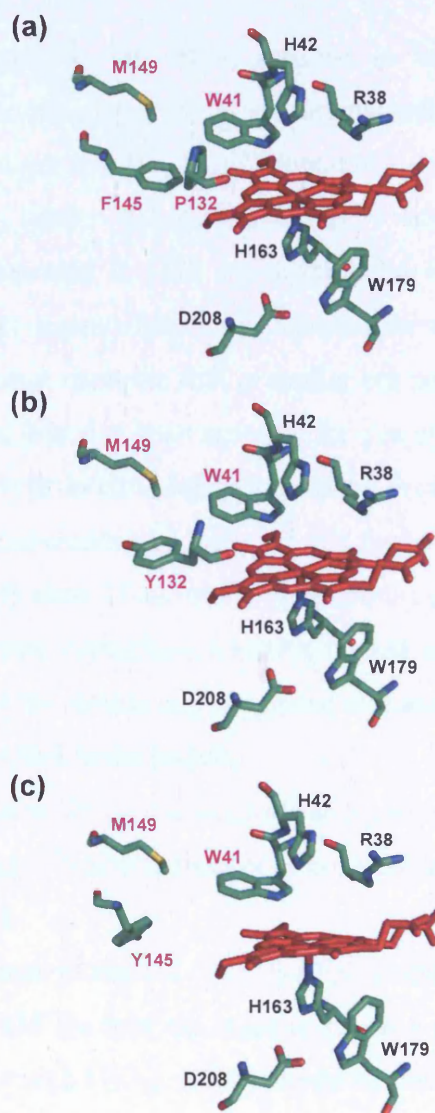
Figure 2.31: (a) Active site structure of rsAPX, (b) Model of the active site structure of P132Y variant, (c) Model of the active site structure of F145Y variant. Met149, Trp41, Pro132, Phe145, Y132 and Y145 are labelled in magenta.

---

[e] In order to test the above hypothesis, a tyrosine residue was engineered in the active site of rsAPX, in place of Tyr229 seen for KatG (Figure 2.30a). More specifically, by comparing the active site structures of rsAPX and KatG, it was found that Pro132 and Phe145 are in very close proximity to Trp41 and Met 149 in rsAPX (Figure 2.31a) and are the two residues most closely occupying the space of Tyr229 of KatG. Thus, P132Y (Figure 2.31b) and F145Y (Figure 2.31c) variants of rsAPX were engineered in an attempt to place a tyrosine residue between Trp41 and Met149 and test if formation of a Met-Tyr-Trp cross-link could be accommodated in these structures after reaction with H_2O_2. Unfortunately, expression problems with both these variants did not make it possible for these experiments to proceed.

This chapter, presents a series of experiments that show that Trp41 can covalently link to the heme in rsAPX, after treatment of the enzyme with H_2O_2, in a reaction that implicates formation of a radical at Trp41 The main experimental observations are:

- Reaction of rsAPX with H_2O_2 resulted in initial formation of a green Compound I intermediate, which was immediately converted to a more stable Compound II-type species. This Compound II-type species has a UV/visible spectrum (λ_{max} (nm) = 412, 528, 558, 682^{sh}) very similar but not identical to authentic Compound II (*43*), *i.e.* Compound I that has been reduced by ascorbate. This intermediate then decays over a period of ~8 h to a final product that has a spectrum that is similar but not identical to that of rsAPX. This behaviour has also been reported for pea cytosolic APX (*44*) when this Compound II-type intermediate was referred to as Compound I*.

- A pyridine hemochromagen assay of this ferric-like final product suggested possible modification of one of the vinyl groups of the heme group.

- An acid butanone extraction on rsAPX treated with H_2O_2 did not remove all the heme from the protein and suggested that some proportion of the heme is covalently attached to the protein.

- HPLC analyses showed co-elution of the heme and the protein, after reaction with H_2O_2, which is also indicative of covalent attachment between the heme and the protein.

- Mass spectrometry showed that rsAPX treated with H_2O_2 has a mass increased by 634 Da over the mass of the apo-protein (obtained for rsAPX before reaction with H_2O_2), which proves the initial suggestion that the heme group is covalently attached to the protein.

- Tryptic digest and mass spectrometry analysis of the HPLC purified heme containing fragmented, suggested that the heme is linked to the $L^{39}AW^{41}HSAGTFDK^{49}$ peptide fragment, containing Trp41.

- MS/MS analysis of the above peptide fragment confirmed that Trp41 is the protein residue linking to the heme.

- Control experiments with rsAPX reconstituted with deuteroheme and W41A variant, clearly indicated that the covalent link does not form in the absence of either Trp41 or the heme vinyl groups.

- Further control experiments also showed that this link does not form under catalytic conditions (*i.e.* in the presence of substrate). In this case, reaction of rsAPX with H_2O_2 results to initial formation of a Compound I intermediate which returns back to the ferric resting state on reaction with ascorbate (Scheme 2.2).

The data for S207E variant (acidified butanone extraction, HPLC and mass spectrometry (MALDI-TOF, MS/MS) analyses), show that this Trp41-heme covalent link maybe a general feature of APX variants and is not restricted to the wild type protein.

A possible mechanism for formation of the covalently-bound heme species that embodies all of the available data is presented in Scheme 2.2. In this mechanism, initial formation of a Compound I intermediate (step (i)) is followed by oxidation and deprotonation of Trp41 (step (ii)) and addition of the Trp41 radical across the 4-vinyl group of the heme (steps (iii) and (iv)). Subsequent reduction of the ferryl group and release of H_2O (step (v)) leads to formation of a carbocation. Nucleophilic addition of H_2O as the final step (step (vi)) gives a heme structure that is consistent with the mass spectrometry data. The shortest distance from the C^β on the 4-vinyl group to the C^γ of Trp41 is 4.8 Å. We note that hydroxylation of a covalently-bound heme fragment has also been observed previously (*24*).

In support of the above proposal, EPR spectra obtained shortly after reaction of rsAPX with H_2O_2 showed that reaction of rsAPX with H_2O_2 results in initial formation of a porphyrin π-cation radical, as observed previously (*17*). This is consistent with the proposed mechanism above, suggesting that covalent attachment of the heme to rsAPX occurs *via* a Compound I intermediate. In separate EPR experiments, we observed that although reaction of rsAPX with H_2O_2 led to the initial formation of a porphyrin π-cation radical, over longer timescales this signal decreased in intensity and was replaced with a protein free radical signal (Svistunenko, Pipirou, data not shown). The shape and g-values for the EPR signal of this free radical species were very similar to those found for CcP Compound I (*45, 46*), that is known to use a protein radical at Trp191. Formation of a tryptophan radical under the same conditions has also been reported for pea cytosolic APX (*44*): in this case, and by analogy with CcP, the radical was proposed to be on Trp179. In this work, Trp41 has been shown to covalently link to the heme, thus suggesting that,
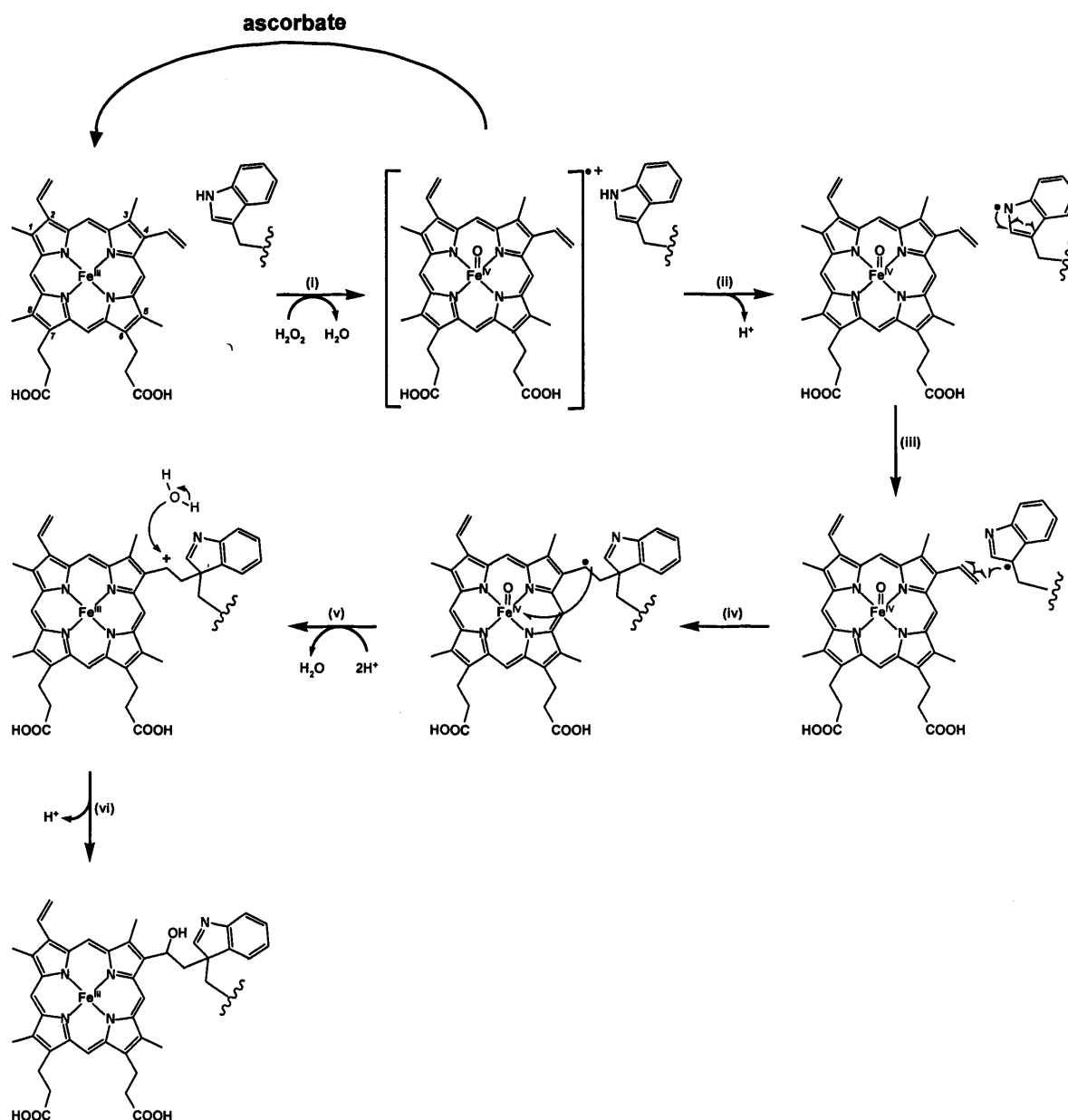
Scheme 2.2: Proposed mechanism for formation of a covalent link between Trp41 and the heme group in ascorbate peroxidase. Steps (i) – (vi) are described in the text.

in contrast to CcP, Trp41 and not Trp179 is the more likely candidate for the protein radical in rsAPX. Formation of a Trp41-heme covalent link is also consistent with the original observations (*44*) that the decay product of Compound I, in the absence of substrate, is not spectroscopically identical to the ferric resting-state. Furthermore, formation of a protein radical at the distal tryptophan closely resembles the initial mechanistic steps after Compound I formation in the KatG enzymes that lead to formation of the Met-Tyr-Trp cross-link (Scheme 2.1).

In summary, these data add a new dimension to our wider understanding of the differences between the KatG enzymes and the monofunctional peroxidase enzymes. In particular, the data indicate that, under non-catalytic conditions, there is no intrinsic barrier to formation of a radical at Trp41 in APX analogous to that thought to be used in the KatGs. The direct implication is that formation of a covalent Trp-Tyr-Met link in APX is limited not by the inherent reactivity of the enzyme but by the absence of a tyrosine residue adjacent to Trp41.

2.5   References

(1)   Dunford, H. B. (1991) in *Peroxidases in Chemistry and Biology* (Everse, J., Everse, K. E., and Grisham, M. B., Eds.) pp 1-24, CRC Press, Boca Ralton FL.

(2)   Welinder, K. G. (1992) Superfamily of plant, fungal and bacterial peroxidases. *Curr. Opin. Chem. Biol. 2*, 388-393.

(3)   Bertrand, T., Eady, N. A. J., Jones, J. N., Bodiguel, J., Jesmin, Nagy, J. M., Raven, E. L., Jamart-Gregoire, B., and Brown, K. H. (2004) Crystal Structure of *Mycobacterium tuberculosis* Catalase-Peroxidase. *J. Biol. Chem. 279*, 38991-38999.

(4)   Carpena, X., Loprasert, S., Mongkolsuk, S., Switala, J., Loewen, P. C., and Fita, I. (2003) Catalase-peroxidase KatG of *Burkholderia pseudomallei* at 1.7 Å resolution *J. Mol. Biol. 327*, 475-489.

(5)   Yamada, Y., Fujiwara, T., Sato, T., Igarashi, N., and Tanaka, N. (2002) The 2.0 angstrom crystal structure of catalase-peroxidase from *Haloarcula marismortui*. *Nat. Struct. Biol. 9*, 691-695.

(6)   Ghiladi, R. A., Knudsen, G. M., Medzihradszky, K. F., and Ortiz de Montellano, P. R. (2005) The Met-Tyr-Trp cross link in *Mycobacterium tuberculosis* catalase peroxidase. *J. Biol. Chem. 280*, 22651-22663.

(7)   Ghiladi, R. A., Medzihradszky, K. F., and Ortiz de Montellano, P. R. (2005) Role of the Met-Tyr-Trp cross link in *Mycobacterium tuberculosis* catalase peroxidase (KatG) as revealed by KatG(M255I). *Biochemistry 44*, 15093-15105.

(8)   Jakopitsch, C., Kolarich, D., Petutschnig, G., Furtmuller, P. G., and Obinger, C. (2003) Distal side tryptophan, tyrosine and methionine in catalase-peroxidases are covalently linked in solution. *FEBS Lett. 552*, 135-140.

(9)   Regelsberger, G., Jakopitsch, C., Ruker, F., Krois, D., Peschek, G. A., and Obinger, C. (2000) Effect of Distal Cavity Mutations on the Formation of Compound I in Catalase-Peroxidases. *J. Biol. Chem. 275*, 22854-22861.

(10)   Jakopitsch, C., Ivancich, A., Schmuckenschlager, F., Wanasinghe, A., Poltl, G., Furtmuller, P. G., Ruker, F., and Obinger, C. (2004) Influence of the unusual covalent adduct on the kinetics and formation of radical intermediates in *Synechocytic* catalase peroxidase. *J. Biol. Chem. 279*, 46082-46095.

(11)   Jakopitsch, C., Auer, M., Ivancich, A., Ruker, F., Furtmuller, P. G., and Obinger, C. (2003) Total conversion of bifunctional catalase-peroxidase (KatG) to monofunctional peroxidase by exchange of a conserved distal side tyrosine. *J. Biol. Chem. 278*, 20185-20191.

(12)   Hillar, A., Peters, B., Pauls, R., Loboda, A., Zhang, H., Mauk, A. G., and Loewen, P. C. (2000) Modulation of the activities of catalase-peroxidase HPI of *Escherichia coli* by site-directed mutagenesis. *Biochemistry 39*, 5868-5875.

(13)   Goodin, D. B., Mauk, A. G., and Smith, M. (1987) The peroxide complex of yeast cytochrome *c* peroxidase contains two distinct radical species, neither of which resides at methionine 172 or tryptophan 51. *J. Biol. Chem. 262*, 7719-7724.

(14)   Yonetani, T., and Schleyer, H. (1966) Studies on cytochrome *c* peroxidase. VII. Electron paramagnetic resonance absorptions of the enzyme and complex ES in dissolved and crystalline forms. *J. Biol. Chem. 241*, 3240-3243.

(15)   Sivaraja, M., Goodin, D. B., Smith, M., and Hoffman, B. M. (1989) Identification by ENDOR of Trp191 as the free-radical site in cytochrome *c* peroxidase Compound ES. *Science 245*, 738-740.

(16)   Dolphin, D., Forman, A., Borg, D. C., Fajer, J., and Felton, R. H. (1971) Compounds I of catalase and horse radish peroxidase: pi-cation radicals. *Proc. Natl. Acad. Sci. U S A 68*, 614-618.

(17)   Patterson, W. R., Poulos, T. L., and Goodin, D. B. (1995) Identification of a porphyrin pi cation radical in ascorbate peroxidase compound I. *Biochemistry 34*, 4342-4345.

(18)   Dalton, D. A., Diaz del Castillo, L., Kahn, M. L., Joyner, S. L., and Chatfield, J. M. (1996) Heterologous expression and characterization of soybean cytosolic ascorbate peroxidase. *Arch. Biochem. Biophys. 328*, 1-8.

(19)   Jones, D. K., Dalton, D. A., Rosell, F. I., and Raven, E. L. (1998) Class I heme peroxidases: characterization of soybean ascorbate peroxidase. *Arch. Biochem. Biophys. 360*, 173-178.

(20)   Patterson, W. R., and Poulos, T. L. (1994) Characterization and crystallization of recombinant pea cytosolic ascorbate peroxidase. *J. Biol. Chem. 269*, 17020-17024.

(21)   Lad, L., Mewies, M., and Raven, E. L. (2002) Substrate binding and catalytic mechanism in ascorbate peroxidase: evidence for two ascorbate binding sites. *Biochemistry 41*, 13774-13781.

(22)   Antonini, M., and Brunori, E. (1971) *Hemoglobin and Myoglobin and their reactions with ligands*, North Holland Publishers, Amsterdam.

(23)   Daltrop, O., Smith, K. M., and Ferguson, S. J. (2003) Stereoselective *in vitro* formation of *c*-type cytochrome variants from *Hydrogenobacter thermophilus* containing only a single thioether bond. *J. Biol. Chem. 278*, 24308-24313.

(24)   Metcalfe, C. L., Ott, M., Patel, N., Singh, K., Mistry, S. C., Goff, H. M., and Raven, E. L. (2004) Autocatalytic formation of green heme: evidence for H_2O_2-dependent formation of a covalent methionine-heme linkage in ascorbate peroxidase. *J. Am. Chem. Soc. 126*, 16242-16248.

(25)   LeBrun, L. A., Xu, F., Kroetz, D. L., and Ortiz de Montellano, P. R. (2002) Covalent attachment of the heme prosthetic group in the CYP4 cytochrome P450 family. *Biochemistry 41*, 5931-5937.

(26)   Colas, C., Kuo, J. M., and Ortiz de Montellano, P. R. (2002) Asp225 and Glu375 in autocatalytic attachment of the prosthetic heme group of lactoperoxidase. *J. Biol. Chem. 277*, 7191-7200.

(27)   Colas, C., and Ortiz de Montellano, P. R. (2004) Horseradish peroxidase mutants that autocatalytically modify their heme prosthetic group. *J. Biol. Chem. 279*, 24131-24140.

(28)   Limburg, J., LeBrun, L. A., and Ortiz de Montellano, P. R. (2005) The P450$_{cam}$ G248E mutant covalently binds its prosthetic heme group. *Biochemistry 44*, 4091-4099.

(29)   Henne, K. R., Kunze, K. L., Zheng, Y.-M., Christmas, P., Soberman, R. J., and Rettie, A. E. (2001) Covalent linkage of prosthetic heme to CYP4 family of P450 enzymes. *Biochemistry 40*, 12925-12931.

(30) Huang, L., Colas, C., and Ortiz de Montellano, P. R. (2004) Oxidation of carboxylic acids by horseradish peroxidase results in prosthetic heme modification and inactivation. *J. Am. Chem. Soc. 126*, 12865-12873.

(31) Badyal, S. K., Joyce, M. G., Sharp, K. H., Seward, H. E., Mewies, M., Basran, J., Macdonald, I. K., Moody, P. C. E., and Raven, E. L. (2006) Conformational mobility in the active site of a heme peroxidase. *J. Biol. Chem. 281*, 24512-24520.

(32) Colas, C., Kuo, J. M., and Ortiz de Montellano, P. R. (2002) Asp225 and Glu375 in autocatalytic attachment of the prosthetic heme group of lactoperoxidase. *J. Biol. Chem. 277*, 7191-7200.

(33) Newmyer, S. L., and Ortiz de Montellano, P. R. (1995) Horseradish peroxidase His-42 --> Ala, His-42 --> Val, and Phe-41 --> Ala mutants. Histidine catalysis and control of substrate access to the heme iron. *J. Biol. Chem. 270*, 19430-19438.

(34) Colas, C., and Ortiz de Montellano, P. R. (2003) Autocatalytic radical reactions in physiological prosthetic heme modification. *Chem. Rev. 103*, 2305-2332.

(35) Metcalfe, C. L., Ott, M., Patel, N., Singh, K., Mistry, S. C., Goff, H. M., and Raven, E. L. (2004) Autocatalytic formation of green heme: evidence for H_2O_2-dependent formation of a covalent methionine-heme linkage in ascorbate peroxidase. *J. Am. Chem. So.c 126*, 16242-16248.

(36) Colas, C., and De Montellano, P. R. (2004) Horseradish peroxidase mutants that autocatalytically modify their prosthetic heme group: insights into mammalian peroxidase heme-protein covalent bonds. *J. Biol. Chem. 279*, 24131-24140.

(37) Sharp, K. H., Mewies, M., Moody, P. C., and Raven, E. L. (2003) Crystal structure of the ascorbate peroxidase-ascorbate complex. *Nat. Struct. Biol. 10*, 303-307.

(38) Colas, C., and Ortiz de Montellano, P. R. (2003) Autocatalytic radical reactions in physiological prosthetic heme modification. *Chem. Rev. 103*, 2305-2332.

(39) Yonetani, T., Chance, B., and Kajiwara, S. (1966) Crystalline cytochrome *c* peroxidase and complex ES. *J. Biol. Chem. 241*, 2981-2982.

(40) Yonetani, T., and Ray, G. S. (1965) Studies on cytochrome *c* peroxidase. Purification and some properties. *J. Biol. Chem. 240*, 4503-4514.

(41) Sivaraja, M., Goodin, D. B., Smith, M., and Hoffman, B. M. (1989) Identification by ENDOR of Trp191 as the free-radical site in cytochrome *c* peroxidase compound ES. *Science 245*, 738-740.

(42) Fishel, L. A., Farnum, M. F., Mauro, J. M., Miller, M. A., Kraut, J., Liu, Y. J., Tan, X. L., and Scholes, C. P. (1991) Compound I radical in site-directed mutants of cytochrome c peroxidase as probed by electron paramagnetic resonance and electron-nuclear double resonance. *Biochemistry 30*, 1986-1996.

(43) Lad, L., Mewies, M., and Raven, E. L. (2002) Substrate binding and catalytic mechanism in ascorbate peroxidase: evidence for two ascorbate binding sites. *Biochemistry 41*, 13774-13781.

(44) Hiner, A. N. P., Martínez, J. I., Arnao, M. B., Acosta, M., Turner, D. D., Raven, E. L., and Rodríguez-López, J. N. (2001) Detection of a radical intermediate in the reaction of ascorbate peroxidase with hydrogen peroxide. *Eur. J. Biochem. 268*, 3091-3098.

(45) Hori, H., and Yonetani, T. (1985) Powder and single-crystal electron paramagnetic resonance studies of yeast cytochrome *c* peroxidase and its peroxide and its peroxide compound, Compound ES. *J. Biol. Chem. 260*, 349-355.

(46) Hoffman, B. M., Roberts, J. E., Kang, C. H., and Margoliash, E. (1981) Electron paramagnetic and electron nuclear double resonance of the hydrogen peroxide compound of cytochrome *c* peroxidase. *J. Biol. Chem. 256*, 6556-6564.

Chapter 3

Investigation of heme-protein covalent link formation in C*c*P and the W191F variant

3.1   Introduction

As mentioned in Chapter 2, the class I heme peroxidase enzymes – the most prominent members of which are cytochrome *c* peroxidase (CcP), ascorbate peroxidase (APX), and the bifunctional catalase-peroxidases (KatG) (*1*) – are distinguished from other heme peroxidases by the presence of a distal tryptophan residue in place of the more usual phenylalanine residue, and a second active site tryptophan adjacent to the proximal histidine ligand (Figure 3.1). A key distinguishing feature of the KatG enzymes is that they contain a Met-Tyr-Trp cross-link (*2-4*), (Figure 3.1), which is believed to form through an autocatalytic mechanism (Chapter 2, Scheme 2.1) that involves radical formation at the distal tryptophan. Although both CcP and APX contain the same distal tryptophan residue in an essentially identical structural environment to that observed in KatG (Figure 3.1a), the Trp-Tyr-Met link is not observed in either of these enzymes (Figure 3.1b,c).
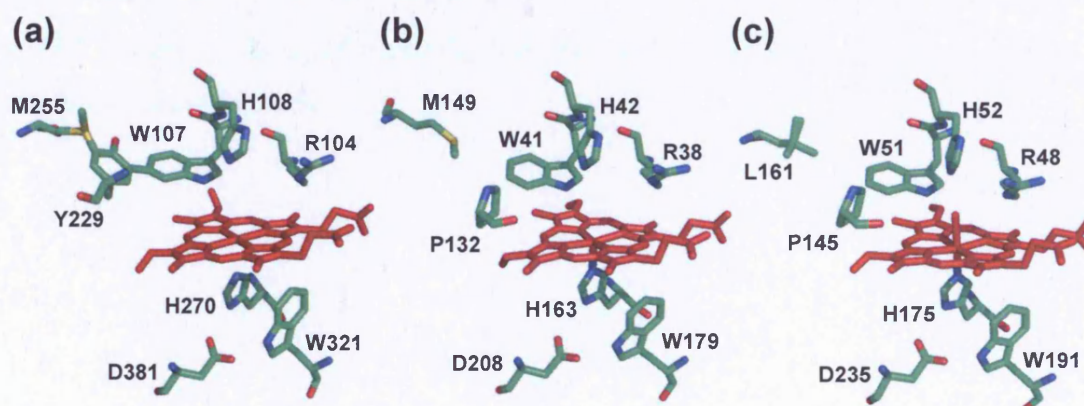
Figure 3.1: Comparison of active site structures of (a) mtKatG (PDB accession code 1SJ2), (b) rsAPX (1OAG) and (c) CcP (2CYP), showing the covalent links between residues W107, Y229 and M255 in mtKatG and the residues occupying the equivalent positions in rsAPX and CcP.

In Chapter 2, evidence was presented (*1*) to demonstrate that covalent linking of Trp41 to the heme group in APX can occur under non-catalytic conditions on exposure of the enzyme to peroxide, and a reaction mechanism involving formation of a protein radical at Trp41 has been implicated. This was interpreted to mean that radical formation at the distal tryptophan residue is not an exclusive feature of the

KatG enzymes and that this reaction intermediate is accessible in other, related peroxidases. If this is the case, it follows that the route by which APX and C*c*P legislate against formation of this link is largely structural (*i.e.* due to the absence of Tyr/Met residues, Figure 3.1b,c) rather than mechanistic (*i.e.* an inability to form a tryptophan radical).

In this chapter, preliminary experiments on C*c*P (*1*), showed no evidence for formation of an analogous link to Trp51 and we proposed that this was because C*c*P immediately diverts oxidizing equivalents to Trp191 as the immediate product of H_2O_2 oxidation without formation of the obligate porphyrin π-cation radical. To test this hypothesis, we have examined the W191F variant of C*c*P, in which formation of a radical at Trp191 is not possible. It has been shown previously that W191F is capable of forming an oxyferryl porphyrin π-cation radical intermediate, on reaction with H_2O_2, while at the same time the main protein radical signal is destabilised ~100-fold and there is also a dramatic decrease in enzymatic activity (*2-4*). In this work, we present evidence to show that formation of a covalently-linked product indeed occurs in the W191F variant and that this is related to the ability of the W191F variant to form a Compound I intermediate bearing a porphyrin π-cation radical, as seen for rsAPX.

3.2   Results

3.2.1   Expression and purification of CcP

Samples of CcP were prepared from *Escherichia coli* BL21 gold DE3 cells (the vector that supports the gene is a version of PemBL8 modified to incorporate the T7 promoter sequence and also includes ampicillin resistance) and purified as described in Chapter 6. Samples of CcP were stored at -80 °C as a crystalline suspension in water.

All CcP protein samples used for this work were kindly prepared and provided by Dr Clive Metcalfe.

3.2.2   Spectroscopic characterization

Purified samples of CcP showed wavelength maxima at 409, 508, 544[sh] and 645 nm (100 mM potassium phosphate, pH 6.0), as reported previously (*5*) (Figure 3.2). Enzyme concentrations for CcP were determined using absorption coefficients of ε_{409} = 95 mM^{-1}cm^{-1} [a].
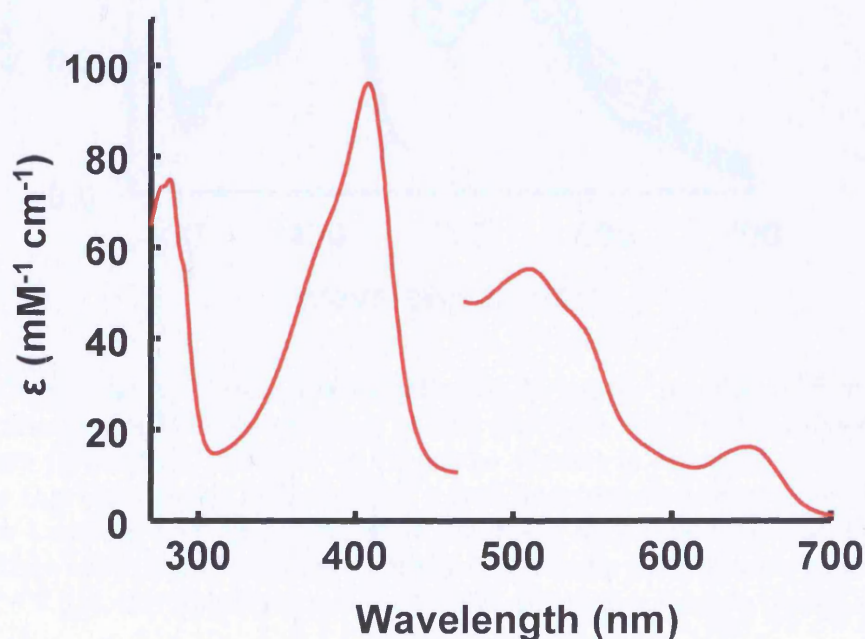
Figure 3.2: UV-visible absorption spectra of CcP. The visible region has been multiplied by a factor of 5. Conditions: 100 mM potassium phosphate, pH 6.0, 25 °C.

---

[a] The absorption coefficient value for CcP was calculated by Dr Clive Metcalfe, using the pyridine hemochromagen assay.

3.2.3 Reaction of CcP with H$_2$O$_2$ and HPLC analysis

In order to examine whether wild-type CcP exhibits similar behaviour to rsAPX, *i.e* whether it forms a link from Trp51 to the heme on reaction with H$_2$O$_2$, we reacted CcP with 6 equivalents of H$_2$O$_2$ and followed the reaction using UV-visible spectroscopy, as reported previously for rsAPX (1). Reaction of CcP with H$_2$O$_2$ resulted in initial formation of an intermediate with wavelength maxima at 420, 530 and 561 nm, as reported for CcP Compound I bearing an oxyferryl iron species and a protein radical (6, 7). This Compound I species decays to a species with wavelength maxima at 413, 532 and 569^{sh} nm over ~2 h (Figure 3.3).
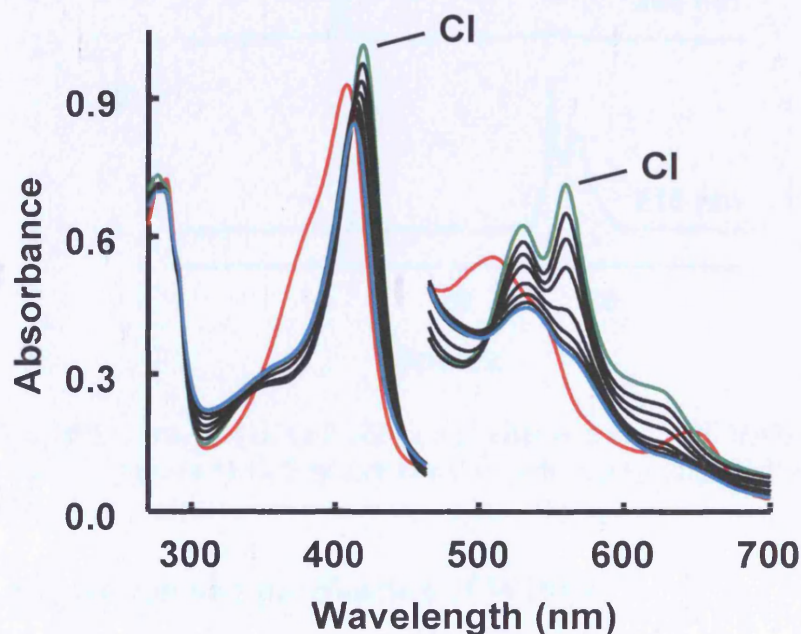
Figure 3.3: Selected electronic spectra collected during the reaction of ferric CcP with 6 equivalents of H$_2$O$_2$. Conversion of CcP (red line) to the initial Compound I intermediate (green line, indicated as CI on the Figure) is observed, followed by conversion to a final species indicated with a cyan line. Intermediate spectra between Compound I and the final species are shown as black lines. The total reaction time was 2 h. The visible region has been multiplied by a factor of 5. Sample conditions: [Enzyme] = 9 μM, [Hydrogen peroxide] = 54 μM, 100 mM potassium phosphate, pH 7.0, 25 °C.

HPLC analysis was carried out before (Figure 3.4a,b) and after (Figure 3.4c,d) treatment of CcP with hydrogen peroxide under the same conditions as those used for rsAPX (1). There was no co-elution of the heme with the protein and this suggests a lack of formation of a covalent link between the heme and the protein.
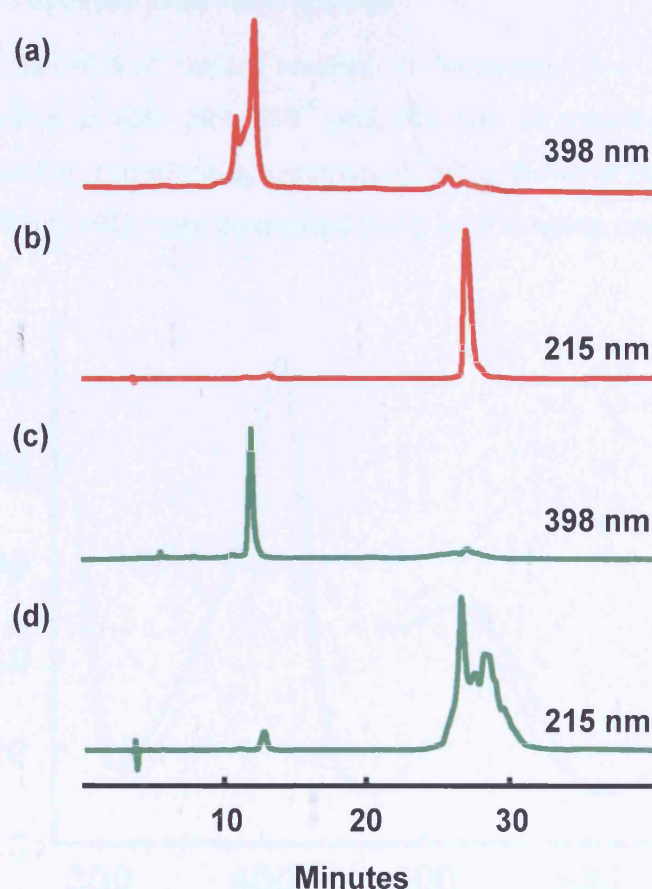
Figure 3.4: HPLC analyses of CcP before and after reaction with H_2O_2 monitored at 398 nm and 215 nm. (a,b) CcP before reaction with H_2O_2, (c,d) CcP after reaction with H_2O_2.

3.2.4   Expression and purification of W191F

Site-directed mutagenesis was performed, according to the Quickchange™ protocol, as described in Chapter 6. The W191F variant was expressed and purified as described in Chapter 6.

The purity of freshly isolated W191F variant was checked using SDS-PAGE analysis, and the preparations were judged to be homogeneous by the observation of a single band on a Coomassie Blue-stained reducing SDS-PAGE gel.

All W191F protein samples used for this work were kindly prepared and provided by Miss Emma Murphy.

3.2.5   Spectroscopic characterization

Expression of the W191F variant resulted in formation of a red enzyme with absorption maxima at 409, 509, 539[sh] and 642 nm, as reported previously (2). Comparison with the corresponding spectrum of CcP is shown in Figure 3.5. Enzyme concentrations for W191F were determined using an absorption coefficients of ε_{409} = 102 mM^{-1}cm^{-1} [b].
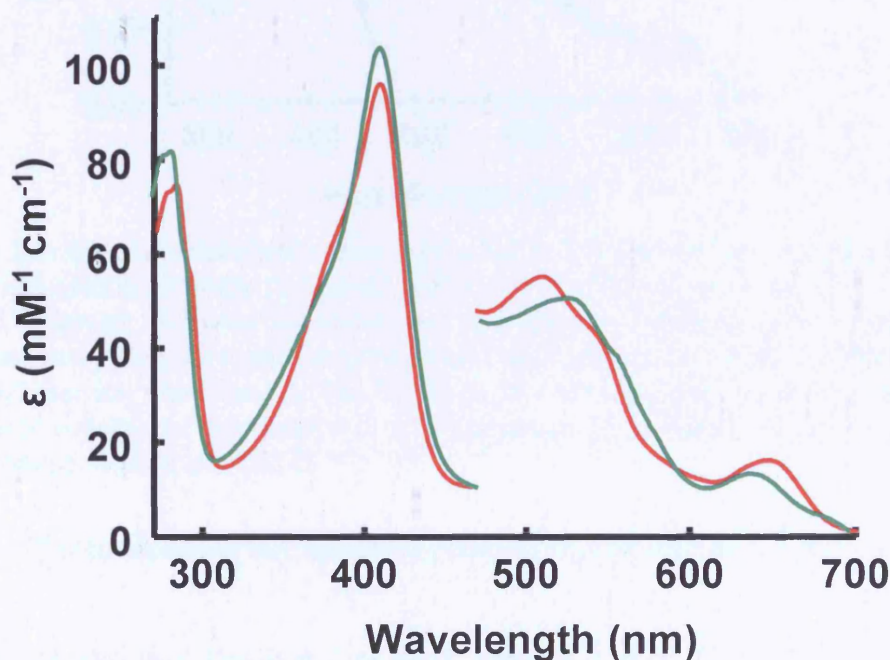
Figure 3.5: UV-visible absorption spectra of W191F (green line) and CcP (red line). The visible region has been multiplied by a factor of 5. Conditions: 100 mM potassium phosphate, pH 7.0, 25.0 °C

3.2.6   Reaction of W191F variant with H_2O_2

Reaction of W191F with 6 equivalents of H_2O_2 was followed by UV-visible spectroscopy (Figure 3.6), and showed initial formation of a species with wavelength maxima at 421, 532 and 563 nm, similar to the spectrum of CcP Compound I (Figure 3.3) as reported previously (*2*). This Compound I species decayed to a species with wavelength maxima at 415, 533 and 564 nm over a period ~2 h (Figure 3.6).

---

[b] The absorption coefficient value for W191F was calculated by Miss Emma Murphy, using the pyridine hemochromagen assay.
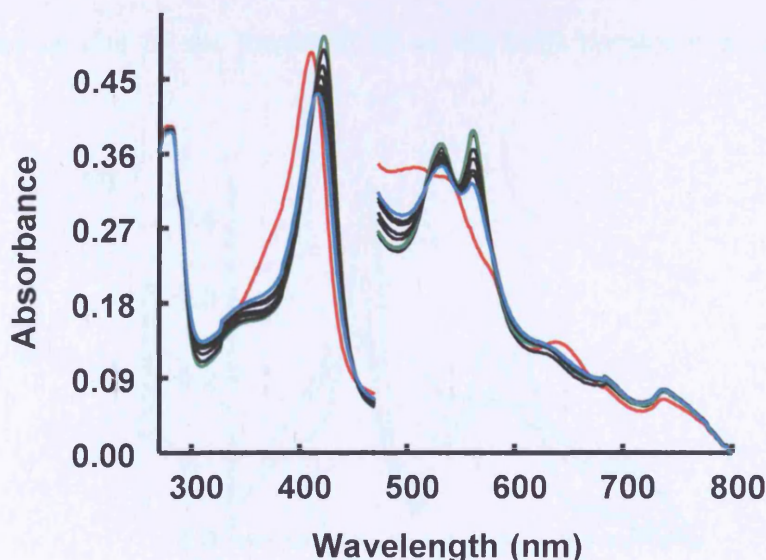
Figure 3.6: Selected electronic spectra collected during the reaction of ferric W191F with 6 equivalents of H_2O_2. Conversion of W191F (red line) to a Compound I (green line) is observed, followed by conversion to a species indicated with a cyan line. Intermediate spectra between Compound I and final species are shown as black lines. The total reaction time was 2 h. The visible region has been multiplied by a factor of 5. Sample conditions: [Enzyme] = 5 μM, [Hydrogen peroxide] = 30 μM, 100 mM potassium phosphate, pH 7.0, 25 °C.

3.2.7 Photodiode-array spectroscopy of the reaction of W191F with H_2O_2

Previous stopped-flow kinetic studies on the reaction of W191F with H_2O_2, revealed the presence of a spectrally distinct intermediate that occurs before formation of the Compound I species observed by UV-visible spectroscopy (*2*). This intermediate was assigned as a Compound I species bearing a porphyrin π-cation radical, as seen for APX. To confirm this observation, stopped-flow studies were used to monitor the reaction of W191F with H_2O_2. W191F was reacted with different concentrations of H_2O_2 and the spectral changes were monitored for a period of up to 1 s; for each experiment the first spectrum was recorded 1.28 ms after the mixing event. In all cases there was an initial decrease in absorbance of the Soret peak (409 nm) followed by an increase in absorbance at 424 nm (Figure 3.7a). This initial decrease in absorbance is characteristic of formation of an intermediate with lower absorptivity, that has been shown for APX to belong to a Compound I intermediate bearing a porphyrin π-cation radical (*8*). The similarity of the spectral characteristics of this intermediate (λ_{max}/nm = 409, 532, 570[sh] and 654), (Figure 3.7a, green line) with HRP (*9*) and APX Compound I (λ_{max}/nm = 409, 530, 569[sh], and 655) (*8*), suggests that it

may also be due to the formation of an oxyferryl porphyrin π-cation radical in W191F.
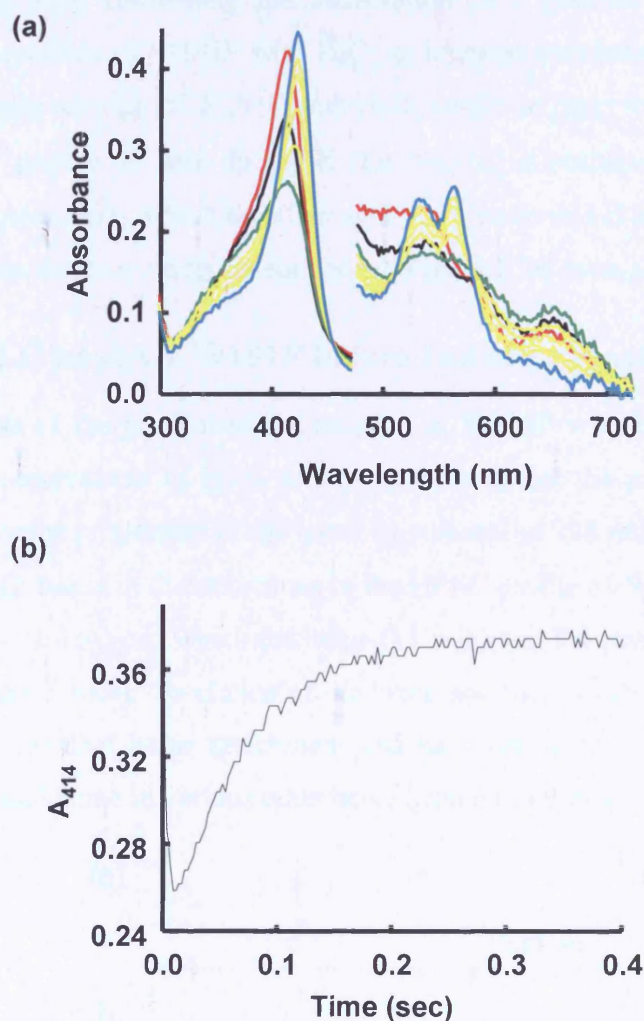
Figure 3.7: (a) Spectral changes observed upon reaction of W191F with H_2O_2, monitored by stopped-flow photodiode array spectroscopy. Conditions: [Enzyme] = 3.5 μM, [Hydrogen peroxide] = 17.5 μM, 100 mM potassium phosphate buffer, pH 7.0, 25 °C. The spectral changes were monitored over a period of 1 s after the mixing event. For reference, the spectrum of the ferric W191F is shown in red. The first spectrum (recorded at 1.28 ms after mixing) is shown in black and rapidly converts to a typical Compound I species bearing a porphyrin π-cation radical, shown in green. This Compound I species decays to a typical Compound II species, shown in cyan. Intermediate spectra between Compound I and Compound II are shown in yellow. For clarity, only selected spectra are shown. In all cases the visible region has been multiplied by a factor of 5. (b) Change in absorbance at 414 nm after mixing W191F with 6 equivalents of H_2O_2 (reaction concentrations as in (a)).

By following the absorbance change at 414 nm (the isosbestic point between ferric W191F and the Compound I intermediate observed at 421 nm), we saw a rapid

decrease in absorbance (0 to 10 ms), followed by a slower increase in absorbance (10 ms to 250 ms) up to the level corresponding to that of the Compound I species (Figure 3.7b), thus confirming the observation of a distinct intermediate being formed after reaction of W191F with H_2O_2 as reported previously (*2*). Hence, these data suggest that reaction of W191F with H_2O_2 results in rapid formation of a typical Compound I species as seen for APX (*i.e.* bearing a porphyrin π-cation radical, Figure 3.7a, green line), which then converts to a Compound II species (*i.e* oxyferryl species that has lost one oxidising equivalent, Figure 3.7a, cyan line).

3.2.8 HPLC analyses W191F before and after reaction with H_2O_2

HPLC analysis of the product of the reaction of W191F with H_2O_2 (prepared with addition of 6 equivalents of H_2O_2 as above) showed that the protein (monitored at 215 nm) and some proportion of the heme (monitored at 398 nm) co-elute at 30 min (Figure 3.8c,d); this is in direct contrast to the HPLC profile of W191F which has not been treated with H_2O_2, in which the heme (13 min) and the protein (30 min) do not co-elute (Figure 3.8a,b). Co-elution of the heme and the protein fragments is a clear indication of covalent heme attachment and has been used previously to identify covalently linked heme in various other heme proteins (*10-16*).
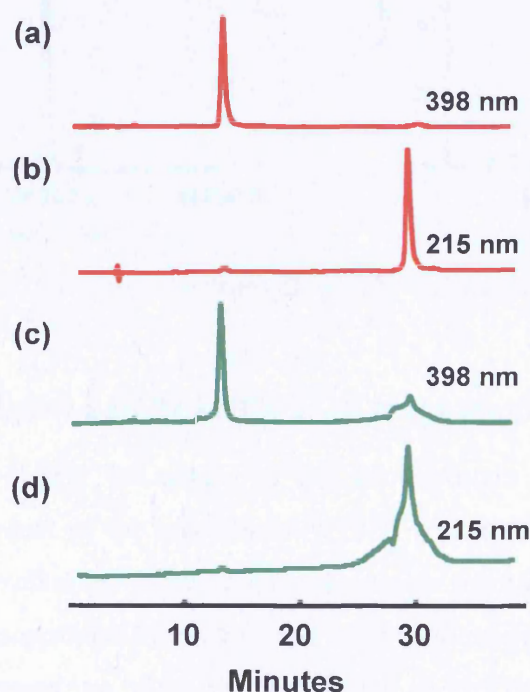
Figure 3.8: HPLC analyses of W191F before and after reaction with H_2O_2 monitored at 398 nm and 215 nm. (a,b) W191F before reaction with H_2O_2, (c,d) W191F after reaction with H_2O_2.

3.2.9 MALDI-TOF analysis of W191F before and after reaction with H_2O_2

Mass spectrometry can be used not only to confirm the presence of a covalent link but also to establish the identity of the residue(s) making the link (*1*). The MALDI-TOF mass spectrum of W191F before treatment with H_2O_2 showed a mass of 33561.10 Da (Figure 3.9a), which corresponds closely to the predicted mass (33554.4 Da) of the apo-protein and is consistent with non-covalent attachment of the heme (as found in rsAPX). After treatment with H_2O_2, two peaks were observed in the MALDI-TOF spectrum, Figure 3.9b. The first is at 33578.66 Da, which is consistent with the mass of the apo-protein (as above). The second peak is at 34195.77 Da, which corresponds to an increase in mass of 617 Da compared to the mass assigned to the apo-protein, and is consistent with covalent attachment of the heme (616 Da) to the protein.
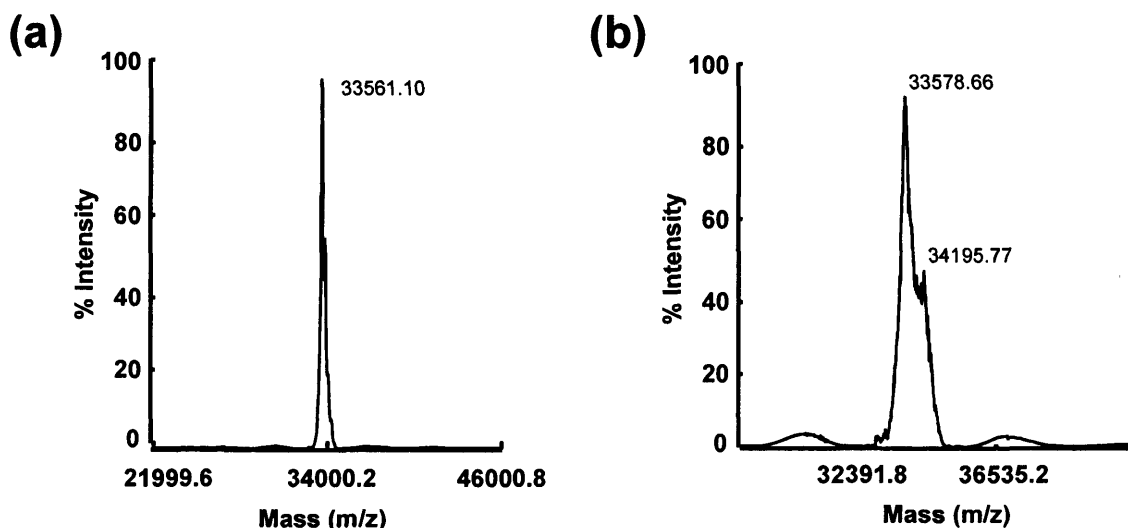
Figure 3.9: MALDI-TOF mass spectrum of W191F before (a) and after (b) reaction with 6 equivalents of H_2O_2.

3.2.10 Tryptic digest and MALDI-TOF mass spectrometry

To establish more clearly the nature of the heme-protein covalent link, tryptic digestion of the product of the reaction of W191F with H_2O_2 was carried out and HPLC was used to isolate the heme-containing peptide fragments (*i.e.* showing both heme and protein absorbancies) from the resulting peptide mixture (Figure 3.10). The MALDI-TOF mass spectrum of the product eluting at 35.7 min gave a mass of 616 Da, indicating that this HPLC peak corresponds to free heme species, as reported earlier in the case of rsAPX. MALDI-TOF mass spectrometry of the peptide

fragment eluting at 30.0 min gave a spectrum with a mass of 1915.22 Da, which is 2 Da lower than the calculated mass of 1917 Da expected for the L[49]AW[51]HTSGTWDK[59] peptide fragment containing heme covalently bound to Trp51 (Figure 3.11a).

Further evidence for heme incorporation into the peptide mentioned above came from the characteristic heme isotope pattern of this peptide (Figure 3.11a). As reported previously (*17*), iron exhibits a very distinct isotope pattern when incorporated into protoporphyrin IX to form heme such that it produces very characteristic signals in the mass spectrum (Figure 3.11b). The fact that the peptide with mass of 1915.22 Da (Figure 3.11a) exhibits the same characteristic isotope pattern as heme (Figure 3.11b) (*17*) gives further confirmation to its assignment as a heme-containing peptide.
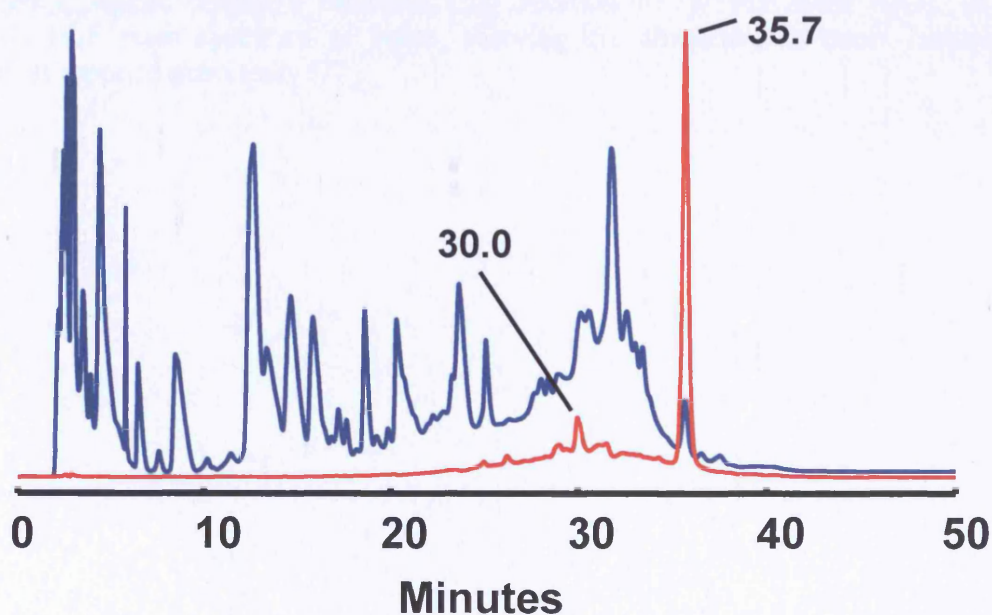
Figure 3.10: HPLC analyses of a tryptic digest of W191F after reaction with H_2O_2, monitored at 215 nm (blue line) and 398 nm (red line). Elution times of heme-containing peptides (30.0 min) as well as free heme (35.7 min) are indicated.
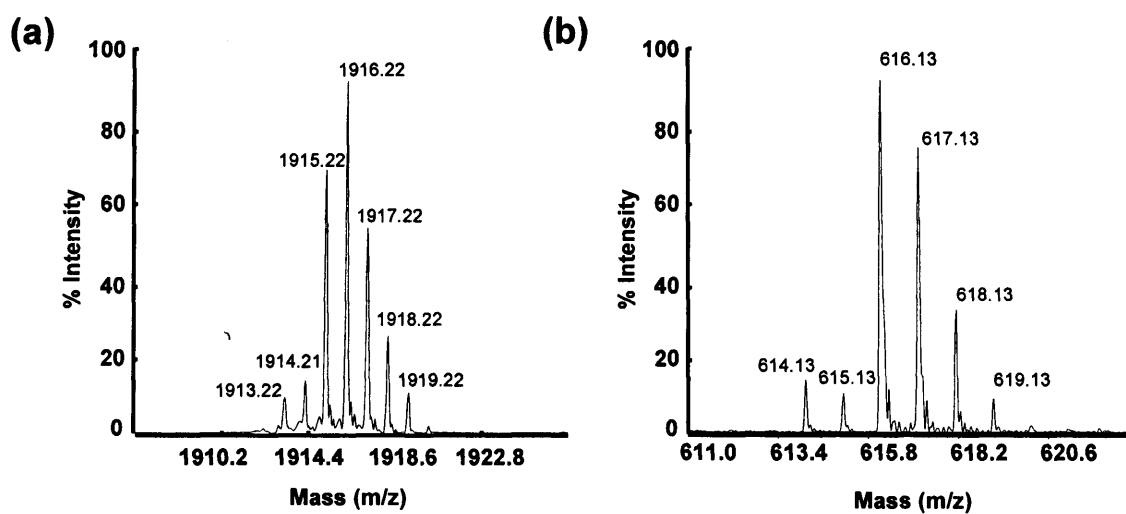
Figure 3.11: (a) MALDI-TOF mass spectrum of the HPLC-purified heme-containing peptide fragment obtained after reaction of W191F with H_2O_2. (b) MALDI-TOF mass spectrum of heme, showing the characteristic heme isotope pattern as reported previously (*17*).

3.3 Discussion

As mentioned earlier, the three most prominent members of the class I super-family of heme peroxidases, CcP, APX and the KatG (*18*), share very similar active site structures and are distinguished from other peroxidases by the presence of a distal tryptophan residue. The KatG, however, have another distinct feature as their distal tryptophan is involved in a covalently bound Trp-Tyr-Met cross-link (*19-23*) that has been proposed to be responsible for their catalatic activity (*24-27*). The proposed mechanism for formation of this cross-link involves radical formation on Trp107 (Scheme 2.1). Although both APX and CcP bear the same distal tryptophan residue, no such cross-link has been observed in either of these enzymes.

In Chapter 2, evidence was presented that was consistent with APX supporting radical formation on the distal tryptophan, Trp41, which results in covalent attachment of the tryptophan to the 4-vinyl group of the heme (*1*). We proposed that radical formation on the distal tryptophan could be a common feature among the members of the Class I peroxidases and that absence of a Trp-Tyr-Met cross-link in APX and CcP could be assigned to the absence of the suitable Tyr residue (and both Tyr and Met in the case of CcP) adjacent to Trp41 (Trp51 in the case of CcP).

The aim of this chapter was to test this proposal further, with parallel experiments on CcP. CcP is unique amongst the class I peroxidases in that it utilises a protein amino acid during its catalytic cycle. A porphyrin radical is not observed in the Compound I of CcP, so an alternative site for X$^\bullet$ had long been sought. Several residues have been implicated as possible radical sites, including Trp51 (*28-32*), Trp191 (*2, 29, 32*), Met172 (*28, 33*), and Met230 and Met231 (*34, 35*). EPR, ENDOR spectroscopy and mutagenesis studies finally identified Trp191 as the position of radical formation in CcP Compound I (*32, 36, 37*). Hence, the enzyme diverts oxidising equivalents to Trp191 as the immediate product of H_2O_2 oxidation without formation of a porphyrin π-cation radical.

As a result of the very similar active site structure of CcP and APX and the presence of Trp51 in CcP in the same position as Trp41 in APX, we examined the reaction of CcP with H_2O_2 to investigate if the same behaviour, leading to covalent linkage of the heme to the protein, could also be observed in CcP. However, no evidence for formation of an analogous link to Trp51 was observed in CcP. We suggested (*1*) that diversion of the radical to Trp191 would preclude formation of a radical at Trp51,

according to the mechanism proposed in Scheme 2.2 in Chapter 2, and we proposed that this might account for the fact that no heme-protein linkage is seen in CcP similar to that observed in APX. To test this hypothesis further, we examined the W191F variant of CcP and investigated its reaction with H_2O_2. In this variant, formation of a radical at Trp191 is not possible and hence formation of a porphyrin π-cation radical occurs instead (2).

Expression of the W191F variant of CcP was first reported in 1988 by Mauro et al. and it was shown to exhibit a dramatic decrease in enzymatic activity compared to wild-type CcP (4). EPR studies by the same group also revealed that the mutant forms a Compound I like species with a stable oxyferryl centre upon reaction with H_2O_2, but the stability of the site responsible for the radical signal is reduced ~100-fold compared to wild-type CcP (4). In 1989, EPR and ENDOR studies from Scholes et al. further supported the above hypothesis (32). Furthermore, Erman et al. reported stopped-flow data on W191F which demonstrated that on reaction with H_2O_2 the variant forms a spectrum characteristic of a porphyrin π-cation radical as seen for HRP and APX (2).

It is also interesting to note that when the crystal structure of W191F was published in 1990, Wang et al. proposed that the reaction of the W191F mutant with H_2O_2 proceeds by formation of a porphyrin π-cation radical which slowly breaks down by an endogenous reduction reaction (3). Nine years later, Gengenbach et al. proposed that although Trp51 had been ruled out as the *primary* radical site in CcP, its close position to the heme makes it an attractive candidate site for the radical in the W191F mutant. Their studies showed that Compound I decays slower in the W191F/W51F double mutant and suggested that Trp51 may be an alternate radical site for CcP mutants lacking Trp191 (38).

In this chapter, as previously for APX and CcP, the W191F variant was reacted with H_2O_2 and subsequently tested for heme-protein covalent link formation. More specifically:

- UV-visible spectroscopy showed formation of a Compound I species on reaction of W191F with H_2O_2 with spectral properties similar to those for CcP as reported previously (2).

- However, stopped-flow analysis of the same reaction revealed that this Compound I species was more likely to be similar to a typical Compound II

species as seen for APX (*8*) and was preceded by formation of a typical Compound I intermediate, bearing a porphyrin π-cation radical. These observations are in agreement with previous studies (*2*) which suggested that the W191F variant, unlike C*c*P, is capable of forming a short-lived porphyrin π-cation radical on reaction with H_2O_2.

- HPLC analyses showed co-elution of some proportion of the heme and the protein after reaction with H_2O_2, which is indicative of covalent attachment between the heme and the protein.

- Mass spectrometry showed that W191F treated with H_2O_2 has a mass which increased by 617 Da compared to the mass of the apo-protein (obtained for W191F before reaction with H_2O_2), which confirms the initial suggestion that the heme group is covalently attached to the protein.

- Tryptic digest and mass spectrometry analysis of the HPLC purified heme containing fragment, suggested that the heme is linked to the $L^{49}AW^{51}HTSGTWDK^{59}$ peptide fragment, containing Trp51. However, in this case there was no additional mass to indicate that addition of an extra hydroxyl group to the heme-containing fragment had occurred, as previously seen for rAPX (*1*).

- Analysis of the isotope pattern of the mass spectrum of the HPLC purified peptide fragment provided further evidence supporting its assignment as a heme-containing peptide.

Based on both our initial observations for formation of a covalent link between Trp41 and the 4-vinyl group of the heme in rsAPX, as well as the striking resemblance between the active site structure of W191F and rsAPX (Figure 3.1), we propose a similar mechanism for formation of a Trp51-heme link in W191F in Scheme 3.1, as proposed for rsAPX (Chapter 2, Scheme 2.2). In this mechanism, initial formation of a Compound I intermediate (step (i)) is followed by oxidation and deprotonation of Trp51 (step (ii)) and addition of the Trp51 radical across the 4-vinyl group of the heme (steps (iii) and (iv)). Subsequent reduction of the ferryl group and release of H_2O (step (v)) leads to formation of a carbocation. Deprotonation at this position (instead of addition of a H_2O molecule as proposed for rsAPX) as the final step (step (vi)) gives a heme structure that is consistent with the mass spectrometry data.
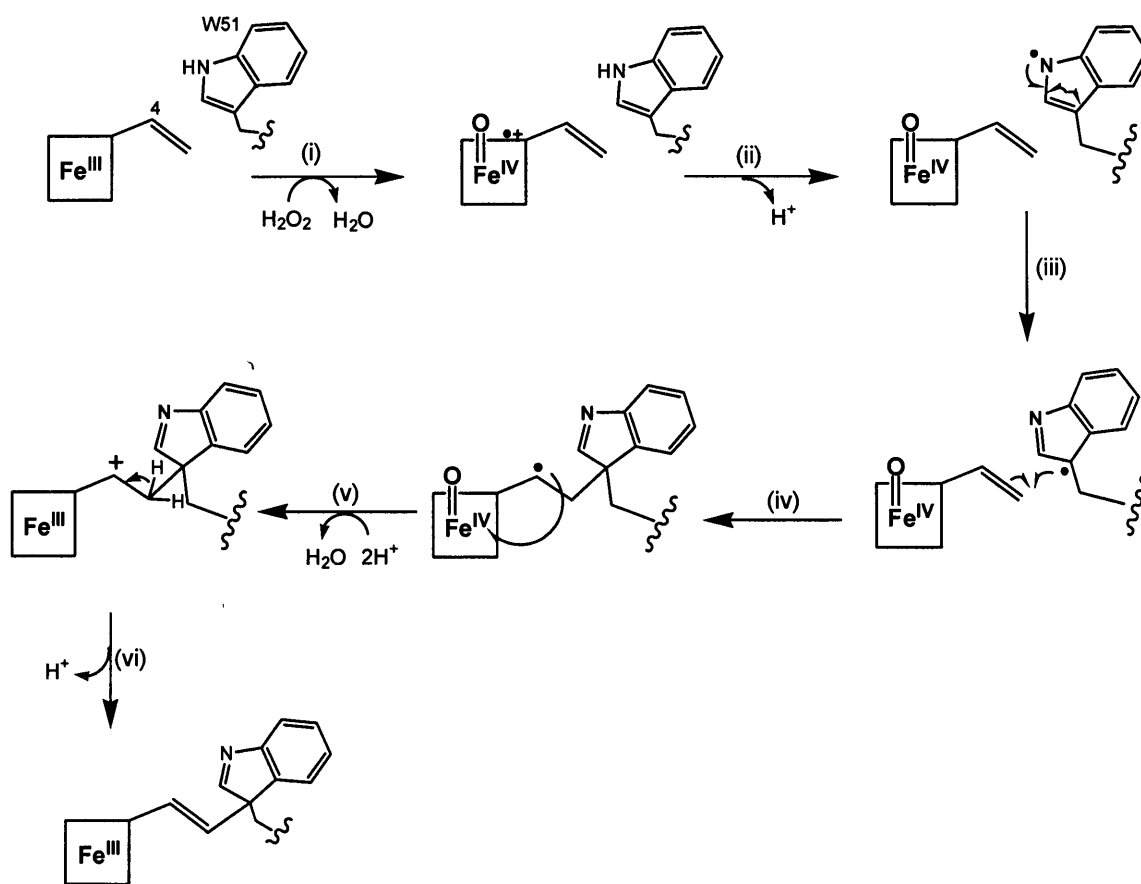
Scheme 3.1: Proposed mechanism for formation of a covalent link between Trp51 and the heme group in W191F variant of CcP. Steps (i) – (vi) are described in the text.

One key element of the mechanism proposed above is that formation of a porphyrin π-cation radical is followed by radical formation on Trp51. Although no studies have clearly established Trp51 as a site of radical formation in W191F, our proposal is in agreement with previous hypotheses which suggested that Trp51 is a very attractive candidate for radical formation in W191F (*38*). Interestingly, there is separate evidence that formation of a radical on Trp51 in CcP may occur under certain conditions (*39*). Hence, Poulos and co-workers have shown that peroxide-dependent formation of a Trp51-Tyr52 link occurs in the H52Y variant of CcP and the formation of this link is proposed to involve oxidation of Trp51 to Trp• and oxidation of Tyr52 to Tyr• in a mechanism that is analogous to that proposed for KatG (*20, 40*) (*i.e.* without formation of the expected Compound I species, with a radical on Trp191).

116

A second observation came from HPLC analyses of W191F after reaction with H_2O_2 (Figure 3.8c,d). Although we propose that covalent link formation between the heme and the protein in W191F occurs at the same position as in rsAPX (Chapter 2), we noted that the yield of covalent linkage was decreased in the case of W191F (average yields were calculated from % peak assigned to covalently bound heme on HPLC chromatograms). Although it has been well documented that Trp191 is the principal site of protein radical formation in Compound I of CcP, numerous studies have shown that radical migration to aromatic residues occurs subsequently (*41-44*) and that the stability of Compound I depends on the number of endogenous oxidisable amino acids (*42*). Furthermore, Zhang *et al.* reported radical formation at Tyr39 and Tyr153 and suggested that the porphyrin ring is the primary conduit of electron transfer from these tyrosyl residues rather than Trp191 cation radical (*45*). We believe that the high percentage of aromatic residues near the active site of W191F in comparison to APX could aid radical diffusion and thus decrease the percentage of specific radical formation on Trp51 and as a consequence the yield of covalent linkage of Trp51 to the heme.

Overall, the work in this chapter provides further evidence for radical formation on Trp51 in W191F variant and further supports our initial hypothesis that the absence of a porphyrin π-cation radical in wild-type CcP was the reason for its inability to form a heme-protein covalent link as seen for rsAPX (Chapter 2). These observations further support our proposal that radical formation at the distal tryptophan is a general feature of both the KatG and the monofunctional peroxidases, under certain conditions, and that formation of a porphyrin π-cation radical seems to be the only prerequisite. Thus, in the presence of suitable residues in the distal cavity, both APX and CcP should be capable of forming a Met-Trp-Tyr cross-link, as seen for the KatG enzymes, whilst in the absence of the residues required for formation of such a cross-link it seems that covalent linkage to the heme is the most likely 'escape' route after radical formation on the distal tryptophan has occurred.

3.4 References

(1)   Pipirou, Z., Bottrill, A. R., Metcalfe, C. M., Mistry, S. C., Badyal, S. K., Rawlings, B. J., and Raven, E. L. (2007) Autocatalytic formation of a covalent link between tryptophan 41 and the heme in ascorbate peroxidase. *Biochemistry 46*, 2174-2180.

(2)   Erman, J. E., Vitello, L. B., Mauro, J. M., and Kraut, J. (1989) Detection of an oxy-ferryl porphyrin pi-cation radical in the reaction between hydrogen peroxide and a mutant yeast cytochrome *c* peroxidase. Evidence for tryptophan-191 involvement in the radical site of compound I. *Biochemistry 28*, 7992-7995.

(3)   Wang, J. M., Mauro, M., Edwards, S. L., Oatley, S. J., Fishel, L. A., Ashford, V. A., Xuong, N. H., and Kraut, J. (1990) X-ray structures of recombinant yeast cytochrome *c* peroxidase and three heme-cleft mutants prepared by site-directed mutagenesis. *Biochemistry 29*, 7160-7173.

(4)   Mauro, J. M., Fishel, L. A., Hazzard, J. T., Meyer, T. E., Tollin, G., Cusanovich, M. A., and Kraut, J. (1988) Tryptophan-191-phenylalanine, a proximal-side mutation in yeast cytochrome *c* peroxidase that strongly affects the kinetics of ferrocytochrome *c* oxidation. *Biochemistry 27*, 6243-6256.

(5)   Yonetani, T., and Ray, G. S. (1965) Studies on cytochrome *c* peroxidase. Purification and some properties. *J. Biol. Chem. 240*, 4503-4514.

(6)   Yonetani, T., Chance, B., and Kajiwara, S. (1966) Crystalline cytochrome *c* peroxidase and complex ES. *J. Biol. Chem. 241*, 2981-2982.

(7)   Coulson, A. F., and Yonetani, T. (1972) Oxidation of cytochrome *c* peroxidase with hydrogen peroxide: identification of the "endogenous donor". *Biochem. Biophys. Res. Commun. 49*, 391-398.

(8)   Lad, L., Mewies, M., and Raven, E. L. (2002) Substrate binding and catalytic mechanism in ascorbate peroxidase: evidence for two ascorbate binding sites. *Biochemistry 41*, 13774-13781.

(9)   Dolphin, D., Forman, A., Borg, D. C., Fajer, J., and Felton, R. H. (1971) Compounds I of catalase and horse radish peroxidase: pi-cation radicals. *Proc. Natl. Acad. Sci. U S A 68*, 614-618.

(10)   Colas, C., Kuo, J. M., and Ortiz de Montellano, P. R. (2002) Asp225 and Glu375 in autocatalytic attachment of the prosthetic heme group of lactoperoxidase. *J. Biol. Chem. 277*, 7191-7200.

(11)   Henne, K. R., Kunze, K. L., Zheng, Y.-M., Christmas, P., Soberman, R. J., and Rettie, A. E. (2001) Covalent linkage of prosthetic heme to CYP4 family of P450 enzymes. *Biochemistry 40*, 12925-12931.

(12)   Metcalfe, C. L., Ott, M., Patel, N., Singh, K., Mistry, S. C., Goff, H. M., and Raven, E. L. (2004) Autocatalytic formation of green heme: evidence for H_2O_2-dependent formation of a covalent methionine-heme linkage in ascorbate peroxidase. *J. Am. Chem. So.c 126*, 16242-16248.

(13)   Limburg, J., LeBrun, L. A., and Ortiz de Montellano, P. R. (2005) The $P450_{cam}$ G248E mutant covalently binds its prosthetic heme group. *Biochemistry 44*, 4091-4099.

(14)   LeBrun, L. A., Xu, F., Kroetz, D. L., and Ortiz de Montellano, P. R. (2002) Covalent attachment of the heme prosthetic group in the CYP4 cytochrome P450 family. *Biochemistry 41*, 5931-5937.

(15)   Colas, C., and De Montellano, P. R. (2004) Horseradish peroxidase mutants that autocatalytically modify their prosthetic heme group: insights into mammalian peroxidase heme-protein covalent bonds. *J. Biol. Chem. 279*, 24131-24140.

(16)   Reeder, B. J., Svistunenko, D. A., Sharpe, M. A., and Wilson, M. T. (2002) Characteristics and mechanism of formation of peroxide-induced heme to protein cross-linking in myoglobin. *Biochemistry 41*, 367-375.

(17)   Pipirou, Z., Bottrill, A. R., Svistunenko, D. A., Efimov, I., Basran, J., Mistry, S. C., Cooper, C. E., and Raven, E. L. (2007) The reactivity of heme in biological systems: autocatalytic formation of both tyrosine-heme and tryptophan-heme covalent links in a single protein architecture. *Biochemistry 46*, 13269-13278.

(18)   Welinder, K. G. (1992) Superfamily of plant, fungal and bacterial peroxidases. *Curr. Opin. Chem. Biol. 2*, 388-393.

(19)   Jakopitsch, C., Kolarich, D., Petutschnig, G., Furtmuller, P. G., and Obinger, C. (2003) Distal side tryptophan, tyrosine and methionine in catalase-peroxidases are covalently linked in solution. *FEBS Lett. 552*, 135-140.

(20)   Ghiladi, R. A., Knudsen, G. M., Medzihradszky, K. F., and Ortiz de Montellano, P. R. (2005) The Met-Tyr-Trp cross link in *Mycobacterium tuberculosis* catalase peroxidase. *J. Biol. Chem. 280*, 22651-22663.

(21)   Bertrand, T., Eady, N. A. J., Jones, J. N., Bodiguel, J., Jesmin, Nagy, J. M., Raven, E. L., Jamart-Gregoire, B., and Brown, K. H. (2004) Crystal Structure of *Mycobacterium tuberculosis* Catalase-Peroxidase. *J. Biol. Chem. 279*, 38991-38999.

(22)   Carpena, X., Loprasert, S., Mongkolsuk, S., Switala, J., Loewen, P. C., and Fita, I. (2003) Catalase-peroxidase KatG of *Burkholderia pseudomallei* at 1.7 Å. *J. Mol. Biol. 327*, 475-489.

(23)   Yamada, Y., Fujiwara, T., Sato, T., Igarashi, N., and Tanaka, N. (2002) The 2.0 angstrom crystal structure of catalase-peroxidase from *Haloarcula marismortui*. *Nature. Struct. Biol. 9*, 691-695.

(24)   Regelsberger, G., Jakopitsch, C., Ruker, F., Krois, D., Peschek, G. A., and Obinger, C. (2000) Effect of distal cavity mutations on the formation of Compound I in catalase-peroxidases. *J. Biol. Chem. 275*, 22854-22861.

(25)   Jakopitsch, C., Ivancich, A., Schmuckenschlager, F., Wanasinghe, A., Poltl, G., Furtmuller, P. G., Ruker, F., and Obinger, C. (2004) Influence of the unusual covalent adduct on the kinetics and formation of radical intermediates in *Synechocytic* catalase peroxidase. *J. Biol. Chem. 279*, 46082-46095.

(26)   Jakopitsch, C., Auer, M., Ivancich, A., Ruker, F., Furtmuller, P. G., and Obinger, C. (2003) Total conversion of bifunctional catalase-peroxidase (KatG) to monofunctional peroxidase by exchange of a conserved distal side tyrosine. *J. Biol. Chem. 278*, 20185-20191.

(27)   Hillar, A., Peters, B., Pauls, R., Loboda, A., Zhang, H., Mauk, A. G., and Loewen, P. C. (2000) Modulation of the activities of catalase-peroxidase HPI of *Escherichia coli* by site-directed mutagenesis. *Biochemistry 39*, 5868-5875.

(28)   Finzel, B. C., Poulos, T. L., and Kraut, J. (1984) Crystal structure of cytochrome *c* peroxidase refined at 1.7 Å resolution. *J. Biol. Chem. 259*, 13027-13036.

(29)   Hori, H., and Yonetani, T. (1985) Powder and single-crystal electron paramagnetic resonance studies of yeast cytochrome *c* peroxidase and its peroxide compound, Compound ES. *J. Biol. Chem. 260*, 349-355.

(30)   Goodin, D. B., Mauk, A. G., and Smith, M. (1987) The peroxide complex of yeast cytochrome *c* peroxidase contains two distinct radical species, neither of which resides at methionine 172 or tryptophan 51. *J. Biol. Chem. 262*, 7719-7724.

(31)   Fishel, L. A., Villafranca, J. E., Mauro, J. M., and Kraut, J. (1987) Yeast cytochrome *c* peroxidase: mutagenesis and expression in *Eschericia coli* show tryptophan-51 is not the radical site in Compound I. *Biochemistry 26*, 351-360.

(32)   Scholes, C. P., Liu, Y., Fishel, L. A., Farnum, M. F., Mauro, J. M., and Kraut, J. (1989) Recent ENDOR and pulsed electron paramagnetic resonance studies of cytochrome *c* peroxidase Compound I and its site-directed mutants. *Isr. J. Chem. 29*, 85-92.

(33)   Goodin, D. B., Mauk, A. G., and M., S. (1986) Studies of the radical species in compound ES of cytochrome *c* peroxidase altered by site-directed mutagenesis. *Proc. Nat. Ac .Sci. USA 83*, 1295-1299.

(34)   Edwards, S. L., Xuong, N., Hamlin, R. C., and Kraut, J. (1987) Crystal structure of cytochrome *c* peroxidase Compound I. *Biochemistry 26*, 1503-1511.

(35)   Hoffman, B. M., Roberts, J. E., Brown, T. G., Kang, C. H., and Margoliash, E. (1979) Electron-nuclear double resonance of the hydrogen peroxide compound of cytochrome *c* peroxidase: identification of the free radical site with a methionyl cluster. *Proc. Natl. Acad. Sci. U S A 76*, 6132-6136.

(36)   Sivaraja, M., Goodin, D. B., Smith, M., and Hoffman, B. M. (1989) Identification by ENDOR of Trp191 as the free-radical site in cytochrome *c* peroxidase compound ES. *Science 245*, 738-740.

(37)   Fishel, L. A., Farnum, M. F., Mauro, J. M., Miller, M. A., Kraut, J., Liu, Y. J., Tan, X. L., and Scholes, C. P. (1991) Compound I radical in site-directed mutants of cytochrome *c* peroxidase as probed by electron paramagnetic resonance and electron-nuclear double resonance. *Biochemistry 30* , 1986-1996.

(38)   Gengenbach, A., Syn, S., Wang, X., and Lu, Y. (1999) Redesign of cytochrome c peroxidase into a manganese peroxidase: role of tryptophans in peroxidase activity. *Biochemistry 38*, 11425-11432.

(39)   Bhaskar, B., Immoos, C. E., Shimizu, H., Sulc, F., Farmer, P. J., and Poulos, T. L. (2003) A novel heme and peroxide-dependent tryptophan-tyrosine cross-link in a mutant of cytohrome c peroxidase. *J. Mol. Biol. 328*, 157-166.

(40)   Ghiladi, R. A., Medzihradszky, K. F., and Ortiz de Montellano, P. R. (2005) Role of the Met-Tyr-Trp cross link in *Mycobacterium tuberculosis* catalase peroxidase (KatG) as revealed by KatG(M255I). *Biochemistry 44*, 15093-15105.

(41)   Fox, T., Tsaprailis, G., and English, A. M. (1994) Fluorescence investigation of yeast cytochrome c peroxidase oxidation by H_2O_2 and enzyme activities of the oxidized enzyme. *Biochemistry 33*, 186-191.

(42)   Pfister, T. D., Gengenbach, A. J., Syn, S., and Lu, Y. (2001) The role of redox-active amino acids on compound I stability, substrate oxidation, and protein cross-linking in yeast cytochrome c peroxidase. *Biochemistry 40*, 14942-14951.

(43)   Ivancich, A., Dorlet, P., Goodin, D. B., and Un, S. (2001) Multifrequency high-field EPR study of the tryptophanyl and tyrosyl radical intermediates in wild-type and the W191G mutant of cytochrome c peroxidase. *J. Am. Chem. Soc. 123*, 5050-5058.

(44)   Tsaprailis, G., and English, A. M. (2003) Different pathways of radical translocation in yeast cytochrome c peroxidase and its W191F mutant on reaction with H_2O_2 suggest an antioxidant role. *J. Biol. Inorg. Chem. 8*, 248-255.

(45)   Zhang, H., He, S., and Mauk, A. G. (2002) Radical formation at Tyr39 and Tyr153 following reaction of yeast cytochrome c peroxidase with hydrogen peroxide. *Biochemistry 41*, 13507-13513.

Chapter 4

The reactivity of heme in biological systems: Autocatalytic formation of both tyrosine-heme and tryptophan-heme covalent links in a single protein architecture

4.1 Introduction

The heme prosthetic group is used commonly in biology. It is usually found associated with proteins as a non-covalent complex, for example in the globins and the b-type cytochromes. As reviewed in Chapter 1, however, there are examples, in which the heme is bound to the protein through a covalent link to one or more amino acids. The cytochromes c (*1*) are probably the most well-known example of this: in this case, one or both of the heme vinyl groups are bound to the protein through thioether bonds to cysteine residues. Recently, however, it has become clear that the presence of a covalently-bound heme group is not a special privilege of the cytochromes c. For example, the mammalian peroxidase enzymes are known to contain sulphonium links between the heme 2-vinyl group and a methionine residue (in myeloperoxidase) and/or two ester links between heme methyl groups and glutamate/aspartate residues (in lactoperoxidase, myeloperoxidase) (*2-5*). Other examples include: the CYP4 family of cytochrome P450s which contain a similar ester link between the heme methyl group and a glutamate residue (*2, 6, 7*); a cyanobacterial hemoglobin, which contains a covalent link between the vinyl group and a histidine residue (*8*); and the heme chaperone CcmE which uses a different vinyl–histidine covalent link (*9, 10*).

Recently, various studies from a number of laboratories have shown that the formation of covalent links to the heme of the type described above are not a unique feature of these particular proteins and can actually be engineered into an existing heme protein framework if an appropriate residue is introduced at an appropriate location and if the correct metal oxidation states are accessible (*11-16*). Collectively, these data have led to an emerging view that the existence of a specific covalent link is largely dictated by structural geometry and, in the catalytic enzymes, heme reactivity. This represents a substantial departure in the way we think about these modified heme groups because it tells us that the strategic positioning of a suitable amino acid within close proximity of the heme group, and contained within a structurally competent protein architecture, is all that is needed for a covalent link from the heme to the protein to form. By implication, this leads one to conclude that the heme group is much more reactive than was originally realized and that 'activation' of the heme substituents is accessible in numerous heme protein architectures and is dictated by the iron chemistry and the structural environment. It

follows logically that some proteins might actually need to be poised in an environment that controls the inherent reactivity of the heme group by specifically "switching off" the machinery required for formation of these covalent links. As a case in point, we have noted (*17*) that a covalent link between the heme and an engineered methionine residue, analogous to that found in the mammalian peroxidases, can be incorporated into the APX framework but that C*c*P, which already contains a methionine residue at this position (Met172), does not form the same covalent heme-Met link under any accessible conditions.

If it is the case that the heme group *per se* is inherently reactive and its reactivity is controlled by the iron and the protein hardware, then it follows that the heme should, in principle, react with *any* nucleophilic amino acid, not just those observed so far in biological systems. In this work, we have tested the generality of this hypothesis by the introduction of a tyrosine residue (S160Y variant, Figure 4.1) into APX at a position that has been shown (*11*) to allow formation of a methionine-heme covalent link (S160M variant) through a H_2O_2-dependent activation process. We find that Tyr160 does indeed form a covalent link to the heme in an autocatalytic reaction that also leads to formation of a second covalent link to Trp41, as seen for rsAPX. We find that the formation of these links has a profound effect on the redox properties of the heme iron. The implications of these data in terms of current understanding of heme group reactivity are discussed.

Figure 4.1: Active site structure of rsAPX showing Ser160 and the 2-vinyl group of the heme.

4.2 Results

4.2.1 Expression and purification of S160Y variant

Site-directed mutagenesis was performed, according to the Quickchange™ protocol, as described in Chapter 6.

The typical yields of purified variant enzyme were ~25 mg/litre LB-media. The purity of freshly isolated S160Y variant was checked using SDS-PAGE analysis, and the preparations were judged to be homogeneous by the observation of a single band on a Coomassie Blue-stained reducing SDS-PAGE gel.

4.2.2 Spectroscopic characterization

4.2.2.1 Electronic absorption spectra and Reinheitzahl values

The S160Y variant was expressed as apo-enzyme, which was reconstituted with hemin. This resulted in formation of a red enzyme with absorption maxima in the visible region at 413, 529 and 562^{sh} nm (Figure 4.2). Comparison with the corresponding spectrum of rsAPX (Figure 4.2), shows that the Soret peak for S160Y is red-shifted compared to rsAPX and that there is no band at 630 nm, both of which are indicative of formation of low-spin heme in S160Y.
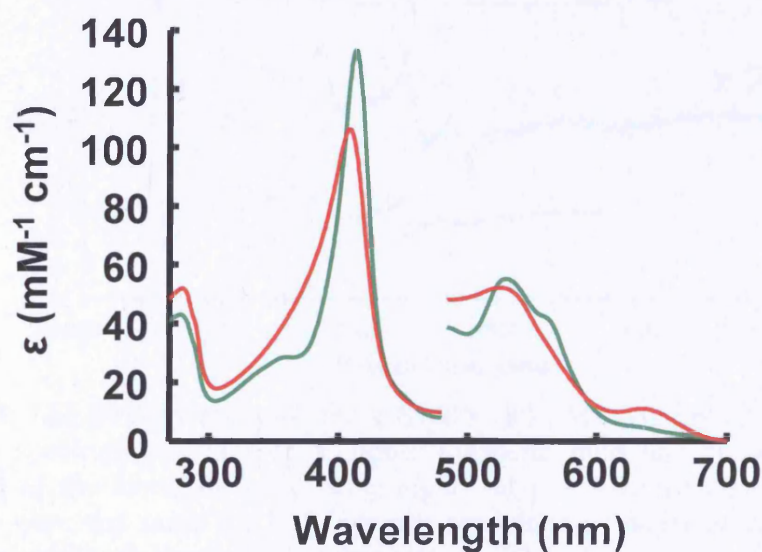
Figure 4.2: UV-visible absorption spectra of ferric rsAPX (red line) and ferric S160Y (green line). The visible region has been multiplied by a factor of 5. Conditions: 100 mM potassium phosphate buffer, pH 7.0, 25 °C.

4.2.2.2 Pyridine hemochromagen assay

The absorption coefficient of S160Y was calculated using an average of three separate determinations of heme contents, measured using the pyridine hemochromagen assay (*18*). An average absorption coefficient value of ε_{413} = 134 ± 1 mM^{-1} cm^{-1} was obtained. This value is higher than that reported for wild type rsAPX (107 mM^{-1}cm^{-1} (*19*)) and is also characteristic of low-spin iron.

4.2.2.3 Electron Paramagnetic Resonance spectroscopy

EPR spectroscopy was used to further characterise the heme environment in S160Y. Low temperature EPR spectra of rsAPX reveals high- and low-spin species (*20*). Consistent with this, the EPR spectrum of S160Y (Figure 4.3) contains features with a high-spin ferric heme of tetragonal symmetry (g$_\perp$ = 5.88, g$_\parallel$ = 1.99) and a low-spin species (g = 2.94, 2.27 and 1.47). These signals are, however, somewhat different from those observed in the EPR spectrum of rsAPX, which has a high-spin signal with less tetragonality (g = 5.96, 5.23 and 1.98), and a less rhombic low-spin signal (g = 2.68, 2.21, and 1.78 (*20*)).

Figure 4.3: The EPR spectrum of ferric S160Y (80 μM). Multiplied by a factor of 2.5 is the spectrum recorded at a higher magnetic field and showing the third component of the low-spin ferric heme signal, at g = 1.5. All other instrumental conditions were the same for both spectra: modulation frequency v_m = 100 kHz, modulation amplitude Am = 5 G, sweep rate v = 22.6 G/s, time constant t = 82 ms, microwave frequency v = 9.4667 GHz, microwave power P = 3.188 mW, number of spectral scans NS = 1, sample temperature 10 K. The ratio of the concentrations [high spin form] / [low spin form] has been measured by integration of the simulated signals in the absence of power saturation and was found to be 1 / 2.83.

4.2.3   Steady-state kinetics

In steady state analyses of S160Y in the presence of ascorbate, the value for k_{cat} (k_{cat} = 43 ± 2 s^{-1}) was lower than that of rsAPX (k_{cat} = 272 ± 32 s^{-1} (*21*)), although K_M values (K_M = 638 ± 66 μM and 389 ± 64 μM (*22*) for S160Y and rsAPX, respectively) were largely similar.

4.2.4   Reaction with H$_2$O$_2$

Reaction of ferric S160Y with 6 equivalents of H$_2$O$_2$ was monitored over ~2 h and the intermediate spectra are presented in Figure 4.3. In contrast to the wild type protein in which a Compound I species (containing a porphyrin π-cation radical) is clearly visible on the stopped-flow timescale and a Compound II species is clearly visible on a timescale of 1-2 min (*21*), reaction of S160Y with H$_2$O$_2$ did not show any evidence for formation of either Compound I or Compound II using conventional electronic spectroscopy. Instead, the reaction resulted in a final product with wavelength maxima at 408, 530 and 563 nm (Figure 4.4).
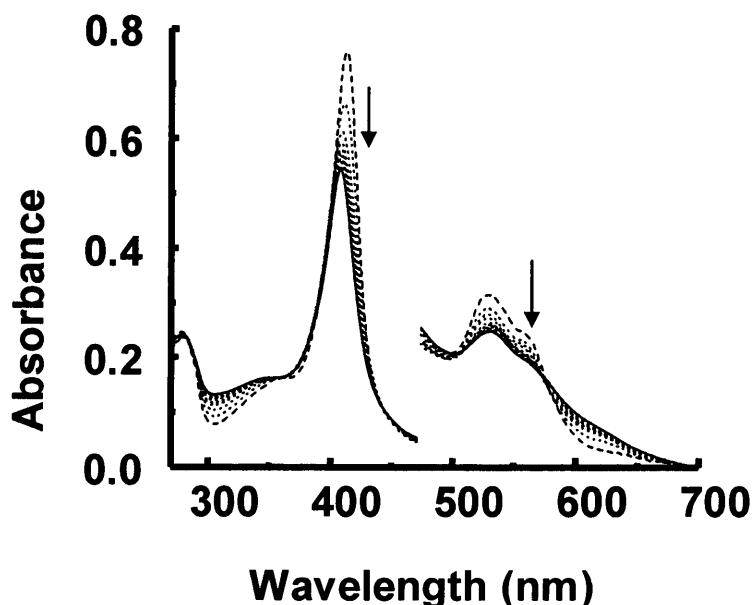
Figure 4.4: Selected spectra collected during the reaction of ferric S160Y (dashed line) with 6 equivalents of H$_2$O$_2$. Intermediate spectra between ferric S160Y and the final product (solid line) are shown as dotted lines. The total reaction time was 2 h. The visible region has been multiplied by a factor of 5. Sample conditions: [Enzyme] = 5 μM, [Hydrogen peroxide] = 30 μM, 100 mM potassium phosphate, pH 7.0, 25 °C.

4.2.5 Pyridine hemochromagen assay

Initial experiments indicated that, on reaction with H_2O_2, the heme group in S160Y became covalently attached to the protein. This was tested, qualitatively, in two ways.

First, a pyridine hemochromagen assay was carried out before and after reaction with H_2O_2. For S160Y before treatment with H_2O_2, the spectrum of the reduced pyridine hemochromagen complex showed a maximum at 556 nm (Figure 4.5). In this experiment, complete extraction of the heme from the protein is observed and the spectrum of the hemochromagen complex is consistent with a non-covalently bound heme structure, in which neither heme vinyl group is modified (18). When the same experiment was carried out with S160Y after treatment with 6 equivalents of H_2O_2, the peak of the reduced pyridine complex at 556 nm was shifted to 551 nm (Figure 4.5). These spectroscopic changes are consistent with covalent modification of the heme vinyl groups (23).
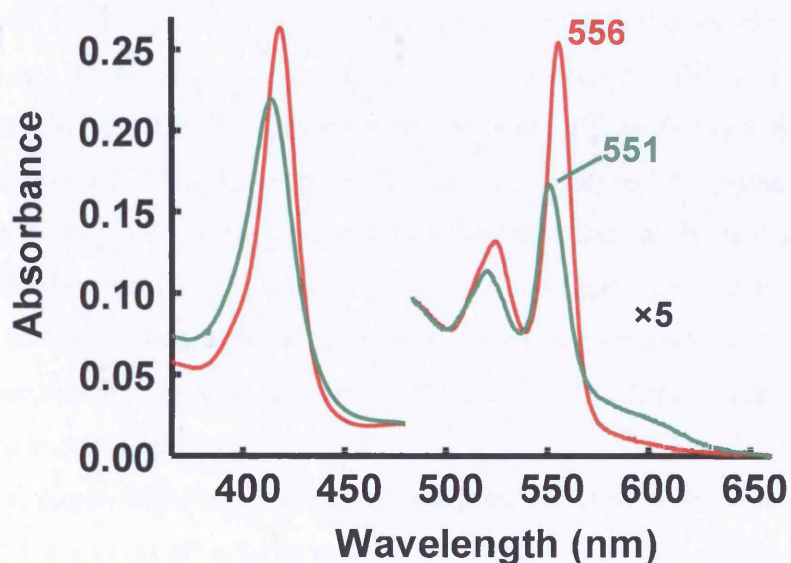
Figure 4.5: Spectra of the reduced pyridine hemochromagen complexes of S160Y before (red line) and after (green line) reaction with H_2O_2.

4.2.6 Acidified butanone extraction

An acid butanone extraction after reaction of S160Y with H_2O_2 did not remove the heme from the protein, which is a clear indication of covalent attachment of the heme to the protein (Figure 4.6b); in contrast, control experiments with S160Y before

129

reaction with H_2O_2 showed complete extraction of heme into the organic layer (Figure 4.6a). These effects were examined in more detail below.
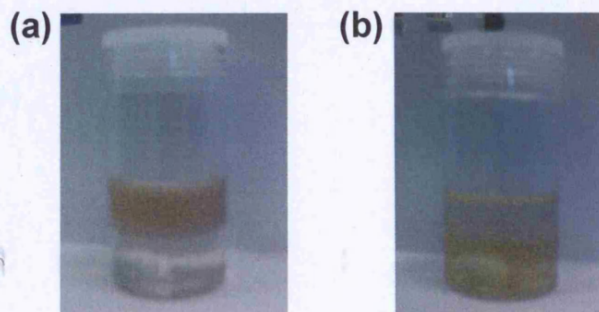
Figure 4.6: Acidified butanone extraction on S160Y before (a) and after (b) reaction with H_2O_2.

4.2.7 HPLC analyses

We sought further confirmation of the proposed heme-protein covalent linkage. HPLC analysis of the product of the reaction of S160Y with H_2O_2 (prepared with addition of 6 equivalents of H_2O_2 as above) showed that the protein (monitored at 215 nm) and the major proportion of the heme (monitored at 398 nm) co-elute at 24 min (Figure 4.7c,d); this is in direct contrast to the HPLC profile of S160Y which has not been treated with H_2O_2, in which the heme (11 min) and the protein (24 min) do not co-elute (Figure 4.7a,b). Co-elution of the heme and the protein fragments is a clear indication of covalent heme attachment and has been used previously to identify covalently linked heme in various other heme proteins (*3, 6, 7, 11, 12, 16, 24*). A commercial sample of hemin eluted at 11 min, confirming the assignment for free heme above (Figure 4.8).

In separate experiments under the same conditions as those used above for Figure 4.4 but in the presence of a large excess of ascorbate, it was shown that no peak corresponding to protein-bound heme was observed at 24 min. This indicates that under turnover conditions no formation of covalently-bound heme occurs.
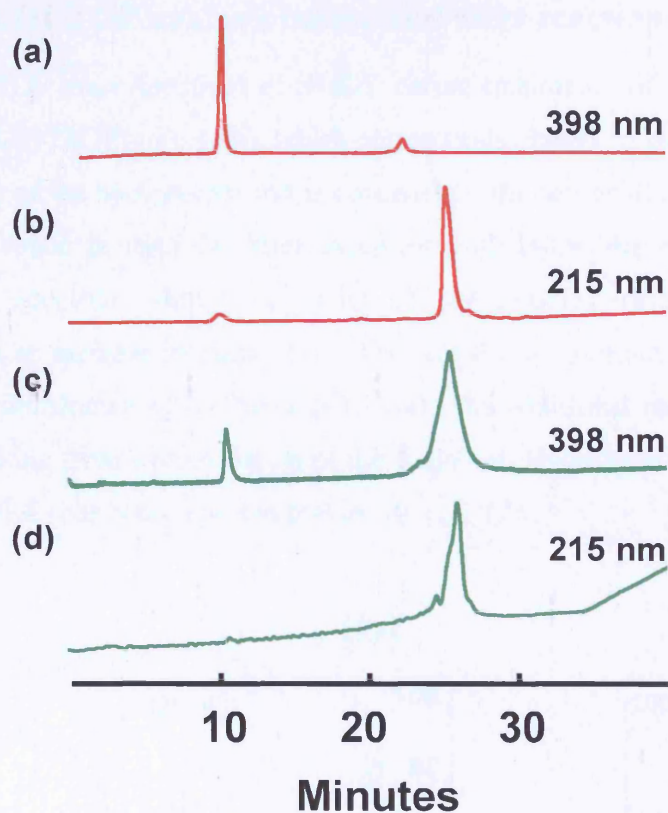
Figure 4.7: HPLC analyses of S160Y before and after reaction with H_2O_2 monitored at 398 nm and 215 nm. (a,b) S160Y before reaction with H_2O_2, (c,d) S160Y after reaction with H_2O_2.
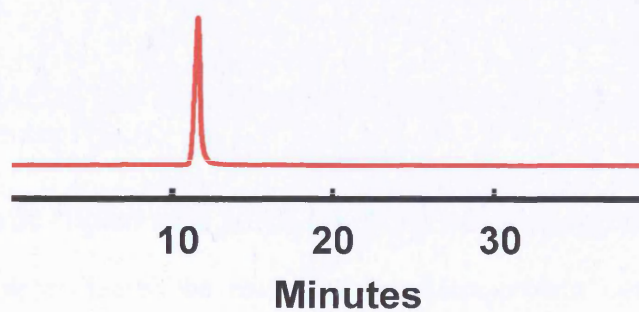
Figure 4.8: HPLC analyses of a commercial sample of free heme.

4.2.8 MALDI-TOF analysis before and after reaction with H_2O_2

The MALDI-TOF mass spectrum of S160Y before treatment with H_2O_2 showed a mass of 28393.63 Da (Figure 4.9a), which corresponds closely to the predicted mass (28394.97 Da) of the apo-protein and is consistent with non-covalent attachment of the heme (as found in rsAPX). After treatment with H_2O_2, the main peak in the MALDI-TOF spectrum showed a mass of 29025.68Da (Figure 4.9b); this corresponds to an increase in mass of 632 Da over the apo-protein and is consistent with covalent attachment of the heme (616 Da). The additional mass of 16 amu is assigned as arising from hydroxylation of the fragment. Hydroxylation of heme after reaction with H_2O_2 has been reported previously (*11, 17*).

(a) **(b)**
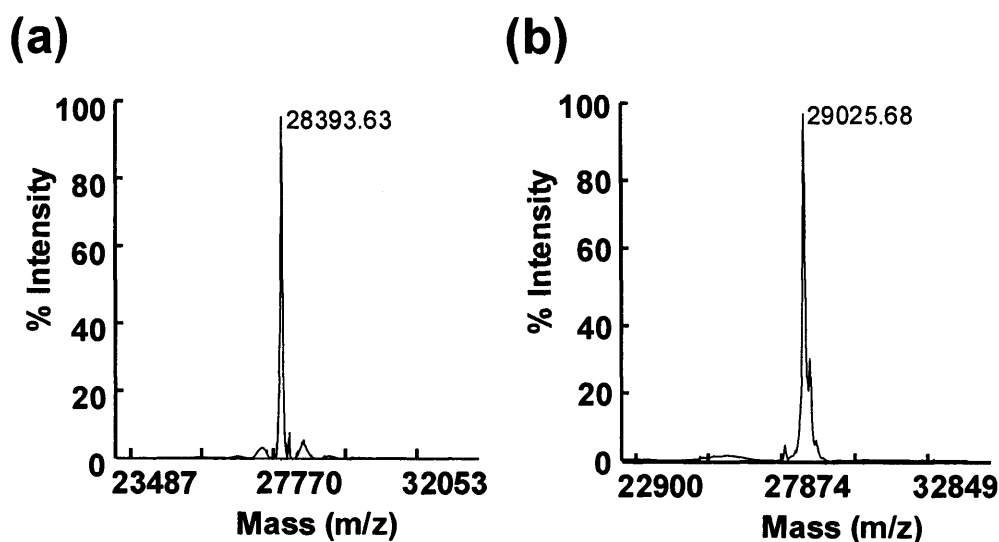
Figure 4.9: MALDI-TOF mass spectrum of S160Y before (a) and after (b) reaction with 6 equivalents of H_2O_2.

4.2.9 Tryptic digest and MALDI-TOF mass spectrometry

To establish more clearly the nature of the heme-protein covalent link, tryptic digestion of the product of the reaction of S160Y with H_2O_2 was carried out and HPLC was used to isolate the heme-containing peptide fragments (*i.e.* showing both heme and protein absorbancies) from the resulting peptide mixture (Figure 4.10). There were three peptide peaks detected on the MALDI-TOF mass spectrum of the main HPLC fragment (Figure 4.11).

(i) The first peak at 1863.96 Da is the same mass as that observed in identical analyses on rsAPX in which a covalent link to Trp41 has been established (*17*). This peak corresponds to the $L^{39}AW^{41}HSAGTFDK^{49}$ peptide fragment containing heme covalently bound to Trp41 (*17*).

(ii) The second peak at 2971.48 Da is 16 Da higher than the calculated mass (2955.18) expected for the $A^{148}MGLTDQDIVALY^{160}GGHTIGAAHK^{170}$ peptide fragment containing heme covalently bound to Tyr160.

(iii) A third peptide fragment was also observed at 4203.39 Da. This is 16 Da higher than the calculated mass (4187.79 Da) expected for the $A^{148}MGLTDQDIVALY^{160}GGHTIGAAHK^{170}$ peptide fragment plus the $L^{39}AW^{41}HSAGTFDK^{49}$ peptide fragment, with both fragments covalently bound to the heme through Tyr160 and Trp41. The proposed structure of this fragment is shown schematically in the inset to Figure 4.12.

Figure 4.10: HPLC analyses of a tryptic digest of S160Y after reaction with H_2O_2, monitored at 215 nm (blue line) and 398 nm (red line). Elution times of heme-containing peptides (23.0, 24.0, 24.7, 27.3 and 28.1 min) as well as free heme (30.6 min) are indicated. The major peak eluting at 24.7 min was analysed by mass spectrometry, according to the text; other peaks were found by mass spectrometry not to be consistent with a Tyr-heme, Trp-heme or any other peptide linking to the heme.
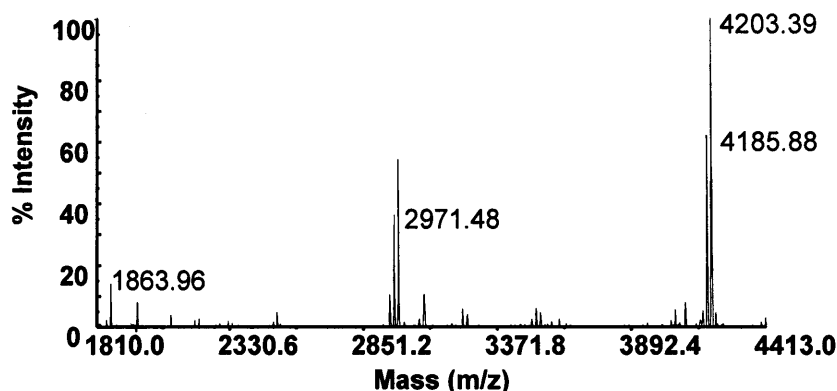
Figure 4.11: MALDI-TOF mass spectrum of the HPLC-purified heme-containing peptide fragment obtained after reaction of S160Y with H_2O_2.

4.2.10 MS/MS analysis of heme-containing peptide fragment

MS/MS mass spectrometry was used to obtain more specific sequence information for the third heme-containing fragment at 4203.39 Da. There were two different fragmentation series identified, indicating the presence of two distinct peptides bound to the heme and consistent with the MALDI-TOF analyses above.

- First, a y-ion fragmentation series allowed amino acids to be identified sequentially from His42 through to Thr46 with the remaining C-terminal mass (409.1 Da) consistent with residues Phe47 through to Lys49, which corresponds to the sequence $H^{42}SAGTFDK^{49}$ (Figure 4.12, series y_B). The absence of fragment ions for the amino acids (LAW^{41}) indicate that the heme forms a covalent link with this part of the peptide and since Leu and Ala are unlikely to be able to form a covalent link to the heme, the data are interpreted as being consistent with the formation of a covalent link from the heme toTrp41. This same link has also been shown, using mass spectrometry, to form when rsAPX is reacted with H_2O_2 (*17*).

- Second, a separate y-ion fragmentation series allowed amino acids to be identified sequentially from His163 through to Lys170, which corresponds to the sequence $H^{163}TIGAAHK^{170}$ (Figure 4.12, series y_A). A combination of a- and b-ion fragmentation series allowed amino acids to be identified sequentially from Ala148 through to Asp152, which corresponds to the sequence $A^{148}MGLTD^{152}$ on the N-terminal end of this peptide (Figure 4.12,

134

series a_A/b_A). As above, the absence of fragment ions for the amino acids (QDIVAL**Y**[160]GG) indicate that the heme forms a covalent link with this part of the peptide (Figure 4.12).
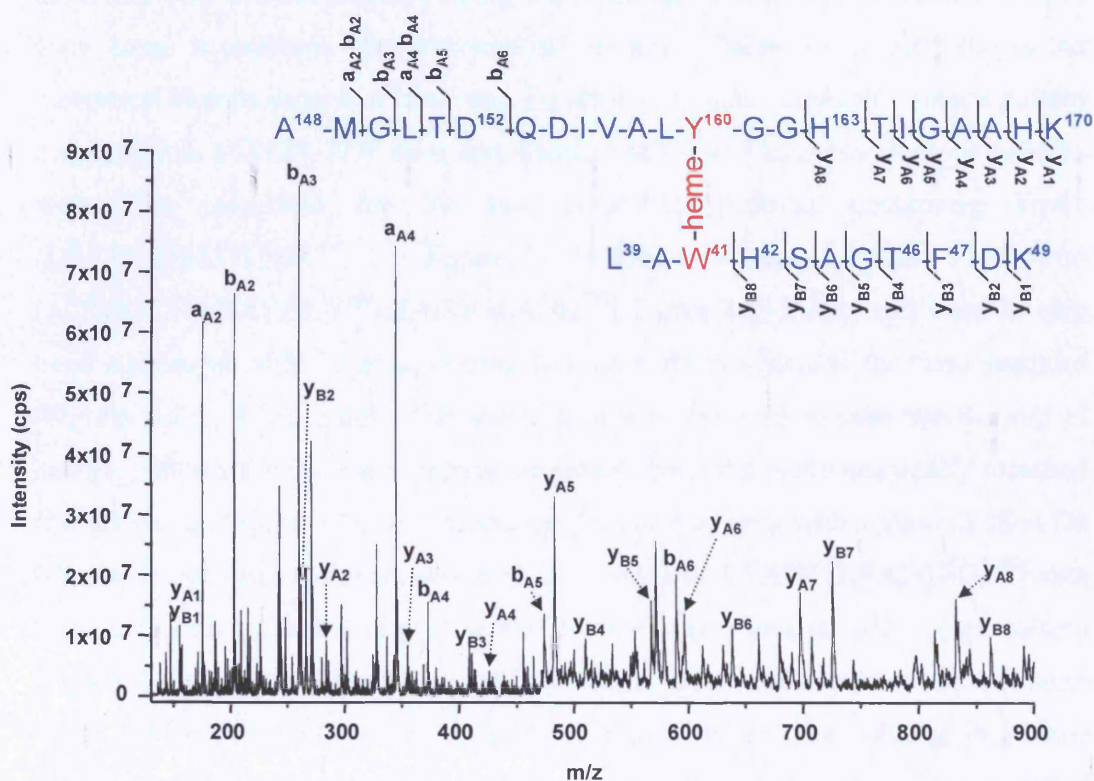
Figure 4.12: MS/MS spectrum of the HPLC-purified heme-containing peptide fragment showing the 4+ charged precursor ion (1051.44 Da). The peptide sequences obtained correspond to the y-ion fragment series for LAW[41]HSAGTFDK peptide and the a-, b- and y-ion fragment series for the AMGLTDQDIVALY[160]GGHTIGAAHK peptide and are shown (inset). The heme and residues W41 and Y160 are indicated in red in the inset.

4.2.11 Isotope patterns for peptide fragments

Further evidence for heme incorporation into the peptides mentioned above came from investigation of the isotope patterns of the peptides in question. Because iron exhibits a very distinct isotope pattern, when incorporated into protoporphyrin IX to form heme it produces very characteristic signals. Figure 4.13a, left, shows the theoretical isotope pattern of heme and Figure 4.13a, right, shows the isotope pattern obtained from MALDI-TOF mass spectrometry of heme. Theoretical isotope patterns were also calculated for the two heme-free peptides containing Trp41 ($L^{39}AW^{41}HSAGTFDK^{49}$, Figure 4.13b, left) and Tyr160 ($A^{148}MGLTDQDIVALY^{160}GGHTIGAAHK^{170}$, Figure 4.13d, left) and were in very good agreement with the experimental isotope patterns obtained for these peptides (Figures 4.13b, 4.13d, right). The same procedure was used to calculate theoretical isotope patterns for the same peptide fragments but with heme covalently attached (*i.e.* after treatment with H_2O_2). Hence, the peptide fragment with a mass of 1864 Da (Figure 4.13c) was assigned above to the fragment $L^{39}AW^{41}HSAGTFDK^{49}$ with heme covalently bound: this peptide exhibits the same characteristic isotope pattern (Figure 4.13c, right) as that predicted theoretically after attachment of heme (Figure 4.13c, left) which confirms the assignment. Similarly, the same change in isotope pattern is observed for the peptide with a mass of 2971 Da (Figure 4.13c), assigned above as $A^{148}MGLTDQDIVALY^{160}GGHTIGAAHK^{170}$ with heme covalently attached, before and after attachment of heme, Figures 4.13d and 4.13e, respectively. The fact that the peptides with masses of 1864 Da (Figure 4.13c) and 2971 Da (Figure 4.13e) exhibit the same characteristic isotope pattern as heme (Figure 4.13a) gives further confirmation of their assignment as heme-containing peptides.

136

(a)

Mass	%
614	6.3
615	2.5
616	100.0
617	41.0
618	9.3
619	1.5
620	0.2
621	0.0

(b)

Mass	%
1232	100.0
1233	68.8
1234	26.3
1235	7.4
1236	1.6
1237	0.3
1238	0.0

(c)

Mass	%
1861	5.7
1862	6.2
1863	93.3
1864	100.0
1865	58.1
1866	23.8
1867	7.8
1868	2.0
1869	0.5
1870	0.1

(d)

Mass	%
2339	79.9
2340	100.0
2341	70.6
2342	36.1
2343	15.0
2344	5.1
2345	1.5
2346	0.4
2347	0.1
2348	0.0

(e)

Mass	%
2967	3.7
2968	6.1
2969	63.4
2970	100.0
2971	88.3
2972	56.3
2973	27.7
2974	12.0
2975	4.2
2976	1.4
2977	0.3
2978	0.1
2979	0.0
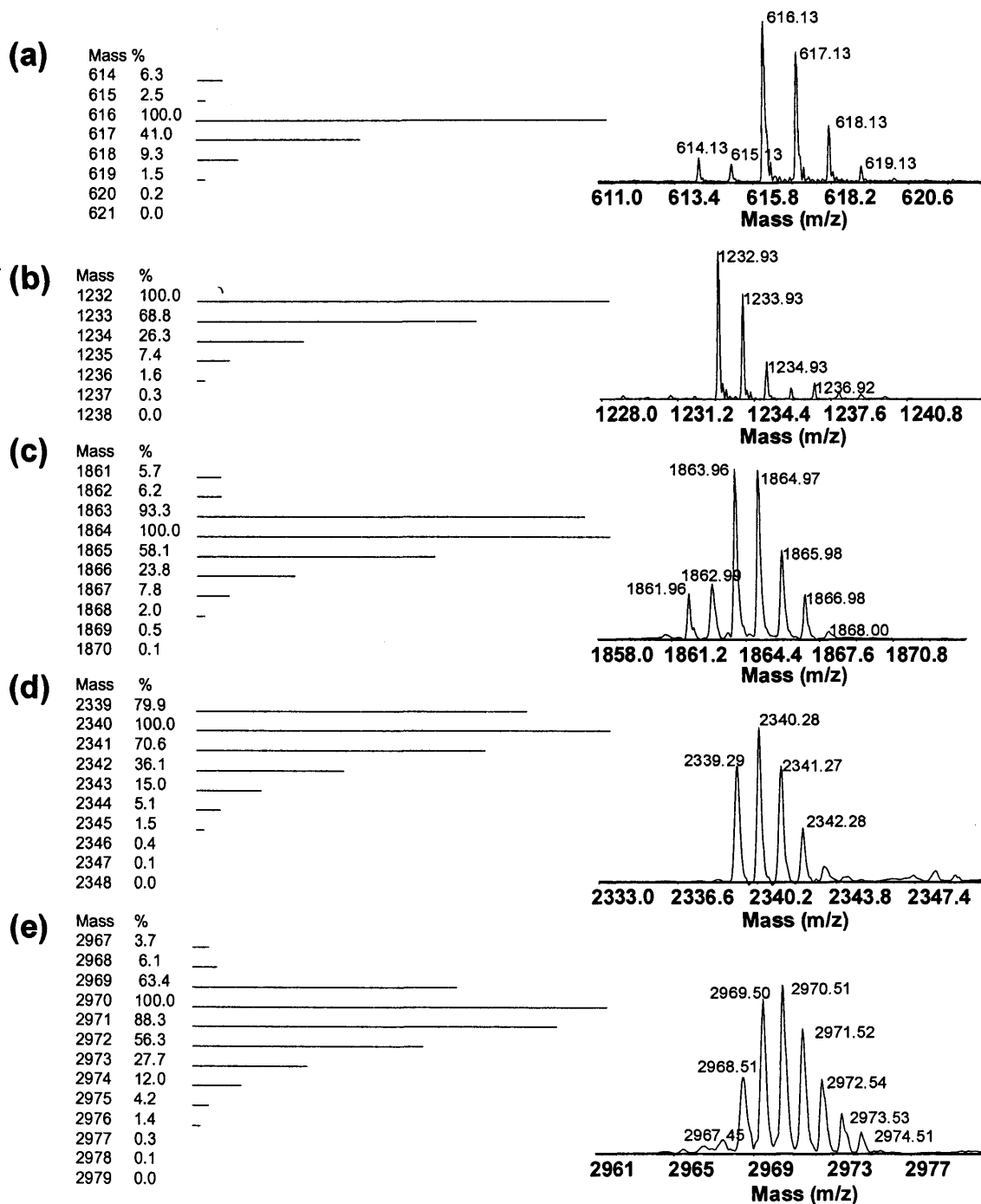
Figure 4.13: Theoretically calculated (figures on the left) and experimentally observed (figures on the right) isotope patterns for heme (a), the LAW[41]HSAGTFDK peptide before (b) and after (c) covalent attachment of heme, and the AMGLTDQDIVALY[160]GGHTIGAAHK peptide before (d) and after (e) covalent attachment of heme.

137

4.2.12 Reconstitution of S160Y with iron (III) deuteroporphyrin IX chloride and reaction with H_2O_2

To provide further information on the nature of the covalent attachment, a sample of apo-S160Y was reconstituted with iron(III) deuteroporphyrin, in which hydrogen atoms replace the 2- and 4-vinyl groups, and subsequently reacted with H_2O_2 as above. The protein was reacted with H_2O_2 under the same conditions used before and the reaction mixture was analysed by HPLC. Substitution of heme with iron(III) deuteroporphyrin reduced the percentage of linked heme but did not seem to eliminate it (Figure 4.14). Mass spectrometry was carried out on heme containing peptides, separated by HPLC after tryptic digest of the H_2O_2 treated protein sample, but no mass was found to be consistent with a peptide linking to the heme.
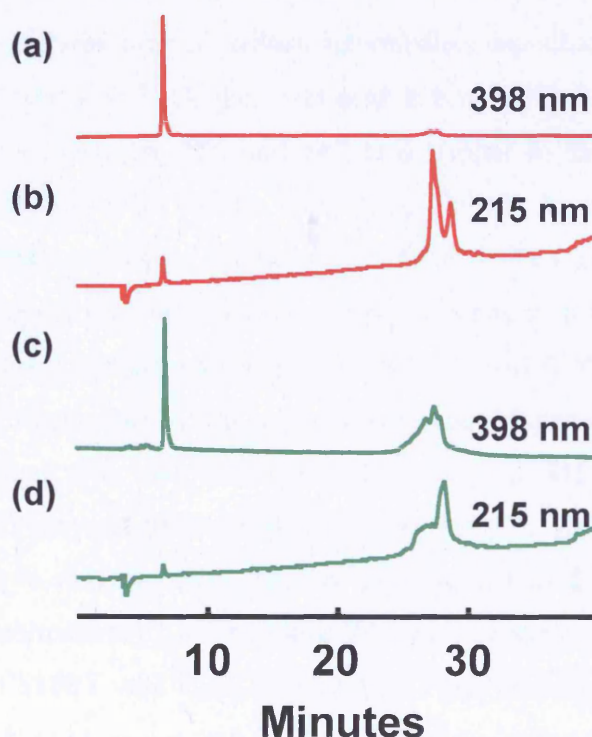
Figure 4.14: HPLC analyses of S160Y reconstituted with deuteroheme, before and after reaction with H_2O_2 monitored at 398 nm and 215 nm. (a,b) S160Y before reaction with H_2O_2, (c,d) S160Y after reaction with H_2O_2.

4.2.13 Mechanistic investigations

4.2.13.1 Diode-array spectroscopy of the reaction of S160Y with H_2O_2

Reaction of ferric S160Y with H_2O_2 was also examined under pre-steady-state conditions (Figure 4.15a), to investigate if reaction of S160Y with H_2O_2 involved initial formation of a Compound I intermediate over shorter (stopped-flow) timescales (as short as 5 ms) and using different H_2O_2 concentrations (1 to 100 equivalents). Unlike rsAPX which shows clear formation of a Compound I intermediate containing a porphyrin π-cation radical (λ_{max}/nm = 409, 530, 569[sh], and 655 (*17*)) on reaction with H_2O_2, no formation of a porphyrin π-cation radical intermediate was observed under any conditions for S160Y. Over timescales <300 ms and >1.28 ms (the dead-time of the stopped flow instrument is ~1 ms), no formation of a porphyrin π-cation radical intermediate was observed either. Instead, on reaction of S160Y with H_2O_2 the Soret peak is blue-shifted and decays to a final spectrum with maxima (408, 530 and 563 nm) similar to those described above (Figure 4.4). Time-dependent spectra were fitted globally by numerical integration methods using Prokin software (Applied Photophysics). Data collected over a period of 1000 s from the mixing event were best fitted to a two-step model (A → B → C, with rate constants for these two steps of 0.028 s^{-1} and 0.0024 s^{-1}, respectively) (Figure 4.15b). Intermediate A has absorption characteristics (λ_{max}/nm = 413, 529 and 562[sh]) consistent with those observed above for ferric S160Y, and clearly arise from the oxidized enzyme. Intermediate B (λ_{max}/nm = 411, 528 and 558[sh]) does not show spectroscopic characteristics that are consistent with either Compound I or Compound II. Intermediate C has maxima that are consistent with the final product of the reaction of S160Y with H_2O_2 (Figure 4.4). These findings show that exposure of the protein to H_2O_2 does not lead to formation of the expected porphyrin π-cation radical, which is in contrast to rsAPX and all other APXs examined so far (*25*). They also indicate that the formation of these links is slower overall than that observed for formation of other cross-links in APX which are known to go through formation of an authentic porphyrin π-cation intermediate (*11*).
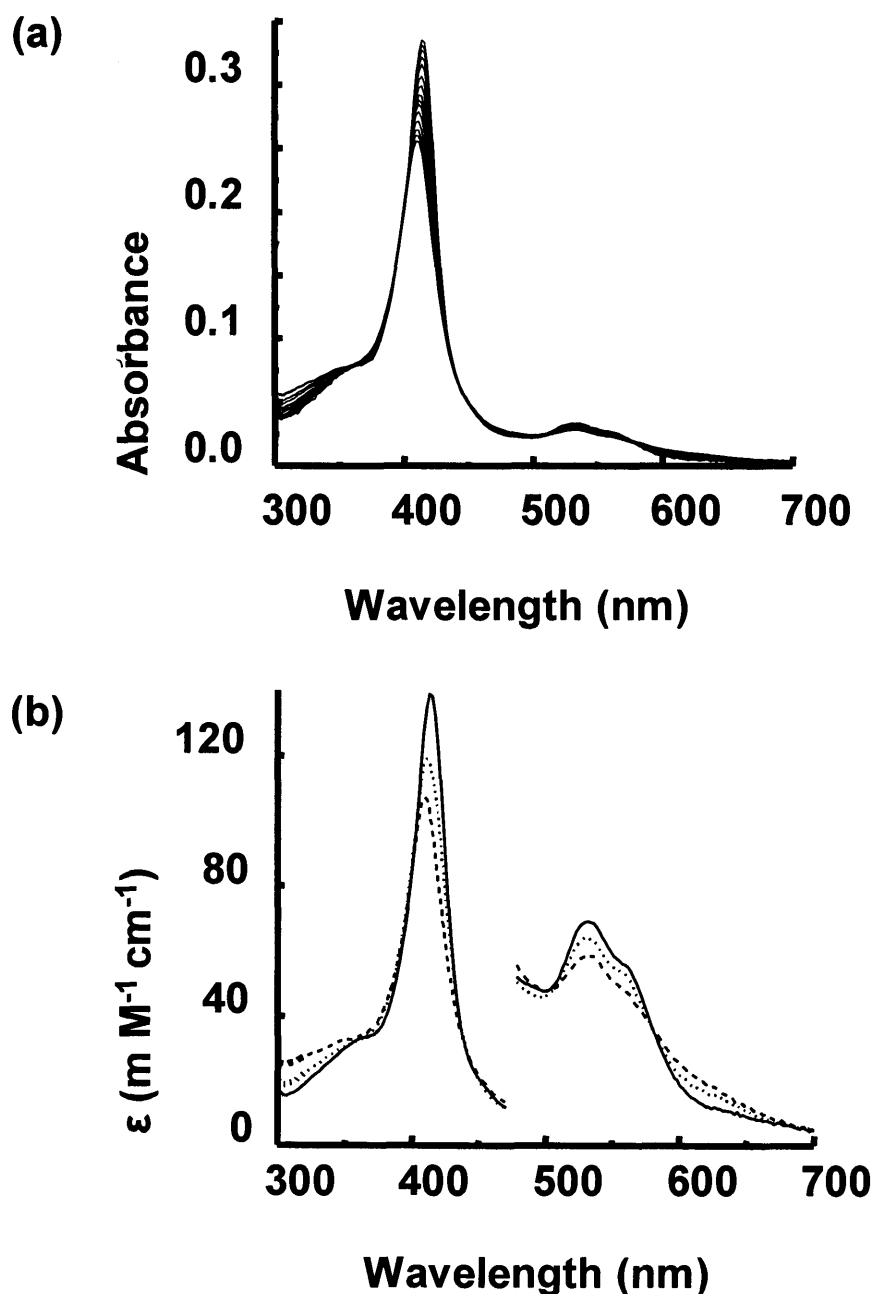
Figure 4.15: (a) Spectral changes observed upon reaction of S160Y with H_2O_2 monitored by stopped-flow diode array spectroscopy. Conditions: [Enzyme] = 20 µM, [Hydrogen peroxide] = 30 mM, 100 mM potassium phosphate buffer, pH 7.0, 25 °C. The experiment was performed over 1000 s. For clarity, only selected spectra are shown. (b) Deconvoluted spectra for the reaction shown in (a). The data were fitted to a two-step model (A → B → C); intermediate A shown in solid line, intermediate B shown in dotted line and intermediate C shown in dashed line.

Reaction of ferric S160Y with buffer alone *i.e.* in the absence of H_2O_2 (Figure 4.16a), was examined to investigate the possibility of light-dependent processes occurring over longer timescales. Incubation of S160Y with buffer for 4200 s resulted in heme bleaching as evidenced by the continuous decrease in absorbance of the Soret peak; no such behaviour was seen when these experiments were carried out using conventional UV-visible spectrophotometer. The absorbance change at 413 nm was fitted to a single-exponential decay with a rate constant of 0.0003 s^{-1} (Figure 4.16b). To verify that thè spectral changes observed upon incubation of S160Y with buffer was due to a light-dependent process, the following experiment was carried out: the reaction of S160Y with buffer was monitored over 4200 s as above, but after 720 s the shutter to the monochromator (and hence the light source) was closed for a period of 720 s, it was then re-opened and the absorbance change at 413 nm (Soret peak) was again monitored. If the process responsible for the decrease in absorbance at 413 nm was not a light-dependent one, then the absorbance decrease would continue even in the absence of light (*i.e* whilst the light shutter remained closed). However, if the decrease in absorbance at 413 nm (A_{413}) was a light-dependent process, no reaction should occur in the absence of light and the A_{413} values before closing and after opening the shutter should be the same. We noticed that no decrease in absorbance occurred in the absence of light which confirmed our initial hypothesis of a light-dependent process occurring due to the intensity of the xenon lamp (Figure 4.16c). Since the rate constant for the heme bleaching process (0.0003 s^{-1}) was much slower than both the rates constants measured for the biphasic reaction of S160Y with H_2O_2 (0.028 s^{-1} and 0.0024 s^{-1}), we concluded that this process does not significantly affect the reaction of S160Y with H_2O_2.

141
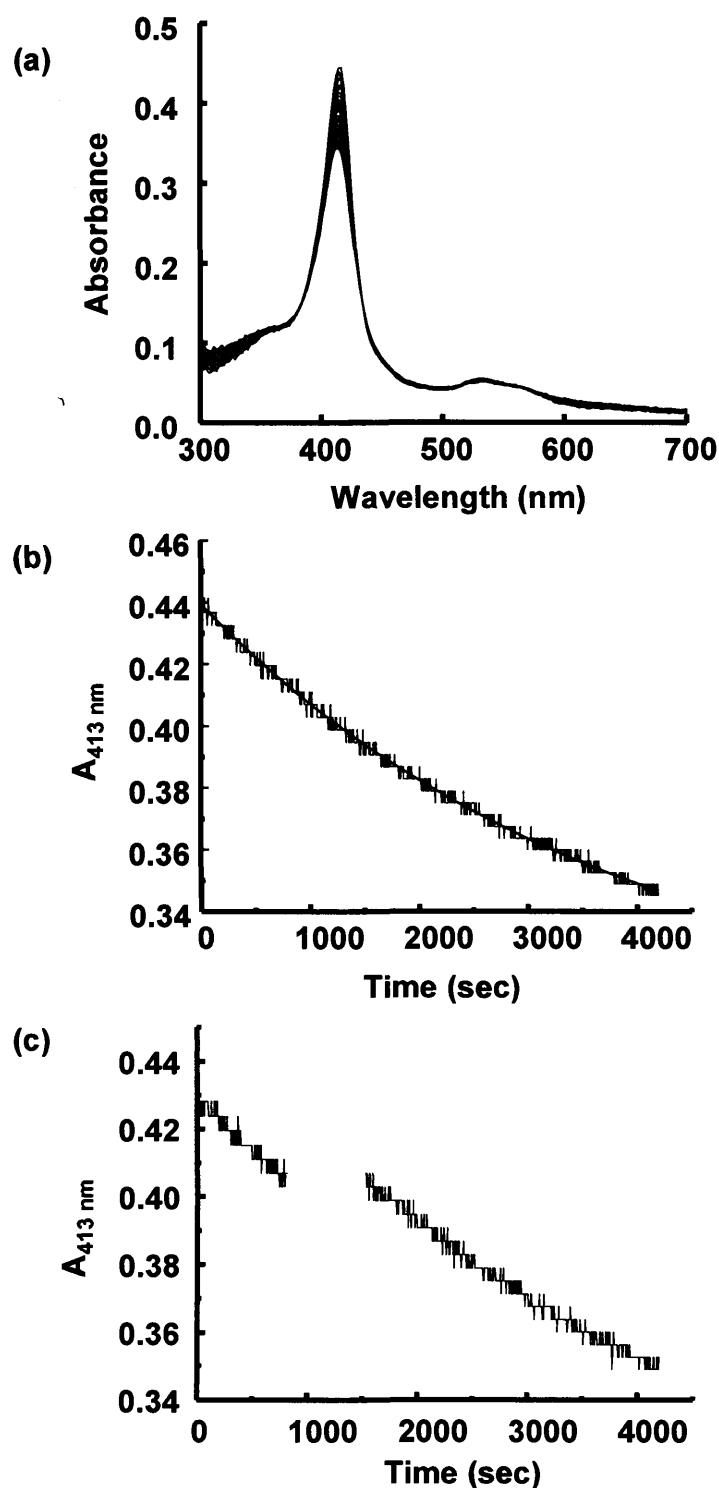
Figure 4.16: (a) Spectral changes occurring upon incubation of S160Y with buffer (100 mM potassium phosphate, pH 7.0, 25 °C) monitored by stopped-flow photodiode array spectroscopy. Conditions: [Enzyme] = 20 μM, 100 mM potassium phosphate buffer, pH 7.0, 25 °C. The spectral changes were monitored for 4200 s; (b) Absorption transient at 413 nm for the reaction shown in (a). Green line represents the fit of the data to a single exponential decay with a rate constant of 0.0003 s^{-1}; (c) As (b) but the lamp shutter was closed after 720 s for a period of time and then re-opened; see main text for details.

4.2.13.2 Electron Paramagnetic Resonance

EPR spectroscopy was used to obtain further evidence for the formation of a protein radical. EPR spectra of rsAPX and S160Y after treatment with H_2O_2 are shown in Figure 4.17a and 4.17b, respectively. In agreement with previous work (26), reaction of rsAPX with H_2O_2 yields a species with g-values (g = 3.52, g = 1.998) consistent with the existence of a porphyrin π cation radical (Figure 4.17a). In contrast, reaction of S160Y with H_2O_2 (Figure 4.17b) reveals a single radical species with g = 2.0053 and a linewidth of 19.2 G. This signal is shown in more detail in Figure 4.17c and is compared with the EPR signal (Figure 4.17d) observed in the human metHb/H_2O_2 system in which a tyrosyl radical has been assigned (27). These EPR signals, Figure 4.17c and d, have identical g-factors and linewidths and have very close overall lineshapes. Taken together, these data are consistent with the stopped-flow data presented above and are consistent with the formation of a tyrosyl radical. Power saturation studies (data not shown) revealed that the radical in the S160Y mutant relaxed faster than an organic radical which suggests proximity to a nearby paramagnetic centre, consistent with its presence on the Tyr160 and close to the heme.

Figure 4.17: The EPR spectra of (a) rsAPX and (b) S160Y (both 80 μM) after addition of 80 μM H_2O_2 (final concentrations, pH 7.0, the samples frozen 4 s after mixture). The spectra were measured at 10 K, other instrumental conditions were: modulation frequency v_m = 100 kHz, modulation amplitude A_m = 5 G, sweep rate v = 22.6 G/s, time constant τ = 82 ms, microwave frequency v = 9.47 GHz, microwave power P = 3.188 mW, number of spectral scans NS = 1. (c) Detailed EPR spectrum of the free radical formed in S160Y after addition of H_2O_2; sample conditions as in (b), instrumental conditions were as in (b) except A_m = 3 G and v = 1.19 G/s. (d) A tyrosyl radical EPR signal recorded under the same conditions as (c) in the human metHb + H_2O_2 system (27).

4.2.14 Redox measurements

The Fe^{3+}/Fe^{2+} reduction potential for rsAPX (determined using the phenosafranine/xanthine/xanthine oxidase method) was found to be −206 mV (Figure 4.18) which is identical to the value reported before (*28*). Redox measurements were also carried out on S160Y, before and after reaction with H_2O_2. To determine the Fe^{3+}/Fe^{2+} reduction potential for S160Y after reaction with H_2O_2, an acid butanone extraction was carried out, as described in Chapter 6, to remove any unreacted, free heme. The UV-visible spectrum of the protein after extraction of free heme is shown in Figure 4.19. HPLC analysis was also carried out to confirm that all free heme had been removed (Figure 4.20). The Fe^{3+}/Fe^{2+} reduction potential for rsAPX before reaction with H_2O_2 (determined using the phenosafranine/xanthine/xanthine oxidase method) was found to be −197 mV (Figure 4.21a); this compares with a value of −206 mV (Figure 4.18) as reported before (*28*) for rsAPX and indicates that no considerable shift in potential occurred as a consequence of the S160Y mutation.
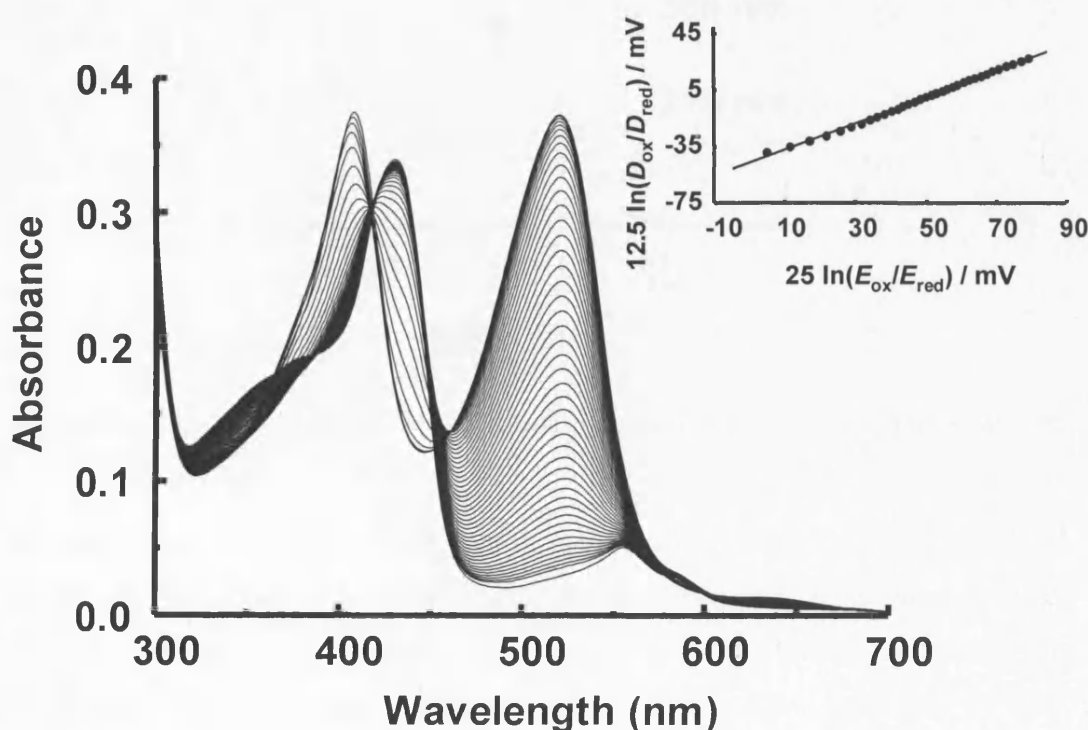
Figure 4.18: Representative family of spectra for determination of Fe^{3+}/Fe^{2+} reduction potential in rsAPX (100 mM potassium phosphate, pH 7.0, 25 °C). Insets: the corresponding linear Nernst plot.
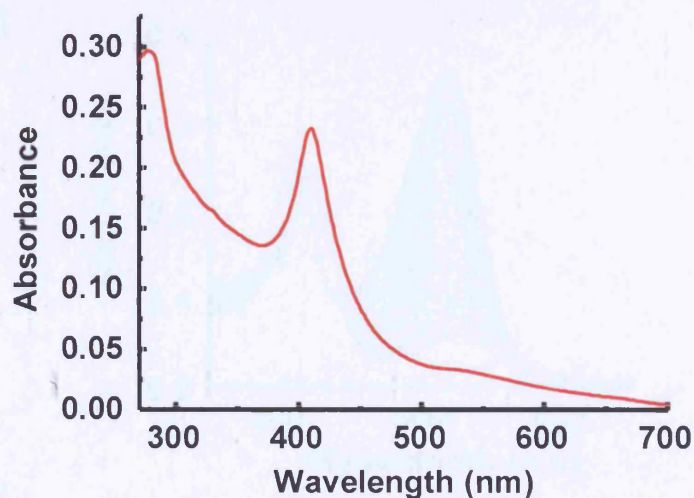
Figure 4.19: UV-visible absorption spectra of S160Y after removal of free heme. Conditions: 100 mM potassium phosphate buffer, pH 7.0, 25 °C.
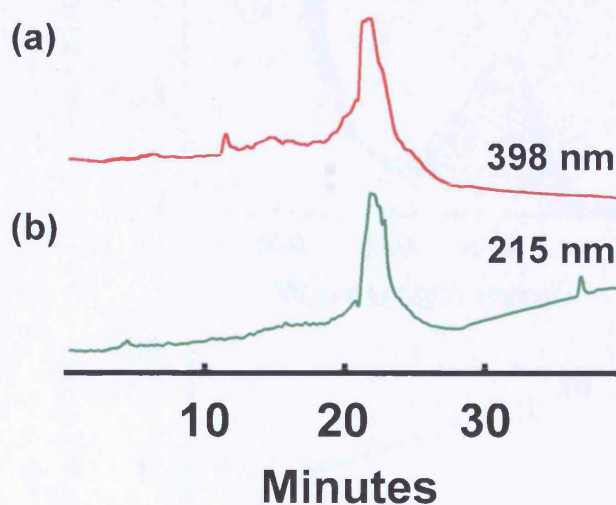
Figure 4.20: HPLC analyses of S160Y after removal of free heme, monitored at 398 nm (a) and 215 nm (b).

The corresponding Fe^{3+}/Fe^{2+} reduction potential for S160Y after reaction with H_2O_2 was determined using the indigotrisulfonate/xanthine/xanthine oxidase method (Figure 4.21b), described in Chapter 6, and was found to be −98 mV, an increase of 99 mV over the protein before hydrogen peroxide treatment. Both sets of data showed linear Nernst plots (Figure 4.21c). This suggests that the formation of two covalent links between the heme and the protein in S160Y leads to a significant stabilisation of the reduced protein.

(a)

(b)

(c)
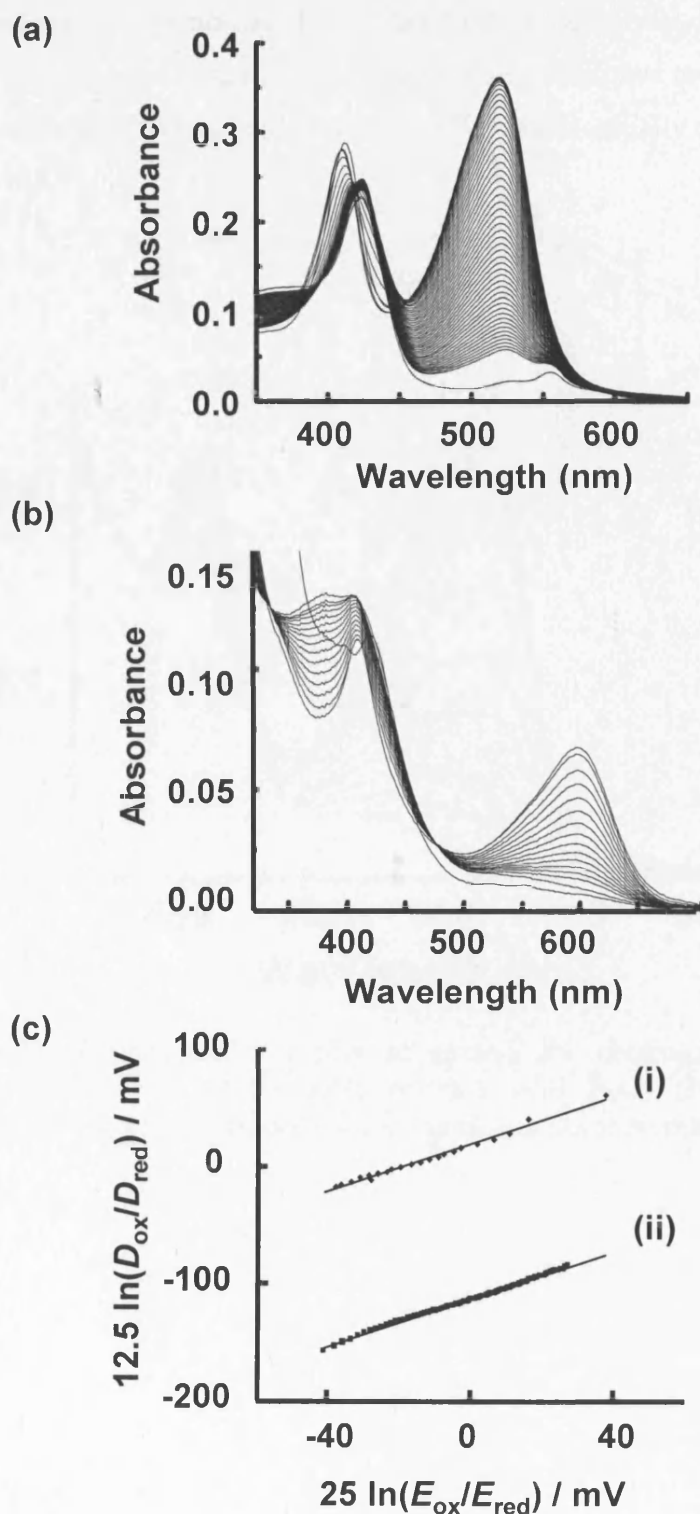
Figure 4.21: Representative family of spectra for determination of Fe^{3+}/Fe^{2+} reduction potential in S160Y before (a) and after (b) reaction with H_2O_2 (100 mM potassium phosphate, pH 7.0, 25 °C). (c) The corresponding linear Nernst plots, where plot (i) corresponds to the data shown in (b) and plot (ii) to the data shown in (a).

To test this and to confirm that the reported potential is correct, the experiment was repeated with a second dye, nile blue (Figure 4.22). This gave measured potential of −92 mV which compares well with the −98 mV that was initially obtained.
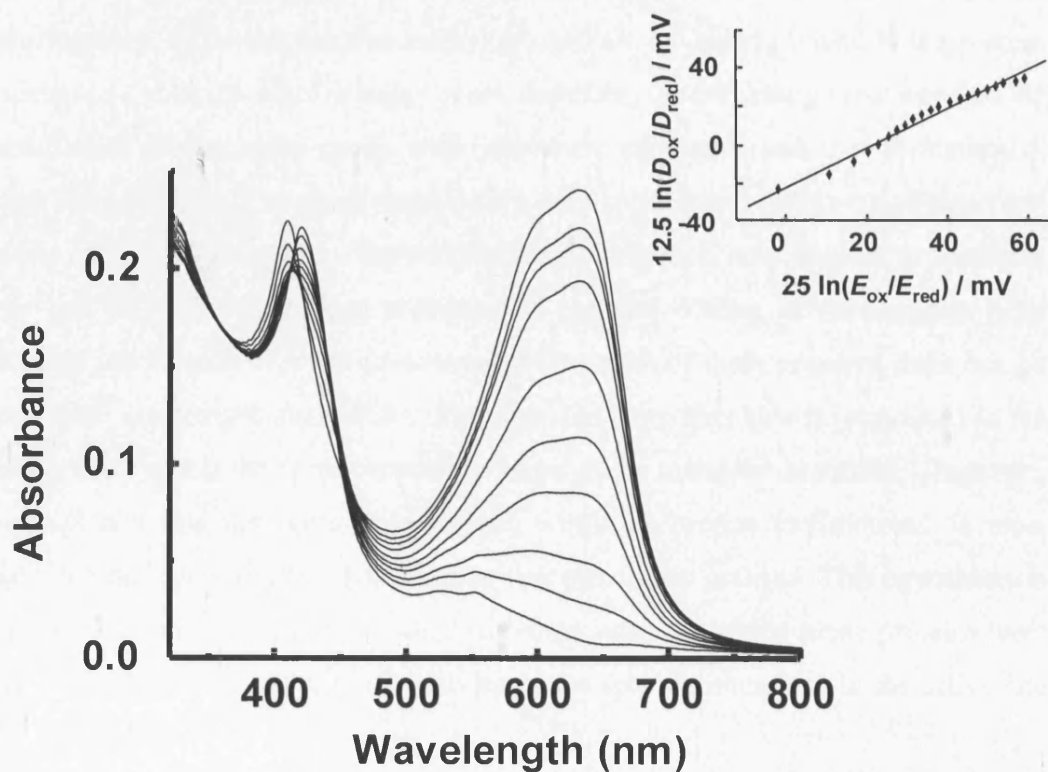
Figure 4.22: Representative family of spectra for determination of Fe^{3+}/Fe^{2+} reduction potential in S160Y after reaction with H_2O_2 (100 mM potassium phosphate, pH 7.0, 25 °C). Insets: the corresponding linear Nernst plot.

4.3   Discussion

The heme prosthetic group is widely distributed in biological systems and in the majority of cases is bound to the protein through non-covalent interactions. There are still relatively few examples of heme proteins or enzymes in which the heme substituents (*i.e.* the vinyl and/or methyl groups) are covalently bound to the protein backbone (*2, 8, 9, 29-32*). For many years, therefore, the prevailing view was that the substituents on the heme group were inherently unreactive and that formation of these links could only be supported within a very specific and highly-tuned structural and/or catalytic framework. This simplistic rationalisation now appears to represent only one part of a much more sophisticated problem. Hence, *in vitro* studies from different laboratories (*11-16*) have revealed that most of these covalent links can be duplicated in other protein architectures when the correct residue is introduced in the correct place and if the correct oxidation states of the metal are accessible. Together, this indicates that the heme, as contained within its protein environment, is most likely a rather more reactive species than was previously realised. This hypothesis is supported by other examples in which covalent links to various heme proteins have also been observed without needing to introduce specific mutations in the active site (*17, 24, 33-35*).

The work presented in this chapter provides further evidence for the idea of an intrinsically reactive heme group. Hence, it has already been shown (*11*) that replacement of Ser160 in APX by a methionine residue leads to formation of a heme-methionine covalent link in an autocatalytic reaction that requires H_2O_2. Here, introduction of a nucleophilic tyrosine residue at this position leads, similarly, to a covalent link to Tyr160. In addition, a second covalent link to Trp41 is observed: this link has been previously shown to form to the 4-vinyl group of the heme in both the wild type protein (*17*) and S207E variant of rsAPX, through an autocatalytic process involving reaction with H_2O_2. To our knowledge, there is only one other example (*15*) in which formation of a doubly-linked heme species has been engineered inside a protein architecture that does not, ordinarily, support such links.

This chapter presents a series of experiments, based on the same methodology used in Chapter 2, which show that both Trp41 and Tyr160 can covalently link to the heme in S160Y variant, after treatment of the enzyme with H_2O_2. The main experimental observations are:

- An acid butanone extraction on S160Y treated with H_2O_2 only removed a small proportion of the heme from the protein and suggested that the largest proportion of the heme is covalently attached to the protein.

- HPLC analyses showed co-elution of the heme and the protein, after reaction with H_2O_2, which is also indicative of covalent attachment between the heme and the protein.

- Mass spectrometry showed that S160Y treated with H_2O_2 has a mass increased by 632 Da over the mass of the apo-protein, which is consistent with the initial suggestion that the heme group is covalently attached to the protein.

- Tryptic digestion and mass spectrometry analysis of the HPLC purified heme containing fragmented, suggested that the heme is linked both to the $L^{39}AW^{41}HSAGTFDK^{49}$ peptide fragment, containing Trp41 and to the $A^{148}MGLTDQDIVALY^{160}GGHTIGAAHK^{170}$ peptide fragment, containing Tyr160.

- MS/MS analysis of the above peptide fragment confirmed that Trp41 and Tyr160 are the most likely protein residues linking to the heme.

- Finally, investigation of the isotope patterns of the above purified peptide fragments gave further evidence confirming their assignment as heme-containing peptides.

The nature of the tyrosine-heme link. Based on previous work in which a covalent link from Met160 to the 2-vinyl was proposed, a similarly modified heme was initially envisaged for the S160Y variant. The peak at 551 nm for the reduced pyridine-heme complex of S160Y after treatment with H_2O_2 has been used as an empirical indication that two vinyl groups on the porphyrin ring have been modified (*18*): since it had already been established that Trp41 links to the 4-vinyl group (*17*), the 551 nm peak indicated that Tyr160 was linked to the 2-vinyl group. There are only a handful of examples in the literature of tyrosine-heme covalent link: in the P460 heme in hydroxylamine oxidoreductase (HAO) (*30, 36*), in myoglobin (*33*) and in leghemoglobin (*34*). In all three cases, the link has been proposed to a *meso*-carbon of the heme (although not the same *meso*-carbon in all cases) but this has not been confirmed crystallographically for all three examples. There is, however, a structure for the cytochrome P460 from *Nitrosomonas europaea* (*31*) in which a

covalent link from the *γ-meso* carbon of the heme to the amine group of a lysine residue has been observed. By analogy, it has been proposed (*31*) that the heme-tyrosine link in HAO is to the hydroxyl group of the Tyr residue and that the heme-tyrosine (in HAO) and heme-lysine (in P460 from *Nitrosomonas europaea*) links are formed either through a radical mechanism or by direct nucleophilic attack. From the data presented above for S160Y, the precise nature of the heme-tyrosine link could not be unambiguously confirmed but analogy with the examples above would suggest that a link to the *meso*-carbon is most likely. This would be consistent with control experiments and parallel HPLC analyses with apo-S160Y reconstituted with deuteroheme (in which hydrogen atoms replace the 2- and 4-vinyl groups) in which it was observed that replacement of the heme vinyl groups reduced the percentage of covalently-linked heme but did not eliminate it completely (Figure 4.14).

The mechanism of formation of the links. Stopped-flow data shows no evidence for formation of a typical Compound I species (containing a porphyrin π-cation radical) on reaction of S160Y with H_2O_2. EPR experiments similarly showed no evidence for formation of a porphyrin π-cation signal as observed for the wild type enzyme (*26*); instead, EPR identifies an initial radical species which was assigned as a tyrosyl radical. This is shown as Intermediate I in Scheme 4.1, which outlines a proposed mechanism for formation of the covalent links to the heme. This initially-formed species may arise in two ways: (a) indirectly, through internal electron transfer within an initial poprhyrin π-cation species that is not observable on the stopped flow timescale (steps (i) and (ii), Scheme 1); (b) or directly through oxidation of Tyr160 on reaction with H_2O_2 (step (iii) in Scheme 4.1), without going through a normal Compound I intermediate. There is separate evidence that formation of tyrosyl radicals can occur independently and not necessarily as a consequence of Compound I formation (*37*). These two possibilities cannot be distinguished from the data presented. We then envisage a further radical addition mechanism to form the heme-tyrosine link, Scheme 4.1, followed by further reaction with H_2O_2 to form the heme-Trp link, step (iv) in Scheme 4.1. Formation of this link to Trp41 has already been proposed (*17*) to involve radical formation on Trp41 (see Chapter 2, Scheme 2.2).
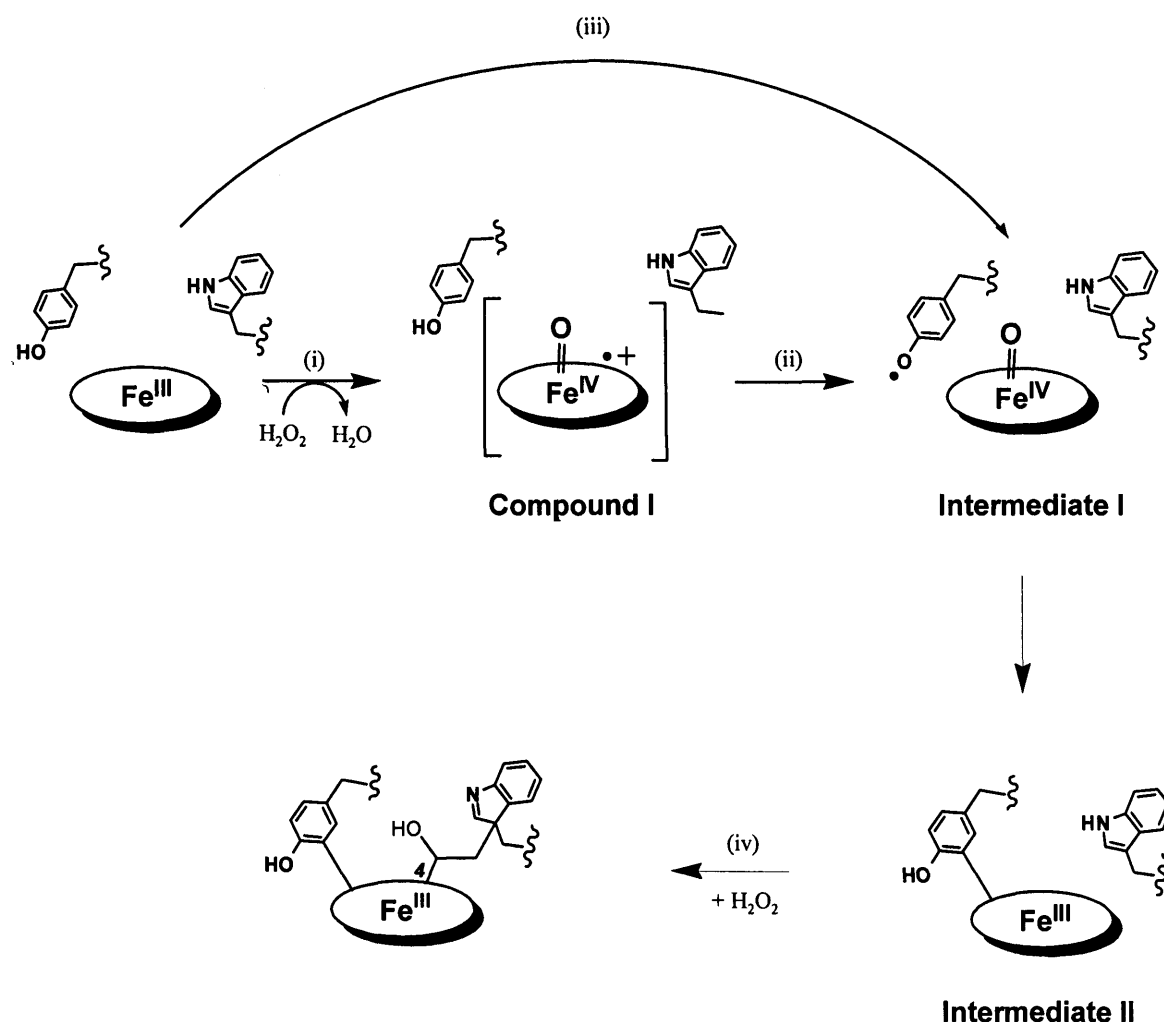
Scheme 4.1: Proposed cartoon mechanism for formation of a covalent link between Tyr160 and the heme in APX. The heme-tryptophan link, step (iv), is at the 4-vinyl group (labeled with a 4 in the scheme) with a suggested structure (17) as shown; this is proposed to be via formation of a tryptophan radical and to be through the C^γ of Trp41, but the various resonance forms of a tryptophan radical mean that a link to other carbon atoms of Trp41 is also possible. The structure of the heme-tyrosine link is not known and is suggested to be as depicted here; an ether link through the O of Tyr160 is also possible, however. The porphyrin π-cation radical is not detected in this work, but is proposed as an intermediate on the basis of the known mechanism in the wild type enzyme (see Discussion).

Functional implications. We have observed that formation of a double link between the heme and Tyr160 and Trp41 resulted in an increase of the Fe^{3+}/Fe^{2+} reduction potential from -197 mV to -98 mV, reflecting a clear stabilisation of the reduced form. Parallel experiments with rsAPX after formation of the Trp41-heme linkage, also showed an increase in the Fe^{3+}/Fe^{2+} reduction potential although this increase was difficult to quantify because of the experimental complications associated with obtaining completely pure samples of the Trp41-heme species. Hence, we cannot assign the 99 mV stabilisation of the reduced form in the modified enzyme as arising from one or other of the two links, although we note also that covalent modification of the flavin (FAD) subunit of the flavocytochrome *p*-cresol methylhydroxylase by a tyrosine residue also raises the reduction potential of the flavin group (*38*). In fact, quantitative rationalisations of the role of individual covalent links on the control of heme redox potential are very poorly defined. The closest analogy is with the mammalian peroxidases, in which the covalent links to the heme have been linked with their redox properties. Although there is no overall consensus on exactly how and why these links are influential, disruption of the Asp94–heme ester linkage in myeloperoxidase has been shown to lead to a change in heme potential, suggested to be a result of increased heme flexibility introduced as a consequence of the removal of one of the three physiological covalent links (*39*). It is possible that similar effects on the heme structure are responsible for the changes we observe in this work.

4.4   References

(1)   Stevens, J. M., Daltrop, O., Allen, J. W., and Ferguson, S. J. (2004) *C*-type cytochrome formation: chemical and biological enigmas. *Acc. Chem. Res. 37*, 999-1007.

(2)   Colas, C., and Ortiz de Montellano, P. R. (2003) Autocatalytic radical reactions in physiological prosthetic heme modification. *Chem. Rev. 103*, 2305-2332.

(3)   Colas, C., Kuo, J. M., and Ortiz de Montellano, P. R. (2002) Asp225 and Glu375 in autocatalytic attachment of the prosthetic heme group of lactoperoxidase. *J. Biol. Chem. 277*, 7191-200.

(4)   Rae, T. D., and Goff, H. M. (1998) The heme prosthetic group of lactoperoxidase. Structural characteristics of heme l and heme l-peptides. *J. Biol. Chem. 273*, 27968-27977.

(5)   Oxvig, C., Thomsen, A. R., Overgaard, M. T., Sorensen, E. S., Hojrup, P., Bjerrum, M. J., Gleich, G. J., and Sottrup-Jensen, L. (1999) Biochemical evidence for heme linkage through esters with Asp-and Glu241 in human eosinophil peroxidase. The ester with Asp93 is only partially formed in vivo. *J. Biol. Chem. 274*, 16953-16958.

(6)   LeBrun, L. A., Xu, F., Kroetz, D. L., and Ortiz de Montellano, P. R. (2002) Covalent attachment of the heme prosthetic group in the CYP4 cytochrome P450 family. *Biochemistry 41*, 5931-5937.

(7)   Henne, K. R., Kunze, K. L., Zheng, Y.-M., Christmas, P., Soberman, R. J., and Rettie, A. E. (2001) Covalent linkage of prosthetic heme to CYP4 family of P450 enzymes. *Biochemistry 40*, 12925-12931.

(8)   Hoy, J. A., Kundu, S., Trent III, J. T., Ramaswamy, S., and Hargrove, M. S. (2004) The crystal structure of *Synechocystis* hemoglobin with a covalent heme linkage. *J. Biol. Chem. 279*, 16535-16542.

(9)   Lee, D., Pervushin, K., Dischof, D., Braun, M., and Thony-Meyer, L. (2005) Unusual heme-histidine bond in the active site of a chaperone. *J. Am. Chem. Soc. 127*, 3716-3717.

(10)   Uchida, T., Stevens, J. M., Daltrop, O., Harvat, E. M., Hong, L., Ferguson, S. J., and Kitagawa, T. (2004) The interaction of covalently bound heme with the cytochrome *c* maturation protein CcmE. *J. Biol. Chem.* *279*, 51981-51988.

(11)   Metcalfe, C. L., Ott, M., Patel, N., Singh, K., Mistry, S. C., Goff, H. M., and Raven, E. L. (2004) Autocatalytic formation of green heme: evidence for H_2O_2-dependent formation of a covalent methionine-heme linkage in ascorbate peroxidase. *J. Am. Chem. Soc.* *126*, 16242-16248.

(12)   Colas, C., and De Montellano, P. R. (2004) Horseradish peroxidase mutants that autocatalytically modify their prosthetic heme group: insights into mammalian peroxidase heme-protein covalent bonds. *J. Biol. Chem.* *279*, 24131-24140.

(13)   Huang, L., Wojciechowski, G., and Ortiz de Montellano, P. R. (2006) Role of heme-protein covalent bonds in mammalian peroxidases. Protection of the heme by a single engineered heme-protein link in horseradish peroxidase. *J. Biol. Chem.* *281*, 18983-18988.

(14)   Barker, P. D., Ferrer, J. C., Mylrajan, M., Loehr, T. M., Feng, R., Konishi, Y., Funk, W. D., MacGillivray, R. T., and Mauk, A. G. (1993) Transmutation of a heme protein. *Proc. Natl. Acad. Sci. U S A 90*, 6542-6546.

(15)   Barker, P. D., Nerou, E. P., Freund, S. M., and Fearnley, I. M. (1995) Conversion of cytochrome b562 to *c*-type cytochromes. *Biochemistry 34*, 15191-15203.

(16)   Limburg, J., LeBrun, L. A., and Ortiz de Montellano, P. R. (2005) The $P450_{cam}$ G248E mutant covalently binds its prosthetic heme group. *Biochemistry 44*, 4091-4099.

(17)   Pipirou, Z., Bottrill, A. R., Metcalfe, C. M., Mistry, S. C., Badyal, S. K., Rawlings, B. J., and Raven, E. L. (2007) Autocatalytic formation of a covalent link between tryptophan 41 and the heme in ascorbate peroxidase. *Biochemistry 46*, 2174-2180.

(18)   Antonini, M., and Brunori, E. (1971) *Hemoglobin and Myoglobin and their reactions with ligands*, North Holland Publishers, Amsterdam.

(19) Jones, D. K., Dalton, D. A., Rosell, F. I., and Raven, E. L. (1998) Class I heme peroxidases: characterization of soybean ascorbate peroxidase. *Arch. Biochem. Biophys. 360*, 173-178.

(20) Jones, D. K., Dalton, D. A., Rosell, F. I., and Lloyd Raven, E. (1998) Class I heme peroxidases: characterization of soybean ascorbate peroxidase. *Arch. Biochem. Biophys. 360*, 173-178.

(21) Lad, L., Mewies, M., and Raven, E. L. (2002) Substrate binding and catalytic mechanism in ascorbate peroxidase: evidence for two ascorbate binding sites. *Biochemistry 41*, 13774-13781.

(22) Lad, L., Mewies, M., and Raven, E. L. (2002) Substrate binding and catalytic mechanism in ascorbate peroxidase: evidence for two ascorbate binding sites. *Biochemistry 41*, 13774-13781.

(23) Daltrop, O., Smith, K. M., and Ferguson, S. J. (2003) Stereoselective *in vitro* formation of c-type cytochrome variants from *Hydrogenobacter thermophilus* containing only a single thioether bond. *J. Biol. Chem. 278*, 24308-24313.

(24) Reeder, B. J., Svistunenko, D. A., Sharpe, M. A., and Wilson, M. T. (2002) Characteristics and mechanism of formation of peroxide-induced heme to protein cross-linking in myoglobin. *Biochemistry 41*, 367-375.

(25) Raven, E. L. (2003) Understanding functional diversity and substrate specificity in haem peroxidases: what can we learn from ascorbate peroxidase? *Nat. Prod. Rep. 20*, 367-381.

(26) Patterson, W. R., Poulos, T. L., and Goodin, D. B. (1995) Identification of a porphyrin pi cation radical in ascorbate peroxidase compound I. *Biochemistry 34*, 4342-4345.

(27) Svistunenko, D. A., Dunne, J., Fryer, M., Nicholls, P., Reeder, B. J., Wilson, M. T., Bigotti, M. G., Cutruzzola, F., and Cooper, C. E. (2002) Comparative study of tyrosine radicals in hemoglobin and myoglobins treated with hydrogen peroxide. *Biophys. J. 83*, 2845-2855.

(28) Efimov, I., Papadopoulou, N. D., McLean, K. J., Badyal, S. K., Macdonald, I. K., Munro, A. W., Moody, P. C., and Raven, E. L. (2007) The redox properties of ascorbate peroxidase. *Biochemistry 46*, 8017-8023.

(29)   Stevens, J. M., Daltrop, O., Allen, J. W. A., and Ferguson, S. J. (2004) *C*-type cytochrome formation: chemical and biological enigmas. *Acc. Chem. Res. 37*, 999-1007.

(30)   Arciero, D. M., Hooper, A. B., Cai, M., and Timkovich, R. (1993) Evidence for the structure of the active site heme P460 in hydroxylamine oxidoreductase of Nitrosomonas. *Biochemistry 32*, 9370-9378.

(31)   Pearson, A. R., Elmore, B. O., Yang, C., Ferrara, J. D., Hooper, A. B., and Wilmot, C. M. (2007) The crystal structure of cytochrome P460 of *Nitrosomonas europaea* reveals a novel cytochrome fold and heme-protein cross-link. *Biochemistry 46*, 8340-8349.

(32)   Vu, B. C., Vuletich, D. A., Kuriakose, S. A., Falzone, C. J., and Lecomte, J. T. (2004) Characterization of the heme-histidine cross-link in cyanobacterial hemoglobins from *Synechocystis sp.* PCC 6803 and *Synechococcus sp.* PCC 7002. *J. Biol. Inorg. Chem. 9*, 183-194.

(33)   Catalano, C. E., Choe, Y. S., and Ortiz de Montellano, P. R. (1989) Reactions of the protein radical in peroxide-treated myoglobin. Formation of a heme-protein cross-link. *J. Biol. Chem. 264*, 10534-10541.

(34)   Moreau, S., Davies, M. J., and Puppo, A. (1995) Reaction of ferric leghemoglobin with H_2O_2: formation of heme-protein cross-links and dimeric species. *Biochim. Biophys. Acta 1251*, 17-22.

(35)   Jia, Y., Buehler, P. W., Boykins, R. A., Venable, R. M., and Alayash, A. I. (2007) Structural basis of peroxide-mediated changes in human hemoglobin: a novel oxidative pathway. *J. Biol. Chem. 282*, 4894-4907.

(36)   Igarashi, N., Moriyama, H., Fujiwara, T., Fukumori, Y., and Tanaka, N. (1997) The 2.8 Å structure of a hydroxylamine oxidoreductase from a denitrifying chemoautotrophic bacterium, *Nitrosomonas europaea. Nat. Struct. Biol. 4*, 276-284.

(37)   Zhang, H., He, S., and Mauk, A. G. (2002) Radical formation at Tyr39 and Tyr153 following reaction of yeast cytochrome *c* peroxidase with hydrogen peroxide. *Biochemistry 41*, 13507-13513.

(38)   Efimov, I., Cronin, C. N., and McIntire, W. S. (2001) Effects of noncovalent and covalent FAD binding on the redox and catalytic properties of *p*-cresol methylhydroxylase. *Biochemistry 40*, 2155-2166.

(39)   Zederbauer, M., Furtmuller, P. G., Bellei, M., Stampler, J., Jakopitsch, C., Battistuzzi, G., Moguilevsky, N., and Obinger, C. (2007) Disruption of the aspartate to heme ester linkage in human myeloperoxidase: impact on ligand binding, redox chemistry, and interconversion of redox intermediates. *J. Biol. Chem.* *282*, 17041-17052.

Chapter 5

Summary

As reviewed in Chapter 1, although most heme proteins have a non-covalently bound, *b*-type heme as their prosthetic group, there is now an increasing number of heme proteins that bind their heme covalently by different number and type of links. The most well known examples are cytochromes *c* and the mammalian peroxidases. In both cases, however, there is still little known about the mechanism of formation of these links and the debate on their functional roles still continues as well.

The aim of this work was to use APX as a model system to give more insight into the above questions. APX is a plant protein that bears a non-covalently bound heme group and thus, by using protein engineering we can insert heme-protein links and follow both their mechanism of formation and their effect on enzyme properties. Overall, the data in this thesis give us valuable insight into the requirements for covalent heme binding and build on what has already been proposed in the literature concerning the mechanism of formation and the physiological function of these links (*3, 4*). The data also highlight similarities and differences in heme reactivity between the members of the Class I family of plant peroxidases. This is discussed in more detail below.

5.1   Location, location, location

Previous studies have suggested that a properly positioned amino acid near the heme edge is the sole requirement for covalent binding to the heme and that no further protein characteristics were necessary. Thus, when a suitably placed glutamate residue was engineered into HRP, it was shown that covalent attachment of the heme to the protein through an ester linkage can be achieved, similarly to that seen for the mammalian peroxidases, and hence suggesting that an appropriately situated carboxylic acid group is sufficient for covalent heme attachment (*5*). This suggestion was re-enforced by further studies in P450$_{cam}$ where an ester link was introduced between an engineered glutamate residue and the 5-methyl group of the heme (*6*), thus mimicking the ester link known to exist in the CYP4 family of P450s (*7-10*). Formation of an ester link in an enzyme such as P450$_{cam}$, which has poor sequence identity with the peroxidases, provided even more evidence supporting the proposal that the ability to covalently bind the heme group is unlikely to require additional specific active site assistance (*6*). The above observations are not limited to formation of ester heme-protein links, as a sulfonium link similar to the one seen in

MPO has recently also been engineered into APX by insertion of a methionine residue at a suitable position (*11*).

The results in this thesis have also shown that heme-protein covalent links can be engineered when a suitable residue is introduced or even when an already existing protein residue is correctly positioned towards the heme. Furthermore, we have shown that the level of reactivity of the heme group is such that 'activated' locations close to the heme can support formation of more than one type of covalent link, such as a tyrosine or even a tryptophan. Collectively, this tells us that, in principle, any heme peroxidase, or, indeed any heme protein with appropriately positioned residues, can duplicate the active site architecture of the mammalian peroxidases. That would suggest that covalent heme attachment in the mammalian peroxidases relates to peroxidase biology or stability rather than to intrinsic catalytic properties. However, in suggesting that heme attachment is mainly governed by structural geometry around the active site, it is also important to point out that even slight differences from the optimum could prevent formation of these links. As a case in point, we observed that although insertion of a glutamate residue inside the active site of HRP (*12*) and P450$_{cam}$ (*6*) was sufficient for covalent link formation, this was not the case for S207E variant of APX. Similarly, when an aspartate residue was inserted into P450$_{cam}$ (*6*), instead of a glutamate residue as mentioned above, or when a glutamate residue was inserted in a different position in HRP (*5*), no ester link could be achieved. This reinforces the importance of the length, flexibility or exact location of the amino acid side chain in being able to attach the heme groups and form a covalent link. Finally, incorrect positioning of an amino acid has even been demonstrated in the form of strong coordination to the iron that prevents covalent link formation, as evidenced by studies in P450$_{BM3}$ (*13*).

5.2   How do these links form?

As mentioned in Chapter 1, mechanistic studies in the mammalian peroxidases are hindered by the fact that the covalent links are already fully formed in the mature form of the enzymes. By being able to successfully engineer heme-protein covalent links in APX, we established a model system that can be used as a platform for studying their mechanism of formation.

The results in Chapters 2 and 4 demonstrated that covalent link formation in rsAPX and S160Y variant occurs in an autocatalytic process that only requires reaction of

the enzyme with H_2O_2. Furthermore, formation of the Trp41-heme link in rsAPX involves initial formation of a typical Compound I intermediate, *i.e.* an oxyferryl species bearing a porphyrin π-cation radical. This is consistent with the findings from other groups in the literature. More specifically, studies in LPO provided evidence for covalent heme attachment being an autocatalytic process (*14*). Heme attachment in HRP and P450 variants was also shown to be autocatalytic following reaction with H_2O_2 (*6, 15, 16*). The same conclusion was drawn for formation of a sulfonium link in APX, where a Compound I species was detected as an intermediate for the first time (*11*). Together, these mechanistic studies seem to suggest that heme attachment can be activated if an enzyme is competent for reaction with H_2O_2 by forming an oxidized Compound I species. Once this activated oxyferryl intermediate is formed it seems to have an inherent ability to oxidize an appropriately placed amino acid. This leads us to conclude that heme is inherently reactive and we therefore suggest that modified heme groups might be accessible in a much wider variety of protein architectures than was originally thought.

5.3 Class I plant peroxidases: all the same, all different

As discussed in Chapter 2, APX, CcP and the KatG share very similar active site structures and all bear a distal tryptophan residue in place of the most commonly found phenylalanine. The data in Chapter 2 showed that on reaction of rsAPX with H_2O_2, under non catalytic conditions, a covalent link can be formed between Trp41 and the 4-vinyl group of the heme. Formation of a covalent link in rsAPX was suggested to involve radical formation at the distal tryptophan, thus resembling the mechanism used by the KatG for formation of the Met-Tyr-Trp cross-link. This suggested that the mechanism that lead to formation of this cross-link in the KatG might also be accessible under certain conditions in other Class I peroxidases. However, although APX and CcP exhibit almost identical active site structures and bear the same distal tryptophan residue, the data in Chapter 3 showed that no heme-protein link could be sustained in wild type CcP, as seen for rsAPX. We proposed that after formation of Compound I in rsAPX, the very close proximity of the distal tryptophan to the heme allowed for Trp41 to be oxidized, while the diversion of oxidizing equivalents to the proximal tryptophan in CcP made oxidation of Trp51 not plausible. This hypothesis was tested by studies on W191F variant of CcP, which has

been shown to form a typical Compound I intermediate on reaction with H_2O_2, as seen for rsAPX. It was indeed found that when a Compound I intermediate bearing a porphyrin π-cation radical was accessed, a covalent link between Trp51 and the heme could be engineered in W191F. These results confirmed our proposal that radical formation at the distal tryptophan requires formation of a Compound I species containing a porphyrin π-cation radical.

To our knowledge, this is the first time that a tryptophan residue has been shown to link to the heme. Overall, the ability of the distal tryptophan to host a protein radical that leads to covalent attachment to the heme seems to be a more general feature within the Class I family of plant peroxidases, as a 'distal tryptophan-heme' linkage was observed in all APX variants observed in this thesis and even in a CcP variant where a Compound I species could be formed. This observation leads us to the conclusion that formation of a Met-Tyr-Trp cross-link in APX and CcP is not limited by the inherent reactivity of the enzymes but by the absence of the suitable residue(s) adjacent to the distal tryptophan. Finally, it is also worthwhile mentioning that by comparison of the effectiveness of heme attachment between APX and CcP we can also assume that the fate of protein radicals is also governed by the availability of endogenous oxidisable amino acids near the active site of the protein. We therefore propose that the high percentage of aromatic residues near the active site of W191F, in comparison to APX, could aid radical diffusion and thus decrease the percentage of specific radical formation on Trp51 and consequently the percentage of linkage between Trp51 and the heme.

5.4   What does nature gain from heme attachment?

A complete answer to this question has not yet emerged. In fact, the functional role of heme-protein covalent links has been the centre of debate for several years and many questions still remain unanswered. Heme attachment has been proposed to result in greater stability and rigidity of protein structures (4, 17, 18), to aid the well-defined packing of multiheme proteins (19), to enhance the specificity of catalytic reactions (3) and even protect the heme group from modification from their highly reactive metabolic products (20). Heme attachment has also been related to control of the redox potential in cytochromes c and the mammalian peroxidases. In MPO, the presence of an electron withdrawing sulfonium ion link has been proposed to raise

the reduction potential of the enzyme and thus make it thermodynamically competent to oxidize chloride (*3, 4, 21*). The distortion of the heme plane in MPO, by the presence of three covalent links, has also been implicated in raising the reduction potential of the enzyme (*3*), although no quantitative assignment of the role of individual links has been made so far. Redox measurements presented for S160Y variant in Chapter 4 have shown that formation of a double link between the heme and Tyr160 and Trp41 has resulted in an increase of the reduction potential of the enzyme by ~ 100 mV. These results are consistent with recent studies which showed that disruption of the aspartate to heme ester bond in MPO decreased the reduction potential by 56 mV (*22*), and further support the above proposal on the functional role of heme-protein links and the effect of heme flexibility on the properties of the enzyme. Overall, however, it is not possible to pin-point the precise functional advantage that is bestowed upon the protein through formation of a heme link and further detailed investigations will be necessary before this is fully understood.

5.5   Concluding remarks and future aims

In conclusion, the work in this thesis has given valuable insight into the formation of covalent links in heme proteins, using plant proteins as model systems. Although a number of wide-ranging questions remain unresolved, the conclusions drawn from this work contribute to our general understanding of the chemical and biological properties of enzymes bearing heme-protein links by helping us to understand how nature can 'switch off' their formation by finely tuning the characteristics in the active sites of otherwise very similar heme proteins. This work could, therefore, be used as a basis for further studies that explore alternative routes for covalent heme attachment.

5.6 References

(1) Pipirou, Z., Bottrill, A. R., Metcalfe, C. M., Mistry, S. C., Badyal, S. K., Rawlings, B. J., and Raven, E. L. (2007) Autocatalytic formation of a covalent link between tryptophan 41 and the heme in ascorbate peroxidase. *Biochemistry 46*, 2174-2180.

(2) Pipirou, Z., Bottrill, A. R., Svistunenko, D. A., Efimov, I., Basran, J., Mistry, S. C., Cooper, C. E., and Raven, E. L. (2007) The reactivity of heme in biological systems: autocatalytic formation of both tyrosine-heme and tryptophan-heme covalent links in a single protein architecture. *Biochemistry 46*, 13269-13278.

(3) Colas, C., and Ortiz de Montellano, P. R. (2003) Autocatalytic radical reactions in physiological prosthetic heme modification. *Chem. Rev. 103*, 2305-2332.

(4) Zederbauer, M., Furtmuller, P. G., Brogioni, S., Jakopitsch, C., Smulevich, G., and Obinger, C. (2007) Heme to protein linkages in mammalian peroxidases: impact on spectroscopic, redox and catalytic properties. *Nat. Prod. Rep. 24*, 571-584.

(5) Colas, C., and Ortiz de Montellano, P. R. (2004) Horseradish peroxidase mutants that autocatalytically modify their heme prosthetic group. *J. Biol. Chem. 279*, 24131-24140.

(6) Limburg, J., LeBrun, L. A., and Ortiz de Montellano, P. R. (2005) The P450$_{cam}$ G248E mutant covalently binds its prosthetic heme group. *Biochemistry 44*, 4091-4099.

(7) LeBrun, L. A., Hoch, U., and Ortiz de Montellano, P. R. (2002) Autocatalytic mechanism and consequences of covalent heme attachment in the cytochrome P4504A family. *J. Biol. Chem. 277*, 12755-12761.

(8) LeBrun, L. A., Xu, F., Kroetz, D. L., and Ortiz de Montellano, P. R. (2002) Covalent attachment of the heme prosthetic group in the CYP4F cytochrome P450 family. *Biochemistry 41*, 5931-5937.

(9) Henne, K. R., Kunze, K. L., Zheng, Y. M., Christmas, P., Soberman, R. J., and Rettie, A. E. (2001) Covalent linkage of prosthetic heme to CYP4 family P450 enzymes. *Biochemistry 40*, 12925-12931.

(10)   Hoch, U., and Ortiz De Montellano, P. R. (2001) Covalently linked heme in cytochrome p4504a fatty acid hydroxylases. *J. Biol. Chem.* *276*, 11339-11346.

(11)   Metcalfe, C. L., Ott, M., Patel, N., Singh, K., Mistry, S. C., Goff, H. M., and Raven, E. L. (2004) Autocatalytic formation of green heme: evidence for H_2O_2-dependent formation of a covalent methionine-heme linkage in ascorbate peroxidase. *J. Am. Chem. Soc.* *126*, 16242-16248.

(12)   Colas, C., and De Montellano, P. R. (2004) Horseradish peroxidase mutants that autocatalytically modify their prosthetic heme group: insights into mammalian peroxidase heme-protein covalent bonds. *J. Biol. Chem.* *279*, 24131-24140.

(13)   Girvan, H. M., Marshall, K. R., Lawson, R. J., Leys, D., Joyce, M. G., Clarkson, J., Smith, W. E., Cheesman, M. R., and Munro, A. W. (2004) Flavocytochrome P450 BM3 mutant A264E undergoes substrate-dependent formation of a novel heme iron ligand set. *J. Biol. Chem.* *279*, 23274-23286.

(14)   DePillis, G. D., Ozaki, S., Kuo, J. M., Maltby, D. A., and Ortiz de Montellano, P. R. (1997) Autocatalytic processing of heme by lactoperoxidase produces the native protein-bound prosthetic group. *J. Biol. Chem.* *272*, 8857-8860.

(15)   Lad, L., Mewies, M., Basran, J., Scrutton, N. S., and Raven, E. L. (2002) The role of histidine 42 in ascorbate peroxidase: kinetic analysis of the H42A and H42E variants. *Eur. J. Biochem.* *369*, 3182-3192.

(16)   Baer, B. R., Kunze, K. L., and Rettie, A. E. (2007) Mechanism of Formation of the Ester Linkage between Heme and Glu310 of CYP4B1: (18)O Protein Labeling Studies. *Biochemistry* *46*, 11598-11605.

(17)   Tomlinson, E. J., and Ferguson, S. J. (2000) Conversion of a *c* type cytochrome to a *b* type that spontaneously forms in vitro from apo protein and heme: implications for *c* type cytochrome biogenesis and folding. *Proc. Natl. Acad. Sci. U S A* *97*, 5156-5160.

(18)   Barker, P. D., and Ferguson, S. J. (1999) Still a puzzle: why is haem covalently attached in *c*-type cytochromes? *Structure* *7*, R281-90.

(19)   Page, M. D., Sambongi, Y., and Ferguson, S. J. (1998) Contrasting routes of c-type cytochrome assembly in mitochondria, chloroplasts and bacteria. *Trends Biochem. Sci.* *23*, 103-108.

(20)   Huang, L., Wojciechowski, G., and Ortiz de Montellano, P. R. (2006) Role of heme-protein covalent bonds in mammalian peroxidases. Protection of the heme by a single engineered heme-protein link in horseradish peroxidase. *J. Biol. Chem. 281*, 18983-18988.

(21)   Zederbauer, M., Furtmuller, P. G., Ganster, B., Moguilevsky, N., and Obinger, C. (2007) The vinyl-sulfonium bond in human myeloperoxidase: impact on compound I formation and reduction by halides and thiocyanate. *Biochem. Biophys. Res. Commun. 356*, 450-456.

(22)   Zederbauer, M., Furtmuller, P. G., Bellei, M., Stampler, J., Jakopitsch, C., Battistuzzi, G., Moguilevsky, N., and Obinger, C. (2007) Disruption of the aspartate to heme ester linkage in human myeloperoxidase: impact on ligand binding, redox chemistry, and interconversion of redox intermediates. *J. Biol. Chem. 282*, 17041-17052.

Chapter 6

Experimental

6.1 Materials and Stock Solutions

All chemicals were obtained from commercial sources and used without further purification unless otherwise stated. Buffers (Fisher) were all of the highest analytical grade (99% + purity) and used without further purification. Sinapinic acid and α-cyano-4-hydroxycinnamic acid were purchased from Fluka. Deuteroporphyrin was obtained from Porphyrin Products. All glycerol was sterilised. All buffers and solutions were made using deionised water and are listed in Appendix A. Water was purified by an Elga Purelab purification system and all buffers were filtered (0.2 μm) prior to use. Hydrogen peroxide solutions were freshly prepared by dilution of a 30% (v/v) solution (BDH): exact concentrations were determined using the published absorption coefficient (ε_{240} = 39.4 M^{-1} cm^{-1}) (*1*). All molecular biology kits and enzymes were used according to manufacturer's protocols.

6.2 Recombinant DNA Techniques

6.2.1 Oligonucleotides

Complementary oligonucleotides (29-35 bases in length) were designed to have ~15 bases either side of the residue to be mutated, and to end in G or C (See Appendix B). The melting temperatures (T_m) of primers were calculated according to Equation 6.1,

$$T_m = 64.9 + 0.4(\% \; GC) - 600/l \qquad \qquad ...(6.1)$$

where *l* is the primer length in bases, % GC is the percentage of mismatching bases in the primer. All these numbers are rounded to whole numbers for the formula.

The primers were synthesised and purified by Invitrogen™. Primers, delivered in lyophilized form, were resuspended in sterile water (300 μl) and stored at -20 °C. The complementary pairs of oligonucleotides containing the appropriate mismatch bases (Table II, Appendix B), were used to prepare the variants of rsAPX/CcP studied in this thesis. The W41A variant of rsAPX was prepared, expressed and purified by Miss Sandip Badyal and the W191F variant was prepared, expressed and purified by Miss Emma Murphy.

6.2.2 Site-directed mutagenesis

Site-directed mutagenesis was carried out using the Quickchange^{TM} mutagenesis kit (Stratagene). Two complementary oligonucleotides (Table II, Appendix B) encoding the desired mutation were synthesised and purified (Invitrogen). A set of 6 reaction samples was prepared. All chemicals were added in the order listed in Table 6.1 – with the exception of the DNA polymerase (*pfuTurbo*^{TM} or *KOD Hot Start*^{TM}), which was added last – to a thin-walled PCR tube and kept on ice. Evaporation from the mixture was prevented by addition of 1 drop of Nujol or PCR Mineral oil (Sigma). The DNA polymerase was supplied in the kit along with 10 × reaction buffer and the dNTP mix. A stock solution of 10 OD at 260 nm was used for each primer.

	S207E	S160Y	P132Y	F145Y
10× Buffer	2.5	2.5	2.5	5
Template	1	0.5	1	1
Primer F	0.5	1.5	0.25	3
Primer R	0.5	1.5	0.25	3
dNTPs	0.5	2.5	2.5	5
MgCl$_2$	2	1	1	2
Glycerol	2.5	–	–	–
DMSO	–	1.5	–	1
Water	15.5	13.5	16	29
*pfu*Turbo Polymerase	0.5	–	–	–
KOD Hot Start Polymerase	–	0.5	0.5	1

Table 6.1: Reaction volumes used in site directed mutagenesis PCR (μl).

The tubes were then centrifuged (13,000 rpm, ~10 seconds) and the PCR block (Perkin Elmer, 480 DNA Thermocycler) turned on with the programs set as in Table III, Appendix B. The successful conditions for each PCR experiment are described in Table III, Appendix B. In the 16 or 30 cycles, the time at 68 °C (5 minutes) was calculated from the size of the template (1 minute per kb) and the annealing temperature was calculated using Equation 6.2.

$$\text{Primer } T_m - 5 = \text{Primer annealing temperature} \qquad ...(6.2)$$

At the end of the reaction, samples were placed on ice for 2 minutes to cool. Digestion of the methylated and hemimethylated parental DNA was carried out by the addition of DpnI (1 µl). Mixtures were then centrifuged (1 minute) and immediately incubated at 37 °C for at least 1 hour to digest the parental DNA. Agarose gel electrophoresis was performed to determine successful reaction samples.

6.2.3 Transformation into XL1-Blue Supercompetent/SG cells

XL1-Blue supercompetent/SG cells were gently thawed on ice. The *Dpn* I-treated DNA (1 µl) was transferred into a prechilled Falcon® 2059 polypropylene tube. Cells (100 µl) were added; the reactions were swirled to mix solutions and placed on ice for 30 minutes. The reactions were heat-shocked for 45 seconds at 42°C and placed on ice for another 2 minutes. Psi Broth (500 µl) was added to the Falcon tubes and the reactions were incubated at 37°C, shaking, for 90 minutes. The cultures were then pelleted, 400 µl of the supernatant media were removed and the remaining 100 µl of supernatant solution was used to resuspend the bacterial pellets. The cultures were then plated on LB Amp agar plates (for XL1-Blue supercompetent cells) or LB Amp/Kan agar plates (for SG cells). A single colony from the overnight plate was selected and incubated into LB media (10 ml) containing 100 µg/ml ampicillin (for XL1-Blue supercompetent cells) or 100 µg/ml ampicillin/30 µg/ml kanamycin (for SG cells), at 37 °C with vigorous shaking (225 rpm). DNA was isolated from the overnight cultures using QIAprep® Spin Miniprep kit and analysed as above using agarose electrophoresis and the DNA was re-sequenced to confirm the mutation.

6.2.4 Isolation of DNA

DNA was extracted from 10 ml overnight cultures using a QIAprep® Spin Miniprep kit (Qiagen Cat. No. 27104) and a microcentrifuge. The protocol from the kit (QIAprep® Miniprep handbook, p22) was followed, except that the eluting step was performed with sterile water (not EB buffer). The cells were pelleted in a sterile 50 ml tube, at 1200 rpm for 30 minutes. The pellet was then resuspended in buffer P1 (250 µl, with RNase added, and stored at 4 °C, see Appendix A). Buffer P2 (250 µl, see Appendix A) was added and the tube was gently inverted 4-6 times, after which buffer N3 (350 µl, see Appendix A) was added and the tube inverted 4-6 times. The tube was centrifuged (13,000 rpm) for 10 minutes. The supernatant was added to a QIAprep spin column and centrifuged for 1 minute at 13,000 rpm discarding the flow through. The column was washed with PB buffer (500 µl, see Appendix A) and centrifuged at 13,000 rpm for 1 minute discarding the flow through. The column was then washed with buffer PE (750 µl, with ethanol added, see Appendix A) and centrifuged for 1 minute at 13,000 rpm discarding the flow through. The column was centrifuged for 1 minute at 13,000 rpm to remove residual ethanol. The column was placed in a clean 1.5 ml microcentrifuge tube with sterile water (50 µl) in the centre of the column and left standing for 1 minute before centrifuging at 13,000 rpm for 2 minutes. The DNA sample obtained was stored at -20 °C. The isolated DNA concentration was calculated using Equation 6.3.

$$A_{260} \times 50 \times \text{Dilution factor} = \text{DNA concentration (ng/µl)} \qquad ...(6.3)$$

6.2.5 DNA sequencing

For DNA sequencing, (performed by Protein and Nucleic Acid Chemistry Laboratory, University of Leicester), 18 µl of DNA prepared as above was submitted along with 10 µl of each of the PQEF and PQER sequencing primers (Table I, Appendix B).

6.3 Agarose gel electrophoresis

Agarose gels (0.8 % w/v) containing 0.6 µg/ml ethidium bromide were cast, and electrophoresis was performed in TAE buffer (see Appendix A) at 80 V. Samples (10 µl) were mixed with 2 µl sample loading buffer prior to being loaded on to the gel.

DNA markers (GeneRuler 1 kb DNA ladder) were from MBI Fermentas (Cat. No SM0311), band sizes were 10, 8, 6, 5, 4, 3.5, 3, 2.5, 2, 1.5, 1, 0.75, 0.5 and 0.25 Kb. Nucleic acids were visualised by exposing the gel to long wavelength UV radiation on a transilluminator.

6.4 Protein expression of APX

Recombinant soybean cytosolic APX (rsAPX) was prepared from *Escherichia coli* SG1300 cells (Qiagen, containing pREP4 vector) incorporating pQE30 expression plasmid (Qiagen), (see Appendix C). All LB media used to grow the *E. coli* contained ampicillin (100 µg/ml) and kanamycin (30 µg/ml). SDS-PAGE analysis was used to monitor protein expression.

Agar plates containing ampicillin (100 µg/ml) and kanamycin (30 µg/ml) were streaked with *E. coli* cells from a −80 °C glycerol stock. The plates were inverted, incubated and grown at 37 °C overnight. A single colony was used to inoculate LB media (400 ml). This was incubated overnight at 37 °C with shaking at 225 rpm. This formed the starter culture. An aliquot of this starter culture (750 µl) was added to glycerol (750 µl) to form the new glycerol stock, which was then frozen on dry ice. The starter culture (50 ml per litre) was then added to 8 x 1 litre of LB media. The flasks were shaken (225 rpm) at 37 °C until the culture reached an OD_{600} nm of ≈1.0 (approximately 3 hours). The incubator temperature was then adjusted to 27 °C. IPTG (1 ml, 1 M) was added to each flask to induce expression. The flasks were incubated at 27 °C overnight with shaking (225 rpm). Cells were harvested by centrifugation (8,000 rpm for 5 minutes at 5 °C). The cell pellets were then frozen at -80 °C, until needed.

6.5 Protein isolation and purification of APX

6.5.1 Cell Lysis

The cell pellets were thawed in sonication buffer (150 ml), (see Appendix A). PMSF (50 mg) was dissolved in isopropanol (2 ml) and added to the cell suspension, which was stirred with lysozyme (~5 mg) for 20 minutes at room temperature until the liquid became viscous. DNase (50 µl of 1 mg/ml stock) was added and the suspension was stirred until it became more fluid. The mixture was then sonicated on ice, at maximum power, for 4×1 minute bursts, followed by a cooling period of

approximately one minute. The cell-free extract was obtained through pelleting of the cell debris by centrifugation (20,000 rpm for 40 minutes, 5 °C). The supernatant containing the cell free extract was decanted and kept at 4 °C for protein purification.

6.5.2 Nickel Resin Column

A Ni^{2+}-nitrilotriacetic acid (NTA) agarose column (Qiagen) was used to isolate the APX protein from the cell-free extract. A column of 5 ml Ni^{2+}-NTA super flow resin (Qiagen) was packed and flushed through with water (100 ml). The resin was regenerated with 20 ml of regeneration buffer (see Appendix A) and was equilibrated with sonication buffer (100 ml). The cell-free extract was loaded on at a steady flow rate. The column was flushed with sonication buffer until the eluant gave an absorbance of 0.01 at 280 nm. The column was then washed with wash buffer (600 ml), (see Appendix A). The bound protein was eluted with elution buffer (~250 ml), (see Appendix A) and the pH of eluant was adjusted to 6 (using 1M KH_2PO_4) for reconstitution.

6.5.3 Reconstitution

Hemin solution (5 mg/ml in 0.1 M KOH) was prepared and titrated into the eluant from the Ni^{2+}-NTA column at 20 μl aliquots over a period of 1-2 hours until $R_z > 2$. Another 100 μl of hemin solution was then added and the protein solution was dialysed overnight against FFQ buffer, at 4 °C.

6.5.4 FFQ Column

Excess hemin was removed using a column (2.5 cm diameter and 20 cm long) packed with Q Sepharose fast flow (FFQ) resin. The enzyme and hemin solution was centrifuged (10 minutes, 8000 rpm). FFQ resin (5 ml) was poured into a column and flushed with water (100 ml). The column was equilibrated with FFQ buffer (200 ml). The enzyme solution was decanted off the precipitate, and was concentrated using an Amicon device (Amicon, Bioseparations, Millipore) with nitrogen under pressure using an ultrafiltration regenerated cellulose membrane (MW cut off 10,000, Amicon) to a minimum volume of ~100 ml. This solution was loaded on to the column at maximum flow rate. Then the column was washed with FFQ buffer (100 ml). The protein was eluted with ~50 ml of FFQ elution buffer and concentrated

using an Amicon. The protein was exchanged into deionised water using a centricon (Amicon, Bioseparations, and Millipore) and concentrated to ~1 ml. The spectrum was recorded and the protein was split in 100 µl aliquots, frozen on dry ice and stored at -80 °C.

6.5.5 Fast Protein Liquid Chromatography (FPLC)

Protein samples were purified further by gel filtration (Superdex column 75 HR 10/30, Fast Protein Liquid Chromatography (FPLC), ÄKTA). The protein was eluted with 0.15 M potassium phosphate pH 7.0, monitored at a wavelength of 280 nm. The protein had a retention time of 45 minutes.

6.5.6 Polyacrylamide gel electrophoresis (SDS-PAGE)

To confirm the purity of the protein, SDS-PAGE was carried out. Discontinuous polyacrylamide gels (15 %) containing 0.1 % SDS and 4 % polyacrylamide stacking gel and a mini-Protean II gel system at 0.75 mm thickness were used. Samples were prepared by adding an equal volume of sample buffer and boiling for five minutes. The gels were run in SDS running buffer at 200 V until the dye front reached the end of the gel. The gels were soaked in stain for 10 minutes, then destained by soaking in destain solution overnight. Protein markers (Low Molecular Weight Protein Marker) were from Sigma, band sizes were 97.0, 66.0, 45.0, 30.0, 20.1 and 14.4 kDa.

6.6 Protein expression and purification of CcP

The CcP gene that was kindly supplied from Professor Grant Mauk has been modified in order to improve overexpression in *E. Coli*. Firstly the 67 residues pre-sequence has been dispensed with so when compared to the cDNA obtained from bakers yeast residue 1 is actually residue 68. However for our purposes residue 1 is residue 1 and all numbering is with respect to this. Secondly, the first three residues have been modified from TTT in the wild type gene to MKT in the supplied gene. Therefore our "wild type" is referred to as CcP(MKT). There are also two reported "versions" of the protein. The CcP cDNA predicts residue 53 being Ile and residue 152 being Gly. However the crystal structure shows residue 53 to be Thr and residue 152 to be Asp. Our CcP(MKT) version has Thr53 and Asp152 so is identical to the crystal structure. The vector that supports the gene is a version of PemBL8 modified

to incorporate the T7 promoter sequence. The vector also includes amphicilin resistance.

The CcP construct was transformed into XL1-Blue Super competent cells (Stratagene) and a 5 ml overnight culture was grown and used for a DNA prep. The CcP coding region was sequenced using a standard T7 sequencing primer to check the integrity of the gene. BL21 gold DE3 cells were freshly transformed with the sequences DNA and colonies grown on a LB plate containing amphicilin (100 µg/ml) at 37 °C for 12 hours. A single colony was used to inoculate 50 ml of LB broth containing amphicilin (100 µg/ml) and was grown at 37 °C for 12 hours with shaking. 8 × 1 L flasks of LB broth containing amphicilin (100 µg/ml) were inoculated with 1 ml of the overnight culture and were left to incubate at 37 °C for ~8 hours with shaking (A_{600} ~ 2.0) after which they were induced with IPTG (200 µg/ml final concentration) and left to incubate at 20 °C with stirring for 18 hours. The cells containing large amounts of CcP were harvested by centrifugation giving red pellets. These were frozen at -80 °C to aid lysis.

The cell pellets were resuspended in 100 ml of lysis buffer (0.1 M potassium phosphate, 1 mM EDTA, pH 6.0) along with hemin (10 mg in 1 ml of 0.1 M KOH) and PMSF (1 mM final concentration). The cells were sonicated in 8 × 1 minute bursts with cooling in between. After sonication the lysate was left at 4 °C for 1 hour to allow reconstitution with the hemin. The cell debris was then removed by centrifugation at 20,000 rpm for 40 minutes. The cell free extract was then diluted with water to a total volume of 500 ml and readjusted to pH 6. The crude protein solution was loaded onto a DEAE sepharose ion exchange column (5 cm × 2 cm) that had been pre-equilibrated with 0.1 M potassium phosphate, pH 6.0. The column was then washed with 20 column volumes of buffer and then the protein was eluted with 0.5 M potassium phosphate, pH 6.0 as a single dark red band. The protein was diluted to 100 ml volume and was adjusted to pH 5.0 and left at 4 °C for 1 hour, which resulted in a white precipitate, which was removed by centrifugation. The protein solution was concentrated to 10 ml total volume and loaded onto a sephadex G50 gel filtration column (150 cm × 3 cm) which had been pre-equilibrated with 0.1 M potassium phosphate, pH 6.0 and slowly eluted over 8 hours. The centre of the large red CcP band was collected and concentrated, then this was dialysed against water resulting in a crystalline precipitate. The crystals were dissolved in 0.5 M potassium phosphate, pH 6.0 and recrystallised a further 3 times after which they

were shown by UV and SDS PAGE to be pure CcP. The protein was stored at -80 °C as a crystalline suspension in water.

Purified samples of CcP and W191F showed wavelength maxima at 409, 508, 544^{sh} and 645 nm and 410, 529, 565^{sh} and 642 nm (150 mM potassium phosphate, pH 6.0), respectively. Enzyme concentrations for CcP and W191F were determined using absorption coefficients of ε_{409} = 95 mM^{-1}cm^{-1} (3) and ε_{409} = 102 mM^{-1}cm^{-1}, respectively.

All CcP and W191F protein samples used for this work were kindly prepared and provided by Dr. Clive Metcalfe and Miss Emma Murphy, respectively.

6.7   UV-Visible spectroscopy

Routine absorbance measurements were conducted using variable-slit Perkin-Elmer Lambda 14, Lambda 25, Lambda 35 or Lambda 40 (1 mm slit width) UV-visible spectrometers. Temperature control (25 ± 0.1 °C) was achieved using a thermally-jacketed cell holder that was connected to a circulating water bath (NESLAB RTE-200) or Peltier device (Perkin-Elmer, Peltier thermostatted reference holder, BS0510412). A typical 270-700 nm scan was obtained using a scan speed of 480 nm/minute, acquiring at 0.5 nm intervals, using a 0.5 ml or 1 ml quartz cuvette of 10 mm path length. Baseline corrections were made against the buffers and solvents used.

6.8   Determination of heme absorption coefficients

The total heme content of a heme protein solution and therefore the absorption coefficient of the heme protein was determined using the pyridine hemochromagen method according to the protocol of Antonini and Brunori (2).

An alkaline pyridine solution was prepared from the addition of pyridine (2 ml), 1 M NaOH (600 µl) and distilled water to a final volume of 6 ml. A protein sample with an absorbance of 0.3 – 0.9 in the visible region was required to provide the most reliable data; thus, a spectrum was recorded on a gravimetrically determined sample drawn from the protein stock solution. Pyridine solution (600 µl) was added to the protein solution (200 µl of known concentration) to form the pyridine-heme complex. After five minutes (to enable complete conversion to hemochromagen), the electronic spectrum of the resulting solution (800 µl) of oxidised hemochromagen

(yellow in colour) was recorded. A single crystal of dithionite was added to the oxidised pyridine hemochromagen solution and the spectrum of the unstable reduced hemochromagen was recorded immediately over the wavelength range 450 – 650 nm. The complete transfer of heme from the protein to the pyridine was checked by determining the absorbance at maximum (λ = 557 nm) and minimum (λ = 540 nm) wavelengths; a ratio of A_{557}/A_{540} = 3.5 is found for protoheme. Absorption coefficients were calculated knowing the absorption coefficient for the pyridine-protoheme complex (ε = 32 mM^{-1} cm^{-1}) using Equation 6.4: where A is the absorbance of the stock solution, c is the concentration of the protein, ε is the molar absorption coefficient and l is the pathlength of the cuvette.

$$A = \varepsilon c l \qquad\qquad ...(6.4)$$

6.9   Acidified butanone extraction

Acid butanone extractions were carried out as reported previously (*3*). Specifically, an aqueous solution of protein was titrated with 1 M HCl to a pH of 1.5. An equivalent volume of ice-cold 2-butanone was added with gentle but continuous stirring. After a period of cooling on ice, two distinct layers were observed and a further amount was added to remove the heme. Transfer of heme to the organic layer (visualised by red color) indicated absence of covalent links between the heme and the protein, and *vice versa*.

6.10   Reconstitution with deuteroheme

Apoenzyme was initially prepared by the method of Teale (*3*). Specifically, apoenzyme was prepared by means of an acidified butanone extraction, as described above. The heme was extracted through addition of ice-cold butan-2-one (Aldrich) and the organic layer removed; this process was repeated until a straw-coloured aqueous apo-enzyme layer was observed. The aqueous layer was dialysed sequentially against 5 L of 1 mM NaHCO$_3$, 5 L of 1 mM EDTA, and finally 5 L of 1 mM NaHCO$_3$ at 4 °C. The apo-enzyme was then further dialysed against 10 mM potassium phosphate, pH 8.5 at 4 °C and concentrated.

Iron(III) deuteroporphyrin IX chloride (>97%; Porphyrin Products, Frontier Scientific Inc.) was dissolved in 0.1 M potassium hydroxide (1mg/ml) which was

added dropwise to the apo-enzyme, with stirring on ice, until an *Rz* value of >2 was reached. The solution was incubated on ice for another 30 minutes. An additional amount of iron(III) deuteroporphyrin IX chloride solution was added and the solution was further incubated on ice for another 15 minutes. This solution was dialysed against potassium phosphate (20 mM, pH 7.0) overnight at 4°C. The protein solution was concentrated and exchanged in water. Any precipitated protein or excess heme was removed by centrifugation (13,000 rpm, 5 minutes).

6.11   Steady-state kinetics

Steady-state kinetic measurements were conducted using a Perkin-Elmer spectrophotometer in a fixed wavelength scan mode, acquiring at 0.1 second intervals, monitoring at a wavelength that is dominated by the reducing substrate. Steady-state kinetic assays for measurement of *L*-ascorbic acid activity were performed in 100 mM potassium phosphate buffer, pH 7.0 and the concentrations of stock solutions were measured by UV-visible spectroscopy. Stock solutions made were: 10 mM ascorbate (ε_{290} = 2.8 mM^{-1}cm^{-1}), 10 mM hydrogen peroxide (ε_{240} = 39.4 M^{-1}cm^{-1}), 2-5 μM enzyme. For each assay 10 μl of enzyme stock solution were used. The ascorbate concentration was varied. The final volume was made up to 1 ml with buffer using a 1 ml quartz cuvette. Hydrogen peroxide stock solution (10μl) were added last. The temperature was maintained using a water bath at 27 °C. The decay of ascorbate was measured at 290 nm using the Kinlab program.

6.12   Transient-state kinetics

Rapid reaction kinetic experiments were performed using an Applied Photophysics SX.18MV-R microvolume stopped-flow spectrophotometer fitted with a Neslab RTE200 circulating water bath. Time-dependent spectra of the various reactions, were performed by multiple wavelength stopped-flow spectroscopy using a photodiode array detector and X-SCAN software (Applied Photophysics). Spectral deconvolution was performed by global analysis and numerical integration methods using PROKIN software (Applied Photophysics). To investigate the reaction of S160Y with H_2O_2, the enzyme (20 μM in 100 mM potassium phosphate buffer, pH 7; 25 °C) was reacted with varying concentrations of H_2O_2 and the reaction was followed over time scales ranging from 3 milliseconds to 4000 sec. To investigate

the reaction of W191F with H_2O_2, the enzyme (3.5 µM in 100 mM potassium phosphate, pH 7.0; 25 °C) was reacted with 1 or 5 equivalents of H_2O_2 (3.5 or17.5 µM, respectively, in 100 mM potassium phosphate, pH 7.0; 25 °C) and the reaction was followed over time scales ranging from 3 milliseconds to 1 sec.

6.13 High Performance Liquid Chromatography (HPLC)

HPLC analysis of protein samples before and after reaction with H_2O_2 were conducted on a Varian ProStar HPLC system with an analytical Vydac C4 reverse phase HPLC column under computer control. Solvents were as follows: A = 0.1% w/v trifluoroacetic acid (TFA) (4) in 95% H_2O, 5% acetonitrile; B = 0.1% w/v TFA in 80% acetonitrile, 20% H_2O. The column was pre-equilibrated with 42 % buffer B and protein/heme separation was achieved using the following elution gradient: 42 % B for 5 minutes, 42 – 55 % B for 25 minutes, 55 – 100 % B for 10 minutes, 100 % B for 5 minutes. Chromatograms were monitored at 215 nm for protein-containing fractions and 398 nm for heme-containing fractions.

For separation and collection of fragments, an Agilent Series 1100 binary pump HPLC system was used, fitted with diode array detector. For collection of the hydroxylated heme species, protein samples, after reaction with H_2O_2, were injected onto a Phenomenex JUPITER 5u C4 300A column (250 × 2 mm); fractions eluting at 4 minutes were collected, freeze-dried and resuspended in 200 µl of H_2O to be used for MALDI-TOF mass spectrometry.

Samples for trypsin digestion were treated 50:1 w/w (enzyme:trypsin) in 0.4 M NH_4HCO_3, pH 8, 37 °C for 18 hours. The digest was stopped by addition of TFA (1 µl). The digested mixture was then injected onto a reverse phase C8 column (P.E. BrownLee Columns Aquapore Octyl, RP-300 C8 7 µm, 220×2.1 mm); solvents were as follows: A = 0.1% w/v TFA in 95% H_2O, 5% acetonitrile; B= 0.1% w/v TFA in 80% acetonitrile, 20% H_2O. Separation of peptide fragments was achieved using the following elution gradient: t=0 minutes, B=2%; t=2, B=2%; t=45, B=75%; t=50, B=100%; t=55, B=100%. Peptide fractions showing both heme and protein absorbances were collected and then evaporated to dryness and dissolved in H_2O.

6.14 Mass Spectrometry

6.14.1 Matrix-Assisted Laser Desorption/Ionization-Time of Flight (MALDI-TOF) mass spectrometry

MALDI-TOF analyses were carried out on a Voyager-DE STR Biospectrometry Workstation (Applied Biosystems, Framingham/USA), (Figure 6.1). Spectra of protein samples were acquired in linear mode using external calibration. Protein samples for MALDI-TOF mass spectrometry were exhaustively exchanged into 0.4 M NH_4HCO_3, pH 8 and diluted 1:1 or 1:50 (depending on sample concentration) with matrix (sinapinic acid, 10 mg/ml, 0.1% TFA in 1:1 acetonitrile/H_2O). Analysis was carried out as follows: 1 µl of the protein/matrix mixture was spotted onto a MALDI target plate using the drying droplet method. The MALDI-TOF mass spectrometer was calibrated in the range 2000 – 45000 Da using horse heart myoglobin. Spectra were an average of 1000 shots.

Spectra for peptide samples were acquired in reflectron mode. Peptide samples (1µl) were mixed with matrix (α-cyano-4-hydroxycinnamic acid, 5 mg/ml, 0.1% TFA in 1:1 acetonitrile/H_2O) for MALDI-TOF mass spectrometry. For these experiments, the MALDI-TOF mass spectrometer was calibrated in the range 500-6000 Da with a peptide mass calibration kit (Sigma, Catalogue Number MSCAL2, used according to manufacturer's instructions). Spectra of the HPLC-purified peptide fragments were collected in the same mass range using an average of 250 laser shots. All MALDI-TOF spectra were analysed using Data Viewer software (Applied Biosystems). Theoretical isotope patterns for heme and peptide fragments of interest were calculated by entering the desired chemical formula in the 'Sheffield ChemPuter Isotope Pattern Calculator' (http://winter.group.shef.ac.uk/chemputer/isotopes.html). The results are presented with the most intense line set to 100%.
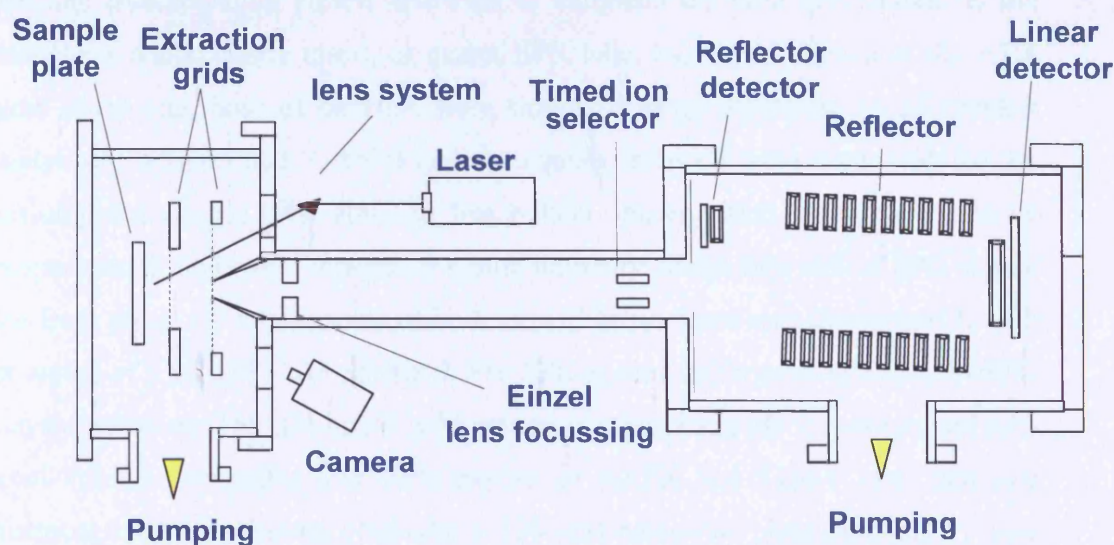
Figure 6.1: Voyager-DE STR workstation layout, Applied Biosystems.

6.14.2 MS/MS analyses

HPLC-purified samples of peptide fragments prepared as above were re-suspended in water (100 µl). The solution was then mixed in a 1:1 ratio with acetonitrile/0.2% formic acid and infused from a syringe pump (Harvard Apparatus Ltd., Edenbridge, Kent, UK) at a flow rate of 0.5 µl/min to the MicroIonspray source of a 4000 Q-Trap mass spectrometer (Applied Biosystems, Warrington, UK). The sample was sprayed directly from a fused-silica PicoTip (New Objective Inc., Woburn, MA, USA) maintained at a potential of 2800 V in positive ion mode. Tandem mass spectrometry was carried out for ions of interest. Spectra of fragment ions were interpreted manually. MS/MS analyses of all protein samples was carried out by Dr. Andrew Bottrill.

6.15 Electronic Paramagnetic Resonance (EPR) Spectroscopy

All EPR spectra were measured using a Bruker EMX EPR spectrometer (X-band) at a modulation frequency of 100 kHz. Accurate g-values were obtained using the built-in microwave frequency counter and a 2,2-diphenyl-1-picrylhydrazyl powder standard (g = 2.0037 ± 0.0002 (5)). A spherical high quality Bruker resonator SP9703 and an Oxford Instruments liquid helium system were used to measure low temperature EPR spectra. Spectra for blank samples (frozen water) were subtracted

from the corresponding protein spectrum to eliminate the base line caused by the resonator's walls, quartz insert, or quartz EPR tube. Individual signals of the APX heme forms and those of metHbA were simulated using SimFonia v.1.25 (Bruker Analytische Messtechnik GmbH) and the signals integrals were compared for the non-saturated signals. The absolute free radical concentration was determined by comparison of the second integral of a pure lineshape of the free radical EPR signal, free from the $g = 2$ components of both the HS ferric heme and Compound I, with the signal of a 98 µM Cu2+ standard. For EPR spectra of ferric rsAPX and S160Y, enzyme solutions (160 µM in 100 mM potassium phosphate, pH 7) were mixed with equal volumes of buffer. For EPR spectra of rsAPX and S160Y after peroxide treatment, enzyme solutions (160 µM in 100 mM potassium phosphate, pH 7) were mixed with equal volumes of hydrogen peroxide solution. Tubes containing protein solutions or water (blanks) were frozen in cold methanol. Once frozen, samples were transferred to liquid nitrogen (77 K) where they were stored before measurements.

6.16 Xanthine/xanthine oxidase method for determination of Fe^{3+}/Fe^{2+} reduction potential

Fe^{3+}/Fe^{2+} reduction potentials for rsAPX and S160Y were determined by simultaneous reduction with a dye of known potential (6) according to previous methodology (7). The assay contained xanthine (300 µM), xanthine oxidase (50 nM), and enzyme (3-4 µM). The buffer (100 mM potassium phosphate buffer, pH 7.0) was made oxygen free using glucose (5 mM), glucose oxidase (50 µg/mL), and catalase (5 µg/mL). For measurement of the reduction potentials of rsAPX and S160Y before reaction with H_2O_2 the reaction also contained phenosafranin ($E_{m,7}$ = -252 mV) (8). Absorbance changes corresponding to reduction of heme were measured at the isosbestic point for phenosafranine (407 nm); reduction of the dye was measured at 520 nm where the change due to heme reduction was negligible. For measurement of the reduction potential of S160Y after reaction with H_2O_2, the same experiment was also carried out using

(i) indigo trisulfonate ($E_{m,7}$ = -81 mV) as a dye (8). Reduction of the dye was measured at the wavelength maximum of the dye (600 nm), where the change due to heme reduction was negligible; absorbance changes corresponding to reduction of heme were measured at 440 nm, subtracting the contribution from the dye.

(ii) nile blue ($E_{m,7}$ = −116 mV) as a dye (*8*). Reduction of the dye was measured at the wavelength maxima of the dye (635 nm), where the change due to heme reduction was negligible; absorbance changes corresponding to reduction of heme were measured at 406 nm.

In all cases, linear Nernst plots for one electron reduction of heme (25 mV $\ln(E_{ox}/E_{red})$) (where E_{ox} = concentration of oxidized enzyme, E_{red} = concentration of reduced enzyme) and two-electron reduction of dye (12.5 mV $\ln(D_{ox}/D_{red})$) (where D_{ox} = concentration of oxidized dye, D_{red} = concentration of reduced dye) produced the expected slope of 1 across a wide range of potentials, and the intercept gives a reliable value for $\Delta E_{m,7}$ with an error of ±2 mV. UV-visible spectra obtained in all experiments were analyzed using SPECFIT (*9*) for singular value decomposition based on factor analysis. All potentials reported in this thesis are given versus the normal hydrogen electrode (NHE).

6.17 Crystal screens

All the screens for the crystallisation of S207E and S160Y rsAPX were carried out using the sitting drop method (Figure 6.2) and using 24 well plates (4 × 6 Cryschem plates with 1 ml reservoirs, Hampton Research).

Screening of crystallisation conditions used the sparse-matrix factorial search method (*10*) using commercially available kits (MDL screens (I) and (II), Molecular Dimensions Ltd, Appendix D). The screens were prepared in a temperature controlled room at 19 °C. The protein solution (10 mg/ml in deionised water) was kept on ice throughout. Each MDL screen solution (700 μl) was added to a separate well. The drops were 1 μl of protein solution and 1 μl of well solution.
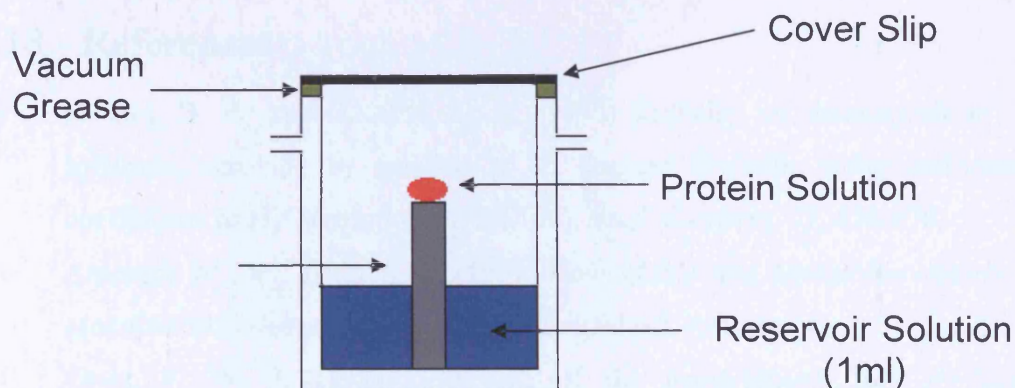
Figure 6.2: Diagrammatic representation of the sitting drop method.

Screens were set up using the crystallisation conditions that have been published for rsAPX (*11*). The screens were set up with 2.25 M lithium sulfate and 0.1 M Hepes pH 8.3 at 19 °C. Screens were also set up with 1.5 to 2.25 M lithium sulfate and 0.1 M Hepes pH 8.1 to 9.5 at 19 °C (Table 6.2). All the well solutions were prepared from the same stock solutions and all the buffer pHs were checked as 1 M stock solutions. Protein solution (2 µl) was added to the first twelve of the small drop wells (6x2). Well solution (2 µl) was added to the drop of protein solution, and the first twelve wells sealed with clear postal tape making sure there were no air bubbles. The process was then repeated to complete the plate. The wells contained 1 ml of reservoir solution. The screens were left in temperature controlled rooms with no vibrations.

Li_2SO_4 (M)	0.1 M HEPES pH					
	8.1	8.3	8.5	8.8	9.0	9.5
1.5						
1.75						
2.0						
2.25						

Table 6.2 Screen conditions.

6.18 References

(1) Nelson, D. P., and Kiesow, L. A. (1972) Enthalpy of decomposition of hydrogen peroxide by catalase at 25 degrees C (with molar extinction coefficients of H_2O_2 solutions in the UV). *Anal. Biochem. 49*, 474-478.

(2) Antonini, M., and Brunori, E. (1971) *Hemoglobin and Myoglobin and their reactions with ligands*, North Holland Publishers, Amsterdam.

(3) Teale, F. W. J. (1959) Cleavage of the haem-protein link by acid methylethylketone. *Biochim. Biophys. Acta 35*, 543.

(4) Pummerer, R., Melamed, D., and Puttfarcken, H. (1922) *Chem. Berr. 55*, 3116-3132.

(5) Weil, J. A., Bolton, J. R., and Wertz, J. E. (1994) *Electron paramagnetic resonance: Elementary theory and practical applications.*, Wiley. xxi, New York.

(6) Massey, V. (1991) in *Flavins and Flavoproteins* (Curti, B., Ronchi, S., and Zanetti, G., Eds.) pp 59-66, Walter de Gruyter & Co., New York.

(7) Efimov, I., Papadopoulou, N. D., McLean, K. J., Badyal, S. K., Macdonald, I. K., Munro, A. W., Moody, P. C., and Raven, E. L. (2007) The redox properties of ascorbate peroxidase. *Biochemistry 46*, 8017-8023.

(8) Clark, W. M. (1972) *Oxidation-Reduction Potentials of Organic Systems*, Robert E. Kreiger Publishing Co., Huntington, NY.

(9) Binstead, R. A., and Zuberbuehler, A. D., Chapel Hill, NC.

(10) Collaborative Computational Project, N. (1994) The *CCP*4 suite: programs for protein crystallography. *Acta Cryst. D50*, 760-763.

(11) Sharp, K. H., Mewies, M., Moody, P. C., and Raven, E. L. (2003) Crystal structure of the ascorbate peroxidase-ascorbate complex. *Nat. Struct. Biol. 10*, 303-307.

Appendix A

LB media

Per 8 L: 168 g LB-Broth, 16.8 g glucose

LB-Amp/Kan agar plates

20 g LB-Broth, 2 g glucose and water to 500 ml. 15 g agar and water to 500 ml

Both solutions sterilised, mixed and supplemented with 100 mg/ml ampicillin and 30 mg/ml kanamycin

Anti-denaturation buffer

100 mM potassium phosphate, pH 7

Regeneration buffer

114.6 g guanidine HCl

40 ml acetic acid

160 ml water

Sonication buffer

100 mM potassium phosphate, pH 8

300 mM KCl (22.36 g)

made up to 1 L with water

Wash buffer

100 mM potassium phosphate, pH 6

300 mM KCl (22.36 g)

made up to 1 L with water

Elution buffer

100 mM potassium phosphate, pH 4.2

300 mM KCl (22.36 g)

made up to 1 L with water

FFQ buffer

10 mM potassium phosphate, pH 7

FFQ elution buffer

10 mM potassium phosphate, pH 7

250 mM KCl (18.64 g/L)

FPLC grade

150 mM potassium phosphate, pH 7

Sample buffer

0.15 g Tris, 1 g SDS, 5 g glycerol, 0.76 g DTT, 0.01 g bromophenol blue

made up to 50 ml with water

Running buffer

(25 mM Tris-HCl, 192 mM glycine, 0.1% w/v SDS)

18 g Tris, 86 g glycine, 6 g SDS

made up to 600 ml with water

Resolving buffer

(1.5 M Tris with 0.4 % SDS, pH 8.8)

30.3 g Tris base in 100 ml water, adjusted to pH 8.8, plus 0.66 g SDS and made up to

166 ml with water

Stacking buffer

(0.5 M Tris with 0.4 % SDS, pH 6.8)

6.05 g Tris base in 40 ml water, adjusted to pH 6.8, plus 0.4 g SDS and made up to

100 ml with water

Resolving gel mix

3.25 ml acrylamide solution, 1.9 ml resolve buffer, 2.4 ml water, 25 μl 10 % APS,

12.5 μl TEMED (add TEMED last and proceed immediately)

Stacking gel mix

325 µl acrylamide solution, 625 µl stacking buffer, 1.525 ml water, 2 µl saturated bromophenol blue, 12.5 µl 10 % APS, 6.5 µl TEMED (add TEMED last and proceed immediately)

Coomassie Brilliant Blue R250

0.25 % in 5:1:5 v/v methanol: acetic acid: water

Staining buffer

30 % v/v methanol, 12 % w/v trichloroacetic acid, 0.01 % w/v Coomassie Brilliant Blue R250, 10 % w/v sulphosalicylic acid

Destaining buffer

7.5 % acetic acid, 5 % methanol in water

DNA gel mix

1.4 g agarose, 200 ml TAE, 20 µl ethidium bromide

50x TAE Buffer (Agarose gel electrophoresis)

242 g Tris base, 57.1 ml glacial acetic acid, 100 ml of 0.5 M EDTA, made up to 1 L with water

Pyridine base solution

1.2 ml 1 M NaOH, 4 ml pyridine, 6.8 ml water

HPLC Buffer A

0.1 % w/v TFA in 5 % v/v acetonitrile in water

HPLC Buffer B

0.1 % w/v TFA in 80 % v/v acetonitrile in water

N3 Buffer (Qiagen)

Contains guanidine hydrochloride and acetic acid

P1 Buffer (Qiagen)

Alkaline buffer that contains RNase

P2 Buffer (Qiagen)

Contains sodium hydroxide

PB Buffer (Qiagen)

Contains guanidine hydrochloride and isopropanol

PE Buffer (Qiagen)

Contains ethanol

Psi Broth

Lennox-LB media autoclaved

Per 100 ml:

      Add 1ml of filter sterilised 1M potassium chloride

      Add 0.4 ml of filter sterilised 1M magnesium sulphate

Appendix B

Table I. The forward and reverse oligonucleotides used for sequencing.

Sequencing Primer	T_m (°C)	% GC
PQEF 5' CGG ATA ACA ATT TCA CAC AG 3'	48	40
PQER 5' GTT CTG AGG TCA TTA CTG G 3'	49	47

Table II. The forward and reverse oligonucleotides used to generate the variants of rsAPX. The mismatched codons are highlighted in red.

Variant	T_m (°C)	% GC
S207E rsAPX Forward: 5' CCTTCAGCTACCT**GAA**GACAAGGCTC 3' Reverse: 5' GAGCCTTGTC**TTC**AGGTAGCTGAAGG 3'	63	54
S160Y rsAPX Forward: 5' CGTTGCTCTA**TAT**GGGGGTCACACTATTGG 3' Reverse: 5' CCAATAGTGTGACCCCC**ATA**TAGAGCAACG 3'	66	53
P132Y rsAPX Forward: 5' GGGTCGCTTG**TAC**GATGCCACTAAGGG 3' Reverse: 5' CCCTTAGTGGCATC**GTA**CAAGCGACCC 3'	66	59
F145Y rsAPX Forward: 5' CCATTTGAGAGATGTG**TAC**GGCAAAGCTATGGGGC 3' Reverse: 5' GCCCCATAGCTTTGCC**GTA**CACATCTCTCAAATGG 3'	69	51

Table III. Temperature cycler program for site directed mutagenesis. [*] See Equation 6.2

(A) S207E rsAPX

Number of Cycles	Temperature (°C)	Time (s)
1	95	30
	95	30
16	58	60
	68	360

(B) S160Y rsAPX

Number of Cycles	Temperature (°C)	Time (s)
1	94	120
	94	15
30	61	30
	68	300

(C) P132Y rsAPX

Number of Cycles	Temperature (°C)	Time (s)
1	95	30
16	95	30
	63	58
	68	300
1	72	600
	4	30

(D) F145Y rsAPX

Number of Cycles	Temperature (°C)	Time (s)
1	94	120
30	94	15
	64	30
	68	60
1	68	600

Appendix C

Vector pQE-30:
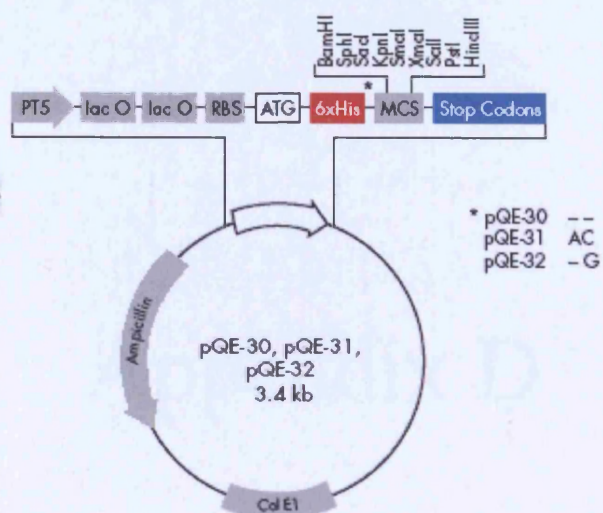
Appendix D

(A)   Structure Screen 1 - Catalogue Number MD1-01

1	0.02 M Calcium chloride dihydrate	0.1 M Na Acetate trihydrate pH 4.6	30% v/v 2-methyl-2,4 pentanediol
2	0.2 M Ammonium acetate	0.1 M Na Acetate trihydrate pH 4.6	30% w/v PEG 4000
3	0.2 M Ammonium sulphate	0.1 M Na acetate trihydrate pH 4.6	25% w/v PEG 4000
4	None	0.1 M Na acetate trihydrate pH 4.6	2.0 M Sodium formate
5	None	0.1 M Na acetate trihydrate pH 4.6	2.0 M Ammonium sulphate
6	None	0.1 M Na acetate trihydrate pH 4.6	8% w/v PEG 4000
7	0.2 M Ammonium acetate	0.1 M tri-sodium citrate dihydrate pH 5.6	30% w/v PEG 4000
8	0.2 M Ammonium acetate	0.1 M tri-sodium citrate dihydrate pH 5.6	30% v/v 2-methyl-2,4-pentanediol
9	None	0.1 M tri-Sodium citrate dihydrate pH 5.6	20% w/v 2-propanol, 20% w/v PEG 4000
10	None	0.1 M Na Citrate pH 5.6	1.0 M Ammonium dihydrogen phosphate
11	0.2 M Calcium chloride dihydrate	0.1 M Na acetate trihydrate pH 4.6	20% v/v 2-propanol
12	None	0.1 M Na Cacodylate pH 6.5	1.4 M Na acetate trihydrate
13	0.2 M tri-sodium citrate dihydrate	0.1 M Na Cacodylate pH 6.5	30% v/v 2-propanol
14	0.2 M Ammoniium sulphate	0.1 M Na Cacodylate pH 6.5	30% w/v PEG 8000
15	0.2 M Magnesium acetate tetrahydrate	0.1 M Na Cacodylate pH 6.5	20% PEG 8000
16	0.2 M Magnesium acetate tetrahydrate	0.1 M Na Cacodylate pH 6.5	30% v/v 2-methyl-2,4-pentanediol
17	None	0.1 M Imidazole pH 6.5	1.0 M Sodium acetate trihydrate
18	0.2 M Sodium acetate trihydrate	0.1 M Na Cacodylate pH 6.5	30% w/v PEG 8000
19	0.2 M Zinc acetate dihydrate	0.1 M Na Cacodylate pH 6.5	18% w/v PEG 8000
20	0.2 M Calcium acetate hydrate	0.1 M Na Cacodylate pH 6.5	18% w/v PEG 8000

21	0.2 M tri-sodium citrate dihydrate	0.1 M Na Hepes pH 7.5	30% v/v 2-methyl-2,4-pentanediol
22	0.2 M Magnesium chloride hexahydrate	0.1 M Na Hepes pH 7.5	30% v/v 2-propanol
23	0.2 M Calcium chloride dihydrate	0.1 M Na Hepes pH 7.5	28% v/v PEG 400
24	0.2 M Magnesium chloride hexahydrate	0.1 M Na Hepes pH 7.5	30% v/v PEG 400
25	0.2 M tri-sodium citrate dihydrate	0.1 M Na Hepes pH 7.5	20% v/v 2-propanol
26	None	0.1 M Na Hepes pH 7.5	0.8 M K, Na tartrate tetrahydrate
27	None	0.1 M Na Hepes pH 7.5	1.5 M Lithium sulphate monohydrate
28	None	0.1 M Na Hepes pH 7.5 0.8 M K dihydrogen phosphate monohyd.	0.8 M Na dihydrogen phosphate
29	None	0.1 M Na Hepes pH 7.5	1.4 M tri-Sodium citrate dihydrate
30	None	0.1 M Na Hepes pH 7.5	2% v/v PEG 400, 2.0 M Amm sulphate
31	None	0.1 M Na Hepes pH 7.5	10% v/v 2-propanol, 20% w/v PEG 4000
32	None	0.1 M Tris HCl pH 8.5	2.0 M Ammoniium sulphate
33	0.2 M Magnesium chloride hexahydrate	0.1 M Tris HCl pH 8.5	30% w/v PEG 4000
34	0.2 M tri-sodum citrate dihydrate	0.1 M Tris HCl pH 8.5	30% v/v PEG 400
35	0.2 M Lithium sulphate monohydrate	0.1 M Tris HCl pH 8.5	30% w/v PEG 4000
36	0.2 M Ammonium acetate	0.1 M Tris HCl pH 8.5	30% v/v 2-propanol
37	0.2 M Sodium acetate trihydrate	0.1 M Tris HCl pH 8.5	30% w/v PEG 4000
38	None	0.1 M Tris HCl pH 8.5	8% w/v PEG 8000
39	None	0.1 M Tris HCl pH 8.5	2.0 M Ammonium dihydrogen phosphate
40	None	None	0.4 M K, Na Tartrate tetrahydrate

41	None	None	0.4M Ammonium dihydrogen phosphate
42	0.2M Ammonium sulphate	None	30% w/v PEG 8000
43	0.2 M Ammonium sulphate	None	30% w/v PEG 4000
44	None	None	2.0 M Ammonium sulphate
45	None	None	4.0 M Sodium formate
46	0.05 M Potassium dihydrogen phosphate	None	20% w/v PEG 8000
47	None	None	30% w/v PEG 1500
48	None	None	0.2 M Magnesium formate
49	1.0 M Lithium sulphate monohydrate	None	2% w/v PEG 8000
50	0.5 M Lithium sulphate monohydrate	None	15% w/v PEG 8000

(B)   Structure Screen 2 - Catalogue Number MD1-02

1	0.1 M Sodium chloride	0.1 M Bicine pH 9.0	30% w/v PEG monomethylether 550
2	None	0.1 M Bicine pH 9.0	2.0 M Magnesium chloride hexahydrate
3	2% w/v Dioxane	0.1 M Bicine pH 9.0	10% w/v PEG 20,000
4	0.2 M Magnesium chloride hexahydrate	0.1 M Tris pH 8.5	3.4M 1,6 Hexanediol
5	None	0.1 M Tris pH 8.5	25% v/v tert-Butanol
6	0.01 M Nickel chloride hexahydrate	0.1 M Tris pH 8.5	1.0 M Lithium sulphate
7	1.5 M Ammonium sulphate	0.1 M Tris pH 8.5	12% v/v Glycerol
8	0.2 M Ammonium phosphate monobasic	0.1 M Tris pH 8.5	50% v/v MPD
9	None	0.1 M Tris pH 8.5	20% v/v Ethanol
10	0.01 M Nickel chloride hexahydrate	0.1 M Tris pH 8.5	20% w/v PEG monomethylether 2000
11	0.5 M Ammonium sulphate	0.1 M Hepes pH 7.5	30% v/v MPD
12	None	0.1 M Hepes pH 7.5	10% w/v PEG 6000, 5% v/v MPD
13	None	0.1 M Hepes pH 7.5	20% v/v Jeffamine M-600
14	0.1 M Sodium chloride	0.1 M Hepes pH 7.5	1.6 M Ammonium sulphate
15	None	0.1 M Hepes pH 7.5	2.0 M Ammonium formate
16	0.05 M Cadmium sulphate octahydrate	0.1 M Hepes pH 7.5	1.0 M Sodium acetate
17	None	0.1 M Hepes pH 7.5	70% v/v MPD
18	None	0.1 M Hepes pH 7.5	4.3 M Sodium chloride
19	None	0.1 M Hepes pH 7.5	10% w/v PEG 8000

8% v/v Ethylene glycol

20	None	0.1 M Mes pH 6.5	1.6 M Magnesium sulphate heptahydrate
21	0.1 M Na phosphate monobasic 0.1 M K phosphate monobasic	0.1 M Mes pH 6.5	2.0 M Sodium Chloride
22	None	0.1 M Mes pH 6.5	12% w/v PEG 20,000
23	1.6 M Ammonium sulphate	0.1 M Mes pH 6.5	10% v/v Dioxane
24	0.05 M Cesium chloride	0.1 M Mes pH 6.5	30% v/v Jeffamine M-600
25	0.01 M Cobalt chloride hexahydrate	0.1 M Mes pH 6.5	1.8 M Ammonium sulphate
26	0.2 M Ammonium sulphate	0.1 M Mes pH 6.5	30% w/v PEG monomethylether 5000
27	0.01 M Zinc sulphate heptahydrate	0.1 M Mes pH 6.5	25% v/v PEG monomethylether 550
28	None	0.1 M Hepes pH 7.5	20% w/v PEG 10,000
29	0.2 M K/Na Tartrate	0.1 M Sodium citrate pH 5.6	2.0 M Ammonium sulphate
30	0.5 M Ammonium sulphate	0.1 M Sodium citrate pH 5.6	1.0 M Lithium sulphate
31	0.5 M Sodium chloride	0.1 M Sodium citrate pH 5.6	4% v/v polyethyleneimine
32	None	0.1 M Sodium citrate pH 5.6	35% v/v tert-butanol
33	0.01 M Ferric chloride hexahydrate	0.1 M Sodium citrate pH 5.6	10% v/v Jeffamine M-600
34	0.01 M Manganese chloride tetrahydrate	0.1 M Sodium citrate pH 5.6	2.5 M 1,6 Hexanediol
35	None	0.1 M Sodium acetate pH 4.6	2.0 M Sodium chloride
36	0.2 M Sodium Chloride	0.1 M Sodium acetate pH 4.6	30% v/v MPD
37	0.01 M Cobalt Chloride hexahydrate	0.1 M Sodium acetate pH 4.6	1.0 M 1,6 Hexanediol
38	0.1 M Cadmium chloride	0.1 M Sodium acetate pH 4.6	30% v/v PEG 400
39	0.2 M Ammonium sulphate	0.1 M Sodium acetate pH 4.6	30% w/v PEG monomethylether 2000
40	2.0 M Sodium Chloride	None	10% w/v PEG 6000

41	0.01 M Cetyl trimethyl ammoniumbromide	None	0.5 M Sodium chloride 0.1 M Magnesium chloride hexahydrate
42	None	None	25% v/v Ethylene glycol
43	None	None	35% v/v Dioxane
44	2.0 M Ammonium Sulphate	None	5% v/v Isopropanol
45	None	None	1.0 M Imidazole pH 7.0
46	None	None	10% w/v PEG 1000, 10% w/v PEG 8000
47	1.5 M Sodium Chloride	None	10% v/v Ethanol
48	None	None	1.6 M Sodium citrate pH 6.5
49	15% w/v Polyvinylpyrolidone		
50	2.0 M Urea;		

Publications

Autocatalytic Formation of a Covalent Link between Tryptophan 41 and the Heme in Ascorbate Peroxidase[†]

Zoi Pipirou,[‡] Andrew R. Bottrill,[§] Clive M. Metcalfe,[‡] Sharad C. Mistry,[§] Sandip K. Badyal,[‡]
Bernard J. Rawlings,[‡] and Emma Lloyd Raven*,[‡]

*Department of Chemistry, University of Leicester, University Road, Leicester LE1 7RH, England, and Protein and Nucleic Acid
Chemistry Laboratory, Hodgkin Building, University of Leicester, Lancaster Road, Leicester LE1 9HN, U.K.*

Received November 3, 2006; Revised Manuscript Received December 13, 2006

ABSTRACT: Electronic spectroscopy, HPLC analyses, and mass spectrometry (MALDI-TOF and MS/MS) have been used to show that a covalent link from the heme to the distal Trp41 can occur on exposure of ascorbate peroxidase (APX) to H_2O_2 under noncatalytic conditions. Parallel analyses with the W41A variant and with APX reconstituted with deuteroheme clearly indicate that the covalent link does not form in the absence of either Trp41 or the heme vinyl groups. The presence of substrate also precludes formation of the link. Formation of a protein radical at Trp41 is implicated, in a reaction mechanism that is analogous to that proposed [Ghiladi, R. A., et al. (2005) *Biochemistry 44*, 15093−15105] for formation of a covalent Trp-Tyr-Met link in the closely related catalase peroxidase (KatG) enzymes. Collectively, the data suggest that radical formation at the distal tryptophan position is not an exclusive feature of the KatG enzymes and may be used more widely across other members of the class I heme peroxidase family.

The three most prominent members of the class I super-family of heme peroxidases (*1*) are cytochrome *c* peroxidase (C*c*P),[1] ascorbate peroxidase (APX), and the bifunctional catalase−peroxidase (KatG) enzymes. These class I enzymes are distinguished from other peroxidases in the superfamily by the presence of a distal tryptophan residue, in place of the more usual phenylalanine residue, and a second active site tryptophan adjacent to the proximal histidine ligand (Figure 1). The catalase−peroxidases contain a unique structural feature, however, that distinguishes them from all other heme peroxidases: in all catalase−peroxidase enzymes for which crystal structures have appeared (*2−4*), a co-valently bound Trp-Tyr-Met cross-link (involving Trp107, Tyr229, and Met255 in the *Mycobacterium tuberculosis* KatG enzyme, Figure 1a) has been observed. The formation of the Trp-Tyr-Met link is therefore believed to be a feature of all KatGs and is proposed (*5, 6*) to be formed through an autocatalytic mechanism involving reaction with H_2O_2. Trp and Tyr residues are essential for complete formation of the link, but replacement of Met is tolerated if both Tyr and Trp are present (*5−7*). The functional role of this covalent link is not clearly established, but the fact that it is not observed in the monofunctional peroxidases (APX and C*c*P,

Figure 1b,c) suggests that it might be connected with catalatic activity in KatGs. Mutagenesis data support this suggestion (*7−11*).

The proposed mechanism (*5, 6*) of formation of the Trp-Tyr-Met link involves initial reaction with peroxide to form a Compound I intermediate (containing a ferryl heme and a porphyrin π-cation radical). This is followed by oxidation of both Trp107 and Tyr229 (numbering according to Figure 1a) by Compound I to form protein radicals at both residues. Radical cross-linking reactions then occur to form the Trp-Tyr link. A second cycle of reaction with H_2O_2 is then proposed for formation of the Tyr-Met link. A key feature is the proposed formation of a protein radical at the distal Trp residue, in a mechanism that can be considered as analogous to the oxidation of the proximal Trp191 residue in Compound I of C*c*P. At present, however, it is not clear whether other, related heme proteins are able to support oxidation of the distal Trp residue.

In this paper, we present the first direct evidence to demonstrate that covalent linking of Trp41 to the heme group in ascorbate peroxidase can occur on exposure of the enzyme to peroxide. A reaction mechanism involving formation of a protein radical at Trp41 is implicated to account for this observation. Together, the data suggest that radical formation at the distal tryptophan position is not an exclusive feature of the KatG enzymes and may be used more widely in other, related peroxidases.

EXPERIMENTAL PROCEDURES

Materials. L-Ascorbic acid (Aldrich Chemical Co.) and all buffers (Fisher) were of the highest analytical grade (99%+ purity) and were used without further purification. Sinapinic acid and α-cyano-4-hydroxycinnamic acid were purchased from Fluka. Water was purified by an Elga purelab

* To whom correspondence should be addressed. Telephone: +44 (0)116 229 7047. Fax: +44 (0)116 252 2789. E-mail: emma.raven@le.ac.uk.
‡ Department of Chemistry, University of Leicester
§ Protein and Nucleic Acid Chemistry Laboratory, University of Leicester.
¹ Abbreviations: APX, ascorbate peroxidase; rsAPX, recombinant soybean cytosolic ascorbate peroxidase; C*c*P, cytochrome *c* peroxidase; KatG, catalase−peroxidase; mtKatG, *Mycobacterium tuberculosis* catalase−peroxidase.
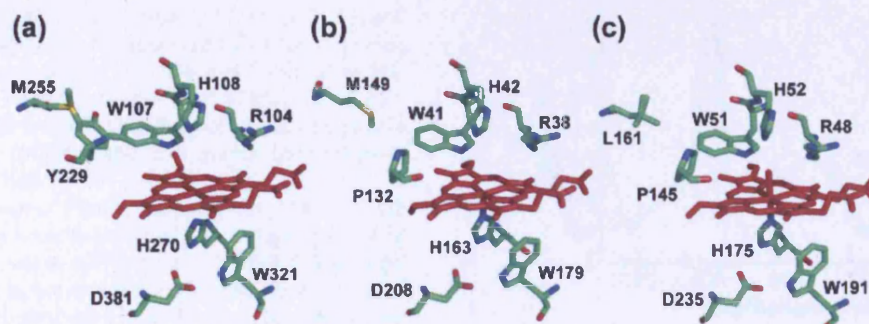
FIGURE 1: Comparison of active site structures of (a) mtKatG (PDB accession code 1SJ2), (b) rsAPX (1OAG), and (c) CcP (2CYP) showing the covalent links between residues W107, Y229, and M255 in mtKatG and the residues occupying the equivalent positions in rsAPX and CcP.

purification system, and all buffers were filtered (0.2 μm) prior to use. Hydrogen peroxide solutions were freshly prepared by dilution of a 30% (v/v) solution (BDH); exact concentrations were determined using the published absorption coefficient ($\epsilon_{240} = 39.4$ M^{-1} cm^{-1}) (*12*). All molecular biology kits and enzymes were used according to manufacturer's protocols.

Mutagenesis, Protein Expression, and Purification. Site-directed mutagenesis on recombinant soybean cytosolic APX (rsAPX) was performed according to the QuikChange protocol (Stratagene Ltd., Cambridge, U.K.). The sequence of the W41A variant was confirmed by DNA sequencing as reported previously (*13*). Bacterial fermentation of cells and purification of rsAPX and W41A were carried out according to published procedures (*13, 14*). Purified samples of rsAPX and W41A showed wavelength maxima at 407 (107), 525, and ≈630 nm and 405 (125), 525, and ≈630 nm, respectively, as reported previously (*13, 15*). Enzyme concentrations for rsAPX and W41A were determined using absorption coefficients of $\epsilon_{407} = 107$ mM^{-1} cm^{-1} (*15*) and $\epsilon_{405} = 125$ mM^{-1} cm^{-1} (*13*), respectively. Cytochrome *c* peroxidase was expressed according to published procedures (*16*). The CcP expression construct was a kind gift from Professor Grant Mauk (University of British Columbia). Purified enzyme showed wavelength maxima at 409 (95), 504, and 529[sh] nm (150 mM potassium phosphate, pH 6). Enzyme concentrations for CcP were determined using an absorption coefficient of $\epsilon_{409} = 95$ mM^{-1} cm^{-1}.

Electronic Absorption Spectroscopy. Spectra were collected using a Perkin-Elmer Lambda 35 or 40 spectrophotometer, linked to a PC workstation running UV-Winlab software. Pyridine−hemochromagen assays before and after reaction of the enzyme with H$_2$O$_2$ were carried out according to established protocols (*17*). The pyridine−hemochromagen experiment proceeds as follows: a solution of protein is mixed with a solution of pyridine in NaOH. Oxidized pyridine−hemochromagen, which is a soluble and stable compound, is formed rapidly. The spectrum between 600 and 500 nm is recorded just after addition of solid sodium dithionite, which yields the relatively unstable reduced pyridine−hemochromagen.

Steady-State Kinetics. Steady-state measurements (100 mM potassium phosphate, pH 7.0, 25 °C) for oxidation of ascorbate were carried out according to published protocols (*18*).

Reconstitution of rsAPX with Iron(III) Deuteroporphyrin IX Chloride. Apoenzyme was initially prepared by the method of Teale (*19*). Iron(III) deuteroporphyrin IX chloride (>97%; Porphyrin Products, Frontier Scientific Inc.) was dissolved in 0.1 M potassium hydroxide (1 mg/mL) which was added dropwise to the apoenzyme, with stirring on ice, until an Rz value of >2 was reached. The solution was incubated on ice for another 30 min. An additional amount of iron(III) deuteroporphyrin IX chloride solution was added, and the solution was further incubated on ice for another 15 min. This solution was dialyzed against potassium phosphate (20 mM, pH 7.0) overnight at 4 °C. The protein solution, which showed wavelength maxima at 402, 521, 557[sh], and 625 nm, was concentrated and exchanged in water. Any precipitated protein or excess heme was removed by centrifugation (13000 rpm, 5 min).

High-Performance Liquid Chromatography. HPLC analyses of protein samples before and after reaction with H$_2$O$_2$ were conducted on a Varian ProStar HPLC system with an analytical Vydac C4 reverse-phase HPLC column under computer control. Solvents were as follows: A = 0.1% (w/v) trifluoroacetic acid (TFA) in 95% H$_2$O and 5% acetonitrile; B = 0.1% (w/v) TFA in 80% acetonitrile and 20% H$_2$O. The column was preequilibrated with 42% buffer B, and protein/heme separation was achieved using the following elution gradient: 42% B for 5 min, 42−55% B for 25 min, 55−100% B for 10 min, and 100% B for 5 min. Chromatograms were monitored at 215 nm for protein-containing fractions and 398 nm for heme-containing fractions.

For separation and collection of fragments, an Agilent Series 1100 binary pump HPLC system was used, fitted with a diode array detector. For collection of the hydroxylated heme species, protein samples, after reaction with H$_2$O$_2$, were injected onto a Phenomenex JUPITER 5u C4 300A column (250 × 2 mm); fractions eluting at 4 min were collected, freeze-dried, and resuspended in 200 μL of H$_2$O to be used for MALDI-TOF mass spectrometry.

Samples for trypsin digestion were treated with 50:1 (w/w) enzyme:trypsin in 0.4 M NH$_4$HCO$_3$, pH 8, at 37 °C for 18 h. The digestion was stopped by addition of TFA (1 μL). The digested mixture was then injected onto a reverse-phase C8 column (P. E. BrownLee Columns Aquapore Octyl, RP-300 C8 7 μm, 220 × 2.1 mm). Solvents were as follows: A = 0.1% (w/v) TFA in 95% H$_2$O and 5% acetonitrile; B =

0.1% (w/v) TFA in 80% acetonitrile and 20% H_2O. Separation of peptide fragments was achieved using the following elution gradient: $t = 0$ min, B = 2%; $t = 2$ min, B = 2%; $t = 45$ min, B = 75%; $t = 50$ min, B = 100%; $t = 55$ min, B = 100%. Peptide fractions showing both heme and protein absorbances were collected and then evaporated to dryness and dissolved in H_2O.

Mass Spectrometry. Protein samples for MALDI-TOF mass spectrometry were exhaustively exchanged into 0.4 M NH_4HCO_3, pH 8, using a Millipore Centricon (Centrifugal Filter Devices) ultrafiltration device (molecular mass cutoff 10 kDa) and by centrifugation at 3000g. The sample was then diluted 1:1 or 1:50 (depending on sample concentration) with matrix (sinapinic acid, 10 mg/mL, and 0.1% TFA in 1:1 acetonitrile/H_2O). Analysis was carried out as follows: 1 μL of the protein/matrix mixture was spotted onto a MALDI target plate using the drying droplet method. The MALDI-TOF mass spectrometer was calibrated in the range 2000–45000 Da using horse heart myoglobin. Spectra were an average of 1000 shots.

Peptide samples (1 μL) were mixed with matrix (α-cyano-4-hydroxycinnamic acid, 5 mg/mL, and 0.1% TFA in 1:1 acetonitrile/H_2O) for MALDI-TOF mass spectrometry. For these experiments, the MALDI-TOF mass spectrometer was calibrated in the range 500–6000 Da with a peptide mass calibration kit (Sigma; used according to manufacturer's instructions). Spectra of the HPLC-purified peptide fragments were collected in the same mass range using an average of 250 laser shots. All MALDI-TOF spectra were analyzed using Data Viewer software (Applied Biosystems).

MS/MS Analyses. HPLC-purified samples of peptide fragments prepared as above were resuspended in water (100 μL). The solution was then mixed in a 1:1 ratio with acetonitrile/0.2% formic acid and infused from a syringe pump (Harvard Apparatus Ltd., Edenbridge, Kent, U.K.) at a flow rate of 0.5 μL/min to the MicroIonspray source of a 4000 Q-Trap mass spectrometer (Applied Biosystems, Warrington, U.K.). The sample was sprayed directly from a fused-silica PicoTip (New Objective Inc., Woburn, MA) maintained at a potential of 2800 V in the positive ion mode. Tandem mass spectrometry was carried out for ions of interest. Spectra of fragment ions were interpreted manually.

RESULTS

Reaction of rsAPX with Hydrogen Peroxide and Characterization of Products. Reaction of rsAPX with 6 equiv of H_2O_2 resulted in the initial formation of a Compound I intermediate, as observed previously (*18*) (data not shown). This is followed by immediate conversion of this Compound I to a more stable Compound II species (Figure 2). Compound II then decays over a period of ≈8 h to a final product that has a spectrum that is similar but not identical to that of rsAPX (Figure 2). The activity of rsAPX against ascorbic acid was monitored before and after reaction with H_2O_2 under the conditions described above. Values for k_{cat} after reaction with H_2O_2 were essentially unchanged from those of the wild-type enzyme (*18*).

A pyridine–hemochromagen assay was carried out on rsAPX both before and after reaction with H_2O_2. For rsAPX before treatment with H_2O_2, the spectrum of the reduced pyridine–hemochromagen complex obtained in this way
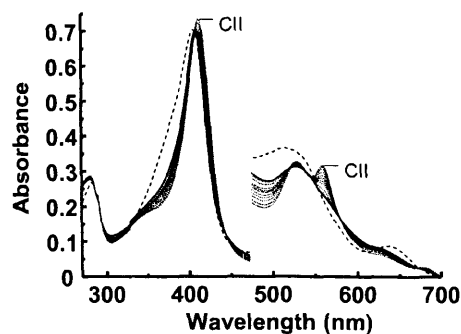

FIGURE 2: Selected electronic spectra collected during the reaction of ferric rsAPX with 6 equiv of H_2O_2. Conversion of rsAPX (dashed line) to the initial Compound II intermediate (indicated as CII on the figure) is observed, followed by conversion back to a ferric-like species (solid line). Intermediate spectra between Compound II and ferric-like are shown as dotted lines. The total reaction time was 8 h. The visible region has been multiplied by a factor of 5. Sample conditions: enzyme, 5 μM; hydrogen peroxide, 30 μM; 0.1 M potassium phosphate, pH 7.0; 25 °C.
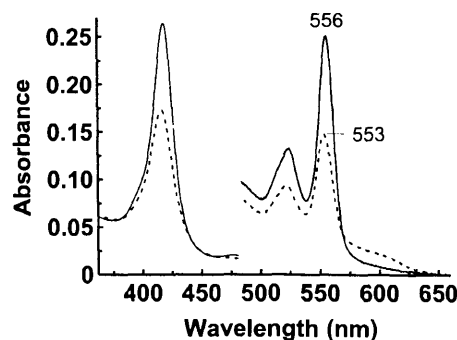

FIGURE 3: Spectra of the reduced pyridine–hemochromagen complexes of rsAPX before (solid line) and after (dashed line) reaction with H_2O_2.

showed a maximum at 556 nm (Figure 3). In this experiment, complete extraction of the heme from the protein is observed, and the spectrum of the hemochromagen complex is consistent with a noncovalently bound heme structure, in which neither heme vinyl group is modified (*17*). When the same experiment was carried out with rsAPX after treatment with H_2O_2, the peak was shifted to 553 nm (Figure 3). These spectroscopic changes are diagnostic of the covalent attachment to one of the two vinyl groups on the heme (*20*).

HPLC Analyses. HPLC analysis of the product of the reaction of rsAPX with H_2O_2 (prepared as above) showed that the protein (monitored at 215 nm) and a significant proportion of the heme (monitored at 398 nm) coelute at 24 min (Figure 4b); this is in direct contrast to the HPLC profile of rsAPX which has not been treated with H_2O_2, in which the heme (11 min) and the protein (24 min) do not coelute (Figure 4a). Coelution of the heme and the protein fragments is a clear indication of covalent heme attachment and has been used previously to identify covalently linked heme in various other heme proteins (*14, 21–25*). In separate experiments (data not shown), a commercial sample of hemin eluted at 11 min, confirming the assignment for free heme above. For the sample of rsAPX treated with H_2O_2, there is a second peak that elutes earlier (4 min) than free heme
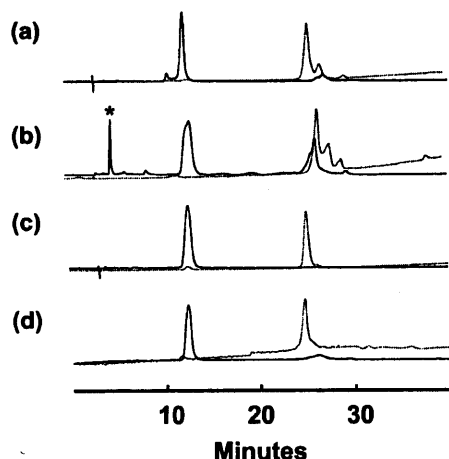
FIGURE 4: HPLC analyses of rsAPX and W41A before and after reaction with H_2O_2 monitored at 398 nm (solid line) and 215 nm (dotted line). (a) rsAPX before reaction with H_2O_2; (b) rsAPX after reaction with H_2O_2; (c) W41A before reaction with H_2O_2; (d) W41A after reaction with H_2O_2.

(labeled with an asterisk in Figure 4b). This is indicative of a hydroxylated heme product (*21*), and a similar assignment is proposed here. MALDI-TOF analysis of this heme fragment confirmed this assignment: a mass of 650 Da was observed (data not shown), which is consistent with a doubly hydroxylated heme species. Nonspecific hydroxylation of heme groups has been reported in other peroxidase systems (*23, 26*).

In separate experiments (data not shown) with rsAPX under the same conditions as those used above for Figure 4b but in the presence of a large excess of ascorbate, it was shown that no HPLC peak corresponding to protein-bound heme was observed at ≈24 min. This indicates that under turnover conditions no formation of covalently bound heme occurs.

Mass Spectrometric Analyses. Mass spectrometry data are consistent with the HPLC analyses above and provided further evidence for partial covalent attachment of the heme to the protein. MALDI-TOF analysis of rsAPX before treatment with H_2O_2 (Figure 5a) showed a mass of 28312.0 Da, which corresponds closely to the predicted mass (28318.9 Da) of the apoprotein and is consistent with noncovalent attachment of the heme to the protein in rsAPX. After treatment with H_2O_2, two peaks were observed in the MALDI-TOF spectrum (Figure 5b). The first is at 28320.6 Da, which is consistent with the mass of the apoprotein (as above). The second peak is at 28954.3 Da, which corresponds to an increase in mass of 634 Da over the apoprotein, and is consistent with covalent attachment of the heme (616 Da) to the protein. The additional mass of 18 amu is assigned as arising from hydroxylation of the fragment.

To establish the nature of the heme—protein covalent link, tryptic digestion of the product of the reaction of rsAPX with H_2O_2 was carried out, and HPLC was used to isolate heme-containing peptide fragments (i.e., showing both heme and protein absorbances) from the resulting peptide mixture (data not shown).[2] The mass of 1863.9 Da observed for this fragment (Figure 5c) is 16 Da higher than the calculated mass of 1848 Da expected for the L[39]AW[41]HSAGTFDK[49] peptide fragment containing heme covalently bound to Trp41.

MS/MS mass spectrometry was used to obtain sequence information for this heme-containing fragment. In this case, a *y*-ion fragmentation series allowed amino acids to be identified sequentially from His42 through to Thr46 with the remaining C-terminal mass (409.1 Da) consistent with residues Phe47 through to Lys49, which corresponds to the sequence HSAGTFDK (Figure 6). The remaining N-terminal mass, together with the absence of fragment ions for the amino acids (LAW[41]), indicates that the heme forms a covalent cross-link with this part of the peptide. Since Leu and Ala are unlikely to be able to form a covalent cross-link to the heme, the data are interpreted as being consistent with the formation of a covalent link from the heme to Trp41.

Experiments with Iron(III) Deuteroporphyrin. To provide further information on the nature of the covalent attachment, a sample of apo-rsAPX was reconstituted with iron(III) deuteroporphyrin, in which hydrogen atoms replace the 2- and 4-vinyl groups, and subsequently reacted with H_2O_2 as above. No peak corresponding to covalently bound heme was observed by HPLC, because heme was released from the protein and eluted at 5 min both before (Figure S1a in the Supporting information) and after (Figure S1b in the Supporting Information) reaction with H_2O_2. A commercial sample of deuteroheme was also shown to elute at 5 min (data not shown).

Examination of the W41A Variant. Further experiments were carried out with the W41A variant, which has been previously shown (*13*) to be catalytically competent for reaction with H_2O_2 and substrate oxidation. Hence, the W41A variant was reacted with H_2O_2 under the same conditions as those used for rsAPX (*vide supra*), and the corresponding HPLC and MALDI-TOF analyses were carried out. HPLC analysis prior to treatment with H_2O_2 (Figure 4c) showed that the heme and the protein elute separately as for rsAPX under the same conditions. However, on treatment with H_2O_2 no change in the HPLC elution profile was observed, indicating that no covalent attachment of the heme to the protein had occurred in this case (Figure 4d). In addition, and in contrast to rsAPX, there is no evidence for formation of a hydroxylated heme species in the HPLC analyses.

MALDI-TOF analyses (Figure S2 in the Supporting Information) confirmed these observations since essentially identical molecular masses are observed for W41A before (28207.1 Da) and after (28202.5 Da) treatment with H_2O_2. Both of these values are in good agreement with the calculated mass for the apo-W41A variant (28203.7 Da).[3]

Examination of CcP. In order to examine whether CcP exhibits similar behavior to rsAPX when treated with hydrogen peroxide, HPLC analysis was carried out before (Figure S1c in the Supporting Information) and after (Figure S1d in the Supporting Information) treatment of CcP with hydrogen peroxide under the same conditions as those used for rsAPX above. No evidence for formation of a covalent link between the heme and the protein was observed in this case.

---

[2] There were three peaks with significant absorbance at 398 nm. The MALDI-TOF mass spectrum of the product eluting at 35.1 min gave a mass of 616 Da, indicating that this HPLC peak corresponds to free heme species. MALDI-TOF mass spectrometry of the peptide fragments eluting at 26.4 and 27.5 min both gave spectra with identical masses of 1863.9 Da, indicating that both HPLC peaks are assigned to a single peptide (Figure 5c).

[3] A minor peak at 27488.2 Da is also observed, which may arise from nonspecific cleavage of the protein.
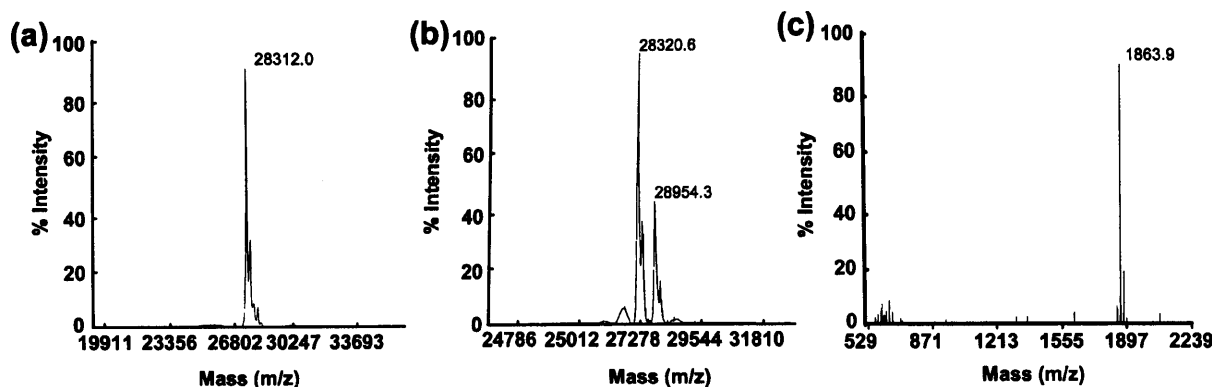
FIGURE 5: MALDI-TOF mass spectrum of rsAPX before (a) and after (b) reaction with 6 equiv of H_2O_2. (c) MALDI-TOF mass spectrum of the HPLC-purified heme-containing peptide fragment obtained after reaction of rsAPX with H_2O_2.
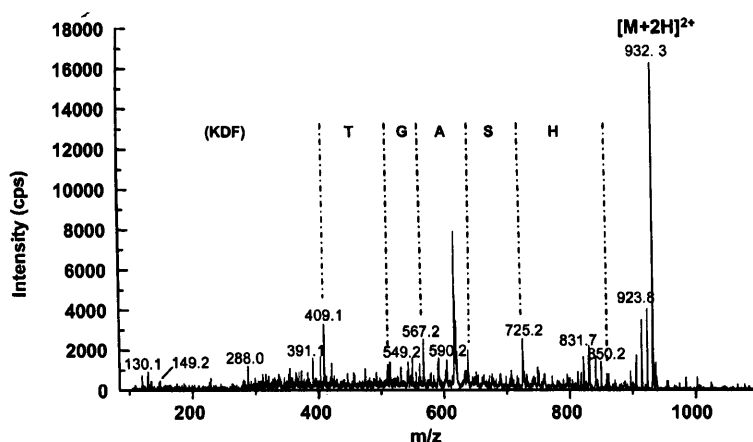

FIGURE 6: MS/MS spectrum of the HPLC-purified heme-containing peptide fragment showing the doubly charged precursor ion (932.56 Da). The annotated peptide sequence corresponds to the *y*-ion fragment series.

DISCUSSION

In the mammalian heme peroxidases, it is known that different types of covalent link from protein amino acids to the heme group are used (*27*). Although covalently bound heme groups are not observed in other peroxidases, there is an increasing amount of evidence to show that these links can be engineered into an existing peroxidase framework if the correct residue is inserted at the correct site and if the peroxidase in question is competent for reaction with H_2O_2 (see, for example, refs *14* and *23*). This represents a substantial change in the way we think about these modified peroxidases: collectively, what it tells us is that there is no intrinsic reason why any peroxidase, or any heme protein for that matter, cannot form a particular covalent link under the right conditions. *In extremis*, this might even mean that some proteins may need to be poised in an environment that specifically "switches off" these covalent links. Collectively, and in view of the very similar active site structures of the class I peroxidase enzymes, these ideas indicated to us that the same principle may apply to the covalent Trp-Tyr-Met link in KatG (at least in the class I enzymes). More specifically, the mechanisms that lead to formation of the Trp-Tyr-Met link in KatG might also be accessible under certain conditions in other class I peroxidases.

The mechanism of formation of the Trp-Tyr-Met link in KatG is proposed to involve initial formation of both Trp

and Tyr radicals through a normal oxidative peroxidase mechanism (*5*, *6*). Although both C*c*P and APX contain a distal Trp residue in an essentially identical structural environment to that observed in KatG (Figure 1), the Trp-Tyr-Met link is not observed in either of these enzymes because the active site Tyr residue is missing in APX (Figure 1b) and because both Tyr and Met are missing in C*c*P (Figure 1c). In this paper, we have presented evidence from electronic spectroscopy, HPLC analyses, and mass spectrometry to show that under noncatalytic conditions (*i.e.* in the absence of substrate) and over long time scales a covalent link from the heme to the Trp41 can be formed in APX. This link does not form in the presence of substrate (ascorbate). Experiments with the W41A variant and with deuteroheme clearly indicate that the covalent link does not form in the absence of either Trp41 or the heme vinyl groups.

A possible mechanism for formation of the covalently bound heme species that embodies all of the available data is presented in Scheme 1. In this mechanism, initial formation of a Compound I intermediate (step i)[4] is followed by oxidation and deprotonation of Trp41 (step ii) and addition of the Trp41 radical across the 4-vinyl group of the heme

---

[4] We assume that formation of the link is not dependent on the exact nature of the oxidant and that any other oxidant that is capable of oxidizing the heme to Compound I (for example, peracetic acid) would also lead to a covalently bound heme.

Scheme 1: Proposed Mechanism for Formation of a Covalent Link between Trp41 and the Heme Group in Ascorbate Peroxidase[a]
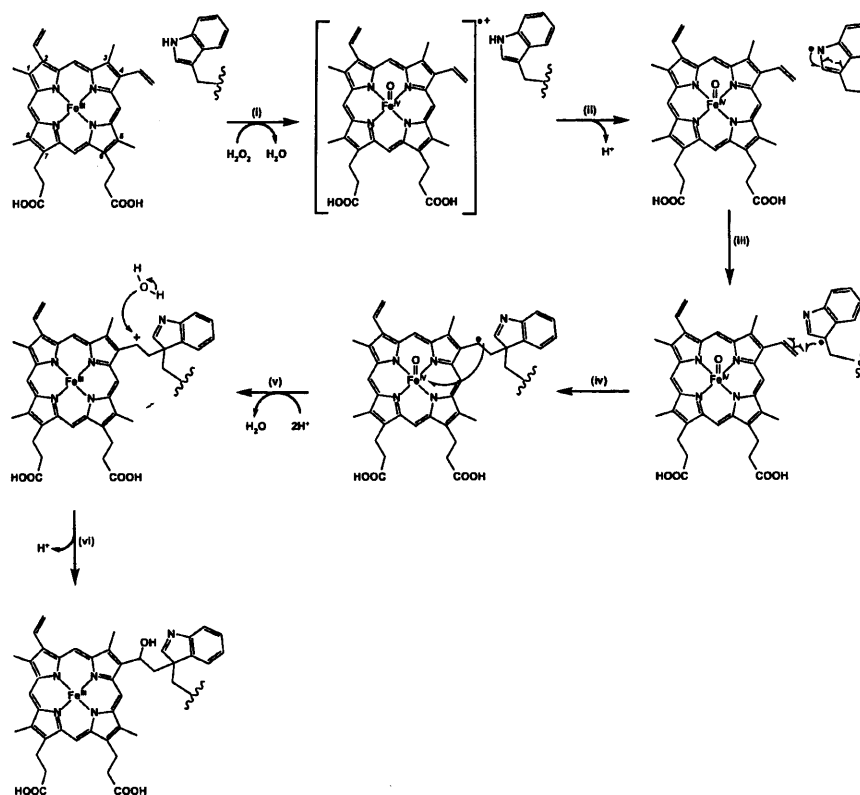
[a] Steps i—vi are described in the text.

(steps iii[5] and iv). Subsequent reduction of the ferryl group and release of H_2O (step v) lead to formation of a carbocation. Nucleophilic addition of H_2O as the final step (step vi) gives a heme structure that is consistent with the mass spectrometry data. The shortest distance from the C^β on the 4-vinyl group to the C^γ of Trp41 is 4.8 Å. We note that hydroxylation of a covalently bound heme fragment has also been observed previously (*14*). Further evidence in support of this mechanism comes from previous work in which formation of a protein-based radical, proposed to be a Trp radical, on reaction of APX with H_2O_2 in the absence of substrate has been reported (*28*).

The data for CcP are curious because no evidence for formation of an analogous link to Trp51 was observed. CcP is unique among the class I peroxidases in that it utilizes a protein amino acid, Trp191, during its catalytic cycle. Hence, the enzyme diverts oxidizing equivalents to Trp191 as the immediate product of H_2O_2 oxidation without formation of a porphyrin π-cation radical. Diversion of the radical to Trp191 would preclude formation of a radical at Trp51 according to the mechanism proposed in Scheme 1. Interestingly, there is separate evidence that formation of a radical on Trp51 in CcP may occur under certain conditions (*29*). Hence, Poulos and co-workers have shown that peroxide-dependent formation of a Trp51-Tyr52 link occurs in the

H52Y variant of CcP and the formation of this link is proposed to involve oxidation of Trp51 to Trp• and oxidation of Tyr52 to Tyr• in a mechanism that is analogous to that proposed for KatG (*5, 6*) (i.e., without formation of the expected Compound I species, with a radical on Trp191).

In summary, these data add a new dimension to our wider understanding of the differences between the KatG enzymes and the monofunctional peroxidase enzymes. The data indicate that, under noncatalytic conditions, there is no intrinsic barrier to formation of a radical at Trp41 in APX analogous to that thought to be used in the KatGs. The direct implication is that formation of a covalent Trp-Tyr-Met link in APX is limited not by the inherent reactivity of the enzyme but by the absence of a tyrosine residue adjacent to Trp41.

A separate question arises, however: how do the KatG enzymes protect their heme groups from modification by Trp? Clearly, the presence of the relevant amino acids close to the distal Trp is essential, but other, more subtle, effects are likely to also be important. For example, very slight differences in the precise orientation of key amino acids may well be critical in defining whether a particular covalent link is formed. As a case in point we note that a covalent link between an engineered methionine residue at position 160 (S160M variant) and the heme, analogous to those found in the mammalian peroxidases, can be incorporated into the APX framework but that cytochrome *c* peroxidase, which already contains a Met residue at this position (Met172), does not form the same covalent heme-Met link under any accessible conditions.

---

[5] We have proposed a radical on C^γ on the basis that this will be more stable (tertiary radical) and because a radical on this carbon retains the aromatic ring structure of Trp41 compared to the other resonance forms.

SUPPORTING INFORMATION AVAILABLE

HPLC analysis of rsAPX reconstituted with iron(III) deuteroporphyrin before (Figure S1a) and after (Figure S1b) reaction with H_2O_2 and of CcP before (Figure S1c) and after (Figure S1d) reaction with H_2O_2 and MALDI-TOF mass spectrum of W41A before (Figure S2a) and after (Figure S2b) reaction with 6 equiv of H_2O_2. This material is available free of charge via the Internet at http://pubs.acs.org.

REFERENCES

1. Welinder, K. G. (1992) Superfamily of plant, fungal and bacterial peroxidases, *Curr. Opin. Chem. Biol. 2*, 388−393.
2. Bertrand, T., Eady, N. A. J., Jones, J. N., Bodiguel, J., Jesmin, Nagy, J. M., Raven, E. L., Jamart-Gregoire, B., and Brown, K. H. (2004) Crystal structure of *Mycobacterium tuberculosis* catalase−peroxidase, *J. Biol. Chem. 279*, 38991−38999.
3. Carpena, X., Loprasert, S., Mongkolsuk, S., Switala, J., Loewen, P. C., and Fita, I. (2003) Catalase−peroxidase KatG of *Burkholderia pseudomallei* at 1.7 Å resolution, *J. Mol. Biol. 327*, 475−489.
4. Yamada, Y., Fujiwara, T., Sato, T., Igarashi, N., and Tanaka, N. (2002) The 2.0 angstrom crystal structure of catalase−peroxidase from *Haloarcula marismortui*, *Nat. Struct. Biol. 9*, 691−695.
5. Ghiladi, R. A., Knudsen, G. M., Medzihradszky, K. F., and Ortiz de Montellano, P. R. (2005) The Met-Tyr-Trp cross link in *Mycobacterium tuberculosis* catalase peroxidase, *J. Biol. Chem. 280*, 22651−22663.
6. Ghiladi, R. A., Medzihradszky, K. F., and Ortiz de Montellano, P. R. (2005) Role of the Met-Tyr-Trp cross link in *Mycobacterium tuberculosis* catalase peroxidase (KatG) as revealed by KatG-(M255I), *Biochemistry 44*, 15093−15105.
7. Jakopitsch, C., Kolarich, D., Petutschnig, G., Furtmuller, P. G., and Obinger, C. (2003) Distal side tryptophan, tyrosine and methionine in catalase−peroxidases are covalently linked in solution, *FEBS Lett. 552*, 135−140.
8. Regelsberger, G., Jakopitsch, C., Ruker, F., Krois, D., Peschek, G. A., and Obinger, C. (2000) Effect of distal cavity mutations on the formation of Compound I in catalase−peroxidases, *J. Biol. Chem. 275*, 22854−22861.
9. Jakopitsch, C., Ivancich, A., Schmuckenschlager, F., Wanasinghe, A., Poltl, G., Furtmuller, P. G., Ruker, F., and Obinger, C. (2004) Influence of the unusual covalent adduct on the kinetics and formation of radical intermediates in Synechocytic catalase peroxidase, *J. Biol. Chem. 279*, 46082−46095.
10. Jakopitsch, C., Auer, M., Ivancich, A., Ruker, F., Furtmuller, P. G., and Obinger, C. (2003) Total conversion of bifunctional catalase−peroxidase (KatG) to monofunctional peroxidase by exchange of a conserved distal side tyrosine, *J. Biol. Chem. 278*, 20185−20191.
11. Hillar, A., Peters, B., Pauls, R., Loboda, A., Zhang, H., Mauk, A. G., and Loewen, P. C. (2000) Modulation of the activities of catalase−peroxidase HPI of *Escherichia coli* by site-directed mutagenesis, *Biochemistry 39*, 5868−5875.
12. Nelson, D. P., and Kiesow, L. A. (1972) Enthalpy of decomposition of hydrogen peroxide by catalase at 25 °C (with molar extinction coefficients of H_2O_2 solutions in the UV), *Anal. Biochem. 49*, 474−478.
13. Badyal, S. K., Joyce, M. G., Sharp, K. H., Seward, H. E., Mewies, M., Basran, J., Macdonald, I. K., Moody, P. C. E., and Raven, E. L. (2006) Conformational mobility in the active site of a heme peroxidase, *J. Biol. Chem. 281*, 24512−24520.
14. Metcalfe, C. L., Ott, M., Patel, N., Singh, K., Mistry, S. C., Goff, H. M., and Raven, E. L. (2004) Autocatalytic formation of green heme: evidence for H_2O_2-dependent formation of a covalent methionine-heme linkage in ascorbate peroxidase, *J. Am. Chem. Soc. 126*, 16242−16248.
15. Jones, D. K., Dalton, D. A., Rosell, F. I., and Lloyd Raven, E. (1998) Class I heme peroxidases: characterisation of soybean ascorbate peroxidase, *Arch. Biochem. Biophys. 360*, 173−178.
16. Ferrer, J. C., Turano, P., Banci, L., Bertinin, I., Morris, I. K., Smith, K. M., Smith, M., and Mauk, A. G. (1994) Active site coordination chemistry of the cytochrome *c* peroxidase Asp235Ala variant: spectroscopic and functional characterization, *Biochemistry 33*, 7819−7829.
17. Antonini, M., and Brunori, E. (1971) *Hemoglobin and Myoglobin and their Reactions with Ligands*, North Holland Publishers, Amsterdam.
18. Lad, L., Mewies, M., and Raven, E. L. (2002) Substrate binding and catalytic mechanism in ascorbate peroxidase: evidence for two ascorbate binding sites, *Biochemistry 41*, 13774−13781.
19. Teale, F. W. J. (1959) Cleavage of the haem-protein link by acid methylethylketone, *Biochim. Biophys. Acta 35*, 543.
20. Daltrop, O., Smith, K. M., and Ferguson, S. J. (2003) Stereoselective in vitro formation of *c*-type cytochrome variants from *Hydrogenobacter thermophilus* containing only a single thioether bond, *J. Biol. Chem. 278*, 24308−24313.
21. LeBrun, L. A., Xu, F., Kroetz, D. L., and Ortiz de Montellano, P. R. (2002) Covalent attachment of the heme prosthetic group in the CYP4 cytochrome P450 family, *Biochemistry 41*, 5931−5937.
22. Colas, C., Kuo, J. M., and Ortiz de Montellano, P. R. (2002) Asp-225 and Glu-375 in autocatalytic attachment of the prosthetic heme group of lactoperoxidase, *J. Biol. Chem. 277*, 7191−7200.
23. Colas, C., and Ortiz de Montellano, P. R. (2004) Horseradish peroxidase mutants that autocatalytically modify their heme prosthetic group, *J. Biol. Chem. 279*, 24131−24140.
24. Limburg, J., LeBrun, L. A., and Ortiz de Montellano, P. R. (2005) The P450$_{cam}$ G248E mutant covalently binds its prosthetic heme group, *Biochemistry 44*, 4091−4099.
25. Henne, K. R., Kunze, K. L., Zheng, Y.-M., Christmas, P., Soberman, R. J., and Rettie, A. E. (2001) Covalent linkage of prosthetic heme to CYP4 family of P450 enzymes, *Biochemistry 40*, 12925−12931.
26. Huang, L., Colas, C., and Ortiz de Montellano, P. R. (2004) Oxidation of carboxylic acids by horseradish peroxidase results in prosthetic heme modification and inactivation, *J. Am. Chem. Soc. 126*, 12865−12873.
27. Colas, C., and Ortiz de Montellano, P. R. (2003) Autocatalytic radical reactions in physiological prosthetic heme modification, *Chem. Rev. 103*, 2305−2332.
28. Hiner, A. N. P., Martínez, J. I., Arnao, M. B., Acosta, M., Turner, D. D., Raven, E. L., and Rodríguez-López, J. N. (2001) Detection of a radical intermediate in the reaction of ascorbate peroxidase with hydrogen peroxide, *Eur. J. Biochem. 268*, 3091−3098.
29. Bhaskar, B., Immoos, C. E., Shimizu, H., Sulc, F., Farmer, P. J., and Poulos, T. L. (2003) A novel heme and peroxide-dependent tryptophan-tyrosine cross-link in a mutant of cytochrome *c* peroxidase, *J. Mol. Biol. 328*, 157−166.

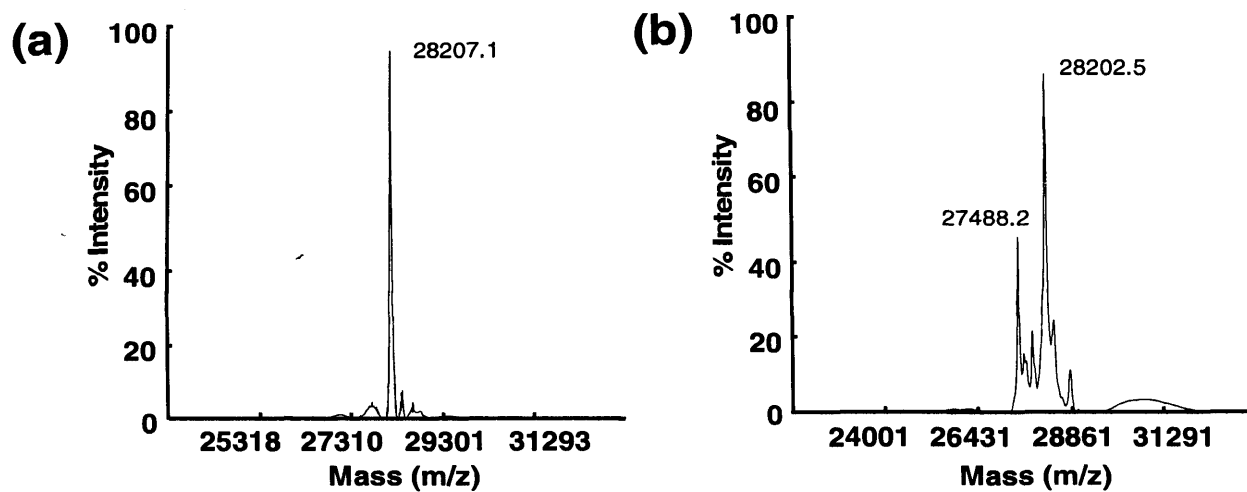BI062274Q

Supporting information

Figure S1: HPLC analysis (monitored at 398 nm) of rsAPX reconstituted with iron (III) deuteroporphyrin, before (a) and after (b) reaction with H_2O_2 and of CcP before (c) and after (d) reaction with H_2O_2.
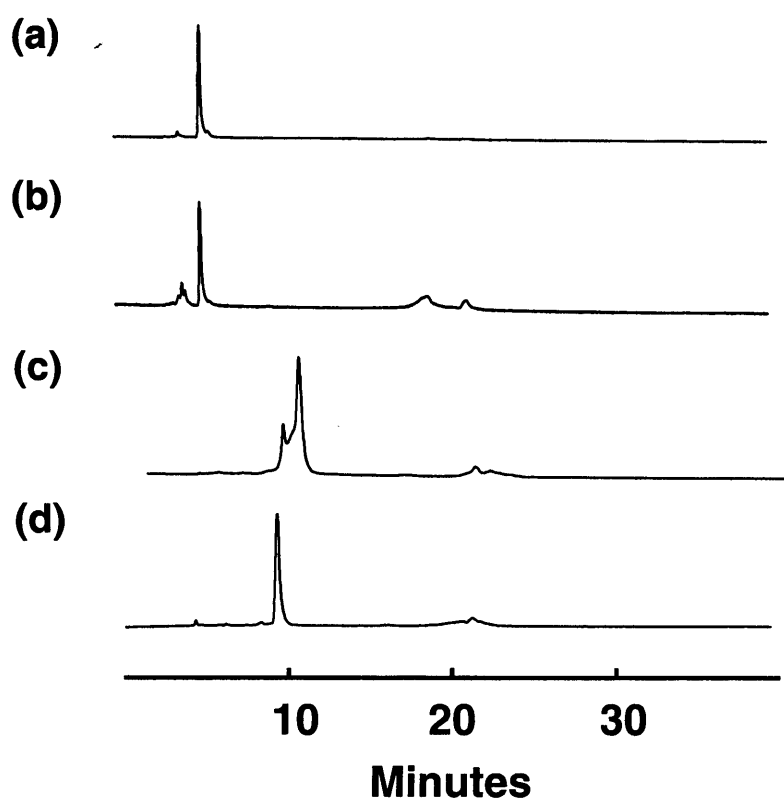
Figure S2: MALDI-TOF mass spectrum of W41A before (a) and after (b) reaction

with 6 equivalents of H_2O_2.

The Reactivity of Heme in Biological Systems: Autocatalytic Formation of Both Tyrosine—Heme and Tryptophan—Heme Covalent Links in a Single Protein Architecture[†]

Zoi Pipirou,[‡] Andrew R. Bottrill,[§] Dimitri A. Svistunenko,[‖] Igor Efimov,[‡] Jaswir Basran,[⊥] Sharad C. Mistry,[§] Christopher E. Cooper,[‖] and Emma Lloyd Raven*[‡]

Department of Chemistry, Henry Wellcome Building, University of Leicester, University Road, Leicester, LE1 7RH, England, Protein and Nucleic Acid Chemistry Laboratory, Hodgkin Building, University of Leicester, Lancaster Road, Leicester LE1 9HN, England, Department of Biochemistry, Henry Wellcome Building, University of Leicester, Lancaster Road, Leicester, LE1 9HN, England, and Department of Biological Sciences, University of Essex, Wivenhoe Park, Colchester, CO4 3SQ, England

Received August 1, 2007; Revised Manuscript Received September 13, 2007

ABSTRACT: We have previously shown that introduction of an engineered Met160 residue in ascorbate peroxidase (S160M variant) leads to the formation of a covalent link between Met160 and the heme vinyl group [Metcalfe, C. L., et al. (2004) *J. Am. Chem. Soc. 126*, 16242—16248]. In this work, we have used electronic spectroscopy, HPLC, and mass spectrometry to show that the introduction of a tyrosine residue at the same position (S160Y variant) leads, similarly, to the formation of a heme—tyrosine covalent link in an autocatalytic reaction that also leads to formation of a second covalent link from the heme to Trp41 [Pipirou, Z., et al. (2007) *Biochemistry 46*, 2174—2180]. Stopped-flow and EPR data implicate the involvement of a tyrosyl radical in the reaction mechanism. The results indicate that the heme can support the formation of different types of covalent links under appropriate conditions. The generality of this idea is discussed in the context of other heme enzymes.

The heme prosthetic group is used commonly in biology. It is usually found associated with proteins as a noncovalent complex, for example in the globins and the *b*-type cytochromes. There are examples, however, in which the heme is bound to the protein through a covalent link to one or more amino acids. The cytochromes *c* (*1*) are probably the most well-known example of this: in this case, one or both of the heme vinyl groups are bound to the protein through thioether bonds to cysteine residues. Recently, however, it has become clear that the presence of a covalently bound heme group is not a special privilege of the cytochromes *c*. For example, the mammalian peroxidase enzymes are known to contain sulfonium links between the heme 2-vinyl group and a Met residue (in myeloperoxidase) and/or two ester links between heme methyl groups and Glu/Asp residues (in myeloperoxidase, lactoperoxidase) (*2—5*). Other examples include the CYP4 family of cytochrome P450s which contain a similar ester link between the heme methyl group and a Glu residue (*2, 6, 7*); a cyanobacterial hemoglobin, which contains a covalent link between the vinyl group and a His residue (*8*); and the heme chaperone CcmE which uses a different vinyl—His covalent link (*9, 10*).

Recently, various studies from a number of laboratories have shown that the formation of covalent links to the heme of the type described above are not a unique feature of these particular proteins and can actually be engineered into an existing heme protein framework if an appropriate residue is introduced at an appropriate location and if the correct metal oxidation states are accessible (*11—16*). Collectively, these data have led to an emerging view that the existence of a specific covalent link is largely dictated by structural geometry and, in the catalytic enzymes, heme reactivity. This represents a substantial departure in the way we think about these modified heme groups because it tells us that the strategic positioning of a suitable amino acid within close proximity of the heme group, and contained within a structurally competent protein architecture, is all that is needed for a covalent link from the heme to the protein to form. By implication, this leads one to conclude that "activation" of the heme substituents is accessible in numerous heme protein architectures and is dictated by the iron chemistry and the structural environment. It follows logically that some proteins might actually need to be poised in an environment that controls the inherent reactivity of the heme group by specifically "switching off" the machinery required for formation of these covalent links. As a case in point, we have noted (*17*) that a covalent link between the heme and an engineered Met residue, analogous to that found in the mammalian peroxidases, can be incorporated into the ascorbate peroxidase framework but that cytochrome *c* peroxidase, which already contains a Met residue at this position (Met172), does not form the same covalent heme—Met link under any accessible conditions.

* To whom correspondence should be addressed. Tel: +44 (0)116 2297047. Fax: +44 (0)116 252 2789. E-mail: emma.raven@le.ac.uk.
‡ Department of Chemistry, University of Leicester.
§ Protein and Nucleic Acid Chemistry Laboratory, University of Leicester.
‖ Department of Biological Sciences, University of Essex.
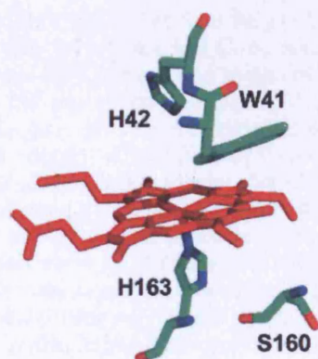⊥ Department of Biochemistry, University of Leicester.

FIGURE 1: The active site of rsAPX.

If it is the case that the heme group *per se* is inherently reactive and its reactivity is controlled by the iron and the protein hardware, then it follows that the heme should, in principle, react with *any* nucleophilic amino acid, not just those observed so far in biological systems. In this work, we have tested the generality of this hypothesis by the introduction of a Tyr residue (S160Y variant, Figure 1) into ascorbate peroxidase at a position that has been shown (*11*) to allow formation of a methionine—heme covalent link (S160M variant) through a H_2O_2-dependent activation process. We find that Tyr160 does indeed form a covalent link to the heme in an autocatalytic reaction that also leads to formation of a second covalent link to Trp41. We find that the formation of these links has a profound effect on the redox properties of the heme iron. The implications of these data in terms of current understanding of heme group reactivity are discussed.

EXPERIMENTAL PROCEDURES

Materials. L-Ascorbic acid (Aldrich Chemical Co.) and all buffers (Fisher) were of the highest analytical grade (99%+ purity) and used without further purification. Sinapinic acid and α-cyano-4-hydroxycinnamic acid were purchased from Fluka. All other chemicals were purchased from Sigma. Water was purified by an Elga purelab purification system, and all buffers were filtered (0.2 μm) prior to use. Hydrogen peroxide solutions were freshly prepared by dilution of a 30% (v/v) solution (BDH): exact concentrations were determined using the published absorption coefficient ($\epsilon_{240} = 39.4 \ M^{-1} \ cm^{-1}$) (*18*). All molecular biology kits and enzymes were used according to manufacturer's protocols.

Mutagenesis, Protein Expression, and Purification. Site-directed mutagenesis on recombinant soybean cytosolic APX[1] (rsAPX) was performed according to the Quikchange protocol (Stratagene Ltd, Cambridge, U.K.). For the S160Y mutation, the primers were 5′-CGTTGCTCTA**TAT**GGGGGT-CACACTATTGG-3′ (forward primer) and 5′-CCAATAGT-GTGACCCCC**ATA**TAGAGCAACG-3′ (reverse primer), with the mutation shown in bold. Bacterial fermentation of cells and purification of rsAPX and S160Y were carried out according to published procedures (*11, 19*). Purified samples of rsAPX and S160Y showed wavelength maxima at 407

---

(107), 525, and ≈630 nm (*20*) and 413 (134), 529, and 562 nm, respectively. Enzyme concentrations for rsAPX and S160Y were determined using absorption coefficients of $\epsilon_{407} = 107 \ mM^{-1} \ cm^{-1}$ (*20*) and $\epsilon_{405} = 134 \ mM^{-1} \ cm^{-1}$, respectively. Preparation of apoenzyme and reconstitution with iron (III) deuteroporphyrin IX chloride was carried out according to published procedures (*17*).

Electronic Absorption Spectroscopy. Spectra were collected using a Perkin-Elmer Lambda 35 or 40 spectrophotometer, linked to a PC workstation running UV-Winlab software. Pyridine hemochromagen assays before and after reaction of enzyme with H_2O_2 were carried out according to published protocols (*17*). The pyridine hemochromagen experiment proceeds as follows: a solution of protein is mixed with a solution of pyridine in NaOH. Oxidized pyridine hemochromagen, which is a soluble and stable compound, is formed rapidly. The spectrum between 600 and 500 nm is recorded just after addition of solid sodium dithionite, which yields the relatively unstable reduced pyridine hemochromagen. An absorbance maximum of 557 nm is expected for protoheme (*17*). The complete transfer of heme from the protein to the pyridine was assessed by determining the absorbance at maximum ($\lambda = 557$ nm) and minimum ($\lambda = 540$ nm) wavelengths; a ratio of $A_{557}/A_{540} = 3.5$ is found for protoheme.

Acidified Butanone Extraction. Acid butanone extractions were carried out as reported previously (*21*). Specifically, an aqueous solution of protein was titrated with 1 M HCl to a pH of 1.5. An equivalent volume of ice-cold 2-butanone was added with gentle but continuous stirring. After a period of cooling on ice, two distinct layers were observed. Transfer of heme to the organic layer (visualized by red color) indicates absence of covalent links between the heme and the protein, and *vice versa*.

Kinetic Measurements. Steady-state measurements (100 mM potassium phosphate, pH 7.0, 25 °C) for oxidation of ascorbate were carried out according to published protocols (*22*). Multiple wavelength absorption studies were carried out using a photodiode array detector and X-SCAN software (Applied Photophysics). Spectral deconvolution was performed by global analysis and numerical integration methods using PROKIN software (Applied Photophysics). To investigate reaction of S160Y with H_2O_2, the enzyme (20 μM in 100 mM potassium phosphate buffer, pH 7, 25.0 °C) was mixed with varying concentrations of H_2O_2 and the reaction was followed over time scales ranging from 300 ms to 4200 s.

Electron Paramagnetic Resonance. All EPR spectra were measured using a Bruker EMX EPR spectrometer (X-band) at a modulation frequency of 100 kHz. Accurate g-values were obtained using the built-in microwave frequency counter and a 2,2-diphenyl-1-picrylhydrazyl powder standard ($g = 2.0037 \pm 0.0002$ (*23*)). A spherical high quality Bruker resonator SP9703 and an Oxford Instruments liquid helium system were used to measure low-temperature EPR spectra. Spectra for blank samples (frozen water) were subtracted from the corresponding protein spectrum to eliminate the baseline caused by the resonator's walls, quartz insert, or quartz EPR tube. Individual signals were simulated using SimFonia v.1.25 (Bruker Analytische Messtechnik GmbH). The absolute free radical concentration was determined by comparison of the second integral of a pure line shape of

the free radical EPR signal, free from the $g = 2$ components of both high-spin ferric heme and Compound I, with the signal of a 98 μM Cu^{2+} standard. For spectra of ferric rsAPX and S160Y, 250 μL of enzyme (160 μM in 100 mM potassium phosphate, pH 7) was mixed with equal volume of buffer; for spectra of rsAPX and S160Y after H_2O_2 treatment, 180 μL of enzyme solution (98 μM in 100 mM potassium phosphate, pH 7) was mixed with 40 μL of H_2O_2 solution (440 μM in 100 mM potassium phosphate, pH 7) (final concentrations = 80 μM enzyme/80 μM H_2O_2).

High Performance Liquid Chromatography. HPLC analysis of protein and peptide samples and tryptic digestion were carried out according to published protocols (*17*).

Mass Spectrometry. MALDI-TOF mass spectrometry analysis of protein and peptide samples and MS/MS analysis of peptide samples were carried out according to published protocols (*17*). Theoretical isotope patterns for heme and peptide fragments of interest were calculated by entering the desired chemical formula in the "Sheffield ChemPuter Isotope Pattern Calculator" (http://winter.group.shef.ac.uk/chemputer/isotopes.html). The results are presented with the most intense line set to 100%. Experiments on peptide isotope patterns were carried out with the assistance of the EPSRC National Mass Spectrometry Service in Swansea.

Determination of Fe^{3+}/Fe^{2+} Reduction Potential. Fe^{3+}/Fe^{2+} reduction potentials for rsAPX and S160Y were determined by simultaneous reduction with a dye of known potential (*24*) according to previous methodology (*25*). The assay contained xanthine (300 μM), xanthine oxidase (50 nM), and enzyme (3–4 μM). The buffer (100 mM potassium phosphate buffer, pH 7.0) was made oxygen free using glucose (5 mM), glucose oxidase (50 μg/mL), and catalase (5 μg/mL). For measurement of the reduction potentials of rsAPX and S160Y before reaction with H_2O_2 the reaction also contained phenosafranin ($E_{m,7} = -252$ mV) (*26*). Absorbance changes corresponding to reduction of heme were measured at the isosbestic point for phenosafranine (407 nm); reduction of the dye was measured at 520 nm where the change due to heme reduction was negligible. For measurement of the reduction potential of S160Y after reaction with H_2O_2, the same experiment was also carried out using indigo trisulfonate ($E_{m,7} = -81$ mV) as a dye (*26*). Reduction of the dye was measured at the wavelength maximum of the dye (600 nm), where the change due to heme reduction was negligible; absorbance changes corresponding to reduction of heme were measured at 440 nm, subtracting the contribution from the dye. In all cases, linear Nernst plots for one-electron reduction of heme (25 mV $\ln(E_{ox}/E_{red})$) (where E_{ox} = concentration of oxidized enzyme, E_{red} = concentration of reduced enzyme) and two-electron reduction of dye (12.5 mV $\ln(D_{ox}/D_{red})$ (where D_{ox} = concentration of oxidized dye, D_{red} = concentration of reduced dye) produced the expected slope of 1 across a wide range of potentials, and the intercept gives a reliable value for $\Delta E_{m,7}$ with an error of ± 2 mV. UV–visible spectra obtained in all experiments were analyzed using SPECFIT (*27*) for singular value decomposition based on factor analysis. All potentials reported in this paper are given versus the normal hydrogen electrode (NHE).

RESULTS

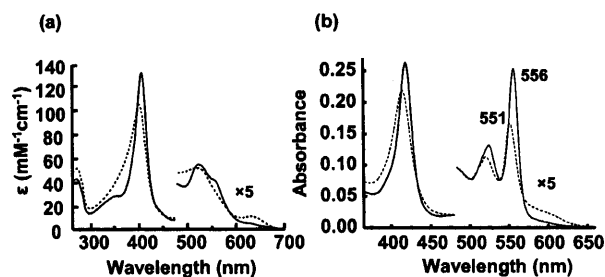*Characterization of S160Y.* The S160Y variant was expressed as *apo*-enzyme, which was reconstituted with

FIGURE 2: (a) Electronic absorption spectra of S160Y (solid line) and rsAPX (dashed line). The visible region has been multiplied by a factor of 5 (100 μM potassium phosphate, pH 7.0, 25.0 °C). (b) Spectra of the reduced pyridine hemochromagen complexes of S160Y before (solid line) and after (dashed line) reaction with H_2O_2.

hemin. This resulted in formation of a red enzyme with absorption maxima at 413, 529, and 562[(sh)] nm (Figure 2a). Comparison with the corresponding spectrum of rsAPX (Figure 2a) shows that the Soret peak for S160Y is red-shifted compared to rsAPX and that there is no band at 630 nm, both of which are indicative of formation of low-spin heme in S160Y.

EPR spectroscopy was used to further characterize the heme environment in S160Y. Low-temperature EPR spectra of rsAPX reveals high- and low-spin species (*20*). Consistent with this, the EPR spectrum of S160Y (Figure S1 in the Supporting Information) contains features with a high-spin ferric heme of tetragonal symmetry ($g_\perp = 5.88$, $g_\parallel = 1.99$) and a low-spin species ($g = 2.94$, 2.27, and 1.47). These signals are, however, somewhat different from those observed in the EPR spectrum of rsAPX, which has a high-spin signal with less tetragonality ($g = 5.96$, 5.23, and 1.98), and a less rhombic low-spin signal ($g = 2.68$, 2.21, and 1.78 (*20*)).

In steady-state analyses of S160Y in the presence of ascorbate, the value for k_{cat} ($k_{cat} = 43 \pm 2$ s^{-1}) was lower than that of rsAPX ($k_{cat} = 272 \pm 32$ s^{-1} (*28*)), although K_M values ($K_M = 638 \pm 66$ μM and 389 $\pm$ 64 μM (*22*) for S160Y and rsAPX, respectively) were largely similar.

Assessment of Covalent Heme Attachment on Reaction with H_2O_2. Initial experiments indicated that, on reaction with H_2O_2, the heme group in S160Y became covalently attached to the protein. This was tested, qualitatively, in two ways. First, a pyridine hemochromagen assay was carried out before and after reaction with H_2O_2. For S160Y before treatment with H_2O_2, the spectrum of the reduced pyridine hemochromagen complex showed a maximum at 556 nm (Figure 2b). In this experiment, complete extraction of the heme from the protein is observed and the spectrum of the hemochromagen complex is consistent with a noncovalently bound heme structure, in which neither heme vinyl group is modified (*29*). When the same experiment was carried out with S160Y after treatment with 6 equiv of H_2O_2, the peak of the reduced pyridine complex at 556 nm was shifted to 551 nm (Figure 2b). These spectroscopic changes are consistent with covalent modification of the heme vinyl groups (*30*). Second, an acid butanone extraction after reaction of S160Y with H_2O_2 did not remove the heme from the protein, which is a clear indication of covalent attachment of the heme to the protein (Figure S2 in the Supporting Information); in contrast, control experiments with S160Y before reaction with H_2O_2 showed complete extraction of
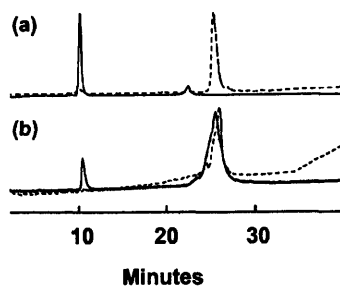
FIGURE 3: HPLC analyses of S160Y before and after reaction with H_2O_2 monitored at 398 nm (solid line) and 215 nm (dotted line). (a) S160Y before reaction with H_2O_2. (b) S160Y after reaction with H_2O_2.

heme into the organic layer. Thése effects were examined in more detail below.

HPLC Analyses. We sought further confirmation of the proposed heme—protein covalent linkage. HPLC analysis (under denaturing conditions) of the product of the reaction of S160Y with H_2O_2 (prepared with addition of 6 equiv of H_2O_2 as above) showed that the protein (monitored at 215 nm) and the major proportion of the heme (monitored at 398 nm) coelute at 24 min (Figure 3b); a proportion of the protein ($\approx 10\%$) remains unreacted. This is in direct contrast to the HPLC profile of S160Y which has not been treated with H_2O_2, in which the heme (11 min) and the protein (24 min) do not coelute (Figure 3a). Coelution of the heme and the protein is a clear indication of covalent heme attachment and has been used previously to identify covalently linked heme in various other heme proteins (*3, 6, 7, 11, 12, 16, 31*). A commercial sample of hemin eluted at 11 min, confirming the assignment for free heme above (Figure S3 in the Supporting Information). In separate experiments (data not shown) under the same conditions as those used above for Figure 3b but in the presence of a large excess of ascorbate, it was shown that no peak corresponding to protein-bound heme was observed at ≈ 24 min. This indicates that under turnover conditions no formation of covalently bound heme occurs.

Mass Spectrometry. Mass spectrometry can be used not only to confirm the presence of a covalent link but also to establish the identity of the residue(s) making the link (*17*). The MALDI-TOF mass spectrum of S160Y before treatment with H_2O_2 showed a mass of 28393.63 Da (Figure 4a), which corresponds closely to the predicted mass (28394.97 Da) of the apoprotein and is consistent with noncovalent attachment of the heme (as found in rsAPX). After treatment with H_2O_2, the main peak in the MALDI-TOF spectrum showed a mass of 29025.68 Da (Figure 4b); this corresponds to an increase in mass of 632 Da over the apoprotein and is consistent with covalent attachment of the heme (616 Da). The additional mass of 16 amu is assigned as arising from hydroxylation of the fragment. Hydroxylation of heme after reaction with H_2O_2 has been reported previously (*11, 17*).

To establish more clearly the nature of the heme—protein covalent link, tryptic digestion of the product of the reaction of S160Y with H_2O_2 was carried out and HPLC was used to isolate the main heme-containing peptide fragment (i.e., showing both heme and protein absorbances, eluting at 24.7 min, Figure S4 in the Supporting Information) from the resulting peptide mixture. There were three peptide peaks

detected on the MALDI-TOF mass spectrum of the main HPLC fragment (Figure 4c). (i) The first peak at 1863.96 Da is the same mass as that observed in identical analyses on rsAPX in which a covalent link to Trp41 has been established (*17*). This peak corresponds to the $L^{39}AW^{41}$-HSAGTFDK^{49} peptide fragment containing heme covalently bound to Trp41 (*17*). (ii) The second peak at 2971.48 Da is 16 Da higher than the calculated mass (2955.18) expected for the $A^{148}MGLTDQDIVALY^{160}GGHTIGAAHK^{170}$ peptide fragment containing heme covalently bound to Tyr160. (iii) A third peptide fragment was also observed at 4203.39 Da. This is 16 Da higher than the calculated mass (4187.79 Da) expected for the $A^{148}MGLTDQDIVALY^{160}GGHTIGAAHK^{170}$ peptide fragment plus the $L^{39}AW^{41}HSAGTFDK^{49}$ peptide fragment, with both fragments covalently bound to the heme through Tyr160 and Trp41. The proposed structure of this fragment is shown schematically in the inset to Figure 4d.

MS/MS mass spectrometry was used to obtain more specific sequence information for the third heme-containing fragment at 4203.39 Da. There were two different fragmentation series identified, indicating the presence of two distinct peptides bound to the heme. First, a y-ion fragmentation series allowed sequential identification of His42 through to Thr46 with the remaining C-terminal mass (409.1 Da) consistent with residues Phe47 to Lys49, which corresponds to the sequence $H^{42}SAGTFDK^{49}$ (Figure 4d, series y_B). The absence of fragment ions for the amino acids (LAW^{41}) indicates that the heme forms a covalent link with this part of the peptide and is interpreted as being consistent with the formation of a covalent link toTrp41. This same link has also been shown to form when rsAPX is reacted with H_2O_2 (*17*). Second, a separate y-ion fragmentation series allowed sequential identification of His163 through to Lys170, which corresponds to the sequence $H^{163}TIGAAHK^{170}$ (Figure 4d, series y_A). A combination of a- and b-ion fragmentation series allowed sequential identification of Ala148 through to Asp152, which corresponds to the sequence $A^{148}MGLTD^{152}$ on the N-terminal end of this peptide (Figure 4d, series a/b_A). As above, the absence of fragment ions for the amino acids ($QDIVALY^{160}GG$) indicates that the heme forms a covalent link with this part of the peptide (in Figure 4d, inset).

Further evidence for heme incorporation into the peptides mentioned above came from isotope patterns of the peptides in question. Because iron exhibits a very distinct isotope pattern, when incorporated into protoporphyrin IX to form heme it produces very characteristic signals. Figure 5a, left, shows the theoretical isotope pattern of heme, and Figure 5a, right, shows the isotope pattern obtained from MALDI-TOF mass spectrometry of heme. Theoretical isotope patterns were also calculated for the two heme-free peptides containing Trp41 ($L^{39}AW^{41}HSAGTFDK^{49}$, Figure 5b, left) and Tyr160 ($A^{148}MGLTDQDIVALY^{160}GGHTIGAAHK^{170}$, Figure 5d, left) and were in very good agreement with the experimental isotope patterns obtained for these peptides (Figures 5b, 5d, right). The same procedure was used to calculate theoretical isotope patterns for the same peptide fragments but with heme covalently attached (i.e., after treatment with H_2O_2). Hence, the peptide fragment with a mass of 1864 Da (Figure 4c) was assigned above to the fragment $L^{39}AW^{41}HSAGTFDK^{49}$ with heme covalently bound: this peptide exhibits the same characteristic isotope pattern (Figure 5c, right) as that predicted theoretically after
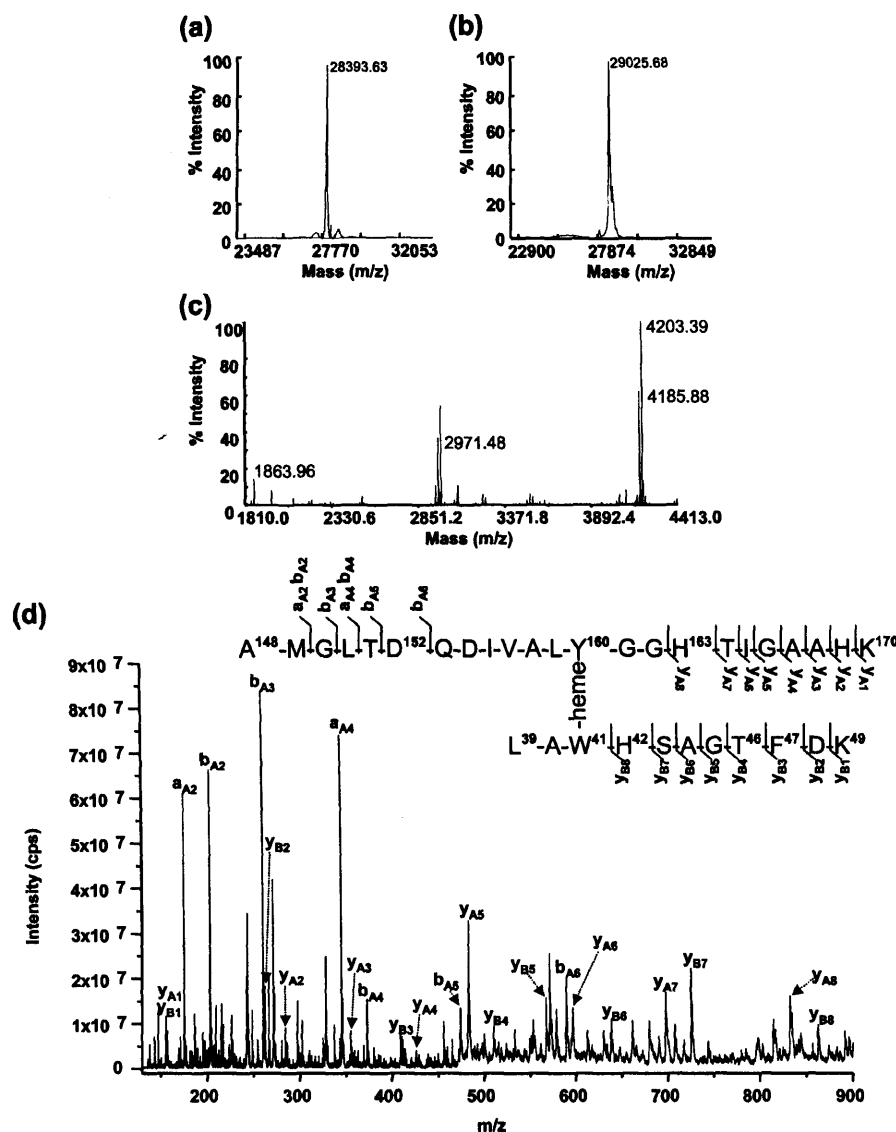
FIGURE 4: MALDI-TOF mass spectrum of S160Y before (a) and after (b) reaction with 6 equiv of H_2O_2. (c) MALDI-TOF mass spectrum of the HPLC-purified heme-containing peptide fragment obtained after reaction of S160Y with H_2O_2. (d) MS/MS spectrum of the HPLC-purified heme-containing peptide fragment showing the 4+ charged precursor ion (1051.44 Da). The peptide sequences obtained correspond to the y-ion fragment series for LAW[41]HSAGTFDK peptide and the a-, b-, and y-ion fragment series for the AMGLTDQDIVALY[160]-GGHTIGAAHK peptide and are shown (inset).

attachment of heme (Figure 5c, left) which confirms the assignment. Similarly, the same change in isotope pattern is observed for the peptide with a mass of 2971 Da (Figure 4c), assigned above as A[148]MGLTDQDIVALY[160]-GGHTIGAAHK[170] with heme covalently attached, before and after attachment of heme, Figures 5d and 5e. The fact that the peptides with masses of 1864 Da (Figure 5c) and 2971 Da (Figure 5e) exhibit the same characteristic isotope pattern as heme (Figure 5a) gives further confirmation of their assignment as heme-containing peptides.

Mechanistic Investigations. Reaction of ferric S160Y with 6 equiv of H_2O_2 was monitored over ~2 h, and the intermediate spectra are presented in Figure 6a. In contrast to the wild type protein in which a Compound I species (containing a porphyrin π-cation radical) is clearly visible on the stopped-flow time scale and a Compound II species

is clearly visible on a time scale of 1–2 min (*28*), reaction of S160Y with H_2O_2 did not show any evidence for formation of either Compound I or Compound II using conventional electronic spectroscopy. Instead, the reaction resulted in a final product with wavelength maxima at 408, 530, and 563 nm (Figure 6a).

The same reaction was also examined under pre-steady-state conditions (Figure 6b), to investigate if reaction of S160Y with H_2O_2 involved initial formation of a Compound I intermediate over shorter time scales (300 ms to 4200 s) and using different H_2O_2 concentrations (6 to 100 equiv). Unlike rsAPX which shows clear formation of a Compound I intermediate containing a porphyrin π-cation radical (λ_{max}/ nm = 409, 530, 569[sh], and 655 (*17*)) on reaction with H_2O_2 under rapid mixing conditions, no formation of a porphyrin π-cation radical intermediate was observed under any condi-
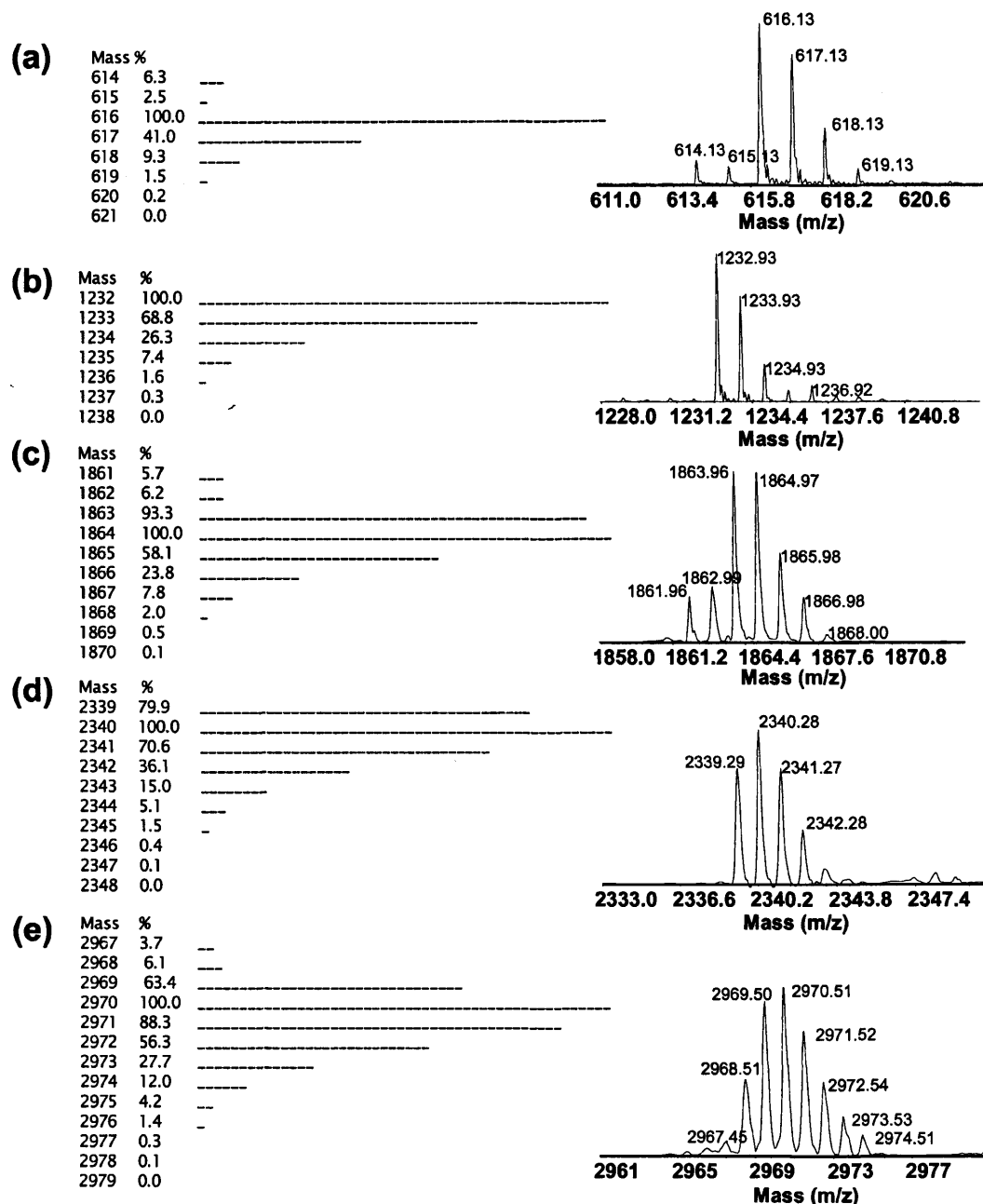
(a)

Mass	%
614	6.3
615	2.5
616	100.0
617	41.0
618	9.3
619	1.5
620	0.2
621	0.0

(b)

Mass	%
1232	100.0
1233	68.8
1234	26.3
1235	7.4
1236	1.6
1237	0.3
1238	0.0

(c)

Mass	%
1861	5.7
1862	6.2
1863	93.3
1864	100.0
1865	58.1
1866	23.8
1867	7.8
1868	2.0
1869	0.5
1870	0.1

(d)

Mass	%
2339	79.9
2340	100.0
2341	70.6
2342	36.1
2343	15.0
2344	5.1
2345	1.5
2346	0.4
2347	0.1
2348	0.0

(e)

Mass	%
2967	3.7
2968	6.1
2969	63.4
2970	100.0
2971	88.3
2972	56.3
2973	27.7
2974	12.0
2975	4.2
2976	1.4
2977	0.3
2978	0.1
2979	0.0

FIGURE 5: Theoretically calculated (figures on the left) and experimentally observed (figures on the right) isotope patterns for heme (a), the LAW[41]HSAGTFDK peptide before (b) and after (c) covalent attachment of heme, and the AMGLTDQDIVALY[160]GGHTIGAAHK peptide before (d) and after (e) covalent attachment of heme.

tions for S160Y. (Over time scales <300 ms and >1.28 ms (the dead-time of the stopped-flow instrument), no formation of a porphyrin π-cation radical intermediate was observed either.) Instead, on reaction of S160Y with H_2O_2 the Soret peak is blue-shifted and decays to a final spectrum with maxima (408, 530, and 563 nm) similar to those described above (Figure 6a). Time-dependent spectra were fitted globally by numerical integration methods using Prokin software (Applied Photophysics). Data collected over a period of 1000 s from the mixing event were best fitted to a two-step model (A → B → C, with rate constants for these two steps of 0.028 s⁻¹ and 0.0024 s⁻¹, respectively) (Figure

6c). Intermediate A has absorption characteristics (λ_{max}/nm = 413, 529, and 562[sh] nm) consistent with those observed above for ferric S160Y, and clearly arise from the oxidized enzyme. Intermediate B (λ_{max}/nm = 411, 528, and 558[sh] nm) does not show spectroscopic characteristics that are consistent with either Compound I or Compound II. Intermediate C has maxima that are consistent with the final product of the reaction of S160Y with H_2O_2 (Figure 6a). These findings show that exposure of the protein to H_2O_2 does not lead to formation of the expected porphyrin π-cation radical, which is in contrast to rsAPX and all other APXs examined so far (*32*). They also indicate that the formation
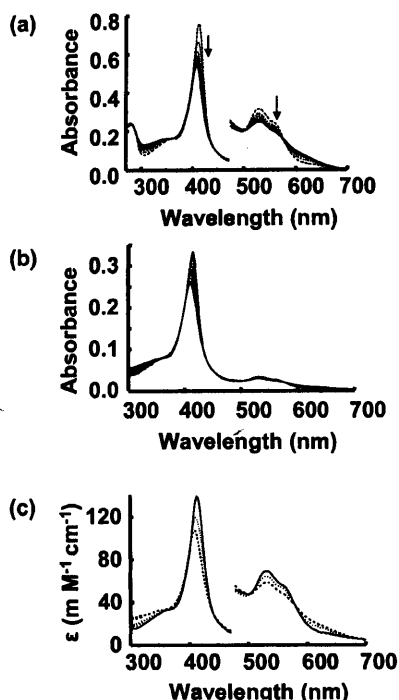
(a)

(b)

(c)

FIGURE 6: (a) Selected spectra collected during the reaction of ferric S160Y (dashed line) with 6 equiv of H_2O_2. Intermediate spectra between ferric S160Y and the final product (solid line) are shown as dotted lines. The total reaction time was 2 h. The visible region has been multiplied by a factor of 5. Sample conditions: enzyme 5 μM, hydrogen peroxide 30 μM, 0.1 M potassium phosphate, pH 7.0, 25.0 °C. (b) Reaction of S160Y with H_2O_2 monitored by stopped-flow diode array spectroscopy. Conditions: 100 mM potassium phosphate buffer, pH 7.0; 25 °C. Enzyme concentration, 20 μM; substrate concentration, 30 mM. The experiment is performed over 1000 s. For clarity, only selected spectra are shown. (c) Deconvoluted spectra for the reaction shown in (b). The data were fitted to a two-step model: intermediate A shown in solid line, intermediate B shown in dotted line, and intermediate C shown in dashed line.

of these links is slower overall than that observed for formation of other cross-links in APX which are known to go through formation of an authentic porphyrin π-cation intermediate (11).

Electron Paramagnetic Resonance. EPR spectroscopy was used to obtain further evidence for the formation of a protein radical. EPR spectra of rsAPX and S160Y after treatment with H_2O_2 are shown in Figure 7a and 7b, respectively. In agreement with previous work (33), reaction of rsAPX with H_2O_2 yields a species with g-values (g = 3.52, g = 1.998) consistent with the existence of a porphyrin π-cation radical (Figure 7a). In contrast, reaction of S160Y with H_2O_2 (Figure 7b) reveals a single radical species with g = 2.0053 and a line width of 19.2 G. This signal is shown in more detail in Figure 7c and is compared with the EPR signal (Figure 7d) observed in the human metHb/H_2O_2 system in which a tyrosyl radical has been assigned (34). These EPR signals, Figures 7c and 7d, have identical g-factors and linewidths and have very close overall lineshapes. The maximal yield of the free radical, observed at the first time points of the reaction (4−10 s), was 0.3 μM for the stoichiometric amount of H_2O_2 added and 0.5 μM for a 6-fold molar excess of H_2O_2 over the heme concentration (80 μM). A low concentration
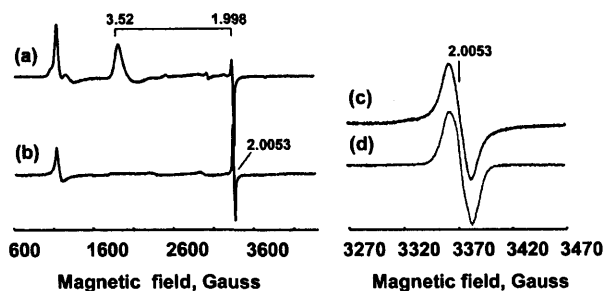

FIGURE 7: The EPR spectra of (a) rsAPX and (b) S160Y (both 80 μM) after addition of 80 μM H_2O_2 (final concentrations, pH 7.0, the samples frozen 4 s after mixture). The spectra were measured at 10 K; other instrumental conditions were modulation frequency ν_m = 100 kHz, modulation amplitude A_m = 5 G, sweep rate ν = 22.6 G/s, time constant τ = 82 ms, microwave frequency ν = 9.47 GHz, microwave power P = 3.188 mW, number of spectral scans NS = 1. (c) Detailed EPR spectrum of the free radical formed in S160Y after addition of H_2O_2; sample conditions as in (b), instrumental conditions were as in (b) except A_m = 3 G and ν = 1.19 G/s. (d) A tyrosyl radical EPR signal recorded under the same conditions as (c) in the human metHb + H_2O_2 system (34).

of free radicals observed (under 1% of protein) is in agreement with previous reports on different heme protein/peroxide systems (34, 35). Taken together, these data are consistent with the stopped-flow data presented above and are consistent with the formation of a tyrosyl radical.[2] Power saturation studies (data not shown) revealed that the radical in the S106Y mutant relaxed faster than many radicals observed so far on proteins, which suggests proximity to a nearby paramagnetic center, consistent with its presence on the Tyr160 and close to the heme.

Redox Measurements. The Fe^{3+}/Fe^{2+} reduction potential for S160Y before reaction with H_2O_2 (determined using the phenosafranine/xanthine/xanthine oxidase method) was found to be −197 mV, Figure 8a; this compares with a value of −206 mV (25) for rsAPX and indicates that no considerable shift in potential occurred as a consequence of the S160Y mutation. The corresponding Fe^{3+}/Fe^{2+} reduction potential for S160Y after reaction with H_2O_2 was determined using indigo trisulfonate as a dye (Figure 8b) and was found to be −98 mV, an increase of 99 mV. Both sets of data show linear Nernst plots, Figure 8c. This suggests that the formation of two covalent links between the heme and the protein in S160Y leads to a significant stabilization of the reduced protein.

DISCUSSION

The heme prosthetic group is widely distributed in biological systems and in the majority of cases is bound to the protein through noncovalent interactions. There are still relatively few examples of heme proteins or enzymes in which the heme substituents (i.e., the vinyl and/or methyl groups) are covalently bound to the protein backbone (1, 2, 8, 9, 36−38). For many years, therefore, the prevailing view was that the substituents on the heme group were inherently unreactive and that formation of these links could only be supported within a very specific and highly tuned structural

---

[2] We note that no such radical is observed before introduction of Tyr at position 160. However, the possibility that the radical might be at a different location to Tyr160 cannot be ruled out.
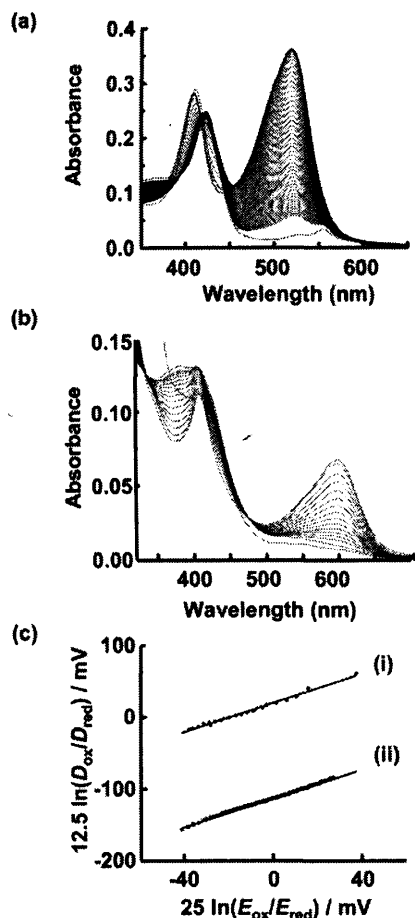
(a)

(b)

(c)

FIGURE 8: Representative family of spectra for determination of Fe^{3+}/Fe^{2+} reduction potential in S160Y before (a) and after (b) reaction with H_2O_2 (100 mM potassium phosphate, pH 7.0). (c) The corresponding linear Nernst plots, where plot (i) corresponds to the data shown in (b) and plot (ii) to the data shown in (a).

and/or catalytic framework. This simplistic rationalization now appears to represent only one part of a much more sophisticated problem. Hence, *in vitro* studies from different laboratories (*11–16*) have revealed that most of these covalent links can be duplicated in other protein architectures when the correct residue is introduced in the correct place and if the correct oxidation states of the metal are accessible. This is supported by other examples in which covalent links to various heme proteins have also been observed without needing to introduce specific mutations in the active site (*17, 31, 39–41*).

This paper provides further evidence in support of the above hypothesis. Hence, we have already shown (*11*) that replacement of Ser160 in ascorbate peroxidase by a methionine residue leads to formation of a heme—methionine covalent link in an autocatalytic reaction that requires H_2O_2. Here, we establish that the introduction of a nucleophilic tyrosine residue at this position leads, similarly, to a covalent link to Tyr160. In addition, a second covalent link to Trp41 is observed: this link has been previously shown (*17*) to form to the 4-vinyl group of the heme in the wild type protein through an autocatalytic reaction involving reaction with H_2O_2. To our knowledge, there is only one other example (*15*) in which formation of a doubly linked heme species

has been engineered inside a protein architecture that does not, ordinarily, support such links.

The Nature of the Tyrosine—Heme Link. Based on our previous work in which a covalent link from Met160 to the 2-vinyl was proposed, we had originally envisaged a similarly modified heme for the S160Y variant. The peak at 551 nm for the reduced pyridine—heme complex of S160Y after treatment with H_2O_2 has been used as an empirical indication that two vinyl groups on the porphyrin ring have been modified (*29*): since we had already established that Trp41 links to the 4-vinyl group (*17*), the 551 nm peak indicated that Tyr160 was linked to the 2-vinyl group. There are only a handful of examples in the literature of tyrosine—heme covalent links: in the cytochrome P460 heme in hydroxylamine oxidoreductase (HAO) (*36, 42*), in myoglobin (*39*), and in leghemoglobin (*40*). In all three cases, the link has been proposed to a *meso*-carbon of the heme (although not the same *meso*-carbon in all cases), but this has not been confirmed crystallographically. There is, however, a structure for the cytochrome P460 from *Nitrosomonas europaea* (*37*) in which a covalent link from the γ-meso carbon of the heme to the amine group of a lysine residue has been observed. By analogy, it has been proposed (*37*) that the heme—tyrosine link in HAO is to the hydroxyl group of the Tyr residue and that the heme—tyrosine (in HAO) and heme—lysine (in P460 from *Nitrosomonas europaea*) links are formed either through a radical mechanism or by direct nucleophilic attack. From the data presented above for S160Y, we cannot confirm unambiguously the precise nature of the heme—tyrosine link, but analogy with the examples above would suggest that a link to the *meso*-carbon is most likely. This would be consistent with our control experiments and parallel HPLC analyses with apo-S160Y reconstituted with deuteroheme (in which hydrogen atoms replace the 2- and 4-vinyl groups) in which we observed that replacement of the heme vinyl groups reduced the percentage of covalently linked heme but did not eliminate it completely (Figure S4 in the Supporting Information[3]).

The Mechanism of Formation of the Links. Stopped-flow data shows no evidence for formation of a typical Compound I species (containing a porphyrin π-cation radical) on reaction of S160Y with H_2O_2. EPR experiments similarly showed no evidence for formation of a porphyrin π-cation signal as observed for the wild type enzyme (*33*); instead, EPR identifies an initial radical species which was assigned as a tyrosyl radical. This is shown as Intermediate I in Scheme 1, in which we outline a proposed mechanism for formation of the covalent links to the heme. This initially formed species may arise in two ways: (a) indirectly, through internal electron transfer within an initial porphyrin π-cation species that is not observable on the stopped-flow time scale (steps (i) and (ii), Scheme 1); or (b) directly through oxidation of Tyr160 on reaction with H_2O_2 (step (iii) in Scheme 1), without going through a normal Compound I intermediate. There is separate evidence that formation of

---

[3] We estimate that the percentage formation of total covalently linked product reduces by $\approx$20% for deuteroheme (from $\approx$90% for S160Y + iron protoporphyrin IX + H_2O_2), and we assume that the link is to the *meso*-carbon for this deuteroheme species (since the vinyl groups are missing). In these experiments, our methods of separation for these modified fragments are not sensitive enough to pick up minor cross-linked components if they were present.

Scheme 1: Proposed Mechanism for Formation of a Covalent Link between Tyr160 and the Heme in Ascorbate Peroxidase[a]
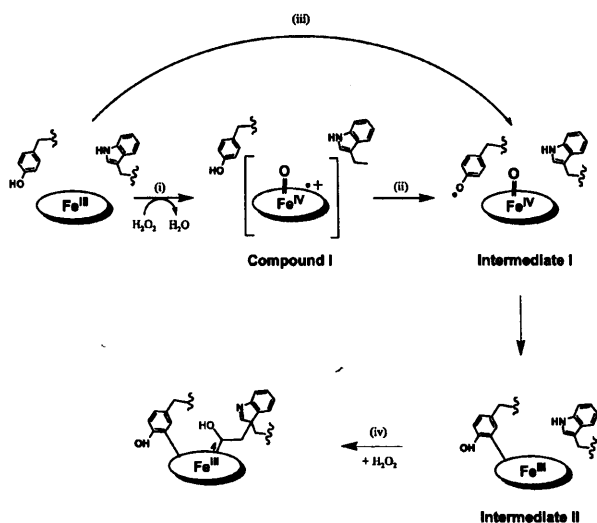
[a] The heme−Trp link, step (iv), is at the 4-vinyl group (labeled with a 4 in the scheme) with a suggested structure (*17*) as shown; this is proposed to be via formation of a Trp radical and to be through the C^γ of Trp41, but the various resonance forms of a Trp radical mean that a link to other carbon atoms of Trp41 is also possible. The structure of the heme−Tyr link is not known and is suggested to be as depicted here; an ether link through the O of Tyr160 is also possible, however. The porphyrin π-cation radical is not detected in this work, but is proposed as an intermediate on the basis of the known mechanism in the wild type enzyme (see Discussion).

tyrosyl radicals can occur independently and not necessarily as a consequence of Compound I formation (*43*). We cannot distinguish these two possibilities from the data presented. We then envisage a further radical reaction mechanism to form the heme−tyrosine link, Scheme 1, followed by further reaction with H_2O_2 to form the heme−Trp link, step (iv) in Scheme 1. We have proposed (*17*) that formation of this link to Trp41 involves radical formation on Trp41.

Functional Implications. We have observed that formation of a double link between the heme and Tyr160 and Trp41 resulted in an increase of the Fe^{3+}/Fe^{2+} reduction potential from -197 mV to -98 mV, reflecting a clear stabilization of the reduced form. Parallel experiments with rsAPX after formation of the Trp41−heme linkage also showed an increase in the Fe^{3+}/Fe^{2+} reduction potential (data not shown) although this increase was difficult to quantify because of the experimental complications associated with obtaining completely pure samples of the Trp41−heme species. Hence, we cannot assign the 99 mV stabilization of the reduced form in the modified enzyme as arising from one or other of the two links, although we note also that covalent modification of the flavin (FAD) subunit of the flavocytochrome *p*-cresol methylhydroxylase by a Tyr residue also raises the reduction potential of the flavin group (*44*). In fact, quantitative rationalizations of the role of individual covalent links on the control of heme redox potential are very poorly defined. The closest analogy is with the mammalian peroxidases, in which the covalent links to the heme have been linked with their redox properties. Although there is no overall consensus on exactly how and why these links are influential, disruption of the Asp94−heme ester linkage in myeloperoxidase has

been shown to lead to changes in heme potential, suggested to be a result of increased heme flexibility introduced as a consequence of the removal of one of the three physiological covalent links (*45*). It is possible that similar effects on the heme structure are responsible for the changes we observe in this work.

ACKNOWLEDGMENT

This paper is dedicated to the memory of Professor Geoff Sykes.

NOTE ADDED AFTER ASAP PUBLICATION

This paper was published ASAP on October 25, 2007 with an error in the Abstract. The correct version published on November 13, 2007.

SUPPORTING INFORMATION AVAILABLE

The EPR spectrum of ferric S160Y (Figure S1), acid butanone extraction for S160Y (Figure S2), HPLC analysis for free heme (Figure S3), HPLC of tryptic digest of S160Y after reaction with H_2O_2 (Figure S4), and HPLC analyses of S160Y reconstituted with deuteroheme (Figure S5). This material is available free of charge via the Internet at http://pubs.acs.org.

REFERENCES

1. Stevens, J. M., Daltrop, O., Allen, J. W. A., and Ferguson, S. J. (2004) *C*-type cytochrome formation: chemical and biological enigmas, *Acc. Chem. Res. 37*, 999−1007.

2. Colas, C., and Ortiz de Montellano, P. R. (2003) Autocatalytic radical reactions in physiological prosthetic heme modification, *Chem. Rev. 103*, 2305−2332.

3. Colas, C., Kuo, J. M., and Ortiz de Montellano, P. R. (2002) Asp-225 and Glu-375 in autocatalytic attachment of the prosthetic heme group of lactoperoxidase, *J. Biol. Chem. 277*, 7191−7200.

4. Rae, T. D., and Goff, H. M. (1998) The heme prosthetic group of lactoperoxidase. Structural characteristics of heme 1 and heme 1-peptides, *J. Biol. Chem. 273*, 27968−27977.

5. Oxvig, C., Thomsen, A. R., Overgaard, M. T., Sorensen, E. S., Hojrup, P., Bjerrum, M. J., Gleich, G. J., and Sottrup-Jensen, L. (1999) Biochemical evidence for heme linkage through esters with Asp-93 and Glu-241 in human eosinophil peroxidase. The ester with Asp-93 is only partially formed in vivo, *J. Biol. Chem. 274*, 16953−16958.

6. LeBrun, L. A., Xu, F., Kroetz, D. L., and Ortiz de Montellano, P. R. (2002) Covalent attachment of the heme prosthetic group in the CYP4 cytochrome P450 family, *Biochemistry 41*, 5931−5937.

7. Henne, K. R., Kunze, K. L., Zheng, Y.-M., Christmas, P., Soberman, R. J., and Rettie, A. E. (2001) Covalent linkage of prosthetic heme to CYP4 family of P450 enzymes, *Biochemistry 40*, 12925−12931.

8. Hoy, J. A., Kundu, S., Trent, J. T., III, Ramaswamy, S., and Hargrove, M. S. (2004) The crystal structure of *Synechocystis* hemoglobin with a covalent heme linkage, *J. Biol. Chem. 279*, 16535−16542.

9. Lee, D., Pervushin, K., Dischof, D., Braun, M., and Thony-Meyer, L. (2005) Unusual heme-histidine bond in the active site of a chaperone, *J. Am. Chem. Soc. 127*, 3716−3717.

10. Uchida, T., Stevens, J. M., Daltrop, O., Harvat, E. M., Hong, L., Ferguson, S. J., and Kitagawa, T. (2004) The interaction of covalently bound heme with the cytochrome *c* maturation protein CcmE, *J. Biol. Chem. 279*, 51981−51988.

11. Metcalfe, C. L., Ott, M., Patel, N., Singh, K., Mistry, S. C., Goff, H. M., and Raven, E. L. (2004) Autocatalytic formation of green heme: evidence for H_2O_2-dependent formation of a covalent methionine-heme linkage in ascorbate peroxidase, *J. Am. Chem. Soc. 126*, 16242−16248.

12. Colas, C., and De Montellano, P. R. (2004) Horseradish peroxidase mutants that autocatalytically modify their prosthetic heme

group: insights into mammalian peroxidase heme-protein covalent bonds, *J. Biol. Chem. 279*, 24131−24140.

13. Huang, L., Wojciechowski, G., and Ortiz de Montellano, P. R. (2006) Role of heme-protein covalent bonds in mammalian peroxidases. Protection of the heme by a single engineered heme-protein link in horseradish peroxidase, *J. Biol. Chem. 281*, 18983−18988.

14. Barker, P. D., Ferrer, J. C., Mylrajan, M., Loehr, T. M., Feng, R., Konishi, Y., Funk, W. D., MacGillivray, R. T., and Mauk, A. G. (1993) Transmutation of a heme protein, *Proc. Natl. Acad. Sci. U.S.A. 90*, 6542−6546.

15. Barker, P. D., Nerou, E. P., Freund, S. M., and Fearnley, I. M. (1995) Conversion of cytochrome b562 to c-type cytochromes, *Biochemistry 34*, 15191−15203.

16. Limburg, J., LeBrun, L. A., and Ortiz de Montellano, P. R. (2005) The P450cam G248E mutant covalently binds its prosthetic heme group, *Biochemistry 44*, 4091−4099.

17. Pipirou, Z., Bottrill, A. R., Metcalfe, C. M., Mistry, S. C., Badyal, S. K., Rawlings, B. J., and Raven, E. L. (2007) Autocatalytic Formation of a Covalent Link between Tryptophan 41 and the Heme in Ascorbate Peroxidase, *Biochemistry 46*, 2174−2180.

18. Nelson, D. P., and Kiesow, L. A. (1972) Enthalpy of decomposition of hydrogen peroxide by catalase at 25 degrees C (with molar extinction coefficients of H_2O_2 solutions in the UV), *Anal. Biochem. 49*, 474−478.

19. Badyal, S. K., Joyce, M. G., Sharp, K. H., Seward, H. E., Mewies, M., Basran, J., Macdonald, I. K., Moody, P. C. E., and Raven, E. L. (2006) Conformational mobility in the active site of a heme peroxidase, *J. Biol. Chem. 281*, 24512−24520.

20. Jones, D. K., Dalton, D. A., Rosell, F. I., and Lloyd Raven, E. (1998) Class I heme peroxidases: characterisation of soybean ascorbate peroxidase, *Arch. Biochem. Biophys. 360*, 173−178.

21. Teale, F. W. J. (1959) Cleavage of the haem-protein link by acid methylethylketone, *Biochim. Biophys. Acta 35*, 543.

22. Lad, L., Mewies, M., and Raven, E. L. (2002) Substrate binding and catalytic mechanism in ascorbate peroxidase: evidence for two ascorbate binding sites, *Biochemistry 41*, 13774−13781.

23. Weil, J. A., Bolton, J. R., and Wertz, J. E. (1994) *Electron paramagnetic resonance: Elementary theory and practical applications*, p xxi, Wiley, New York.

24. Massey, V. (1991) in *Flavins and Flavoproteins* (Curti, B., Ronchi, S., and Zanetti, G., Eds.) pp 59−66, Walter de Gruyter & Co., New York.

25. Efimov, I., Papadopoulou, N. D., McLean, K. J., Badyal, S. K., Macdonald, I. K., Munro, A. W., Moody, P. C., and Raven, E. L. (2007) The Redox Properties of Ascorbate Peroxidase, *Biochemistry 46*, 8017−8023.

26. Clark, W. M. (1972) *Oxidation-Reduction Potentials of Organic Systems*, Robert E. Kreiger Publishing Co., Huntington, NY.

27. Binstead, R. A., and Zuberbuehler, A. D., Chapel Hill, NC.

28. Lad, L., Mewies, M., and Raven, E. L. (2002) Substrate binding and catalytic mechanism in ascorbate peroxidase: evidence for two ascorbate binding sites, *Biochemistry 41*, 13774−13781.

29. Antonini, M., and Brunori, E. (1971) *Hemoglobin and Myoglobin and their reactions with ligands*, North Holland Publishers, Amsterdam.

30. Daltrop, O., Smith, K. M., and Ferguson, S. J. (2003) Stereoselective *in vitro* formation of c-type cytochrome variants from *Hydrogenobacter thermophilus* containing only a single thioether bond, *J. Biol. Chem. 278*, 24308−24313.

31. Reeder, B. J., Svistunenko, D. A., Sharpe, M. A., and Wilson, M. T. (2002) Characteristics and mechanism of formation of peroxide-induced heme to protein cross-linking in myoglobin, *Biochemistry 41*, 367−75.

32. Raven, E. L. (2003) Understanding functional diversity and substrate specificity in haem peroxidases: what can we learn from ascorbate peroxidase, *Nat. Prod. Rep. 20*, 367−381.

33. Patterson, W. R., Poulos, T. L., and Goodin, D. B. (1995) Identification of a porphyrin pi cation radical in ascorbate peroxidase compound I, *Biochemistry 34*, 4342−4345.

34. Svistunenko, D. A., Dunne, J., Fryer, M., Nicholls, P., Reeder, B. J., Wilson, M. T., Bigotti, M. G., Cutruzzola, F., and Cooper, C. E. (2002) Comparative study of tyrosine radicals in hemoglobin and myoglobins treated with hydrogen peroxide, *Biophys. J. 83*, 2845−285.

35. Svistunenko, D. A. (2005) Reaction of haem containing proteins and enzymes with hydroperoxides: the radical view, *Biochim. Biophys. Acta 1707*, 127−155.

36. Arciero, D. M., Hooper, A. B., Cai, M., and Timkovich, R. (1993) Evidence for the structure of the active site heme P460 in hydroxylamine oxidoreductase of Nitrosomonas, *Biochemistry 32*, 9370−9378.

37. Pearson, A. R., Elmore, B. O., Yang, C., Ferrara, J. D., Hooper, A. B., and Wilmot, C. M. (2007) The Crystal Structure of Cytochrome P460 of Nitrosomonas europaea Reveals a Novel Cytochrome Fold and Heme-Protein Cross-link, *Biochemistry 46*, 8340−8349.

38. Vu, B. C., Vuletich, D. A., Kuriakose, S. A., Falzone, C. J., and Lecomte, J. T. (2004) Characterization of the heme-histidine cross-link in cyanobacterial hemoglobins from Synechocystis sp. PCC 6803 and Synechococcus sp. PCC 7002, *J. Biol. Inorg. Chem. 9*, 183−194.

39. Catalano, C. E., Choe, Y. S., and Ortiz de Montellano, P. R. (1989) Reactions of the protein radical in peroxide-treated myoglobin. Formation of a heme-protein cross-link, *J. Biol. Chem. 264*, 10534−10541.

40. Moreau, S., Davies, M. J., and Puppo, A. (1995) Reaction of ferric leghemoglobin with H_2O_2: formation of heme-protein cross-links and dimeric species, *Biochim. Biophys. Acta 1251*, 17−22.

41. Jia, Y., Buehler, P. W., Boykins, R. A., Venable, R. M., and Alayash, A. I. (2007) Structural basis of peroxide-mediated changes in human hemoglobin: a novel oxidative pathway, *J. Biol. Chem. 282*, 4894−4907.

42. Igarashi, N., Moriyama, H., Fujiwara, T., Fukumori, Y., and Tanaka, N. (1997) The 2.8 A structure of a hydroxylamine oxidoreductase from a denitrifying chemoautotrophic bacterium, *Nitrosomonas europaea, Nat. Struct. Biol. 4*, 276−284.

43. Zhang, H., He, S., and Mauk, A. G. (2002) Radical formation at Tyr39 and Tyr153 following reaction of yeast cytochrome c peroxidase with hydrogen peroxide, *Biochemistry 41*, 13507−13513.

44. Efimov, I., Cronin, C. N., and McIntire, W. S. (2001) Effects of noncovalent and covalent FAD binding on the redox and catalytic properties of p-cresol methylhydroxylase, *Biochemistry 40*, 2155−2166.

45. Zederbauer, M., Furtmuller, P. G., Bellei, M., Stampler, J., Jakopitsch, C., Battistuzzi, G., Moguilevsky, N., and Obinger, C. (2007) Disruption of the aspartate to heme ester linkage in human myeloperoxidase: impact on ligand binding, redox chemistry, and interconversion of redox intermediates, *J. Biol. Chem. 282*, 17041−17052.
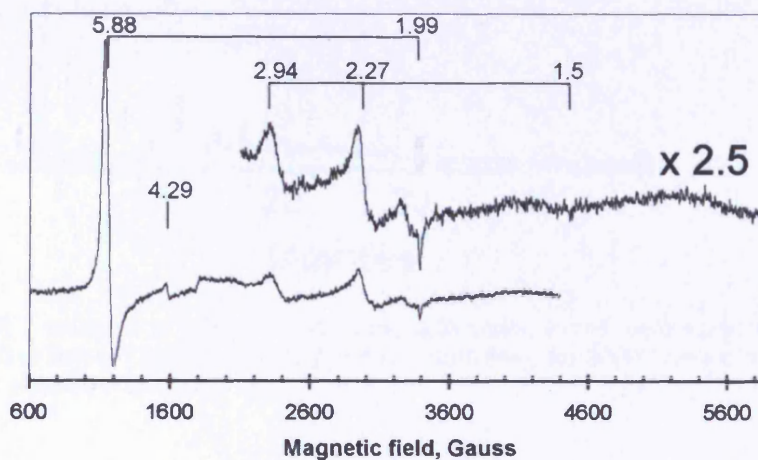
BI7015316

The reactivity of heme in biological systems:
autocatalytic formation of both tyrosine-heme and tryptophan-heme covalent links in a single protein architecture

Zoi Pipirou,[‡] Andrew R. Bottrill,[§] Dimitri A. Svistunenko,[⊥] Igor Efimov,[‡] Jaswir Basran,[‖] Sharad C. Mistry, [§] Christopher E. Cooper,[⊥] and Emma Lloyd Raven*[,‡]
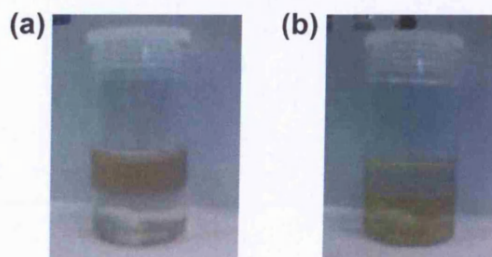
[‡]Department of Chemistry, Henry Wellcome Building, University of Leicester, University Road, Leicester, LE1 7RH, England, [§]Protein and Nucleic Acid Chemistry Laboratory, Hodgkin Building, University of Leicester, Lancaster Road, Leicester LE1 9HN, England, [‖]Department of Biochemistry, Henry Wellcome Building, University of Leicester, Lancaster Road, Leicester, LE1 9HN, England, and [⊥]Department of Biological Sciences, University of Essex, Wivenhoe Park, Colchester, CO4 3SQ, England

Supplementary information

Figure S1: The EPR spectrum of ferric S160Y (80 µM). Multiplied by a factor of 2.5 is the spectrum recorded at a higher magnetic field and showing the third component of the low spin ferric heme signal, at g = 1.5. All other instrumental conditions were the same for both spectra: modulation frequency v_m = 100 kHz, modulation amplitude A_m = 5 G, sweep rate v = 22.6 G/s, time constant τ = 82 ms, microwave frequency v = 9.4667 GHz, microwave power P = 3.188 mW, number of spectral scans NS = 1, sample temperature 10 K. The ratio of the concentrations [high spin form] / [low spin form] has been measured by integration of the simulated signals in the absence of power saturation and was found to be 1 / 2.83.
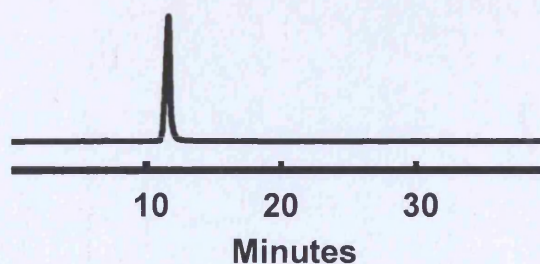

**Figure S2:** Acidified butanone extraction on S160Y before (a) and after (b) reaction with H_2O_2.

Figure S3: HPLC analyses of a commercial sample of free heme.

Figure S4: HPLC of tryptic digest of S160Y after reaction with H_2O_2, monitored at 215 nm (blue line) and 398 nm (red line). Elution times of heme-containing peptides (23.0, 24.0, 24.7, 27.3 and 28.1 minutes) as well as free heme (30.6 minutes) are indicated. The major peak eluting at 24.7 minutes was analysed by mass spectrometry, according to the text; other peaks were found by mass spectrometry not to be consistent with a Tyr-heme, Trp-heme or any other peptide linking to the heme.
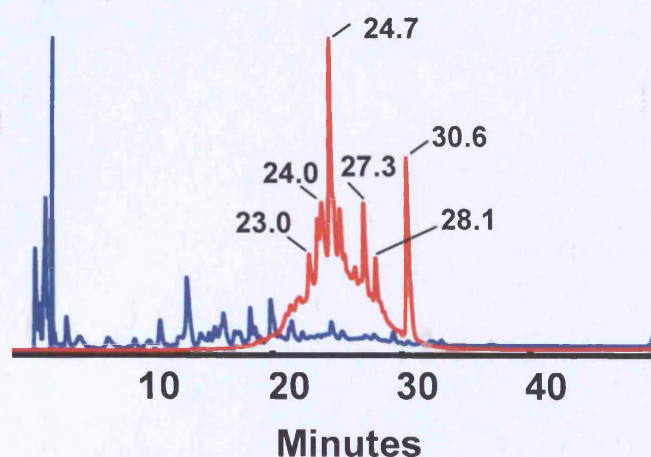
Figure S5: HPLC analyses of S160Y reconstituted with deuteroheme, before and after reaction with H_2O_2 monitored at 398 nm (solid line) and 215 nm (dotted line). (a) S160Y before reaction with H_2O_2; (b) S160Y after reaction with H_2O_2.